

UNIVERSITY OF BIRMINGHAM

EVALUATING THE ROLE OF THE DERMAL PATHWAY IN DRIVING HUMAN EXPOSURE TO PER- AND POLYFLUOROALKYL SUBSTANCES (PFAS)

Oddný Ragnarsdóttir,

M. Sc., B. Sc.

A thesis submitted to the University of Birmingham

for the degree of

DOCTOR OF PHILOSOPHY (Ph. D)

Division of Environmental Health and Risk Management

College of Life and Environmental Sciences

School of Geography, Earth and Environmental Sciences

The University of Birmingham Edgbaston,

B15 2TT United Kingdom

November 2023

UNIVERSITY OF
BIRMINGHAM

University of Birmingham Research Archive

e-theses repository

This unpublished thesis/dissertation is copyright of the author and/or third parties. The intellectual property rights of the author or third parties in respect of this work are as defined by The Copyright Designs and Patents Act 1988 or as modified by any successor legislation.

Any use made of information contained in this thesis/dissertation must be in accordance with that legislation and must be properly acknowledged. Further distribution or reproduction in any format is prohibited without the permission of the copyright holder.

Abstract

Per- and polyfluoroalkyl substances (PFAS) have been identified in multiple sources that come in contact with the skin, i.e., personal care products, fabrics and dust. Despite this, knowledge of dermal uptake as a source of human exposure to PFAS is lacking. The aim of this thesis was to utilize *in vitro* techniques to study the dermal uptake of PFAS from dust. Firstly, physiologically based extraction tests were applied to assess the dermal bioaccessibility of 17 PFAS from indoor dust to synthetic sweat sebum mixtures (SSSM). PFAS bioaccessibility in a 1:1 sweat:sebum mixture ranged from 54-92% for perfluorocarboxylic acids (PFCAs) and 61-77% for perfluorosulfonic acids (PFSAs). The presence of cosmetics significantly impacted the dermal bioaccessibility of target PFAS. Subsequently, *in vitro* 3D-human skin equivalent (3D-HSE) models were used to evaluate the dermal bioavailability of 17 PFAS after exposure to 500 ng/cm^2 PFAS dissolved in methanol over 24-36 hours. PFPeA and PFBS displayed the highest absorbed fraction values, 58.9% and 48.7% respectively. Significant negative correlations were seen for the absorbed fraction and carbon chain length and logK_{OW}. Steady-state flux ($\boldsymbol{J_{SS}}$) and permeation coefficients ($\mathbf{P_{app}}$) were determined for target compounds with significant permeation after 36 h exposure. Combining the data produced in the bioaccessibility and bioavailability studies, the human dermal exposure from contact with dust was estimated. While dust is only one of multiple possible sources of dermal contact to PFAS, this pathway alone contributed meaningfully to the total body burden. Total PFAS exposure via dermal uptake from dust during summer ranged from 25-767 pg/kg bw/week and 91-2761 pg/kg bw/week for adults and toddlers respectively. Finally, phase I *in vitro* metabolism of two novel prototype PFAS in human and rat was investigated. Research on possible PFAS alternatives is urgently required as a result of proposed global restrictions and regulations on current-use PFAS. Following incubation with rat liver S9 (RL-S9) and human liver S9 (HL-S9) fractions, two and one main metabolites were detected respectively. Complete mineralization during the *in vitro* hepatic metabolism of these novel PFAS by HL-S9 and RL-S9 fractions was not observed.

Acknowledgements

Firstly, I would like to express my sincere gratitude to my PhD supervisors Prof. Stuart Harrad and Dr. Mohamed Abdallah for their patience, motivation, and guidance during my PhD. I thoroughly enjoyed our discussions; their door was always open, and their encouragement and insightful comments helped me in so many ways. I truly could not have asked for better supervisors during my PhD.

This project was funded by the European Union's Horizon 2020 research and innovation program under the Marie Skłodowska-Curie grant agreement No 860665.

To all of the Perforce 3 ESRs, you made this experience so much better, and I really enjoyed getting to know all of you. A special thanks to Viktoria and HSF for hosting me during my secondment.

Thank you to everyone in the POPs group, I would like to especially acknowledge Dr. Will Stubbings, Dr. Dan Drage, and Dr. Ovokeroye Abafe for their help and guidance in the lab.

Finally, without the love and support of my family, and friends I would not be where I am today. I am forever grateful for you all.

Table of Contents

Abstract i

Acknowledgements ii

List of tables vi

List of figures vii

List of publications ix

Abbreviations ix

1. INTRODUCTION 1

1.1. Background 1

1.2. The significance of different pathways of human exposure to PFAS 8

1.3. The skin barrier and dermal permeation 15

1.3.1. The skin barrier 15

1.3.2. Dermal bioavailability 16

1.3.3. Dermal bioaccessibility 18

1.3.4. Dermal metabolism 18

1.4. Methods for evaluation of human dermal uptake of chemical contaminants 19

1.4.1. *In vivo* methods 19

1.4.2. *In vitro* and *ex vivo* methods 20

1.4.3. 3D-Human Skin Equivalent Models 24

1.5. Dermal bioavailability and bioaccessibility of halogenated organic pollutants and their significance to overall human exposure 27

1.6. The potential of dermal uptake as a pathway of human exposure to PFAS 31

1.7. Possible sources of human exposure via the dermal pathway 36

1.8. Summary and Aims 39

2. METHODOLOGY 41

2.1. Chemicals and standards 41

2.2. Exposure protocols 45

2.2.1. Dermal bioaccessibility 45

2.2.2. Dermal bioavailability 45

2.2.3. Metabolism of novel PFAS 46

2.3. SPE comparison 46

2.3.1. SPE sample extraction and analysis 46

2.3.2. Results of SPE comparison 47

2.4. Sample types and SPE extraction 48

2.4.1. Sample types 48

2.4.2. Sample extraction with SPE 49

2.5. Instrumental Analysis 49

2.6. Quality Assurance and Quality Control 51
2.7. Data Processing and Statistical Analysis 52
3. DERMAL BIOACCESSIBILITY OF PFAS 53
3.1. Introduction 53
3.2. Materials and Methods 56
3.2.1. Materials 56
3.2.2. Synthetic Sweat and Sebum Mixture Preparation 56
3.2.3. Dermal Bioaccessibility *in vitro* Test Protocol 56
3.2.4. Sample Extraction and Clean-up 57
3.2.5. Chemical Analysis 57
3.2.6. Quality Assurance and Quality Control 57
3.2.7. Assessment of Dermal Bioaccessibility 58
3.2.8. Statistical Analysis 58
3.3. Results and Discussion 59
3.3.1. Dermal bioaccessibility of PFAS in indoor dust 59
3.3.2. Effects of cosmetics on the dermal bioaccessibility of PFAS from indoor dust 63
3.3.3. Preliminary estimates of human dermal exposure to PFAS from indoor dust 66
3.4. Study limitations 70
3.5. Supporting Information 70
3.5.1. Synthetic sweat and sebum preparation: 70
3.5.2. Personal care products ingredients list 72
3.5.3. Sample Extraction and clean-up 73
4. DERMAL BIOAVAILABILITY OF PFAS 89
4.1. Introduction 89
4.2. Materials and Methods 93
4.2.1. Materials 93
4.2.2. Test Matrices and Permeation Assay Protocol 94
4.2.3. Sample Extraction and Chemical Analysis 94
4.2.4. Quality Assurance and Quality Control 95
4.2.5. Data Analysis 96
4.3. Results and Discussion 97
4.3.1. Dermal Bioavailability of PFAS 97
4.3.2. Dermal flux (J_{ss}) and Permeation Coefficients (P_{app}) 103
4.4. Conclusion 106
4.5. Supporting Information 108
4.5.1. Experimental 108
4.5.2. Analysis of PFAS – Sample extraction and clean-up 110

4.5.3. Results and discussion – supporting information. 112
5. EVALUATION OF HUMAN EXPOSURE TO PFAS VIA DERMAL CONTACT WITH INDOOR DUST 115
5.1. Introduction 115
5.2. Materials and Methods 118
5.2.1. Estimations of human dermal uptake of PFAS from dust 119
5.3. Results and discussion 121
5.3.1. Dermal uptake of PFAS from indoor dust 121
5.3.2. Dermal exposure to PFAS via dermal contact with dust; comparison to other exposure pathways 124
5.4. Conclusion and future research 127
6. IN VITRO METABOLISM OF NOVEL PFAS 129
6.1. Introduction 129
6.2. Materials and Methods 132
6.2.1. Chemicals 132
6.2.2. *In vitro* incubation 136
6.2.3. Sample preparation and clean-up 136
6.2.4. Quality Assurance and Quality Control 136
6.2.5. Instrumental Analysis 137
6.2.6. Kinetic modelling 138
6.3. Results and Discussion 139
6.3.1. Metabolic pathways 139
6.3.2. Metabolic profile by targeted analysis 140
6.3.3. Metabolic profile by non-targeted analysis 141
6.3.4. Metabolism kinetics 145
6.3.5. Inter-species metabolic comparison 146
6.4. Study limitations 151
6.5. Supporting Information 152
6.5.1. Specification of S9 fraction 152
6.5.2. Optimization of incubation time 153
6.5.3. Targeted LC-MS/MS analysis 153
6.5.4. Analytical performance of the LC-MS/MS method 154
6.5.5. Non-targeted HRMS analysis 155
6.5.6. Workflow for the identification of further transformation products 157
7. SUMMARY AND CONCLUSIONS 177
References 183

List of tables

Table 1-1: Geometric mean (GM) values of PFAS half-lives in humans.....6
Table 1-2: Summary of the median contributions (expressed as percentage of total exposure via all pathways considered[a]) of various exposure pathways to overall adult human exposure to PFOS and PFOA.....12
Table 1-3: Summary of the median contributions (expressed as percentage of total exposure via all pathways considered[a]) of various exposure pathways to overall infant human exposure to PFOS and PFOA.....13
Table 1-4: Physicochemical properties of various PFAS compared to the Lipinski's rule of 5 criteria. The other two criteria are H bond donors (≤ 5) and H bond acceptors (≤ 10). Also included are the compounds water solubility.....17
Table 2-1: Target PFAS, their abbreviations, molecular structures, and labelled internal standards used. 42
Table 2-2: Fraction of PFAS (%) found in each fraction of eluant from the tested SPEs. 48
Table 2-3: LC conditions used in this study. 50
Table 2-4: Target accurate masses. Estimated method detection and quantification limits (MDL and MQLs) for PFAS. Estimations were based on the S:N ratio 3:1 and 10:1 respectively. 51
Table 3-1: Estimated human daily exposure dose (DED in pg/kg bw/day) to selected PFAS via the dermal pathway from household dust based on contact with 1:1 sweat:sebum mixture. 68
Table 3-2: Chemical composition of synthetic human sweat/sebum mixture (SSSM) applied in this study based on a previously published patent (Stefaniak and Harvey, 2008).....71
Table 3-3: PFAS concentrations determined in SRM2585 (Organics in indoor dust) in this study (n=6) and concentrations reported elsewhere.....75
Table 3-4: Recoveries (expressed as average ± SD percent) of the isotopically labelled internal (surrogate) standards in the analysed samples.....76
Table 3-5: Effect of the composition of synthetic sweat and sebum mixtures on the bioaccessibilty ($f_{bioaccessible}$ (%)) of target PFAS from indoor dust.....77
Table 3-6: Mass balance for target PFAS after dust exposure to 100% sweat (n = 6). 78
Table 3-7: Mass balance for target PFAS after dust exposure to 95:5 sweat:sebum (n = 6)...79
Table 3-8: Mass balance for target PFAS after dust exposure to 1:1 sweat:sebum (n = 6).....80
Table 3-9: Mass balance for target PFAS after dust exposure to 100% sebum (n = 6).....81
Table 3-10: Mass balance for target PFAS after dust exposure to 1:1 sweat:sebum in combination with foundation (n = 3). 83
Table 3-11: Mass balance for target PFAS after dust exposure to 1:1 sweat:sebum in combination with moisturiser (n = 3). 84
Table 3-12: Mass balance for target PFAS after dust exposure to 1:1 sweat:sebum in combination with sunscreen (n = 3).....85
Table 3-13: Mass balance for target PFAS after dust exposure to 1:1 sweat:sebum in combination with deodorant (n = 3).....86
Table 3-14: Parameters used in dermal exposure assessment of target PFAS: 87
Table 4-1: Distribution of target PFAS (expressed as % of exposure dose ± standard deviation) in different compartments of the in vitro diffusion system after 36 or 24[a] hour exposure to 500ng/cm^2.....98

Table 4-2: Flux (J_{ss}, [ng/cm^2·h]), permeation coefficient (P_{app}, [cm/h]) and lag time (t_{lag}, [h]) values estimated from infinite exposure of 3D-HSE models to 500 ng/cm^2 of the target PFAS with significant permeation after 36 h. 105
Table 4-3: Linearity coefficient (R^2) and probability statistics (p) for the linear correlations established between cumulative permeated dose (ng/cm^2) of target PFAS over time (hours) over the established steady-state period.....114
Table 5-1: Median dust concentrations (ng/g) from various countries used for dermal uptake estimations. Concentrations published by Eriksson and Kärrman, 2015 and Norwegian concentrations published by Poothong et al., 2020.....118
Table 5-2: Parameters used in dermal exposure assessment of target PFAS: 119
Table 5-3: Weekly human exposure to PFAS via dermal contact with dust based on age group, country, and time of year (1a. summer, 1b. winter) (pg/kg bw/week). Sum of the EFSA 4 is provided for comparison with EFSA TWI of 4400 pg/kg bw/week. 123
Table 6-1. General information about the targeted chemicals of this study. Adapted from (Licul-Kucera et al., 2023).....134
Table 6-2: Metabolites of CF_3-O-SURF and CF_3-S-SURF identified by HRMS. 143
Table 6-3: Kinetic parameters derived from Michaelis-Menten model for the formation of CF_3-O-CA and CF_3-S-CA following incubation with RL- and HL-S9 146
Table 6-4: Comparison of the intrinsic in vitro hepatic clearance values of PFAS.....150
Table 6-5:. General information about the analyzed prototype molecules and their internal standards (IS), and the liquid chromatographic-tandem mass spectrometric (LC-MS/MS) method.....158
Table 6-6: LC-MS/MS method performance parameters determined for the quantified targeted metabolites. 159

List of figures

Figure 1-1: The various pathways for external human exposure to PFAS. 8
Figure 1-2: Average relative percent contribution of different routes to overall daily human exposure to PFAS in adults and infants. A similar figure based on dietary exposure from USA was presented by Ghassabian et al., 2022 (based on data from (Wu and Kannan, 2019)).....13
Figure 1-3: In vitro dermal exposure experimental configuration using a Franz cell. The skin samples act as a barrier between the two compartments, the upper donor compartment and the lower receptor compartment. The receptor fluid should be kept at a temperature similar to human body temperature. Figure taken from Abdallah and Harrad, 2018. 21
Figure 1-4: Illustration of the parallelogram approach. Figure adapted from Knudsen et al., 2019.....24
Figure 3-1: Dermal bioaccessibility of (a) PFCAs and (b) PFSAs in different composition of synthetic sweat sebum mixtures. Error bars represent the standard deviation (n = 6).....60
Figure 3-2: Plot of PFAS carbon number versus relative standard deviation (RSD) of the bioaccessibility values obtained for individual PFAS across the range of SSSM compositions examined for: (a) PFCAs and (b) PFSAs.....62
Figure 3-3: Comparison of the effects of applied cosmetics on the bioaccessibility of (a) PFCAs and (b) PFSAs. Error bars represent the standard deviation (n = 3). 65
Figure 3-4: Comparison of estimated adult human dermal exposure via contact with dust and other pathways of exposure to target PFAS (high exposure scenario)(Gebbink et al., 2015). 69

Figure 3-5: Average values of $f_{bioaccessible}$ in all SSSM mixtures against PFAS carbon chain length.....82
Figure 4-1: Association of cumulative permeation of PFAS after 36 hours and C chain length (a) and logK_{OW} (b) Error bars represent the cumulative standard deviation (n = 3). Included are values for compounds with C ≤ 9 and C ≤ 8 for both PFCAs and PFSAs respectively. .100
Figure 4-2: Cumulative permeation (ng/cm^2) of PFCAs (a) and PFSAs (b) into the receptor fluid following exposure of 500 ng/cm^2 of target PFAS to 3D-HSE models for 36 hours. Error bars represent the cumulative standard deviation (n = 3).....104
Figure 4-3: General stages of development of 3D human skin equivalent (3D-HSE) model (a). Histological comparison between excised human skin and EPISKIN™(3D-HSE model) tissue (b). Figure published previously by Abdallah et al., 2015b. 108
Figure 4-4: Experimental protocol applied during dermal permeation experiments.....109
Figure 4-5: Flowchart of the applied algorithm for identification of the steady state range as described by Niedorf et al., 2008.....112
Figure 4-6: A representative curve displaying cumulative permeation (ng/cm^2) of target PFCAs (a) and PFSAs (b) at the linear-range region ($R^2 \geq 0.9$), following the parameters described in Figure 4-5. Error bars represent 1 standard deviation (n = 3). 113
Figure 5-1: Human exposure to PFAS via dermal contact to dust compared to other known exposure pathways including (1a.) and excluding (1b.) diet. 126
Figure 6-1: Kinetics of A) CF_3-O-ALC, B) CF_3-O-CA, C) CF_3-S-ALC and D) CF_3-S-CA production during incubation with rat and human S9 hepatic fractions, using the Michaelis-Menten model. Error bars represent standard deviations. (n=3).....148
Figure 6-2: The transformation rate – incubation time relation with rat liver S9 fraction A) in the whole incubation period B) in the linear range.....160
Figure 6-3: Chromatograms of positive control samples 1) before incubation 2) after 120 min incubation with human liver S9 3) after 120 min incubation with rat liver S9 161
Figure 6-4: Proposed transformation pathway of the novel PFAS prototype chemicals. The metabolites in brackets were not detected in this study.....162
Figure 6-5: MS spectrum of TP-NTS-O1. Identified only in the RL fractions. 163
Figure 6-6: MS/MS spectrum of TP-NTS-O1. 164
Figure 6-7: Full-scan MS spectrum of TP-NTS-O2. Identified only in the RL fractions. 165
Figure 6-8: MS/MS spectrum of TP-NTS-O2. 166
Figure 6-9: Full-scan MS spectrum of TP-NTS-S1. Identified only in the HL fractions.....167
Figure 6-10: MS/MS spectrum of TP-NTS-S1.....168
Figure 6-11: Full-scan MS spectrum of TP-NTS-S2. Identified in both the RL and HL fractions.....169
Figure 6-12: MS/MS spectrum of TP-NTS-S2.....170
Figure 6-13: Full-scan MS spectrum of TP-NTS-S3. Identified only in the RL fractions. ...171
Figure 6-14: MS/MS spectrum of TP-NTS-S3.....172
Figure 6-15: Full-scan MS spectrum of TP-NTS-S4. Identified both in the RL and HL fractions.....173
Figure 6-16: MS/MS spectrum of TP-NTS-S4.....174
Figure 6-17: Full-scan MS spectrum of TP-NTS-S5. Identified both in the RL and HL fractions.....175
Figure 6-18: MS/MS spectrum of TP-NTS-S5.....176

List of publications

First author:

i. Ragnarsdóttir, O.; Abdallah, M. A.-E.; Harrad, S. 2022. Dermal Uptake: An Important Pathway of Human Exposure to Perfluoroalkyl Substances? *Environmental Pollution*, 307, 119478. https://doi.org/10.1016/j.envpol.2022.119478.

ii. Ragnarsdóttir, O.; Abdallah, M.A.-E.; Harrad, S., 2023. Dermal bioaccessibility of perfluoroalkyl substances from household dust; influence of topically applied cosmetics. *Environmental Research*, 238, 117093. https://doi.org/10.1016/j.envres.2023.117093

iii. Ragnarsdóttir, O.; Abdallah, M. A.-E.; Harrad, S. 2024. Dermal Bioavailability of Perfluoroalkyl Substances (PFAS) using *in vitro* 3D-Human Skin Equivalent Models. *Under review in Environment International, January 2024.*

Contributing author

i. Licul-Kucera, V.; Ragnarsdóttir, O.; Frömel, T; van Wezel, A.P.; Knepper, T.P.; Harrad, S.; Abdallah, M. A.-E.; 2024. Interspecies comparison of metabolism of two novel prototype PFAS. *Chemosphere*, 351, 141237. https://doi.org/10.1016/j.chemosphere.2024.141237

ii. Namazkar, S.; Ragnarsdóttir, O; Josefsson, A.; Branzell, F.; Abel, S.; Abdallah M. A.-E.; Harrad, S.; and Benskin, J. P., 2024. Characterization and dermal bioaccessibility of residual- and listed PFAS ingredients in cosmetic products. *Environmental Science: Processes & Impacts.*10.139.D3EM00461A. https://doi.org/10.1039/D3EM00461A

Conference Presentations

i. Ragnarsdóttir, O.; Abdallah, M. A.-E.; Harrad, S. Dermal bioaccessibility of per- and polyfluoroalkyl substances (PFAS) from indoor dust. 42nd International Symposium on Halogenated Persistent Organic Pollutants – Dioxin 2022 (presentation).

ii. Ragnarsdóttir, O.; Abdallah, M. A.-E.; Harrad, S. Dermal bioaccessibility of per- and polyfluoroalkyl substances (PFAS) from indoor dust. SETAC Europe 33rd Annual meeting 2023 (presentation).

iii. Ragnarsdóttir, O.; Abdallah, M. A.-E.; Harrad, S. Evaluating dermal bioavailability of per- and polyfluoroalkyl substances (PFAS) using *in vitro* 3D-HSE models. 43rd International Symposium on Halogenated Persistent Organic Pollutants – Dioxin 2023 (presentation – **Otto Hutzinger Student Award**).

Abbreviations

[S]	Surfactant concentration
3D-HSE	3D-Human Skin Equivalent Model
ADME	Absorption, distribution, metabolism, elimination

AFFF	Aqueous fire-fighting foams
BFR	Brominated flame retardants
CF_3-CA	fluoro(trifluoromethoxy)acetic acid
CF_3-O-ALC	2-[1,1,2-trifluoro-2-(trifluoromethoxy)ethoxy]ethan-1-ol
CF_3-O-CA	[1,1,2-trifluoro-2-(trifluoromethoxy)ethoxy]acetic acid
CF_3-O-SURF	1,5-dioxo-1,5-bis({2-[1,1,2-trifluoro-2-(trifluoromethoxy)ethoxy]ethoxy})-3-({2-[1,1,2-trifluoro-2-(trifluoromethoxy)ethoxy]ethoxy}carbonyl)pentane-2-sulfonic acid
CF_3-S-ALC	2-{[1,1,2-trifluoro-2-(trifluoromethoxy)ethyl]sulfanyl}ethan-1-ol
CF_3-S-CA	{[1,1,2-trifluoro-2-(trifluoromethoxy)ethyl]sulfanyl}acetic acid
CF_3-S-SURF	1,5-dioxo-1,5-bis(2-{[1,1,2-trifluoro-2-(trifluoromethoxy)ethyl]sulfanyl}ethoxy)-3-[(2-{[1,1,2-trifluoro-2-(trifluoromethoxy)ethyl]sulfanyl}ethoxy)carbonyl]pentane-2-sulfonic acid
CIC	Combustion ion chromatography
CL_{int}	Apparent intrinsic *in vitro* clearance
$CL_{int, liver}$	Intrinsic *in vitro* hepatic clearance
CYP450	Cytochrome P450
DIA	Data-Independent Acquisition
DMEM	Dubelcos modified eagles medium
DMSO	Dimethyl sulfoxide
DWD	Drinking water directive
DWR	Durable water repellent
ECHA	European Chemicals Acency
ECHA	European Chemicals Agency
EOF	Extractable organic fluorine
FR	Flame retardants
FTACs	Fluorotelomer Acrylates
FTOHs	Fluorotelomer alcohols
G6P	Glucose-6-phosphate
G6P-DH	Glucose-6-phosphate dehydrogenase
GC-MS	Gas chromatography tandem mass spectrometry
HBCDD	HBCDD
HBCDD	Hexabromocyclododecane
HBSS	Hanks balances salt solution
HeptaCD	1, 2, 5, 5, 6, 9, 10-heptachlorodecane
HFPO-DA	2,3,3,3-tetrafluoro-2-(heptafluoropropoxy)propionic acid
HLM	Human liver microsomes
HL-S9	Human liver S9
IDA	Information dependent acquisition
IS	Internal standards
K_m	Michaelis-Menten constant
LOD	Limit of detection
Log Kow	Octanol:water partition coefficient
LOQ	Limit of quantification
MeOH	Methanol
NADPH	Dinucleotide phosphate
OATP	Organic anion transporter polypeptides
OECD	Organication for Economic Co-operation and Development
p	Amount of protein per gram of the liver
PAPs	Polyfluoroalkyl phosphate esters

PBDEs	Polybrominated diphenyl ethers
PCP	Personal care products
PFAS	Per – and polyfluoroalkyl substances
PFBA	Perfluorobutanoic acid
PFBS	Perfluoro-1-butanesulfonate
PFCAs	Perfluorocarboxylic acids
PFDA	Perfluoro-n-decanoic acid
PFDoDA	Perfluoro-n-dodecanoic acid
PFDS	Perfluoro-1-decanesulfonate
PFHpA	Perfluoro-n-heptanoic acid
PFHpS	Perfluoro-1-heptanesulfonate
PFHxA	Perfluoro-n-hexanoic acid
PFHxS	Perfluoro-1-hexanesulfonate
PFNA	Perfluoro-n-nonanoic acid
PFNS	Perfluorono-1-nanesulfonate
PFOA	Perfluoro-n-octanoic acid
PFOS	Perfluoro-1-octanesulfonate
PFPeA	Perfluoropentanoic acid
PFPeS	Perfluoro-1-pentanesulfonate
PFSAs	Perfluorosulfonic acids
PFTeDA	Perfluoro-n-tetradecanoic acid
PFTrDA	Perfluoro-n-tridecanoic acid
PFUnDA	Perfluoro-n-undecanoic acid
PIGE	Particle Induced Gamma Ray Emission spectroscropy
QTOF MS	Quadrupole Time of Flight Mass spectrometry
RLM	Rat liver microsomes
Rat liver S9	RL-S9
REACH	Registration, Evaluation, Authorisation and Restriction of Chemical
RF	Receptor fluid
RfD	Reference dose
SSSFL	Synthetic skin surface film liquid
SSSM	Synthetic skin surface mix
TBB	2-ethylhexyl-2,3,4,5-tetrabromobenzoate
TBBPA	Tetrabromobisphenol A
TBPH	Bis(2-ethylhexyl) 2,3,4,5 tetrabromophthalate
TCEP	Tris-2-chloroethyl phosphate
TCIPP	Tris (1-chloro-2-propyl) phosphate
TDCIPP	Tris- 1,3-dichloropropyl phosphate
TP	Transformation product
UPLC	Ultra Performance Liquid Chromatography
USEPA	United States Environmental Protection Agency
v	Initial velocity of the reaction
vB	Very Bioaccumulative
vM	Very Mobile
vP	Very Persistent
V_{max}	Maximum rate of enzymatic reaction

1. INTRODUCTION

This chapter includes material taken verbatim from the following article:

Ragnarsdóttir, O.; Abdallah, M. A.-E.; Harrad, S. 2022. Dermal Uptake: An Important Pathway of Human Exposure to Perfluoroalkyl Substances? *Environmental Pollution*, 307, 119478. https://doi.org/10.1016/j.envpol.2022.119478.

O.R. wrote the original draft and was the corresponding author. S.H. and M. A.-E. A. reviewed and edited the manuscript.

1.1. Background

Per- and polyfluoroalkyl substances (PFAS) are a class of thousands of chemical substances. These chemicals have been produced since the 1950s and still find use in a wide variety of industrial applications and consumer products. The Organisation for Economic Co-operation and Development (OECD) defines PFAS as fluorinated substances that contain at least one fully fluorinated methyl (CF_3-) or methylene (-CF_2-) carbon atom (without any H/Cl/Br/I attached to it) (OECD, 2021). The perfluoroalkyl moiety is both chemically and thermally stable, as well as having hydrophobic and lipophobic properties. This makes this chemical class very useful and enduring when incorporated as surfactants in firefighting foams and coatings, as well as polymers used in textiles and food packaging materials (Buck et al., 2011; Glüge et al., 2020a). More recent studies have highlighted less well-known applications of PFAS. This includes their use in cosmetic products, such as powders, foundations, sunblocks and more. These products were found to contain perfluorinated carboxylic acids (PFCAs) and polyfluoroalkyl phosphate esters (PAPs) among other fluorinated ingredients (Schultes et al., 2018). PFAS have been identified in other personal care products e.g., hair products, hand sanitisers, and makeup removers and have even been used in guitar strings and piano keys (Glüge et al., 2020a). PFAS have been identified in ski wax products, with a study from Sweden reporting high levels of PFAS, including 9 different ski wax products containing

perfluorooctanoic acid (PFOA) above the EU limit value of 25 ng/g, which promulgated in July 2020 (Fang et al., 2020). Another notable use of PFAS is in water-repellent clothing, which have been found to contain both PFCAs and perfluoroalkyl sulfonic acids (PFSAs) as well as fluorotelomer alcohols (FTOHs) (Greenpeace, 2016, 2013, 2012; van der Veen et al., 2020). FTOHs are a class of PFAS, which can be biotransformed in various living organisms to more stable compounds such as PFCAs and are hence often referred to as precursor compounds. For example, several *in vivo* and *in vitro* studies suggest that 8-2 fluorotelomer alcohol (8-2 FTOH) is metabolised to perfluoropentanoic acid (PFPeA), perfluorohexanoic acid (PFHxA), perfluoroheptanoic acid (PFHpA), PFOA, and perfluorononanoic acid (PFNA). The levels and profiles of resulting metabolites vary between species, suggesting possible pathways for indirect exposure to certain PFAS via precursors (Chen et al., 2020; Fasano et al., 2009; Xie et al., 2020).

In 2001, Giesy and Kannan published one of the first studies highlighting the global distribution of perfluorooctanesulfonic acid (PFOS), caused by the widespread use and production of PFAS. They identified PFOS in the tissue of wildlife, such as fish, birds, and marine mammals in samples collected in both North America and Europe (Giesy and Kannan, 2001). Around the same time, a different study identified four PFAS (PFOS, PFOA, perfluorohexanesulfonate (PFHxS), and perfluorooctanesulfonylamide (PFOSA)) in human serum (Hansen et al., 2001).

A recent report by the European Food Safety Authority (EFSA) highlighted a number of possible adverse human health effects of PFAS. As the liver plays a part in the reabsorption of PFAS there have been studies on the possible effects of PFAS on liver function (EFSA CONTAM Panel, 2020). Salihovic et al. (2018) performed a longitudinal population-based study of 1016 individuals from Sweden. The first samples were collected within two months of each participant's 70th birthday with follow up samples collected at 75 years and 80 years.

Statistical analysis of the results revealed a positive association between plasma concentrations of PFHpA, PFOA, PFNA, and PFOS and those of alanine aminotransferase (ALT). Increased ALT activity is a clinical marker for impaired liver function. Additionally, the study found positive associations of PFHpA, PFOA, PFNA, perfluorodecanoic acid (PFDA), and perfluoroundecanoic acid (PFUnDA) with alkaline phosphatase (ALP) - another marker suggestive of liver dysfunction (Salihovic et al., 2018a). A different study found associations between PFAS exposure and altered lipid and bile acid metabolism (Sen et al., 2022a). These results suggest a possible link between serum concentrations of PFAS and impaired liver function; however, further studies are needed to confirm this. Furthermore, a link between PFOA, PFOS, and PFNA exposure and increased cholesterol levels in serum has been reported (EFSA CONTAM Panel, 2020).

Some studies have suggested that prenatal exposure to PFAS could lead to lower birth weight and increase the risk of preterm birth. A study on the Danish National Birth Cohort which includes maternal samples drawn in the first and second trimester, found a consistent negative association between PFOS and PFOA and birth weight as well as a nearly 2-fold increase in the risk of preterm birth (within the higher quartiles of exposure) (Meng et al., 2018). Similarly, a birth cohort study in eastern Massachusetts, found concentrations of PFNA and PFOS in the plasma of expecting mothers at the early stages of their pregnancies to display a weak inverse association with birth weight and an increased risk of preterm delivery (Sagiv et al., 2018). Both Meng et al. (2018) and Sagiv et al. (2018) used samples collected before 2003 (1996-2002 and 1999-2002 respectively) when environmental levels were at their peak. Thus, the concentrations found in these studies were higher than those found in more recent studies. For example, a study on a Spanish birth cohort revealed a possible negative association between concentrations of PFAS in maternal plasma and birth weight. However, this was not statistically significant (Manzano-Salgado et al., 2017). Yet, taking into consideration the

difference in concentrations of PFAS in serum, the EFSA CONTAM Panel found that "there may well be a causal association between PFOS and PFOA and birth weight" (EFSA CONTAM Panel, 2020).

Another significant health effect of PFAS in humans is reduced antibody response to vaccination. Studies on birth cohorts from the Faroe Islands found negative correlations between vaccine antibodies against diphtheria and tetanus at ages 5 and 7 years and concentrations of PFAS in both maternal pregnancy and children's serum at 5 years (Grandjean et al., 2012, 2017a). Similarly, Abraham et al (2020) conducted a study on samples from a German cohort collected in the late 1990s and found significant associations between concentrations of PFOA in serum and adjusted levels of vaccine antibodies against tetanus, diphtheria and *Haemophilus influenza* type b (Abraham et al., 2020).

Studies on highly exposed cohorts have also linked PFAS exposure and endocrine disruption, e.g. thyroid toxicity and some cancers (Barry et al., 2013; Winquist and Steenland, 2014). The C8 study of a population from the US that was highly exposed to PFOA through their drinking water, found that the high PFOA exposure in this group was associated with increased risk of functional thyroid disease, as well as kidney and testicular cancers (Winquist and Steenland, 2014). Nevertheless, as noted recently, both these adverse effects are only detected at high levels of exposure and there is insufficient evidence to suggest association between PFAS exposure at lower levels and cancers or thyroid disease (EFSA CONTAM Panel, 2020).

A consistency of effects of PFAS exposure is seen between epidemiological studies and *in vivo* animal studies. Animals treated with repeat doses of PFAS revealed similar health effects to human studies. Animals exposed to PFCAs were found to have increased liver weights, disturbed lipid metabolism, elevated ALP and ALT as well as disrupted thyroid

hormone levels. Similarly, for PFSA exposed animals, observed changes were increased liver weight, disruption in thyroid hormones and alterations to the kidneys (PFBS only) as well as changes in lipid metabolism, necrosis and inflammation of the liver for higher exposure groups (EFSA CONTAM Panel, 2020).

Based on these findings, in September 2020, EFSA proposed a group tolerable weekly intake of 4.4 ng (kg bw)$^{-1}$ for the sum of PFOA, PFOS, PFNA, and PFHxS. EFSA also noted various reports suggesting PFAS could have a wider impact on human health but further studies are needed to confirm these findings (EFSA CONTAM Panel, 2020). In 2022 the US EPA also updated their lifetime Health Advisory Levels (HALs) for four PFAS in drinking water. The suggested levels were as follows: PFOA: 0.004 ng/L, PFOS: 0.02 ng/L, PFBS: 2000 ng/L and GenX (hexafluoropropylene oxide dimer acid and its ammonium salt): 10 ng/L (U.S. EPA, 2022). Currently, three PFAS are listed under the Stockholm Convention on persistent organic pollutants (POPs). PFOS, including its salts and perfluorooctane sulfonyl fluoride (PFOSF) are listed in Annex B (Restriction); while PFOA, its salts and PFOA-related compounds (including precursor compounds) are listed in Annex A (Elimination) (Stockholm Convention, 2019). More recently, the POPs Review Committee agreed in 2022 to include PFHxS, its salts and PFHxS-related compounds in Annex A (Stockholm Convention, 2022a). Finally, the POPs Review Committee is evaluating whether to list long-chain PFCAs, with carbon chain lengths from 9-21 as well as their salts in Annex D: screening (Stockholm Convention, 2022b).

Half-lives of PFAS in humans range from a few days for short-chained PFAS up to several years for long-chained PFAS (Table 1-1). The long half-lives of PFAS are due to their ability to interact with various transporters involved in reabsorption processes in the liver, intestine and kidneys (EFSA CONTAM Panel, 2020). The physicochemical properties - e.g. the octanol-water partitioning coefficient - of PFAS can affect their absorption in humans (Lipinski et al., 2001). While perfluoroalkyl acids (PFAAs) are not metabolised in humans,

precursor compounds such as 8:2 FTOH and PFOSA can be biotransformed to PFOA and PFOS, respectively and thus contribute to human exposure to these compounds (Nilsson et al., 2013; Vestergren et al., 2008a). Currently, studies investigating human exposure routes of PFAS suggest the main pathways for human exposure are: diet and drinking water, followed by indoor dust and air (Haug et al., 2011; Poothong et al., 2020; Vestergren et al., 2008a). However, few studies have included dermal uptake as a possible route for human exposure. This is partly because very few studies have examined the dermal permeation ability of PFAS (Fasano et al., 2005; Franko et al., 2012). Other studies however, have revealed dermal absorption to be a significant contributor to the total human exposure to chemicals such as brominated flame retardants (Abdallah and Harrad, 2018; Pawar et al., 2017).

Table 1-1: Geometric mean (GM) values of PFAS half-lives in humans

PFAS	Mean Half-life (years)	Gender	Volume distribution (mL/kg)[a]	Reference
PFOA	3.6	Both	170	Fu et al., 2016
	2.7	Both	N/A[b]	Li et al., 2018
	3.5	Both	N/A	Olsen et al., 2007
	1.5	Young females	170	Zhang et al., 2013
	1.2	Males and older females	170	Zhang et al., 2013
	3.3	Both	N/A	Brede et al., 2010
	2.3	Both	N/A	Bartell et al., 2010
	8.2-14.5	Both	N/A	Yeung et al., 2013
PFBS	0.07 (25.8 days)	Both	N/A	Olsen et al., 2009
PFHxS	1.7	Both	230	Fu et al., 2016
	5.3	Both	N/A	Li et al., 2018
	7.3	Both	N/A	Olsen et al., 2007
	7.1	Young females	230	Zhang et al., 2013

	25	Males and older females	230	Zhang et al., 2013
PFOS	1.9	Both	230	Fu et al., 2016
	3.4	Both	N/A	Li et al., 2018
	4.8	Both	N/A	Olsen et al., 2007
	5.8	Young females	230	Zhang et al., 2013
	18	Males and older females	230	Zhang et al., 2013
	4.7	Males	230	Wong et al., 2014
	3.7	Females (non-menstruating)	230	Wong et al., 2014
	4.0	Females (menstruating)	230	Wong et al., 2014
	4.3-4.8	Both	N/A	Yeung et al., 2013b
PFNA	1.7	Young females	170	Zhang et al., 2013
	3.2	Males and older females	170	Zhang et al., 2013
PFDA	4	Young females	170	Zhang et al., 2013
	7.1	Males and older females	170	Zhang et al., 2013
PFUnDA	4	Young females	170	Zhang et al., 2013
	7.4	Males and older females	170	Zhang et al., 2013

[a]The volume distribution is defined as the total amount of a substance in the body divided by its concentration in the serum. The half-lives are often calculated based on the volume distribution (Fu et al., 2016; Zhang et al., 2013).

[b]Not available

Recent studies highlight the use of PFAS in various consumer products that come in prolonged contact with human skin. This includes anything from cosmetics to water repellent clothing (Glüge et al., 2020a; Greenpeace, 2016; Schultes et al., 2018; van der Veen et al., 2020; Whitehead et al., 2021). However, the extent of dermal absorption upon skin contact with these consumer products and its significance as a pathway of human exposure to PFAS is currently unknown. The limited understanding of the dermal exposure route may constitute a serious knowledge gap, especially in light of the use of PFAS at relatively high concentrations in consumer products that come in contact with human skin for prolonged periods.

1.2. The significance of different pathways of human exposure to PFAS

Different studies on the various pathways of external human exposure to PFAS have been conducted in different regions of the world (Haug et al., 2011; Kim et al., 2019; Trudel et al., 2008). Figure 1-1 summarises the diverse pathways of human exposure to PFAS.

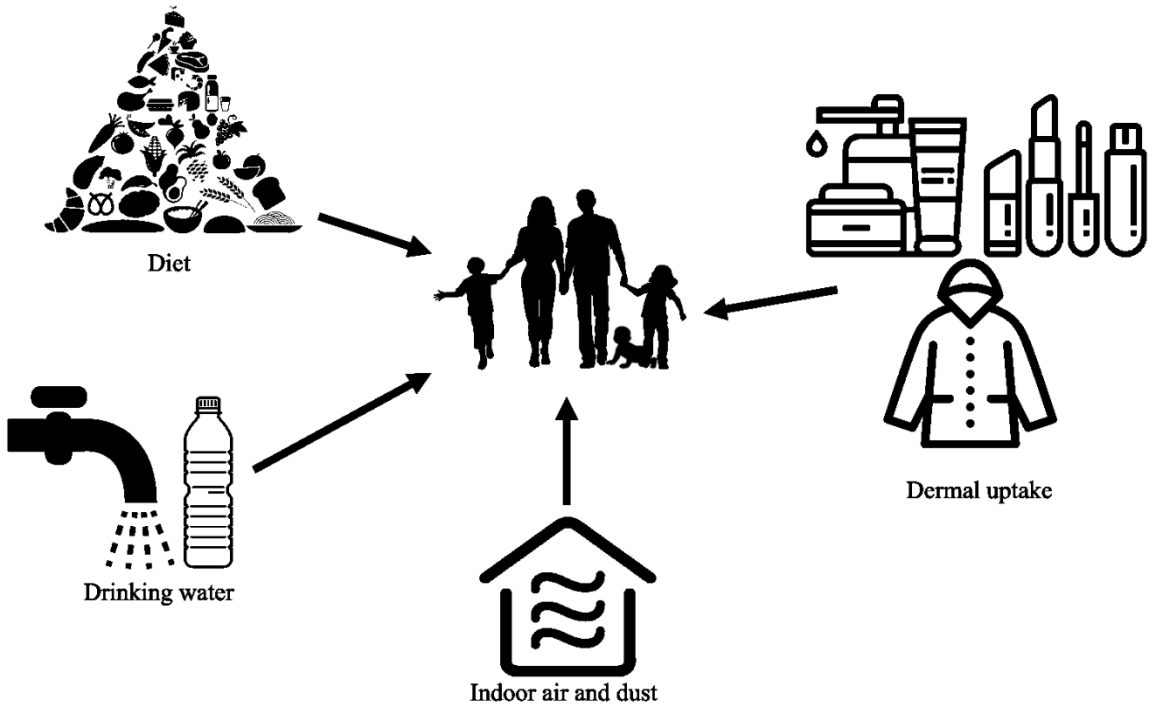


Figure 1-1: The various pathways for external human exposure to PFAS.

A recent study on PFAS concentrations in human milk from Ireland used a first-order pharmacokinetic (PK) model to examine the relationship between concentrations in human milk and predicted exposure intakes via different pathways. Median non-dietary intakes via inhalation of indoor air, dust ingestion, and drinking water, accounted for about 1.5 % of the median total exposure to PFOS and ~6 % of that for PFOA. This suggests that in Ireland at least, diet is the main exposure route for PFOS and PFOA, although the authors noted that dermal absorption (not studied directly) could also be an important contributor to the observed human body burdens of PFAS (Abdallah et al., 2020).

Similarly, a study on Norwegian women and infants focused on different exposure pathways of PFOS and PFOA in humans and related them to concentrations in serum (Haug et al., 2011). The study used a first-order PK model and three different exposure scenarios, with varying dust ingestion rates as well as biotransformation factors of precursor compounds. Diet was found to be the main source of exposure accounting for 67 – 84% of the median total intake of PFOA and 88 – 99% of PFOS intake in women. The only biotransformations considered were FOSAs/FOSEs to PFOS and FTOHs to PFOA; otherwise only direct exposure to PFOA and PFOS was considered. Drinking water represented 4.6-22% of PFOA and 0.13- 3.3% of PFOS exposure. For participants in the highest dust ingestion scenario (200 mg/day), estimated indoor air inhalation and dust ingestion accounted for more than 40% of the PFOA and 61% of PFOS intake. However, for most participants the greatest exposure was from food consumption with indoor air and dust contributing as little as 1.2% - 1.7% of overall exposure for PFOA and 0.7% - 0.1% for PFOS respectively. When comparing the results of the PK model and measured concentrations in serum, the best agreement was seen for scenario 1, which suggested diet to be the predominant contributor to total exposure, followed by drinking water, dust ingestion, and air inhalation. Infant exposure to PFOA and PFOS was reported to be mainly due to PFAS in breast milk, representing over 90% of overall exposure for both PFOA and PFOS. Dust ingestion was found to be the second highest contributor to PFOA and PFOS exposure in infants, followed by air inhalation (Haug et al., 2011). This study did not take dermal absorption into account, based on the low skin absorption of ammonium perfluorooctanoate, (APOF) reported by Fasano et al (Fasano et al., 2005; Haug et al., 2011). Tables 1-2 and 1-3 summarise the average values of various exposure routes found by different studies and figure 1-2 compares different exposure routes for infants and adults. A similar figure based on dietary exposure from USA has been presented by Ghassabian et al., 2022 (based on data from (Wu and Kannan, 2019))

As part of another study of human exposure to consumer chemicals (A-TEAM), the daily intakes of PFAAs and precursor compounds, were evaluated for a cohort of 61 adults in Norway (Poothong et al., 2020). The aim was to characterise exposure to PFAS from dermal contact (based on hand wipe samples), diet, house dust, and indoor air as well as the relative contributions from different exposure pathways to concentrations in human serum. Dermal absorption was estimated by assuming that the total mass of PFAS available for dermal uptake was that on hands as identified via hand wipes and was constant over an exposure duration of 24 h. To avoid overestimation, this study only included dermal absorption from the hand wipe samples. Hand-to-mouth contact based on hand wipe samples was not included as dust ingestion was considered to include dust adhered to hands. The absorption factor of PFAS was adopted from a study which found that 48% of PFOA applied to the human epidermis had penetrated it (Franko et al., 2012). Poothong et al. (2020) concluded that: 91% of the total estimated intake originated from diet, ingestion of house dust and inhalation of indoor air represented 3% and 2% of the total PFAAs respectively, while dermal absorption represented 0.3% of the total PFAS intake. On an individual PFAS basis, diet was the main source of exposure of PFOA, contributing to 92% of total exposure respectively followed by indoor air inhalation (4%), dust ingestion (3%), and dermal absorption (1%). Similarly, for PFOS, diet contributed to 95% of the total intake, followed by indoor air inhalation (3%), while dermal absorption and dust ingestion each contributed <1% of total exposure. The authors note a few limitations to their study, including the relatively small study group. Additionally, lack of knowledge on absorption and biotransformation rates of PFAS increases uncertainty. Finally, only dermal exposure through hands was considered. Depending on the source material e.g. clothing or cosmetics, dermal uptake could occur from a much larger area (Poothong et al., 2020).

A study by Kim et al. (2019) assessed individual-based exposure to PFAS via various exposure pathways. In this study, serum from 50 individuals was analysed along with one day composite food, drinking water, dust, and hand-wipe samples following both indoor and outdoor activity. Interestingly, a positive correlation was found between PFOA concentrations in serum and dust, indicating that dust was potentially a significant contributor to body burdens of PFAS in humans. For food and drinking water, the only PFAS that showed positive correlation to serum concentrations was PFUnDA. The outdoor hand-wipe samples revealed significant correlation with concentrations in serum for PFOA and PFUnDA as well as for total PFAS. However, the indoor hand-wipe samples revealed no correlation with concentrations in serum. The authors suggest that the uneven pattern of correlations between serum and the different external exposure metrics for the various target PFAS is due to the fact that only a single hand-wipe sample was collected for each individual, representing only one hour of exposure whereas serum samples reflect long-term exposure (Kim et al., 2019). The authors also estimated the contribution of each exposure route to total PFOA and PFOS exposure on an individual basis. Only PFOA and PFOS were included as they were representative of PFAS with high detection frequencies in the samples analysed. For both PFOA and PFOS, food ingestion was the biggest contributor to the total body burden at 96% and 94% respectively. Indoor hand-to-mouth activity came second contributing to 2.4% of PFOA and 3.8% of PFOS intake. For PFOS intake, dust contributed 1% to the total intake, drinking water 1.4%, and outdoor hand-to-mouth activity 0.2%. This study did not consider dermal uptake as a possible exposure route (Kim et al., 2019).

A Scenario-Based Risk Assessment of exposure of North Americans showed similar results when investigating direct consumer exposure to PFOA and PFOS. The study found that under a high exposure scenario, food and water contributed to around 80% of adult PFOS exposure followed by dust ingestion (ca. 15%) and hand-to-mouth contact with mill treated

carpets (ca. 5%). Similarly, around 73% of adult exposure to PFOA under the high exposure scenario was from diet, with most such exposure originating from food packaging. Under the same scenario, inhalation accounted for 15% of adult PFOA exposure, followed by dust ingestion (10%) and hand-to-mouth exposure (2%). For infants however, 45% of PFOS exposure was due to diet, followed by hand-to-mouth exposure (40%), and dust ingestion (15%). Infant PFOA exposure was mainly found to be due to hand-to-mouth exposure (40%) followed by diet (35%), and dust ingestion (20%) (Trudel et al., 2008).

Table 1-2: Summary of the median contributions (expressed as percentage of total exposure via all pathways considered[a]) of various exposure pathways to overall adult human exposure to PFOS and PFOA

PFAS	Diet	Drinking water	Indoor air and/or dust	Hand-to-mouth contact	Dermal exposure	Reference
PFOA[b]	84	11	5.3	NM[c]	NM	Haug et al., 2011
PFOS[b]	99	0.7	0.5	NM	NM	
PFOA	92	NM	7	NM	<1[f]	Poothong et al., 2020
PFOS	95		3		<1	
PFOA	96	0.9	NM	2.6	NM	Kim et al., 2019
PFOS	94	1.4	1	4	NM	
PFOA[d]		73[e]	25	2	NM	Trudel et al., 2008
PFOS[d]		80[e]	15	5	NM	

[a]Numbers may not add to 100% due to rounding

[b]The values shown are from exposure scenario 1 (estimated dust ingestion 50 mg/day and biotransformation of FOSA/FOSEs to PFOA: 1% and FTOH to PFOA: 0.02%).

[c]Not measured.

[d]Only direct exposure to PFOA and PFOS considered, high exposure scenarios.

[e]Diet and drinking water combined.

[f] Based on hand wipe samples and assuming 24 h constant exposure and an absorption factor of 48%.

Table 1-3: Summary of the median contributions (expressed as percentage of total exposure via all pathways considered[a]) of various exposure pathways to overall infant human exposure to PFOS and PFOA

PFAS	Breast milk	Dust ingestion	Inhalation	Hand-to-mouth	Reference
PFOS	99	1.2	0.004		Haug et al., 2011
PFOA	98	1.4	0.02		
PFOS	45	15		40	Trudel et al., 2008
PFOA	35	20	2	40	

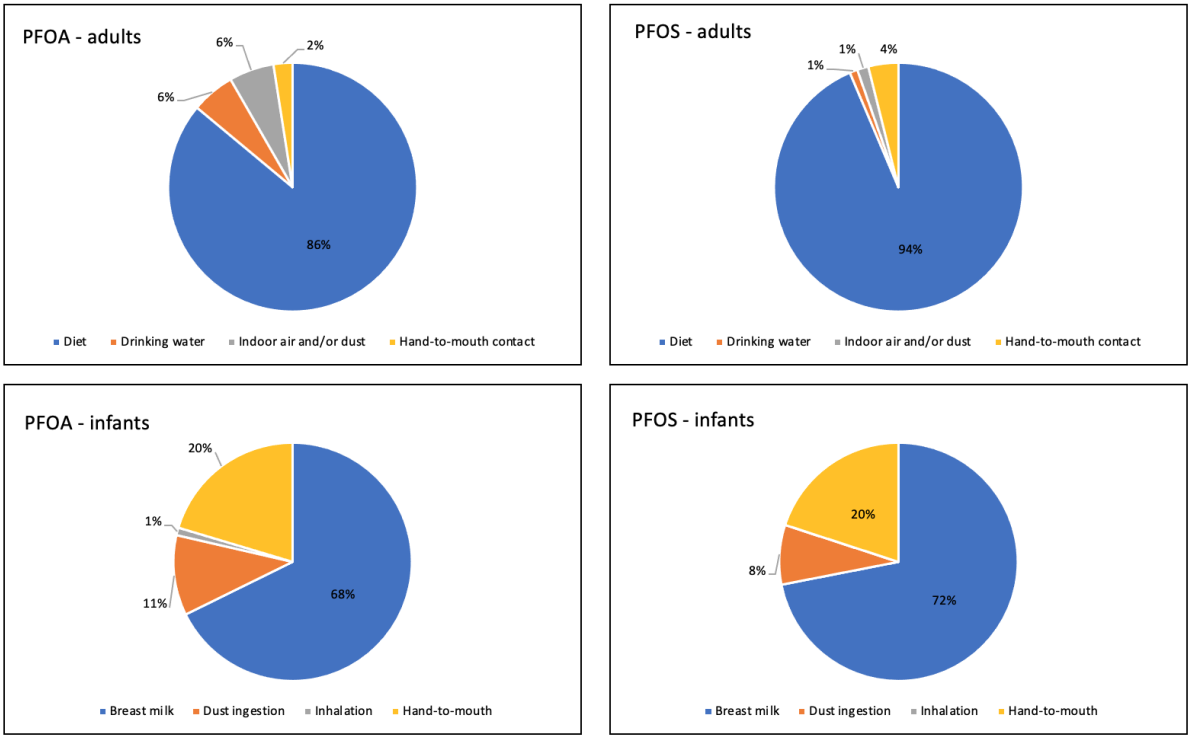


Figure 1-2: Average relative percent contribution of different routes to overall daily human exposure to PFAS in adults and infants. A similar figure based on dietary exposure from USA was presented by Ghassabian et al., 2022 (based on data from (Wu and Kannan, 2019)).

Building upon the study of Trudel et al., Vestergren et al. (2008) performed a Scenario-Based Risk Assessment to quantify consumer exposure to precursor compounds to assess their contribution to total daily doses of PFOS and PFOA. To account for the metabolic transformation of precursors to PFOA and PFOS, the load of precursors absorbed into the human body was multiplied by a biotransformation factor. Due to the large variability of metabolic transformation between different studies, they used a modelling approach to generate biotransformation factors relevant to 3 different exposure scenarios (low, intermediate, and

high) for each of the studied precursor groups. The possible routes for dermal exposure that this study included were: contact with treated clothing, deposition of spray droplets while using impregnation sprays, as well as skin contact with upholstery, and house dust deposited on skin. Looking at PFOS exposure for adults and teens, the study concluded that in both the low-exposure and intermediate scenarios, direct exposure to PFOS via diet was the main route of exposure, accounting for 99% and 94-98% respectively. For the intermediate group, precursor-based exposure was a minor pathway (2.3-5.4%). However, under the high-exposure scenario, precursor-based exposure was a substantial contributor to overall exposure to PFOS accounting for 60-80% of the total exposure. Direct exposure to PFOS accounted for only 18-46% under the high-exposure scenario. Similarly, direct PFOA exposure accounted for 92-100% of the total exposure of adults and teens in the low- and intermediate exposure scenarios. For the intermediate exposure scenario, precursor-based exposure was a minor pathway (4.3-7.7%). In contrast, in the high-exposure scenario, precursor-based exposure was more significant, accounting for 48-55% of the total PFOA exposure in adults and teens. Direct PFOA exposure was slightly less significant (36-45%) for adults and teens in the high-exposure group. Similar patterns were seen for children for both PFOS and PFOA exposures. The main routes of exposure in the low- and intermediate scenarios were direct exposure to PFOS/PFOA, with precursor-based exposures more significant for the high-exposure scenario (Vestergren et al., 2008b).

A report by Knepper et al. researched durable water repellent (DWR) clothing as a possible source of exposure to PFAS. One of the exposure pathways considered was dermal uptake via consumers using commercial impregnation sprays containing PFAS to treat DWR clothing. Other pathways of exposure considered were: inhalation of said impregnation sprays, dermal uptake from wearing treated clothes, hand-to-mouth transfer from treated clothes, inhalation of indoor air, and ingestion of indoor dust. It was concluded that overall exposure to

PFAS via DWR was mainly attributable to inhalation of indoor air (for both indirect and direct exposure), followed by dust ingestion. Dermal uptake was found to be minimal, but this is likely attributed to the low absorption rate assumed (0.001% of the chemical absorbed per hour). In the absence of experimental data, the uptake of PFCAs and FTOHs was derived from a study by Fasano et al., (2005) that assessed *in vitro* human dermal absorption of ammonium perfluorooctanoate, which could be an underestimation. It was concluded that the overall exposure from DWR outdoor jackets contribute to a small part of the overall exposure to PFCAs compared to dietary intake for the general population. Still, taking into consideration the substantial variability in exposure to consumer products, this study concluded that DWR jackets could represent a source of elevated exposure to some population groups (Knepper et al., 2014).

1.3. The skin barrier and dermal permeation

1.3.1. The skin barrier

Skin is the body's largest organ, with the skin of a human adult having a surface area of approximately 2 m^2 and weighing around 5 kg. This multi-layered organ plays an essential role in protecting the body from the surrounding environment. While it is an effective barrier for exogenous molecules, the degree of protection is not complete (Godin and Touitou, 2007). Therefore, elucidating the potential significance of dermal uptake as a pathway of human exposure to chemical contaminants is an important area of research. Human skin is composed of 3 main layers: epidermis layer, dermis, and hypodermis. The outermost layer, the epidermis is a non-vascular layer that serves as a protective obstacle to penetration of chemicals to the underlying vascular dermis. Healthy human epidermis is made up of 4 layers: stratum corneum (SC), stratum granulosum, stratum spinosum, and stratum basale. It is with the outermost layer - the SC - where the barrier properties of the skin mainly lie. This highly hydrophobic layer is composed of differentiated non-nucleated cells, corneocytes, which are filled with keratins and embedded in the lipid domain.

1.3.2. Dermal bioavailability

Dermal bioavailability is defined as the fraction of a chemical that is able to penetrate the skin and reach the bloodstream (Ertl and Butte, 2012; Pawar et al., 2017). The main pathway of transdermal permeation of chemicals through the SC is via passive diffusion. This is greatly affected by the compound's physicochemical properties including: molecular weight, presence and number of hydrogen bond donors/acceptors, water solubility, and octanol-water partitioning coefficient. The general rules that a compound should follow are known as Lipinski's rule of 5 and chemicals should fulfil at least three of the four criteria to be absorbed effectively by the body (see table 1-4). However, it is important to note that these rules were developed for evaluation of drug delivery; thus although a chemical may not obey completely these rules, some fraction may still be absorbed by the skin (Abdallah et al., 2015a; Knudsen et al., 2016; Lipinski et al., 2001). Other factors that can affect percutaneous absorption of chemicals are e.g. exposure conditions (dose, duration, surface area, exposure frequency), conditions of the skin surface (hydration, temperature, pH) and application sites (regional variation in penetration) (Law et al., 2020).

Table 1-4: Physicochemical properties of various PFAS compared to the Lipinski's rule of 5 criteria. The other two criteria are H bond donors (≤ 5) and H bond acceptors (≤ 10). Also included are the compounds water solubility.

	Average Mass (Da)	**Log(Kow) Experimental[a]**	**Log(Kow) Predicted[b]**	**Water solubility (mg/L)[d]**
Lipinski's rule of 5	**< 500 Da**	**≤ 5**	**≤ 5**	**N/A**
PFBA	214.04	-[e]	3.43	765.70
PFPeA	264.05	3.26	4.06	61.11
PFHxA	314.05	4.15	4.67	4.70
PFHpA	364.06	5.02	5.3	0.35
PFOA	414.07	5.91	5.92	0.03
PFNA	464.08	6.79	6.50	0.002
PFDA	514.08	-[e]	7.15	-[e]
PFUnDA	564.09	-[e]	7.77	-[e]
PFDoDA	614.10	-[e]	8.25	-[e]
PFTrDA	664.10	-[e]	8.9[c]	-[e]
PFTeDA	714.11	-[e]	3.90	-[e]
PFBS	300.10	2.81	4.36[c]	107
PFPeS	350.11	-[e]	5.17	8.07
PFHxS	400.12	4.57	6.14	0.60
PFHpS	450.12	5.45	6.43	0.04
PFOS	500.13	-[e]	6.14	-[e]
PFNS	550.14	-[e]	7.66	-[e]
PFDS	600.15	-[e]	3.43	-[e]

[a] Values taken from *Chemspider*, 2021. Note that it is stated that these values are "old".

[b] Data predicted in COSMOtherm(Wang et al., 2011).

[c] Data predicted by ACD/Labs(*Chemspider*, 2023).

[d] Data predicted in EpiSuite (not available from ACD/Labs) (*Chemspider*, 2023).

[e] Data not available.

After a chemical passes through the SC, it may be metabolized *in situ* or move by diffusion through the viable epidermis and into the vascular dermis layer, where it enters the

systemic circulation (Knudsen et al., 2016). Transdermal permeation may also occur via sweat glands and hair follicles directly to the dermis (Abdallah et al., 2015a). Chemicals retained in the epidermis may not reach the circulation but are removed by the natural desquamation process (Knudsen et al., 2016).

1.3.3. Dermal bioaccessibility

The skin's surface is covered with a mixture of aqueous sweat and oil-based sebum. The mixture of the two is called skin surface film liquid (SSFL) (Buckley and Lewis, 1960; Nicolaides, 1974). For a chemical present in a matrix such as dust or a consumer product/material to become dermally bioavailable (i.e. transported through the skin and reach the bloodstream), it has first to be released into surface skin fluids, as it is from such skin fluids that dermal uptake occurs. The total mass of a given chemical that is released from the source matrix into the body fluid (referred to as bioaccessible) will likely not all be absorbed through the skin and reach the circulation (become *bioavailable*). Therefore, bioaccessibility data in combination with dermal absorption data is needed to establish the ability of a chemical present in a matrix to be released from that matrix and become available for absorption by the skin (Pawar et al., 2017).

1.3.4. Dermal metabolism

Along with the SC, increasing evidence suggests that xenobiotic metabolizing enzymes, in addition to transport proteins, play an important role in the transdermal penetration process. Human epidermal keratinocytes have been found to express various transport associated enzymes as well as detoxifying metabolic enzymes (Baron et al., 2001). CYP450 enzymes can metabolise a wide variety of small molecular weight exogenous as well as endogenous compounds. Although CYP450 enzymes have been identified in both human keratinocytes and some 3D-Human Skin Equivalent (3D-HSE) models, the levels detected in skin are lower than those detected in liver cells (Oesch et al., 2014). However, relative levels of the xenobiotic metabolizing enzyme carboxylesterase 1 (CES 1) in whole skin and liver were 0.62 with no significant difference ($p = 0.21$) (van Eijl et al., 2012). Furthermore, Abdallah et al. (2019)

performed a study on the *in vitro* dermal metabolism of 2-ethylhexyl-2,3,4,5-tetrabromobenzoate (EH-TBB). The study revealed that human skin cells metabolised EH-TBB mainly to tetrabromobenzoic acid (TBBA) and concluded that the dermal metabolism of EH-TBB was catalysed by carboxylesterases rather than CYP450 (Abdallah et al., 2019). A study by Liu et al. demonstrated strong binding affinity of PFAS towards both CES 1 and CES 2 *in vitro.* PFAS tested were: PFHxA, PFOA, perfluorodecanoic acid (PFDA), perfluorododecanoic acid (PFDoA), perfluorotetradecanoic acid (PFTeDA), perfluorooctadecanoic acid (PFOcDA), PFOS, perfluorohexyl iodide (PFHxI), perfluorooctyl iodide (PFOI), the fluorotelomer alcohols 4:2 FTOH, 5:1 FTOH, 6:2 FTOH, 7:1 FTOH, and 6:2 fluorotelomer sulfonic acid (6:2 FTSA). The compounds with the greatest binding affinity which caused greater inhibition ability were longer chain PFAS: PFDoDA, PFTeDA, and PFTOcDA. The preliminary results suggested a relationship between carbon chain lengths and inhibition ability, with longer chain lengths showing greater CES 1 inhibition (Liu et al., 2020). The ability of these longer chain PFAS to inhibit the liver CES1 enzymes suggests a lesser risk of dermal absorption of those compounds and their metabolites. However, this must be interpreted with some caution as the inhibition of dermal CES1 at realistic environmentally relevant concentrations was not investigated. Moreover, the resulting metabolites from these chemicals, be it via the partially inhibited CES1 enzymes or other metabolic pathways (e.g., CYP450), have not been identified or risk assessed. Thus, it is still important to experimentally investigate the bioavailability and biotransformation of these long chain PFAS.

1.4. Methods for evaluation of human dermal uptake of chemical contaminants

1.4.1. *In vivo* methods

Dermal absorption studies are currently hindered by various difficulties. For example, several ethical and technical limitations are related to studies involving human volunteers. Although such studies would be the most reliable when evaluating human dermal absorption, their use

has been, and likely will continue to be limited. *In vivo* studies were used to study the dermal absorption of PCBs (polychlorinated biphenyls) through various pathways. Three different studies were conducted using either rhesus monkeys and/or guinea pigs, in association with *in vitro exposure* using human cadaver skin. These studies provided important early insights into the dermal absorption, systemic elimination, and dermal wash efficiency of lipophilic environmental contaminants (Wester et al., 1993, 1990, 1983). However, there are increasing ethical restrictions on the use of animal studies in toxicological studies. Additional uncertainties exist with data derived from animal studies when applied to humans, due to interspecies variation in parameters such as: skin barrier function, intercellular subcutaneous lipids, hair follicles, etc (Abdallah et al., 2015b). Notwithstanding this, there are benefits to the use of *in vivo* animal models for dermal absorption studies as they represent a complete metabolic and physiological system (Abdallah et al., 2015a).

1.4.2. *In vitro* and *ex vivo* methods

With increasing restrictions on *in vivo* animal models due to factors such as ethical concerns, the use of such models is in decline. This has led to increased development and validation of various *in vitro* methods, which then aid the development of predictive pharmacokinetic models (Abdallah et al., 2015a). An example of an *in vitro* experimental configuration using Franz cells is illustrated in Figure 1-3. Guidance documents for *in vitro* skin absorption studies are currently available from various institutions (OECD, 2004a, 2004b; U.S. EPA, 2004; WHO, 2006).

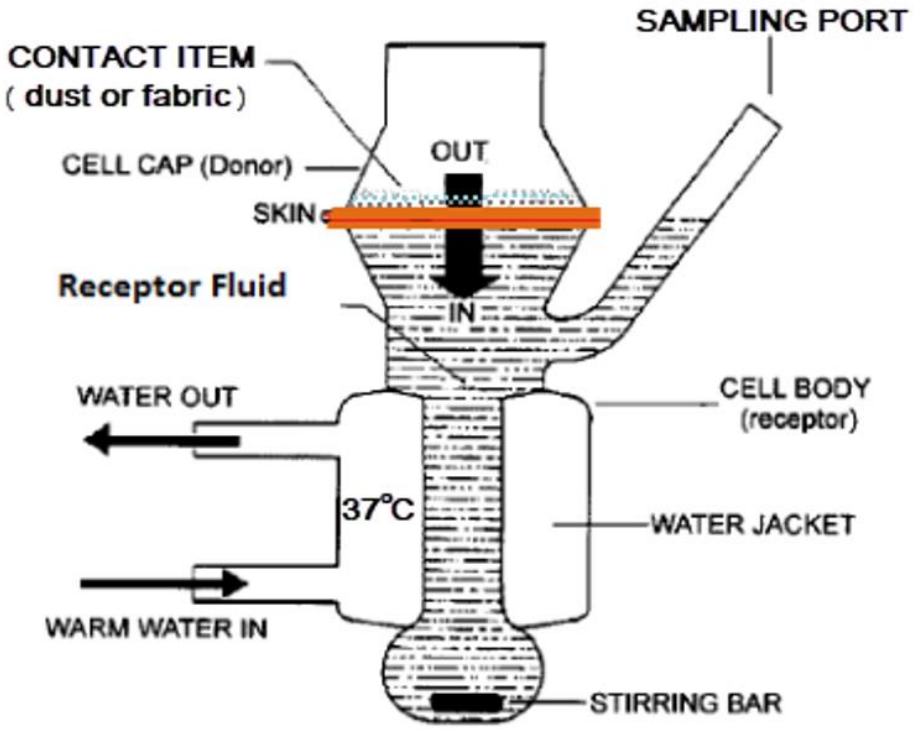


Figure 1-3: In vitro dermal exposure experimental configuration using a Franz cell. The skin samples act as a barrier between the two compartments, the upper donor compartment and the lower receptor compartment. The receptor fluid should be kept at a temperature similar to human body temperature. Figure taken from Abdallah and Harrad, 2018.

Various skin models have been applied for *in vitro* testing, using either excised human skin from surgery or cadavers (*ex vivo*) or animal (e.g. pig or rat) skin as well as reconstructed human skin models (Abdallah et al., 2015a; Sartorelli et al., 2000; van de Sandt et al., 2004). Several factors in the experimental configuration can affect the results of *in vitro* experiments. Different types of diffusion cells have been used in various studies. Both static and flow-through cells showed comparable results for dermal absorption rates of caffeine, benzoic acid, and testosterone. The OECD recommends the use of these three chemicals to establish the reliability and performance of test systems as they cover a wide range of hydrophobicities and have been thoroughly studied (OECD, 2004a, OECD, 2004b). The type of receptor fluid (intended to mimic the blood stream into which dermally- absorbed chemicals pass) used in studies, can also affect the outcome based on the physicochemical properties of the tested

chemicals. Specifically, the receptor fluid could become a rate-limiting factor in dermal permeation studies if the test compound is poorly soluble in the chosen receptor medium. According to the OECD guidelines, the solubility of the test chemical in the receptor fluid should not be the rate limiting step in the *in vitro* diffusion process (OECD, 2004a, 2004b). This is of particular importance for hydrophobic compounds, where use of simple saline solutions as the sole component of the receptor fluid, can prove problematic as it is likely to underestimate the dermal absorption rate of poorly water-soluble compounds (Abdallah et al., 2015a; Jakasa and Kezic, 2008; OECD, 2011). The use of bovine serum albumin (BSA, up to 5%) has been suggested to improve the solubility of hydrophobic compounds in the receptor fluid (OECD, 2011; Sartorelli et al., 2000). Overall, it is always preferable that the receptor fluid mimics as accurately as possible, the actual biological conditions in terms of composition and temperature (Abdallah et al., 2015a).

In vitro pig skin models show the most biological similarities with human skin models. The thickness of the skin layers, hair follicles, and blood vessel density, are all similarities shared by pig and human skin, as well as content of SC ceramides, elastin, and dermal collagen. As a waste product from meat production, pig skin can be easily acquired. Pig ear skin shows the closest structure to human skin layers and the permeability of pig ear skin has been shown to be comparable to that of human skin (Moniz et al., 2020).

For *ex vivo* dermal permeation experiments, freshly excised human skin (typically acquired from volunteers undergoing cosmetic surgery) is favoured over human cadaver skin although this is not always available (Van Gele et al., 2011). The skin permeability of fresh skin to tritiated water was not affected after storage for up to 3 days at 10°C and for over a year for skin stored at -20°C. However, storage at very low temperatures i.e. -80°C has been shown to enhance the permeability of skin (OECD, 2004b). The types of *ex vivo* skin samples used for *in vitro* testing can vary from (1) full-thickness skin, composed of the SC, viable epidermis,

and dermis, (2) split-thickness skin where the lower dermis has been discarded, and (3) epidermal membranes, which includes the viable epidermis and SC (Jakasa and Kezic, 2008). The thickness of skin samples used for dermal uptake testing could affect the variation in absorption of the tested compounds. Thicker skin, i.e. full-thickness and split-thickness samples, can result in a higher fraction of the chemical retained within the skin while thinner skin samples could show an increased flux (OECD, 2011; Wilkinson et al., 2006). According to OECD recommendations, the impact of this can be minimised by including all or part of the compound retained in the skin in the dermal absorption value (OECD, 2011).

A different approach, the Parallelogram, has also been applied for dermal absorption studies (Knudsen et al., 2016, 2019; Van Ravenzwaay and Leibold, 2004a). In this approach, *in vivo* animal studies are combined with *ex vivo* animal, and human skin models. This allows for *in vivo* human exposure to be estimated as a function of *ex vivo* human exposure multiplied by a normalization factor based on the same dose applied to rat skin *in vivo* and *in vitro* (Figure 1-4). This approach assumes the ratio of *in vivo* to *in vitro* dermal penetration of a chemical is the same through animal (i.e. rat) and human skin. It has been used to study the dermal uptake of brominated flame retardants (BFRs), such as novel BFRs (EH-TBB and BEH-TEBP) and tetrabromobisphenol A bis(2,3-dibromopropyl) ether (TBBPA-BDBPE) (Knudsen et al., 2019, 2016).

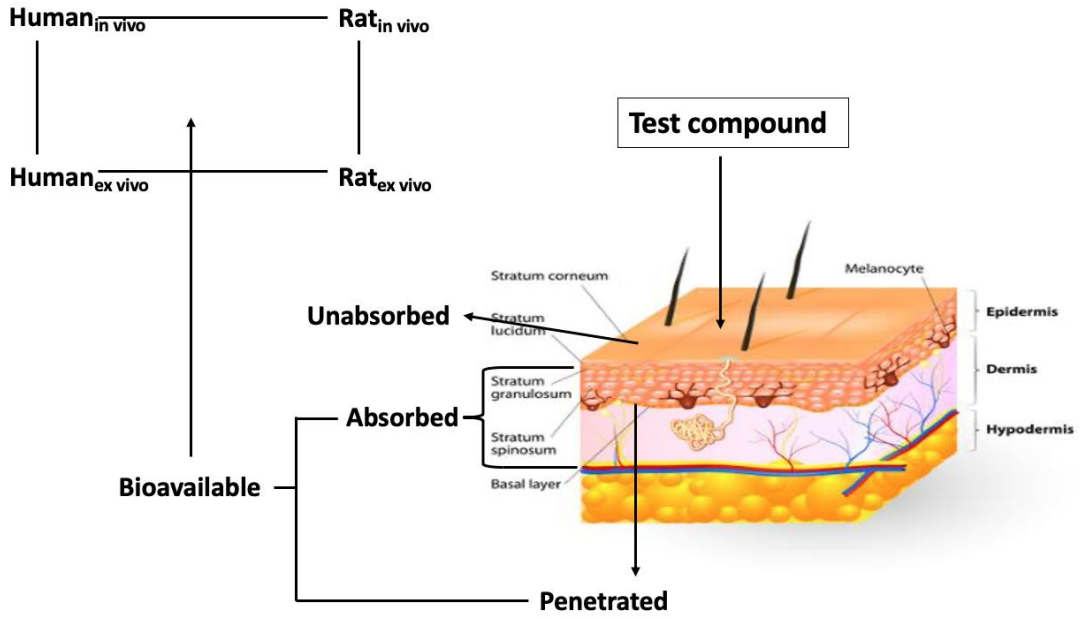


Figure 1-4: Illustration of the parallelogram approach. Figure adapted from Knudsen et al., 2019

1.4.3. 3D-Human Skin Equivalent Models

3D-Human skin equivalent (3D-HSE) models were developed to overcome the ethical issues and differences between species, in addition to increasing restrictions on the use of laboratory animals in toxicological studies (Abdallah et al., 2015b, 2015c; Ackermann et al., 2010; Schäfer-Korting et al., 2008). There are two main types of 3D-HSE models. Reconstructed human epidermis (RHE) models consist of human keratinocytes cultured on an inert polycarbonate medium. The cells are cultured at the air-liquid interphase in a serum-free culture environment. Rapidly proliferating preparative keratinocyte cultures generate epidermal cells which are seeded on inert filter substrates. They are then raised to the air-liquid interface in a humidified-air incubator and the basal cells are fed by nutrient medium through the filter substratum (Abdallah et al., 2015a). A stratified epidermis is formed after 14 days which closely resembles human skin in terms of morphology, lipid composition, and differentiation markers (Abdallah et al., 2015a; Schäfer-Korting et al., 2008). Furthermore, studies have shown that 3D-HSE models display similar activity of enzymes involved in

xenobiotic metabolism to those seen in real human skin samples (Hewitt et al., 2013; Wiegand et al., 2014).

Schafer-Korting et al. compared the permeability of three RHE models using 9 different compounds varying in physicochemical properties, including testosterone, caffeine, and benzoic acid (Schäfer-Korting et al., 2008). This was compared to the permeability of excised human epidermis and pig skin. Results showed that the 3D-HSE model proved more permeable than the human epidermis and pig skin, with the permeation coefficient (P_{app}) for one of the HSE models ranging from two– to seven-fold higher compared to P_{app} values of human epidermis sheets (HES), with the other 3D-HSE models tested showing a greater overestimation compared to HES. It is important to note that since this study was performed, available 3D-HSE models have improved according to developers, with models possessing "enhanced barrier function" now available. Notwithstanding this, the ranking of substance permeation through the human epidermis was similar to that of the HSE models as well as the pig skin, making 3D-HSE models feasible for *in vitro* dermal penetration studies (Schäfer-Korting et al., 2008). Since then, validated 3D-HSE protocols have been approved by the OECD and European Centre for Validation of Alternative Methods (ECVAM) for testing of skin irritation, phototoxicity and corrosion by xenobiotic chemicals (Abdallah et al., 2015b; OECD, 2004a, 2004b).

The second type of 3D-HSE models are full-thickness (FT) models. These models consist of an epidermis, made up of keratinocytes and fibroblasts, a basement membrane, and a dermis. FT models present morphology and tissue functionality similar to those of human skin. For the prediction of biotransformation-linked toxic endpoints, the FT skin models may be better suited than RHE models, as the biotransformation of compounds within the skin can vary between the major cell types that make up the skin (Ackermann et al., 2010).

Ackerman et al. tested the percutaneous absorption of the Phenion® FT skin model (full thickness HSE model) for four compounds, namely the OECD recommended reference compounds: caffeine, benzoic acid, and testosterone, as well as nicotine (Ackermann et al., 2010). The absorption of testosterone and caffeine was compared to the absorption of pig skin. Results showed that the FT models were more permeable than pig skin (P_{app} values for FT models were 6 – 25 fold higher than th_{ose} obtained for pig skin), while still being comparable to RHE models when compared to previous studies, showing good data reproducibility (Ackermann et al., 2010).

Methods using 3D-Human Skin Equivalent (3D-HSE) models (RHE and FT types) have been developed for the evaluation of human dermal exposure to halogenated flame retardants i.e. brominated and chlorinated organophosphate flame retardants (Abdallah et al., 2016, 2015b). Additionally, methods using 3D-HSE models (FT models) have been developed for evaluation of dermal toxicity, e.g. of PFAS (Han et al., 2020) as well as for an *in vitro* genotoxicity assay, 3D Skin Comet assay for dermal exposure (Reisinger et al., 2018).

A comparison of two commercially available 3D-HSE models and human *ex vivo* skin, found no statistically significant differences when investigating the dermal bioavailability of BFRs at two exposure levels (500 ng/cm^2 and 1000 ng/cm^2). Comparison of the permeation coefficients revealed that the P_{app} for 3D-HSE models were only 1.1-1.3 times higher than those observed for *ex vivo* skin (Abdallah et al., 2015b). Similar results were obtained when comparing the dermal permeation of chlorinated organophosphate flame retardants (PFRs) using a 3D-HSE model, with that observed using human *ex vivo* skin. The difference in the absorbed fraction of the tested chemicals was 1.2 – 5.4 % higher for 3D-HSE models compared to *ex vivo* human skin (Abdallah et al., 2016). While both studies found the 3D-HSE model showed less barrier function than *ex vivo* human skin, the differences were not statistically significant ($P > 0.05$) (Abdallah et al., 2016, 2015b).

As mentioned above, while they have not yet been employed to measure dermal uptake of PFAS, 3D-HSE models have been used to evaluate the dermal toxicity of PFCAs. This was done by repeated topical application for 6 days of two low dosages (0.25 mM and 2.5 mM) of PFPeA, PFHpA, PFHxA, and PFOA onto EpiDermFT full thickness models. This study also included *in vivo* tests, where rats were treated with PFHpA at different doses (0, 250 and 1000 mg/kg b.w.) for 6 h a day for 2 weeks. Each application site was shaved before application and covered with bandages after application. The results of the *in vitro* study revealed that 2.5 mM PFOA could induce keratinocyte membrane perturbation, however this was not found sufficient to cause cell death. Additionally, 2.5 mM PFOA-treated tissues showed decreased skin thickness compared to controls. The *in vivo* study revealed an 86% mortality in the 1000 mg/kg/day group during the treatment period with signs of ulceration and inflammatory cell infiltration at the application cites. The lower dose group (250 mg/kg/day) however, showed minimal to slight epidermal hyperplasia and parakeratosis, although minimal to slight ulceration was seen in a minority in the group (Han et al., 2020).

1.5. Dermal bioavailability and bioaccessibility of halogenated organic pollutants and their significance to overall human exposure

While little is currently known about dermal absorption of PFAS, recent studies on other halogenated organic pollutants exposure suggest dermal absorption could be a significant contributor to body burdens e.g. for chlorinated and brominated flame retardants (Abdallah et al., 2016; Abdallah and Harrad, 2018).

A study on exposure of Americans to polybrominated diphenyl ethers (PBDEs) using a PK model assumed that 3% of PBDEs in soil that adhered to skin were absorbed. The study found that dermal uptake was the second biggest contributor to the total body burden of PBDEs (following dust ingestion) (Lorber, 2008). Similarly, Trudel et al. investigated total consumer exposure to PBDEs, both in North America and Europe as well as the most important exposure pathways. They found that for North Americans, dermal uptake from dust could play a

significant role (up to 40% for those exposed at the 99th percentile level) in total human exposure to PBDEs (Trudel et al., 2011). These studies based their dermal absorption factor on reported dermal absorption of either dioxins or polychlorinated biphenyls from soil in laboratory animal models and neither study considered possible dermal absorption from contact with BFR-treated materials (Lorber, 2008; Trudel et al., 2011).

Other *in vitro* studies on BFR exposure via dermal uptake showed that their absorption varied according to the physicochemical properties of each compound. The general trends seen were a negative correlation between a compound's absorbed fraction and its log K_{OW}, while a positive corelation was observed between log K_{OW} and the fraction retained within the skin tissue (Abdallah and Harrad, 2018; Frederiksen et al., 2016). Moreover, Abdallah and Harrad (2018) found that the total dermal uptake of BFRs was not only caused by contact with dust but also, and to a greater extent, via contact with treated fabrics in consumer products, such as sofas. This study used exposure parameters from the USEPA exposure factors handbook and typical apparel in summer and winter to estimate the exposure to dust and fabric. They assumed contact with indoor dust to be for 6 h/day for adults and 9h/day for toddlers (assuming toddlers have greater proximity to the floor and lower hygiene standards) and contact with sofa fabric for 4 h/day for adults and 2 h/day for toddlers (assuming toddlers display greater physical activity than adults – i.e. less sedentary). In fact, they considered the values assigned to dermal uptake from dust in previous studies to be overestimates, especially for adults. This then led to an inflated estimation of the relative contribution of the dermal pathway via contact with dust to the overall daily exposure to BFRs. Conversely, in some cases the total dermal uptake of BFRs was an underestimation due to overlooking dermal uptake via contact with consumer products (e.g. fabrics), according to their findings. For example, based on a conservative estimate, they found the dermal uptake of penta-BDE for an adult via contact with a flame-retarded sofa to be 8.1 ng/kg bw/day during summer which exceeds the estimated average total

exposure via all pathways of American adults by Lorber (5.4 ng/kg bw/day) and Trudel et al. (3.1 ng/kg bw/day) (Abdallah and Harrad, 2018; Lorber, 2008; Trudel et al., 2011). However, the contribution of dermal uptake of toddlers via contact with a sofa was less significant compared to the adult group. Abdallah and Harrad found the dermal uptake for toddlers (1-5 years) to be 6.1 ng/kg bw/day, which was lower than the total exposure of toddlers (1-5 years) reported by Lorber (34.5 ng/kg bw/day) and Trudel et al (10 ng/kg bw/day). These latter two studies included: BDE-28, BDE-47, BDE-99, BDE-100, BDE-153, BDE-154, BDE-183, and BDE-209; while the study by Abdallah and Harrad included the same compounds excluding BDE-183, and BDE-209 which could explain the difference in results to some extent (Abdallah and Harrad, 2018; Lorber, 2008; Trudel et al., 2011).

Other studies have supported the potential importance of the dermal pathway (Liu et al., 2017; Watkins et al., 2011). A study of exposure to PBDEs in office environments revealed positive correlations between PBDEs in indoor dust, hand wipes and serum samples. This could either be explained by dermal absorption and/or ingestion due to hand-to-mouth contact (Watkins et al., 2011). Similarly, an estimation of human exposure to halogenated flame retardants using skin wipes, suggested that dermal absorption could be a significant route of human exposure (Liu et al., 2017).

Assessment of the dermal bioavailability of BFRs found a negative correlation between dermal penetration and the octanol:water partition coefficient (expressed as Log K_{OW}) (Abdallah et al., 2015b). Conversely, a positive correlation was found between Log K_{OW} and the fraction of BFRs remaining within the skin tissue after 24 h exposure. This is likely caused by the time needed for more hydrophobic and higher molecular weight BFRs to reach from the stratum corneum through the aqueous-based epidermis implying higher resistance to diffusion of highly hydrophobic compounds (Abdallah and Harrad, 2018).

Furthermore, studies on different dosing vehicles used when determining dermal penetration of chemicals, found small differences in percutaneous penetration when exposing skin to chemicals dissolved in acetone, 30% acetone in water, and 20% Tween 80 in water. Although the differences were not statistically significant, more hydrophilic compounds showed higher penetration abilities in 20% Tween 80 (non-ionic surfactant (emulsifier)) in water. This could possibly be relevant to human exposure as several polar and non-polar compounds are naturally present in human skin surface film liquid (sweat/sebum mixture) (Abdallah et al., 2015b; Abdallah et al., 2016).

Pawar et al (2017) assessed the bioaccessibility of FRs. The study found that compound-specific physicochemical properties (mainly log K_{OW} and water solubility) as well as the composition of the synthetic sweat/sebum mixture used were the factors that most greatly influenced the bioaccessibility of the target compounds. The compounds examined were: α-, β-, and γ-hexabromocyclododecane (HBCDD), tetrabromobisphenol A (TBBPA), tris-2-chloroethyl phosphate (TCEP), tris (1-chloro-2-propyl) phosphate (TCIPP), and tris- 1,3-dichloropropyl phosphate (TDCIPP). Additionally, this study established that the presence of cosmetics such as moisturising cream, sunscreen lotion, shower gel, and body spray significantly impacted the bioaccessibility of all but one (TBBPA) of the target FRs. The presence of all tested cosmetics decreased the bioaccessibility of HBCDDs while an increased bioaccessibility of TCEP, TCIPP, and TDCIPP was observed when combined with shower gel and sunscreen (Pawar et al., 2017). A different study (Abdallah and Harrad, 2018) found that a further factor affecting dermal absorption of BFRs, was the type of matrix with which dermal contact occurs (dust or fabrics). The study revealed greater dermally absorbed mass after 24 h contact with fabrics in comparison to contact with indoor dust. However, when expressed as a percentage of the applied dose in the contact material, the fraction absorbed from fabrics was significantly lower than from indoor dust. Thus, they concluded that when expressed as a

percentage of the applied dose, dermal absorption was influenced by both the applied dose and the contact matrix. Additionally, the degree of skin hydration during exposure also affected the dermal uptake of BFRs. More "sweaty" skin led to higher absorption of PBDEs and HBCDD, likely caused by the lipophilic sebum components in the skin fluid mixture (Abdallah and Harrad, 2018).

1.6. The potential of dermal uptake as a pathway of human exposure to PFAS

Few studies have explored the possible dermal penetration of PFAS. An *in vitro* study of the permeability of APOF through human skin used human epidermal membranes and degassed physiological saline (0.9% NaCl) as receptor fluid. Analysis of the receptor fluid revealed that only 0.048 ± 0.01% of the applied APOF had penetrated the skin after a 48 hour exposure period (Fasano et al., 2005). Importantly, the use of saline solution as receptor fluid does not accurately mimic actual biological conditions. This could reduce diffusion of chemicals to the receptor fluid leading to an underestimation of dermal absorption (Abdallah et al., 2015a; Jakasa and Kezic, 2008; OECD, 2011). Furthermore, this study only analysed the receptor fluid samples, and not the skin samples themselves, skin washes, or donor/receptor compartment washes.

A study by Franko et al (2012) used both *ex vivo* human full-thickness and epidermis skin samples exposed to a single dose of 50 µL solution 0.1 mg/µL PFOA in acetone solution for 24 h. HEPES-buffered Hanks balanced salt solution (HBSS) consisting of 5.96 g HEPES, 0.32 g $NaHCO_3$, and 0.05 g gentamicin sulphate added to 1 L of Hanks balanced salt solution (pH adjusted to 7.4) was used as a receptor fluid. The skin patches were washed with solvent prior to analysis of the receptor fluid and skin samples. Analysis of the receptor fluid samples revealed that 24% of the applied PFOA had penetrated human skin epidermis samples after 24 hours of exposure. When including PFOA found within the skin samples (skin depot), the total absorbable fraction of PFOA was found to be 48% and 69% for epidermis and full-thickness

skin samples respectively (Franko et al., 2012). Varying the pH of the PFOA dosing solutions revealed a great difference in the median permeability coefficient of the free acid ($5.5x10^{-2}$ cm/h) and the charged species (4.4×10^{-5} cm/h) (Franko et al., 2012). Thus, the effect of PFOA ionisation state on dermal penetration could explain the different results of these two studies (Fasano et al., 2005; Franko et al., 2012). A more recent *in vivo* study exposed a single male volunteer to exposed to $^{13}C_4$-PFOA (110 μg) mixed into 30 g of commercial sunscreen. The sunscreen was then applied to the volunteer's whole skin who didn't shower until 48 h after application. Serum samples were then taken periodically over 115 days. The plasma concentration peaked at 132 ng/L, 22 days after application suggesting that dermal exposure can be long-lasting and indeed contribute to total body burdens of PFAS (Abraham and Monien, 2022).

An *in vivo* study using male Sprague-Dawley rats exposed the animals to 15 PFAS (C_4 - C_{12} and C_{14} PFCAs, C_4, C_6, and C_8 PFSAs as well as 6:2 and 8:2 diPAPs) at two dose levels in acetone (1.25 μg/cm^2 (low-dose group) and 6.25 μg/cm^2 (high-dose group)). Samples of blood were taken at fixed timepoints over the exposure period. At the end of the experiments, 144 h after exposure, 34.1-18.0% and 5.3-15.1% of the applied dose had been absorbed into the rats for the low-dose and high-dose groups respectively. The observed trend in permeation was parabolically associated with the compounds carbon chain length, with PFHpA having the highest permeation through the rat skin. Interestingly, the peak blood concentrations of PFAS were at 8-72 h after the dermal exposure which is significantly later than after oral administration (1-24h). This further supports the findings of Abraham and Monien that dermal exposure can be long-lasting (Chen et al., 2022).

Two studies from the same laboratory examined the effects of topically applied PFOA and PFBS in murine models (Shane et al., 2020; Weatherly et al., 2021).The first study topically applied PFOA in acetone on the dorsal surface of each ear in concentrations ranging

from 0.5-2% w/v. After 4 days of dermal exposure (2%) the IgM antibody response was significantly reduced. Additionally, dermal exposure to PFOA caused a significant decrease in thymus (1 and 2%) and spleen weight (0.5-2%) as well as an increased liver weight (0.5-2%). This study raises concern on the potential adverse effects of dermal exposure and the immunotoxicity of PFOA after dermal exposure (Shane et al., 2020). Similarly, in the other study PFBA in acetone was topically applied on the dorsal surface of each ear in concentrations ranging from 3.75-7.5% v/v for 28 day or 15% v/v for 15-day exposures. At all exposure levels significant increases in liver and kidney weights were seen as well as altered serum chemistries. The adverse effects seen after dermal exposure to PFBA were like those reported for oral PFBA exposure and dermal and oral PFOA exposure. The authors note that as the study was conducted for hazard identification the highest non-overtly toxic concentrations were selected for exposure (Weatherly et al., 2021). It is important to keep in mind that mouse skin differs from human skin in relation to skin barrier function, hair follicles etc. However, murine models can still give a good indication for potential human exposure.

A study evaluating the potential dermal absorption of neutral PFAS from the gas phase using a modelling approach. Many of the compounds included in this study are precursors to the more stable PFCAs and PFSAs. The study was based on the compounds physicochemical properties and it identified 11 PFAS, e.g., N-Methyl- and N-Ethyl- perfluorobutyl sulfonamido ethanol (N-MeFBSE and N-EtFBSE) for which transdermal absorption could be a bigger exposure pathway than inhalation (Kissel et al., 2023).

Although little is known about the function of influx transport proteins in human skin, e.g. their interaction in uptake of xenobiotics, various transporter proteins have been identified in human skin. For example, the solute carrier transporter, SCL21 family genes encode various organic anion transporter polypeptides (OATP) family transporters, which can mediate absorption, distribution, and excretion of an array of environmental toxins and clinically used

drugs (Fujiwara et al., 2015). The expression of various OATPs as well as organic anion transporters (OAT, e.g. OAT4) has been confirmed in the skin (Fujiwara et al., 2015; Schiffer et al., 2003). Interestingly, many of the same OATPs are expressed in the liver, where they have been demonstrated to be able to transport PFBS, PFHxS, and PFOS, as well as PFOA and PFNA (Zhao et al., 2016). Furthermore, OAT4 has been linked to placental transfer of PFAS, with studies suggesting the chain length of a PFAS being related to its binding affinity to OAT4 (Kummu et al., 2015; Lu et al., 2021).

Hand wipes have been used to evaluate PFAS exposure through dermal and hand-to-mouth contact. In a study conducted in Oslo, Norway, hand wipe samples collected to evaluate indoor PFAS exposure and composite samples from both hands of 60 adults were analysed (Poothong et al, 2019). The exposure via dermal absorption was calculated based on body weight, the results of the hand wipe samples, time (set to 24 h exposure), and fraction of PFAS absorbed through the skin over 24 h (48%), which was based on the previous findings of Franko et al (2012) on dermal absorption of PFOA. These calculations generated estimates of the daily dermal uptake of PFOA and PFOS of 11 ng $(kg\ bw)^{-1}$ and 3.6 ng $(kg\ bw)^{-1}$ respectively (Poothong et al., 2019). Importantly, the Poothong et al (2019) study only accounted for the PFAS found on hand wipes and did not consider the presence and dermal uptake of PFAS on other areas of the skin, for example due to the use of cosmetics. Additionally, the study was based on samples collected at one time point only; and therefore, did not account for daily/temporal fluctuations (e.g. seasonal differences in dust loading and varying use of products on different days and/or seasons). Moreover, assuming a 24-hour exposure to a fixed dose does not reflect variations in dust/PFAS loading on the hands due to washing frequency and/or hand-to-mouth behaviour and other hand contact events. Therefore, the actual dermal uptake and relative significance of dermal exposure to PFAS could deviate substantially from these estimates.

A Spanish study on PFAS concentrations in breast milk also estimated the possible exposure routes associated with the breast milk PFAS levels (Serrano et al., 2021). The study participants filled out a questionnaire disclosing information such as their socio-demographic characteristics, diet, lifestyle, and use of personal care products. A multivariate regression analysis was then used to evaluate factors related to individual and total PFAS concentrations. This revealed a positive association between PFAS levels in breast milk and the use of various personal care products suggesting dermal uptake as a source of PFAS exposure. Positive association was seen both for short- and long-chain PFAS and personal care products such as cosmetics, skin care and hair products, perfume, and deodorant. Additionally, foundation use was positively associated with the sum of PFOA, PFOS, PFNA and PFHxS concentrations. The authors discuss how the current knowledge regarding dermal exposure to PFAS have led to it being a considered as minor contribution to total human exposure in many exposure assessments. They suggest this should be reconsidered as newer studies such as this one identify positive associations between PFAS levels and the use of personal care products. Furthermore, various studies have identified PFAS in products that come in contact with the skin i.e. personal care products (Glüge et al., 2020a; Schultes et al., 2018). The authors do acknowledge the small sample size of this study (n = 82) as a limiting factor as it reduces the capacity to detect possible determinants of PFAS exposure, especially for compounds with a low detection frequency. Additionally, the questionnaire used was not specifically designed for exhaustive investigation of sources of PFAS exposure which could have prevented identifications of other possible pathways. Finally, the large number of explanatory factors evaluated could have revealed some false statistically significant associations and that a possible bias may have resulted from a misreporting of dietary intakes and other factors. However, the authors state that misclassification was unlikely to be driven by exposure levels (Serrano et al., 2021).

Furthermore, biomonitoring studies from both Norway and Belgium have identified positive associations between PFAS (e.g. PFNA, PFTrDA, PFBS, and 6:2 diPAP) serum levels and the use of personal care products (Colles et al., 2020; Thépaut et al., 2021).

1.7. Possible sources of human exposure via the dermal pathway

A growing number of studies reveal sources and scenarios for which dermal exposure to PFAS can occur. Studies on PFAS and their potential precursors in various consumer products and clothing could indicate dermal absorption as a potentially important route of human exposure (Fujii et al., 2013; Greenpeace, 2016, 2013, 2012; Schultes et al., 2018; van der Veen et al., 2020; Whitehead et al., 2021). A report on several cosmetics revealed that some products, e.g., foundations and powders, contained 25 different PFAS. The compounds most frequently detected in the samples were PFHpA and PFHxA, along with polyfluoroalkyl phosphate esters (PAPs). Up to 470 μg g^{-1} of total PAPs were identified in products that listed combinations of PAPs as an ingredient. However, the total identified PFAS only represented a small fraction of the extractable organic fluorine (EOF) in the samples when analysed by combustion ion chromatography (CIC) (Schultes et al., 2018). Moreover, a recent study on fluorinated compounds in North American cosmetics identified up to 13 different PFAS in various cosmetic products such as mascaras, foundations, and lip products. Targeted PFAS analysis was conducted using LC-MS/MS and GC/MS, while total (organic and inorganic) fluorine concentrations were measured by particle-induced gamma-ray emission (PIGE) spectroscopy (Whitehead et al., 2021). Another study reported total PFCA concentrations to range from not detected up to 5.9 μg g^{-1} in cosmetics and up to 19 μg g^{-1} in sunscreens (Fujii et al., 2013). This study did not include the analysis of PAPs or EOF, thus the total concentration of fluorinated compounds in the samples tested is unknown. Moreover, a recent paper highlighted the wide range of products that contain PFAS (Glüge et al., 2020a). The authors identified many consumer products that come in contact with the skin such as: hand sanitiser, cosmetics (body

lotion, foundation, blush, eye cream, eye pencil, eye shadow, mascara, lipstick, moisturiser, nail polish, makeup remover, powder, shampoo, hair cream, conditioner, hair spray, hair mousse, shaving cream, and sunscreen), as well as guitar strings and piano keys.

Another potential source of exposure is dermal contact with water repellent clothing, e.g., rain jackets, rain pants, and footwear. Three different studies by Greenpeace found PFAS in outdoor clothing and hiking gear. When testing various samples of outdoor clothing they found that most of the samples contained some form of PFAS, such as PFOA, PFBS, and PFHxA, as well as 8:2 FTOH and 6:2 FTOH (Greenpeace, 2016, 2013, 2012). Furthermore, a recent study on the effect of weathering on water repellent clothing revealed an increase in concentrations of most perfluoroalkyl acids (PFAAs) in weathered articles compared to those in the original unweathered samples. Moreover, an increase in volatile PFAS such as 6:2 FTOH and 8:2 FTOH was also seen in some samples after weathering. The authors suggest a few explanations for the increase in volatile PFAS caused by weathering. One proposed explanation was the degradation of fluorotelomer based polymers with fluorinated alcohol and/or acrylate side chains. Other suggestions were that previously non-extractable organic fluorine was rendered extractable by weathering, or that other unknown precursors were degrading or transforming to the identified volatile PFAS (van der Veen et al., 2020). A study of 160 textile samples from the United States compared PFAS concentrations determined via two different extraction methods. Firstly, the textile samples were extracted by a simple solvent extraction and the second used an oxidative treatment. This second method, the total oxidizable precursor (TOP) assay helps with the analysis of unknown precursors. The samples included water repellent textiles, flame retarded textiles and infant clothing. Before oxidation, the sum concentration of 13 PFAAs (C4, C6, C8 and C10 PFSAs and C4-C12 PFCAs) ranged from <LOD to 63.7 $\mu g/m^2$ (mean value: 3.18 $\mu g/m^2$), with the highest PFAS concentrations seen in flame retarded textiles, followed by water repellent textiles and infant clothes. In samples

analysed after the oxidative treatment, the sum PFAA levels were 10-fold higher than in the samples before oxidation, suggesting the use of PFAA precursors in textiles. This study estimated the dermal exposure to PFAAs in infant clothing based on the concentration of PFAAs found in the clothing, the total body surface for infants (2543 cm^2), the daily migration rate of PFAAs from textiles to the skin (0.001 day^{-1}) and the penetration rate of PFAAs into the body (0.5, unitless). None of the PFAAs exceeded the proposed reference dose (RfD) of 20,000 pg/kg bw/day suggested by the USEPA for PFOA and PFOS in 2016 with the mean exposure doses of total PFAAs calculated based on values after TOP assay being 69.9 pg/kg bw/day (maximum 622 pg/kg bw/day) (Zhu and Kannan, 2020). Dermal exposure was only estimated based on PFAA levels from infant clothing which had the lowest PFAS concentrations of the three types of fabric samples analysed. However, the US EPA announced in 2021 that they would be re-evaluating the RfD for PFOS and PFOA based on scientific data and new analysis indicating negative health effects occurring at much lower levels of exposure than previously thought (U.S. EPA, 2021). Finally, in 2022 the US EPA amended their lifetime Health Advisory Levels (HALs) for PFAS in drinking water. The new levels suggested for PFOS and PFOA were 0.02 ng/L and 0.004 ng/L respectively (U.S. EPA, 2022).

A study from the US also found PFAS in children's school uniforms, which were marketed as stain resistant. The products were first screened for total fluorine using PIGE spectroscopy (n = 72), after which a targeted analysis of 49 neutral and ionic PFAS was performed on 57 samples. Hydrolysis and TOP assay revealed that PFAA precursors were a big contribution to the total PFAS concentrations in the school uniforms. Interestingly, the products made from 100% cotton had higher targeted PFAS concentrations compared to uniforms made from synthetic blends. The concentration of PFAS in school uniforms are alarming as they are worn directly on the skin for many hours per day (up to 10 h), five days a week. They authors estimated the median potential children's exposure to the total target PFAS

through dermal exposure to be 1.03 ng/kg/bw/day. The authors note that no reference doses exist for neutral PFAS, which are detected in the highest concentrations in the uniforms. However, an FDA study indicated that 6:2 FTOH is more toxic than PFHxA (Xia et al., 2022).

1.8. Summary and Aims

Dermal uptake has been overlooked as a possible pathway of human exposure to PFAS. However, growing numbers of studies are identifying many different PFAS-containing consumer products such as fabrics and cosmetics that can come in contact with the skin. Additionally, studies on other halogenated organic pollutants suggest that contaminated dust contributes greatly to dermal exposure of those contaminants with dust also being a source of possible PFAS exposure. Previous studies show that structurally related brominated and chlorinated chemicals are dermally bioavailable and can result in significant contributions to the body burdens of these hazardous chemicals. While this may indicate dermal exposure as an important pathway of exposure to PFAS, especially with dermally relevant consumer applications i.e., stain- and water-proof fabrics as well as cosmetics, it is difficult to estimate the dermally absorbed fraction of PFAS based on those of chlorinated and brominated FRs. This is due to the unique physico-chemical properties of PFAS (due to the strength of the C-F bond) and the diverse nature of PFAS in terms of the large number of chemicals with varying numbers of carbon atoms, fluorine content and functional groups leading to a broad spectrum of physico-chemical properties within PFAS.

Our understanding of dermal absorption of PFAS remains incomplete and experimental data scarce. As knowledge and understanding of the health impact of PFAS increases, it is increasingly important to fill the knowledge gaps that exist regarding human dermal exposure to these chemicals. 3D-HSE models mimic human skin and provide an effective and ethical alternative to the issues associated with human dermal absorption studies. Thus, these models make it possible to perform dermal uptake experiments which are urgently required to address

the crucial research gap and provide necessary information on the dermal flux and permeability coefficients of major PFAS in different homologue groups (e.g., C_4-C_{14}, PFAAs, PFSAs…etc). Such information could then be applied in QSAR-modelling approaches to estimate dermal permeability coefficients for structurally related PFAS with an acceptable level of confidence based on the relative similarity of physico-chemical properties among chemicals within the same PFAS homologous group.

Thus, the objectives of this study are to:

- Evaluate the dermal bioaccessibility of 17 PFAS (11 PFCAs and 6 PFSAs) from contaminated household dust into synthetic sweat:sebum mixtures under physiological conditions.
- Evaluate dermal bioavailability of 17 PFAS (10 PFCAs and 7 PFSAs) using 3D-HSE models. The distribution of PFAS within the different compartments of the *in vitro* set-up are assessed and compared. Finally, based on the results of this experiment the dermal flux ($\boldsymbol{J_{ss}}$) and permeation coefficients ($\boldsymbol{P_{app}}$) are calculated.
- Evaluate potential human exposure to PFAS from household dust and other sources using the combined results from the bioaccessibility and bioavailability experiments. This will provide a better understanding of the contribution of this pathway to total human exposure to PFAS.
- Evaluate the hepatic *in vitro* metabolism of two novel prototype PFAS compounds and compare interspecies differences between humans and rats. These novel compounds are suggested as replacement chemicals for the more persistent legacy PFAS.

2. METHODOLOGY

This chapter includes material taken verbatim from the following articles:

Ragnarsdóttir, O.; Abdallah, M. A.-E.; Harrad, S. Dermal Bioaccessibility of Perfluoroalkyl Substances from Household Dust; Influence of Topically Applied Cosmetics. *Environmental Research* **2023**, *238*, 117093. https://doi.org/10.1016/j.envres.2023.117093.

Ragnarsdóttir, O.; Abdallah, M. A.-E.; Harrad, S. 2023. Dermal Bioavailability of Perfluoroalkyl Substances (PFAS) using *in vitro* 3D-Human Skin Equivalent Models. *Under review in Environment International, January 2024.*

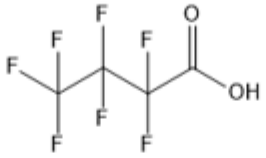
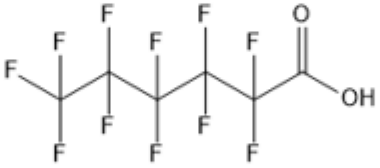
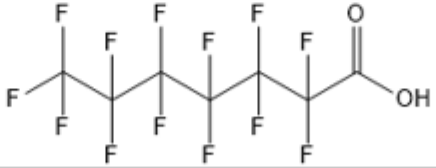
Licul-Kucera, V.; Ragnarsdóttir, O.; Frömel, T; van Wezel, A.P.; Knepper, T.P.; Harrad, S.; Abdallah, M. A.-E.; 2024. Interspecies comparison of metabolism of two novel prototype PFAS. *Chemosphere*, 351, 141237. https://doi.org/10.1016/j.chemosphere.2024.141237

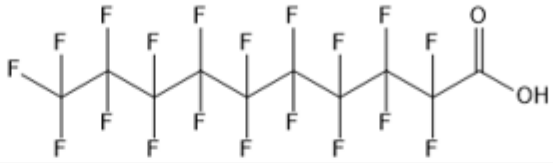
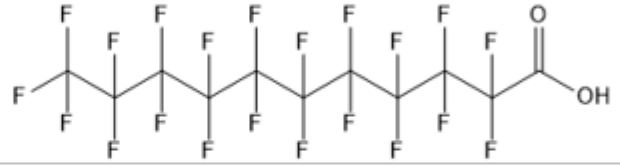
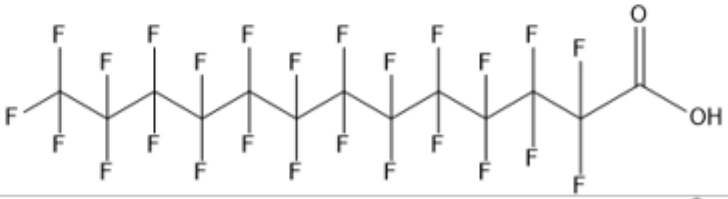
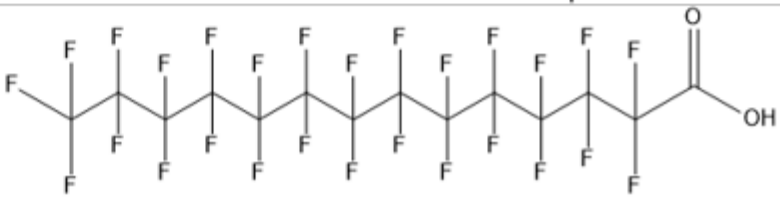
Each authors contribution is described in chapters 3, 4, and 6 in this thesis.

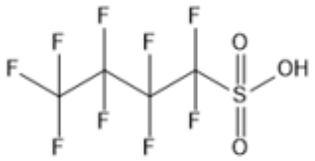
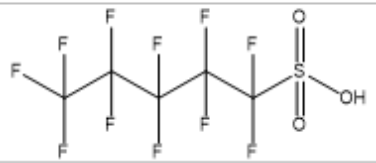
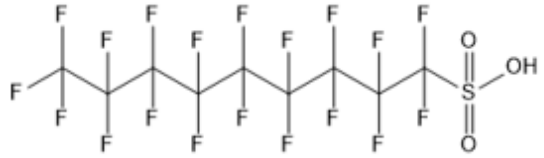
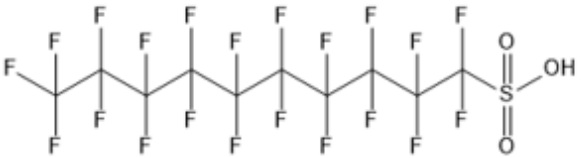
2.1. Chemicals and standards

PFAS are a huge class comprising of thousands of compounds and very little is known about the possible dermal uptake of these chemicals (Ragnarsdóttir et al., 2022). It was therefore decided that the main focus of this study would be on PFCAs and PFSAs as these are the PFAS classes that have been the most studied so far. The impact of these compounds on human health is well documented as well as their presence in products that could lead to dermal exposure to PFAS (EFSA CONTAM Panel, 2020; Glüge et al., 2020a). Thus, 18 PFAS were included in the targeted instrumental method, C_4 – C_{14} PFCAs and C_4 – C_{10} PFSAs. Table 2-1 lists the targeted compounds and the labelled internal standards (ISTD) used for their quantification. Standard stock solutions were prepared in methanol. All standards were purchased from Wellington Laboratories (Guelph, Canada). Ammonium acetate, ammonium hydroxide, Dulbecco's Modified Eagle Medium (DMEM) and all solvents were of HPLC grade or higher, and were purchased from Fisher Scientific (Loughborough, UK). MilliQ water was used for cleaning and sample extraction. Standard reference material (SRM2585, organics in house dust, particle size <100 µm and total moisture content = 2.11 ± 0.06%) was purchased from NIST (Gaithersburg, MD, USA). Details on the chemicals and standards used for the investigation of metabolism of the two novel prototype PFAS can be found in chapter 6.

Table 2-1: Target PFAS, their abbreviations, molecular structures, and labelled internal standards used.

Target compounds	Abbreviation, C-chain length	Molecular formula	Molecular structures	ISTD
Perfluorobutanoic acid	PFBA, C = 4	C_3F_7COOH		MPFBA
Perfluoropentanoic acid	PFPeA, C = 5	C_4F_9COOH		M5PFPeA
Perfluoro-n-hexanoic acid	PFHxA, C = 6	$C_5F_{11}COOH$		MPFHxA
Perfluoro-n-heptanoic acid	PFHpA, C = 7	$C_6F_{13}COOH$		M4PFHpA
Perfluoro-n-octanoic acid	PFOA, C = 8	$C_7F_{15}COOH$		M8PFOA

Perfluoro-n-nonanoic acid	PFNA, C = 9	$C_8F_{17}COOH$		MPFNA
Perfluoro-n-decanoic acid	PFDA, C = 10	$C_9F_{19}COOH$		M6PFDA
Perfluoro-n-undecanoic acid	PFUnDA, C = 11	$C_{10}F_{21}COOH$		M7PFUdA
Perfluoro-n-dodecanoic acid	PFDoDA, C = 12	$C_{11}F_{23}COOH$		MPFDoA
Perfluoro-n-tridecanoic acid	PFTrDA, C = 13	$C_{12}F_{25}COOH$		MPFDoA
Perfluoro-n-tetradecanoic acid	PFTeDA, C = 14	$C_{13}F_{27}COOH$		M2PFTeDA

Perfluoro-1-butanesulfonate	PFBS, C = 4	$C_4F_9SO_3H$		MPFBS
Perfluoro-1-pentanesulfonate	PFPeS, C = 5	$C_5F_{11}SO_3H$		MPFBS
Perfluoro-1-hexanesulfonate	PFHxS, C = 6	$C_6F_{13}SO_3H$		MPFHxS
Perfluoro-1-heptanesulfonate	PFHpS, C = 7	$C_7F_{15}SO_3H$		MPFHxS
Perfluoro-1-octanesulfonate	PFOS, C = 8	$C_8F_{17}SO_3H$		M8PFOS
Perfluorono-1-nanesulfonate	PFNS, C = 9	$C_9F_{19}SO_3H$		M8PFOS
Perfluoro-1-decanesulfonate	PFDS, C = 10	$C_{10}F_{21}SO_3H$		M8PFOS

2.2. Exposure protocols

2.2.1. Dermal bioaccessibility

Dermal bioaccessibility tests were based on a previously reported protocol (Ertl and Butte, 2012; Pawar et al., 2017). Both pure SRM2585 dust as well as SRM2585 dust in the presence of personal care products ((PCP) moisturiser, sunscreen, foundation, and deodorant, all tested separately) were included in the tests. In both cases dust or dust/PCP were exposed to synthetic sweat and sebum mixtures (SSSM) for 1 h with gentle stirring. The dust-to-sweat ratio on human skin can vary. For this study "wet skin conditions" were chosen based on a previous study (Ertl and Butte, 2012). At the end of exposure, the dust and SSSM were separated by centrifugation and the samples extracted and analysed separately. A more detailed description of the exposure protocol can be found in a later section focusing on dermal bioaccessibility (3.3. Dermal bioaccessibility *in vitro* test protocol).

2.2.2. Dermal bioavailability

Upon receipt of the 3D-HSE models, the tissues were prepared according to supplier directions. The exposure protocol used was based on OECD guidelines (OECD, 2004a). In short, 500 ng/cm^2 (100 µL of 10 ng/µL spiking solutions in MeOH) net loading of each target PFAS was applied to each skin tissue based on the exposed surface area and DMEM-based culture medium was used as receptor fluid (RF). Samples of RF was collected at 15 preselected time intervals over 36 hours. All tests were done in triplicates. At the end of the exposure the following samples were collected: donor compartment washes, receptor compartment washes, skin surface washes, skin cells, and RF samples (from 15 different timepoints). Samples were extracted and analysed separately. A more detailed description of the exposure protocol and set-up can be found in a later section focusing on dermal bioavailability (4.3. Test matrices and permeation assay protocol).

2.2.3. Metabolism of novel PFAS

Test assays were prepared by adding 1 mg/mL of RL-S9 or HL-S9 and 2.5 µL of the corresponding prototype PFAS (CF_3-O-SURF/ CF_3-S-SURF) dosing solution to phosphate buffer (pH=7.4). They were then pre-incubated for 5 min at 37 °C, with constant shaking. After that NADPH regenerating system (final concentration: 1.0 mM $NADP^+$, 5.0 mM G6P and 2 units/mL G6P-DH) was added to make a final volume of 250 µL. Samples were then incubated at 37 °C, with constant stirring, for 120 min. Finally, the reaction was stopped with the addition of 250 µL of ice-cold MeOH. A more detailed description of the exposure protocol and the subsequent sample extraction and clean-up is described in chapters 6.2 and 6.5 of this thesis.

2.3. SPE comparison

2.3.1. SPE sample extraction and analysis

Three SPE cartridge types from different manufacturers were tested and results from PFAS analysis compared. The SPE cartridges selected were OASIS WAX (6 cc, 150 mg, Sorbent: Copolymer (Waters)), Strata XAW (6 cc, 200 mg, Sorbent: Polymer based (Phenomenex)) and Chromabond™ PFAS (6 mL, 300 mg, Sorbent: Polymer based (Chromabond)). For all tested SPE cartridges, the compound separation was based on weak anion exchange. Each SPE cartridge was pre-conditioned with 2 x 6 mL methanol containing 0.1% NH_4OH followed by 2 x 6 mL of MilliQ water. The SPEs were then spiked directly with 25 µL (2000 ng/mL) native PFAS standard mixture and 30 µL (1000 ng/mL) PFAS ISTD mixture. Following this the SPE cartridges were dried under vacuum for 5 min. PFAS were eluted in three batches of 6mL MeOH + 0.1% NH_4OH with each fraction collected separately, resulting in 9 fractions in total. The samples were then concentrated to 200 µL under gentle N_2 flow and transferred to autosampler vials for analysis. The samples were analysed on a Sciex Exion UPLC coupled to a Sciex 5600+ triple TOF MS operated in negative mode. A detailed description of the instrumental method can be found in chapter 2.4. Instrumental analysis. Individual PFAS were identified and peak areas of native and mass labelled compounds were determined in

Multiquant 3.0.2 based accurate mass and retention time. Compound area from each fraction was evaluated and compared based on the area in each fraction divided by the sum area of each SPE type using Microsoft Excel (Microsoft Office 365).

2.3.2. Results of SPE comparison

Results revealed similar results for Chromabond^{TM} PFAS and Oasis WAX SPE cartridges. The Strata XAW showed slightly lower retention of PFAS compared to the other two SPEs. For all SPE type, the majority of PFAS were eluted in fractions F1 and F2 (Table 2-2). While the majority of shorter chain PFAS were eluted in the first fraction, more solvent was needed to elude the longer chain compounds. Thus, it was decided to use Chromabond^{TM} PFAS SPE cartridges and elute PFAS with 12 mL of MeOH + 0.1% NH_4OH moving forward.

Table 2-2: Fraction of PFAS (%) found in each fraction of eluant from the tested SPEs.

	Oasis WAX			Chromabond PFAS			Strata XAW		
	F1	F2	F3	F1	F2	F3	F1	F2	F3
PFBA	98.7	1.3	x	98.9	1.1	x	99.9	0.1	x
PFPeA	96.4	3	0.6	96.9	2.7	0.4	97.8	1.9	0.2
PFHxA	94	5.2	0.8	94.8	4.7	0.5	96.1	3.6	0.3
PFHpA	94.3	5.1	0.6	95.4	4.3	0.3	96.4	3.3	0.3
PFOA	90.9	8.1	1	94.5	5.2	0.3	95.3	4.3	0.4
PFNA	88.3	10.8	0.9	94.8	4.9	0.2	94.8	4.9	0.3
PFDA	82.8	16.2	1.1	94	5.8	0.2	93.5	6.2	0.3
PFUdA	69.4	29.1	1.5	87.7	12	0.3	89.3	10.4	0.3
PFDoA	36.2	61.8	2	55.4	43.9	0.6	67.6	31.8	0.6
PFTrDA	15.6	82.3	2.1	30.7	67.9	1.3	43.9	54.9	1.2
PFTeDA	15.9	82.5	1.7	28.4	70.7	0.9	50.2	49.1	0.7
PFBS	93.3	5.7	1	95	4.5	0.5	95.6	3.9	0.5
PFHxS	88	10.8	1.2	93.2	6.3	0.4	93.1	6.4	0.5
PFHpS	83.7	14.9	1.4	92.9	6.7	0.3	92.4	7.1	0.5
PFOS	78.5	20.1	1.4	92.4	7.3	0.3	91.1	8.5	0.5
PFNS	68.2	30	1.8	89.3	10.4	0.3	86.7	12.8	0.5
PFDS	50.7	47.3	2	72	27.5	0.6	70.6	28.7	0.7
	Oasis WAX			Chromabond PFAS			Strata XAW		
	F1	F2	F3	F1	F2	F3	F1	F2	F3
MPFBA	97.1	2.5	0.4	96.8	3.1	0.1	98.1	1.9	0.1
M5PFPeA	97.1	2.4	0.5	96.6	3.2	0.2	97.2	2.6	0.2
MPFHxA	95.9	3.5	0.6	95.1	4.6	0.3	95.9	4	0.2
M4PFHpA	95.4	4	0.6	95.1	4.7	0.2	95.5	4.4	0.2
M8PFOA	93.6	5.7	0.8	94.3	5.5	0.2	94.4	5.4	0.2
MPFNA	91.7	7.5	0.8	94.9	4.9	0.2	94	5.8	0.2
M6PFDA	88.3	10.7	0.9	94.7	5.2	0.1	93.9	5.9	0.2
M7PFUdA	73.6	24.9	1.5	88	11.8	0.2	89.4	10.4	0.2
MPFDoA	43.6	54.1	2.3	62.5	36.9	0.6	74.1	25.3	0.6
M2PFTeDA	16.8	81.8	1.3	29.7	69.5	0.9	53.4	45.9	0.7
MPFBS	94.5	4.6	0.9	94.4	5.2	0.4	94.6	5	0.4
MPFHxS	91.1	7.8	1.1	92.9	6.7	0.4	92	7.6	0.4
M8PFOS	84.1	14.4	1.5	92.7	7	0.3	91	8.6	0.4

2.4. Sample types and SPE extraction

2.4.1. Sample types

Both the bioaccessibility and bioavailability experiments produced various sample types. The bioaccessibility experiment resulted in dust samples (solid, n = 42) and SSSM (liquid, n = 42) samples. The bioavailability exposures produced five different sample types: donor

compartment washes (liquid, n = 27), receptor compartment washes (liquid, n = 27), skin surface wash (solid, n = 27), skin cells (solid, n = 27), and RF (liquid, n = 180) samples. Different sample extraction protocols were used for PFAS extraction for each sample type. However, the SSSM and RF samples were both extracted by SPE, the protocol for which is described in the next section. For all other sample types, the extraction procedure is described in the appropriate sections.

2.4.2. Sample extraction with SPE

Extraction and preparation of SSSM (6 mL) and receptor fluid samples (2 mL) was based on a method previously reported (Harrad et al., 2019). In short, each sample was spiked with 30 μL internal standard mixture before being loaded onto a Chromabond™ PFAS (6 mL/300mg, Chromabond) SPE cartridge. Cartridges were pre-conditioned with 6 mL MeOH (0.1% NH_4OH) followed by 6 mL MilliQ water. After sample addition, cartridges were dried under vacuum for 5 min. PFAS were eluted with 12 mL MeOH (0.1% NH_4OH) and the eluent collected and concentrated to ~0.5 mL under gentle N_2-flow at 38°C. Samples were then loaded onto a pre-conditioned (6 mL MeOH + 0.1% NH_4OH) EnviCarb™ (3 mL/250 mg, Merck) SPE cartridge. PFAS were eluted with 5 mL methanol (0.1% NH_4OH), with the eluate concentrated to incipient dryness and reconstituted to 200 μL in MeOH containing $^{13}C_4$-PFOS recovery determination standard before transfer to autosampler vials for analysis.

2.5. Instrumental Analysis

Samples were analysed on a Sciex Exion UPLC coupled to a Sciex 5600+ triple TOF MS. The instrumental method was based on a method reported previously (Harrad et al., 2019). In short, ten microlitres of sample were injected onto a Zorbax Eclipse™ PlusC_{18} column (1.8 μm particle size, 2.1 x 100 mm, Agilent) equipped with a Zorbax Eclipse™ Plus C_{18} Fast Guard column (internal diameter: 2.1 x 5 mm; particle size 1.8 μm, Agilent). Details of the UPLC method are provided in Table 2-3. The TOF-HRMS was equipped with a Turbo V source

operated in negative mode using ESI at a voltage of -4500 V and the temperature was set to 450°C. The curtain gas and nebuliser (source gas 1) were set to 25 psi and the drying gas (source gas 2) was set to 30 psi. Mass spectrometric data was acquired using automatic information-dependent acquisition (IDA) using survey scan (TOF-MS data). Individual PFAS were quantified in Multiquant 3.0.2 using accurate mass and retention time for identification with calibration plots comprising 5 points of regression (5 ng/mL, 50 ng/mL, 100 ng/mL, 500 ng/mL and 1000 ng/mL), displaying good linearity (Table 2-4).

Table 2-3: LC conditions used in this study.

Mobile Phase	A: 2 mM ammonium acetate in water B: 2 mM ammonium acetate in methanol		
Column	Zorbax Eclipse Plus C18 column 1.8 μm particle size, 100 mm length, 2.1 mm internal diameter		
Flow Rate	0.5 mL/min		
Gradient	**Time**	**A (%)**	**B (%)**
	0.00	80	20
	2.00	5	95
	5.00	5	95
	5.01	80	20
	7.00	80	20

Table 2-4: Target accurate masses. Estimated method detection and quantification limits (MDL and MQLs) for PFAS. Estimations were based on the S:N ratio 3:1 and 10:1 respectively.

Compound	Accurate mass (-H)	MDL (ng/mL)	MQL (ng/mL)	R^2	Linear equation
PFBA	244.9513	1.791	5.970	0.9999	y = 0.008x + 0.0076
PFPeA	294.9481	0.127	0.424	1.0000	y = 0.0091x + 0.0416
PFHxA	344.9449	0.102	0.339	0.9844	y = 0.0068x + 0.3475
PFHpA	394.9417	0.104	0.348	0.9999	y = 0.0087x + 0.0333
PFOA	444.9385	0.045	0.151	0.9999	y = 0.01x + 0.0447
PFNA	494.9353	0.087	0.290	1.000	y = 0.0091x - 0.0012
PFDA	544.9321	0.029	0.097	0.9998	y = 0.0336x + 0.0456
PFUdA	594.9289	0.048	0.161	0.9995	y = 0.0067x + 0.0507
PFDoA	644.9257	0.034	0.115	0.9995	y = 0.0079x + 0.052
PFTrDA	694.9225	0.213	0.710	0.9997	y = 0.0099x + 0.0256
PFTeDA	744.9193	0.049	0.162	0.9996	y = 0.0076x + 0.0369
PFBS	298.9430	0.079	0.265	0.9988	y = 0.0078x + 0.1084
PFPeS	348.9393	0.064	0.214	0.9975	Y = 0.0073x + 0.1804
PFHxS	398.9366	0.033	0.111	0.9996	y = 0.0093x + 0.0859
PFHpS	448.9334	0.025	0.084	0.9996	y = 0.0095x + 0.1373
PFOS	498.9302	0.046	0.155	0.9998	y = 0.0071x + 0.0126
PFNS	548.9270	0.023	0.077	0.9994	y = 0.0092x + 0.0824
PFDS	598.9238	0.016	0.055	0.9984	y = 0.0108x + 0.0886

2.6. Quality Assurance and Quality Control

All experiments were performed in triplicate. In the bioaccessibility tests, one procedural blank comprising of SSSM without dust addition was included for every 6 samples as well as a blank for each PCP (n = 7). For bioavailability tests, a procedural blank comprising of a skin tissue exposed to solvent only was included in each sample batch (n = 3). Further details on QA/QC measures for each experiment can be found in their appropriate sections.

2.7. Data Processing and Statistical Analysis

All data processing was conducted using Microsoft Excel (Microsoft Office 365). Statistical analysis of data was performed using Microsoft Excel and SPSS 26 for Windows. A more detailed description of calculations and statistical analysis performed can be found in their appropriate sections.

3. DERMAL BIOACCESSIBILITY OF PFAS

This chapter includes material taken verbatim from the following article:

Ragnarsdóttir, O.; Abdallah, M. A.-E.; Harrad, S. 2023. Dermal bioaccessibility of perfluoroalkyl substances from household dust; influence of topically applied cosmetics. *Environmental Research*, 238, 117093. https://doi.org/10.1016/j.envres.2023.117093.

O.R. conducted the experiments, interpreted the data, wrote the original draft and was the corresponding author. S.H. and M. A.-E. A. conceived and designed the experiment, assisted with the interpretation of the data, reviewed, and edited the manuscript.

3.1. Introduction

Per- and polyfluoroalkyl substances (PFAS) have been in production and widely used since the 1940s. Their chemical and thermal stability, as well as their hydrophobic and lipophobic properties make PFAS suitable for use in a broad range of products, such as: aqueous fire-fighting foams (AFFF), textiles and personal care products (Buck et al., 2011; Glüge et al., 2020a; Harrad et al., 2019; Whitehead et al., 2021). However, the physicochemical properties of PFAS also result in their global distribution, with perfluorooctane sulfonate (PFOS) being identified in polar bears and other wildlife in remote areas, as far back as the early 2000s (Giesy and Kannan, 2001). Moreover, different PFAS have been identified in human sera from all over the world (Haug et al., 2011; Kim et al., 2019; Sunderland et al., 2019). Consequently, many studies have focused on the possible adverse human health effects of PFAS exposure, with the European Food Safety Authority (EFSA) highlighting the reduced immune response to vaccination (Abraham et al., 2020; Grandjean et al., 2012, 2017a), decreased birth weight (Meng et al., 2018; Sagiv et al., 2018), and impaired liver function (Salihovic et al., 2018a) leading to a recommended tolerable weekly intake of 4.4 ng/kg bw/week for the sum of four PFAS (perfluorohexane sulfonic acid (PFHxS), PFOS, perfluorooctanoic acid (PFOA) and perfluorononanoic acid (PFNA)) (EFSA CONTAM Panel, 2020).

Studies on human exposure have found diet and drinking water to be the greatest contributors to total human adult exposure to PFAS, followed by inhalation of indoor air and ingestion of indoor dust (Harrad et al., 2019; Haug et al., 2011; Sunderland et al., 2019). However, despite the known presence of PFAS in indoor dust and the adherence of such dust to skin, dermal uptake arising from indoor dust is poorly understood. Moreover, recent studies have highlighted the huge variety of PFAS applications in products that come in contact with the skin e.g., personal care products and clothing (Glüge et al., 2020a; Schultes et al., 2018; Whitehead et al., 2021; Xia et al., 2022). Finally, recent *in vivo* studies on rats and one human subject showed that PFAS are able to penetrate the skin and considerably contribute to total body burdens (Abraham and Monien, 2022; Chen et al., 2022). Despite this, very little is known about the human dermal uptake of PFAS and very few studies have investigated this exposure pathway (Ragnarsdóttir et al., 2022).

The surface of human skin is covered with a skin surface film liquid (SSFL) composed of a mixture of sweat and sebum. Sebum is a clear, oily substance secreted by sebaceous glands which are found in most areas of the body. Sweat is an aqueous solution containing various electrolytes, vitamins, amino acids, organic acids, and nitrogenous substances (Nicolaides, 1974; Stefaniak and Harvey, 2008). As a first step in the process via which chemicals present in materials coming into contact with the skin may undergo dermal uptake; chemicals must dissolve from such materials into the SSFL, in order to become available for dermal absorption (i.e. *bioaccessible*) (Luo et al., 2020). Dermal *in vitro* physiologically-based extraction tests have been used to determine the dermal bioaccessibility of various xenobiotics, both inorganic and organic, e.g. sensitising metals, flame retardants, plasticisers, and pesticides (Ertl and Butte, 2012; Pawar et al., 2017; Stefaniak et al., 2014; Zeng et al., 2019).

To differentiate, *bioavailability* is defined as “the fraction of a chemical that reaches the systemic circulation”, *bioaccessibility*, on the other hand, refers to the fraction of a chemical

that is released into the body's fluids (SSFL for skin) from a matrix (*e.g., dust*) making it available for absorption (Ertl and Butte, 2012; Pawar et al., 2017; Ruby et al., 1996). In other words, a chemical within a matrix (*e.g., dust*) or product (*e.g., fabric*) must become *bioaccessible* first, in order to be available for absorption by the skin. However, it is not guaranteed that all the *bioaccessible* fraction of a chemical will penetrate the skin barrier to reach the systemic circulation (*i.e.,* become bioavailable). A potential oversight therefore is that *in vitro* dermal absorption studies rarely account for chemical release from a source matrix into the fluids on the skin surface, which could be a rate limiting step in dermal absorption(Collins et al., 2015). Thus, a combination of data on bioaccessibility and subsequent percutaneous penetration is necessary to fully understand the extent of human dermal uptake of chemicals (*e.g.,* PFAS) (Abdallah et al., 2012; Pawar et al., 2017).

Certain ingredients of cosmetics (*e.g.,* sunscreens and moisturisers) can remain on the skin for a long time and affect the properties of the SSFL. Furthermore, this could alter the skin´s hydration or interact with the proteins in the skin barrier, altering the lipid-protein domain of the skin and enhancing the dermal permeability for other chemicals (Lane, 2013). This has been shown in previous studies where sunscreen lotions enhanced the dermal penetration of contaminants such as herbicides and flame retardants (Pawar et al., 2017; Pont et al., 2004). Thus, it is important to investigate the possible effects of topically applied cosmetics when studying the dermal bioaccessibility of PFAS in indoor dust.

In the current study, we investigate for the first time, the dermal bioaccessibility of several PFAS, including C_4-C_{14} perfluorocarboxylic acids (PFCAs) and C_4-C_{10} perfluorosulfonic acids (PFSAs). The bioaccessible fractions of these PFAS from indoor dust to various physiologically relevant mixtures of synthetic human SSFL were quantified and the impact of different topically applied cosmetics on PFAS bioaccessibility was investigated. Finally, the

potential for human exposure to PFAS via dermal contact with indoor dust was assessed and compared to other well-studied exposure pathways (*i.e.,* diet and drinking water).

3.2. Materials and Methods

3.2.1. Materials

The standard reference material (SRM2585, organics in house dust, particle size <100 μm and total moisture content = 2.11 ± 0.06%) was purchased from NIST (Gaithersburg, MD, USA). HPLC grade methanol, ammonium acetate, ammonium hydroxide, Optima LC-MS grade methanol, and Optima LC/MS grade water were obtained from Fisher Scientific (Loughborough, UK). Native and mass labelled PFAS standards were purchased from Wellington Laboratories Inc. (Guelph, Canada). Target compounds included C_4 - C_{14} PFCAs and C_4, C_6 – C_{10} PFSAs

3.2.2. Synthetic Sweat and Sebum Mixture Preparation

Synthetic sweat and sebum mixtures (SSSM) simulating physiological human skin surface film liquid were prepared according to a previously reported US patent (Stefaniak and Harvey, 2008). Artificial sweat and sebum mixtures were prepared separately (See table 3-2 for detailed ingredients list), the sweat mixture was pH adjusted to that of normal human skin (5.3 ± 0.1) and both solutions stored at 5°C. Sweat:sebum mixtures were prepared at different, physiologically relevant ratios (100% sweat, 95:5 sweat:sebum, 1:1 sweat:sebum and 100% sebum), using drops of Tween-80 to prevent phase-separation and simulate naturally secreted SSFL (Pawar et al., 2017; Stefaniak and Harvey, 2008).

3.2.3. Dermal Bioaccessibility *in vitro* Test Protocol

The bioaccessibility test was based on protocols reported previously (Ertl and Butte, 2012; Pawar et al., 2017). In brief, 60 mg SRM2585 dust were accurately weighed into a clean, dry test tube. When tested, ca. 6 mg of personal care products (moisturiser, sunscreen, foundation, and deodorant, all tested separately) were accurately weighed into the same test tube. As the dust-to-sweat ratio on human skin can vary, “wet skin conditions“ were chosen based on a

previous study (Ertl and Butte, 2012). Thus, 1:100 w/v dust:SSSM ratio was used and 6 mL sweat:sebum mixture was added to the test tube. The mixture was gently stirred and kept at physiological skin temperature (32-34°C) using a heated magnetic stirrer plate. After 1 h the two phases were separated by centrifugation at 3900 RPM for 15 min. All experiments were conducted in triplicate. The resulting dust (solid residue, n = 42) and the SSSM (supernatant, n = 42) samples were analysed separately.

3.2.4. Sample Extraction and Clean-up

3.2.4.1.Dust samples

Dust sample extraction and preparation was based on a previously reported method (Harrad et al., 2020). Triplicate samples (ca. 60 mg each) of unexposed SRM2585 were analysed separately in addition to the exposed dust samples. Briefly, samples were extracted with basic methanol by ultrasonication followed by a clean-up with EnviCarb™ SPE cartridges. A detailed description of the method is provided in the Supporting Information.

3.2.4.2.SSSM samples

The extraction and preparation of SSSM supernatant samples was based on a method previously reported (Harrad et al., 2019). In short, samples were extracted using a Chromabond™ PFAS (6 mL/300 mg, Chromabond) SPE cartridge followed by clean-up using EnviCarb™ SPE cartridges. A detailed description of the extraction method is provided in the Supporting Information.

3.2.5. Chemical Analysis

Target PFAS were analysed on a Sciex Exion UPLC coupled to a Sciex 5600+ triple TOF MS operated in negative mode based on a previously reported method (Harrad et al., 2019). Detailed instrumental parameters are provided in the Supporting Information

3.2.6. Quality Assurance and Quality Control

All experiments were performed in triplicate and one procedural blank prepared for every 6 samples. Additionally, sample blanks containing only SSSM and personal care product were

included for each tested personal care product. Identification and quantification of target analytes were performed according to the relative retention times to the corresponding isotope labelled surrogate standard and the accurate mass of each target PFAS. In most blanks, none of the target compounds were detected. However, a few showed measurable concentrations of some target PFAS (PFDoA in 40% of blanks, PFTrDA in 16% and PFNA, PFOA, PFPeA, PFDoA, PFTrDA, and PFTeDA, in 25% of cosmetics blanks) In such instances, no blank correction was performed when the concentration in the blank was <5% of the average sample concentration from the same sample batch. Blank correction was performed in the instances where the blank concentration was between 5-20% of average sample concentrations. Further details on QA/QC measures including recoveries of internal (surrogate) standards, method accuracy, precision, and limits of quantification, as well as mass balance results for each SSSM composition and cosmetic product studied are provided as Supporting Information (tables 3-4 and 3-6 to 3-13).

3.2.7. Assessment of Dermal Bioaccessibility

Bioaccessibility is expressed as $f_{bioaccessible}$, calculated as the percentage of each target PFAS detected in the supernatant after exposure compared to the unexposed dust (eq. 1). All experiments were carried out in triplicate, thus average values were used:

$$f_{bioaccessible}(\%) = \frac{Average\ mass\ of\ PFAS\ in\ supernatant}{Average\ mass\ of\ PFAS\ in\ dust} * 100 \qquad (1)$$

3.2.8. Statistical Analysis

Statistical analysis of data was conducted using Microsoft Excel (Microsoft Office 365) and SPSS 26 for Windows. Means of various data sets were estimated and compared using ANOVA followed by Tukey's Honest Significant Difference (HSD) *post hoc* test or the Games -Howell test when a test of homogeneity showed no equal variance ($p < 0.05$). P-values of < 0.05 were considered significant.

3.3. Results and Discussion

3.3.1. Dermal bioaccessibility of PFAS in indoor dust

Figure 3-1 depicts the $f_{bioaccessible}$ of target PFCAs and PFSAs from indoor dust in the different SSSM. Average $f_{bioaccessible}$ values of target PFAS can be found in Table 3-5. Our results show that four of the target PFCAs were 100% bioaccessible from dust particles; PFHxA in 100% sweat, PFPeA in 95:5 sweat:sebum, and PFDA and PFTeDA in 100% sebum. While the composition of SSSM in real-life varies, 1:1 sweat:sebum is considered the most physiologically relevant ratio (Buckley and Lewis, 1960, Stefaniak and Harvey, 2006). The ratios examined here were chosen to account for different physiologically relevant SSSM, as well as the two extremes (100% sweat and 100% sebum). When comparing the total PFAS bioaccessibility between the different SSSM compositions; a Games-Howell Post Hoc test revealed that total PFAS bioaccessibility in 100% sebum significantly exceeded that in 100% sweat ($p = 0.01$), and the same was seen when comparing 100% sebum and 95:5 sweat: sebum ($p = 0.028$). Our results show that the target PFAS are bioaccessible at varying levels in all SSSM mixtures, making those PFAS available for absorption through human skin.

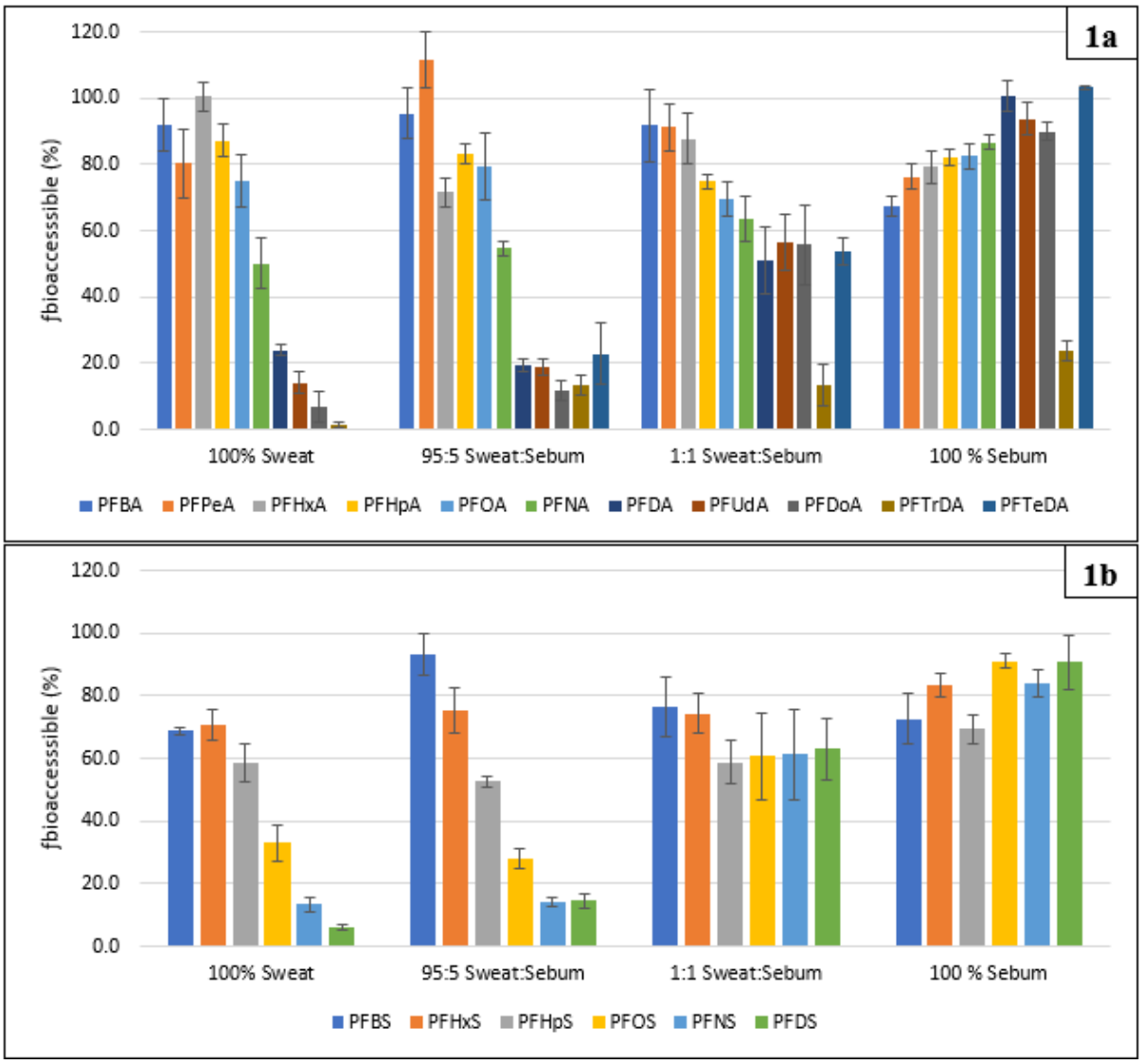


Figure 3-1: Dermal bioaccessibility of (a) PFCAs and (b) PFSAs in different composition of synthetic sweat sebum mixtures. Error bars represent the standard deviation (n = 6).

Comparison of the bioaccessibility of PFAS in 100% sweat and 100% sebum revealed a clear trend for both PFCAs and PFSAs (Figure 3-1). The general trend observed in 100% sweat was that the bioaccessibility decreased with increasing chain length with the $f_{bioaccessible}$ ranging from <LOD (PFTeDA) to 92.0 ± 7.9% (PFBA) for PFCAs ($r = -0.95$, $p \leq 0.001$), and 6.1 ± 0.7% (PFDS) to 68.9 ± 1.1% (PFBS) for PFSAs ($r = -0.92$, $p = 0.008$). The opposite trend was seen in 100% sebum with $f_{bioaccessible}$ values ranging from 103.3 ± 0.54% (PFTeDA) to 67.4 ± 2.8% (PFBA) for PFCAs ($r = 0.91$, $p \leq 0.001$(PFTrDA excluded)). While the same trend appeared for PFSAs, it was not significant ($r = 0.68$, $p = 0.14$) with the $f_{bioaccessible}$ ranging from

90.8 ± 8.9% (PFDS) to 72.6 ± 8.1% (PFBS). These trends are indicative of the physicochemical properties of the PFAS examined, *i.e.*, the more ionic character of the short-chain PFAS that leads to low $\log K_{ow}$ and high water solubility and the less ionic character of the long-chain PFAS has the opposite effects.

In general, PFAS $f_{bioaccessible}$ values were more similar for the shorter chain compounds (Carbon number ≤ 7 for PFCAs and ≤ 6 for PFSAs) in the different SSSM compositions with no significant differences noted. For longer chain compounds however, the $f_{bioaccessible}$ in 1:1 sweat:sebum significantly exceeded those in 100% sweat ($p = 0.001$ (PFTrDA excluded). The, $f_{bioaccessible}$ trends in 95:5 sweat:sebum were akin to those in 100% sweat, with no significant differences in bioaccessibility seen for neither short-chain or long-chain compounds ($p = 0.990$). The $f_{bioaccessible}$ in the most physiologically relevant SSSM (1:1 sweat:sebum) (Stefaniak and Harvey, 2006) exceeded 50% for all studied PFAS (except PFTrDA, 10.2 ± 6.3), ranging from 51.3 ± 10.1% (PFDA) 91.7 ± 10.8 (PFBA) for PFCAs and 60.7 ± 13.7% (PFOS) 76.6 ± 9.4 (PFBS) for PFSAs.

As PFAS chain length increased, the dependence of bioaccessibility on the SSSM composition increased, with the shorter chain compounds less affected by the SSSM composition. This is illustrated in Figure 3-2 which plots the relative standard deviation of the $f_{bioaccessible}$ of a given PFAS across the range of SSSM compositions examined, against PFAS carbon number for both PFCAs and PFSAs.

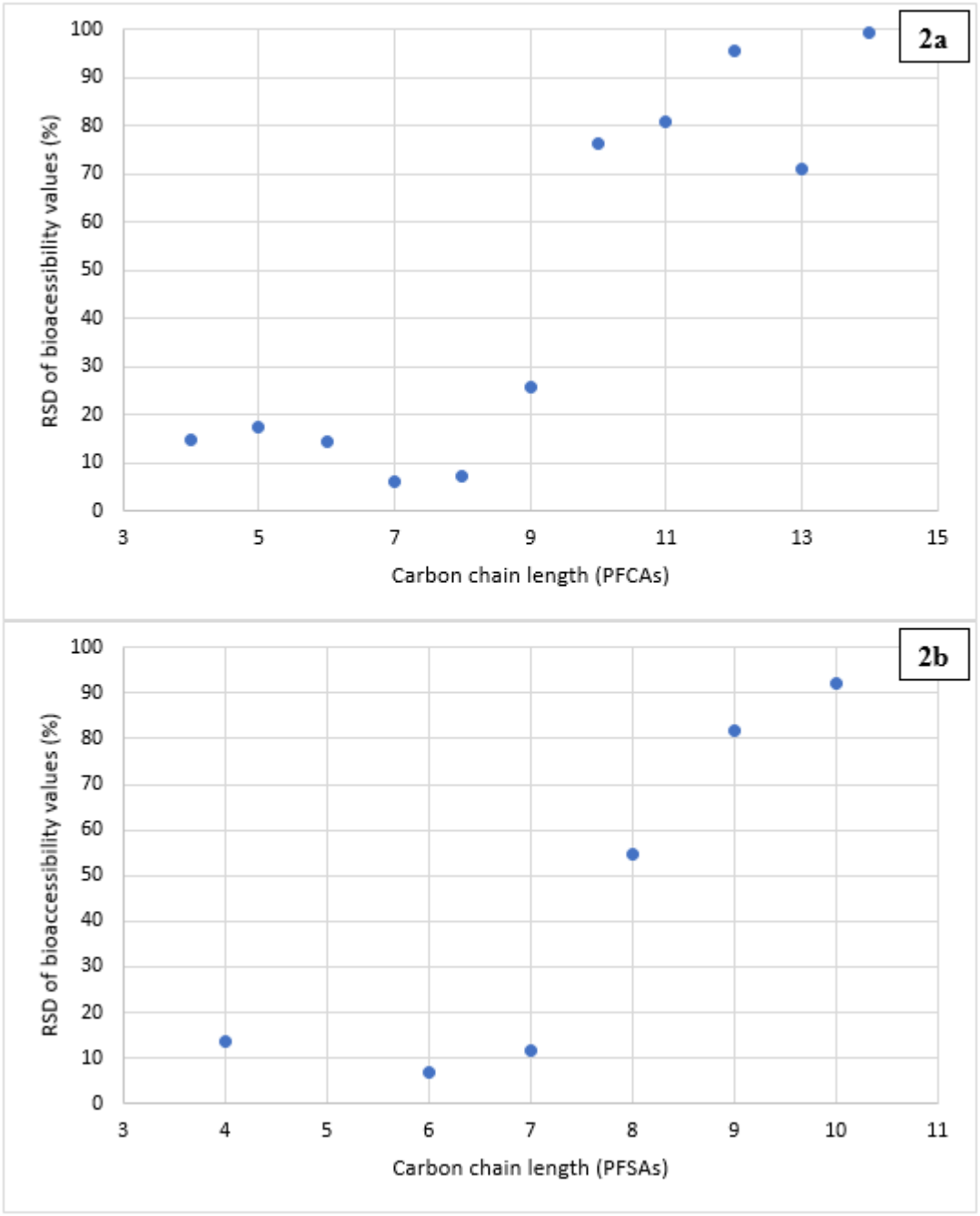


Figure 3-2: Plot of PFAS carbon number versus relative standard deviation (RSD) of the bioaccessibility values obtained for individual PFAS across the range of SSSM compositions examined for: (a) PFCAs and (b) PFSAs.

The overall trends seen for both PFCAs and PFSAs can be attributed to the different properties of the aqueous-based sweat compared to the oily sebum and the varying physicochemical properties of our target PFAS based on chain length (e.g., $\log K_{OW}$ and water solubility. There is a significant negative correlation between $f_{bioaccessible}$ and $\log K_{ow}$ in 100%

sweat for both PFCAs ($r = -0.95$, $p \leq 0.001$) and PFSAs ($r = -0.93$, $p = 0.006$). In 100% sebum however, the $f_{bioaccessible}$ and the $\log K_{ow}$ PFCAs did not show a correlation ($r = 0.06$, $p = 0.85$), while PFSAs showed a moderate positive correlation although not significant ($r = 0.68$, $p = 0.14$). In the most physiologically-relevant SSSM (1:1 sweat:sebum) a significant negative correlation was seen for PFCAs for the $f_{bioaccessible}$ and the $\log K_{ow}$ ($r = -0.86$, $p \leq 0.001$). While a negative correlation was also seen for PFSAs in the 1:1 mixture, it was not significant ($r = 0.76$, $p = 0.08$). Figure 3-5, which shows the $f_{bioaccessible}$ values of each individual PFAS averaged across all 4 SSSMs further supports this overall trend, where the PFAS average $f_{bioaccessible}$ decreased with increasing chain length.

When calculating the correlation between $f_{bioaccessible}$ and water solubility, no clear correlation was seen in 100% sweat ($r = 0.32$, $p = 0.54$ and $r = 0.36$, $p = 0.76$ for PFCAs and PFSAs, respectively). Similarly, in the 1:1 sweat:sebum mixture, no correlation was seen ($r = 0.53$, $p = 0.28$ (PFCAs) and $r = 0.60$, $p = 0.59$ (PFSAs)). In 100% sebum a negative correlation was seen between $f_{bioaccessible}$ and water solubility ($r = -0.88$, $p = 0.02$) for PFCAs, while this trend was not seen for PFSAs ($r = -0.29$, $p = 0.14$). It is worth noting that a unified single experimental and/or modelled approach that provides accurate values of physicochemical properties for all the studied PFAS could not be found in the available literature, which may affect the reliability of the statistical analysis conducted because the reported values for e.g., $\log K_{ow}$ and water solubility of different PFAS were obtained from different sources using different approaches for their estimation.

3.3.2. Effects of cosmetics on the dermal bioaccessibility of PFAS from indoor dust

The topical application of personal care products or cosmetics may either enhance or diminish the release of a chemical ($f_{bioaccessible}$) from particles adhering to the skin (Pawar et al., 2017). To evaluate the effect of cosmetics on the dermal bioaccessibility of PFAS in indoor dust, we estimated the $f_{bioaccessible}$ of target PFAS from dust into 1:1 sweat:sebum mixture in the presence

of four different, widely used personal care products (each tested separately). The 1:1 sweat:sebum mixture was used as the control as it is considered the most physiologically relevant composition (Buckley and Lewis, 1960). The products evaluated were sunscreen lotion, moisturising cream, deodorant stick, and foundation. As the aim of our study was to investigate the impact of cosmetics on the bioaccessibility of PFAS from indoor dust, rather than the release of PFAS from cosmetics; none of the chosen cosmetic products contained PFAS. Sample blanks containing a personal care product and SSSM mixture not exposed to dust were included for each tested product.

3.3.2.1. Influence of topically applied cosmetics on the dermal bioaccessibility of PFAS

The effects of the application of cosmetics on the overall $f_{bioaccessible}$ of PFCAs from indoor dust was compared to the $f_{bioaccessible}$ in the control SSSM mixture, and the statistical significance of the observed differences were determined using a paired t-test. Two products significantly affected the overall $f_{bioaccessible}$ of PFCAs: sunscreen ($p = 0.04$) and moisturising cream ($p = 0.03$), both of which decreased PFCAs bioaccessibility from dust (Figure 3-3). This is especially evident for the longer chain PFCAs (PFDoA, PFTrDA and PFTeDA) which were not detected in the SSSM (*i.e., were not bioaccessible*) after the addition of sunscreen. For PFDA and PFUdA however, the addition of sunscreen seemed to increase their $f_{bioaccessible}$ values, while no difference was seen for PFHxA, PFOA and PFNA. The inclusion of deodorant increased the $f_{bioaccessible}$ values for selected PFCAs (PFHxA, PFHpa, PFNA, PFDA, PFUdA and PFTeDA) while the $f_{bioaccessible}$ for ∑PFAS was not significantly increased.

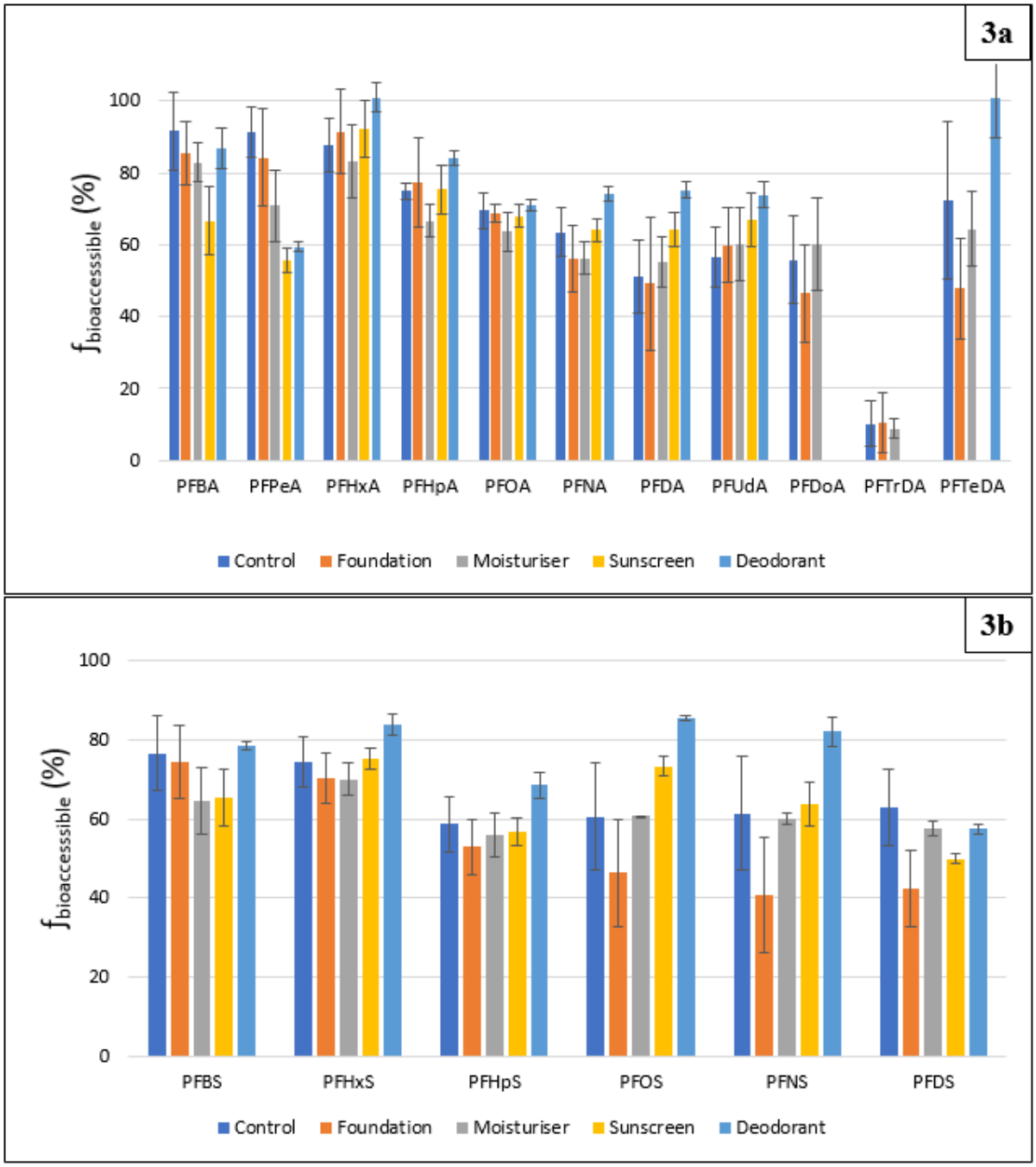


Figure 3-3: Comparison of the effects of applied cosmetics on the bioaccessibility of (a) PFCAs and (b) PFSAs. Error bars represent the standard deviation (n = 3).

All but one of the personal care products examined, significantly affected the overall $f_{bioaccessible}$ of PFSAs compared to the 1:1 sweat:sebum mixture (Figure 3-3). The $f_{bioaccessible}$ values of PFSAs decreased in the presence of foundation ($p = 0.01$) and moisturiser ($p = 0.03$). While all compounds showed a decrease in $f_{bioaccessible}$ with the inclusion of foundation, the effects of moisturiser were less apparent for PFOS and PFNS compared to other PFSAs.

However, a significant increase in $f_{bioaccessible}$ was seen when deodorant was included (p= 0.04), although PFDS had a lower $f_{bioaccessible}$ in the presence of deodorant. The decrease in $f_{bioaccessible}$ seen for both PFSAs and PFCAs has been reported previously for the dermal bioaccessibility of flame retardants (FRs) and polychlorinated biphenyls in the presence of sun- and moisturising creams (Ertl and Butte, 2012; Pawar et al., 2017). This could be explained by a possible retention of the more lipophilic compounds by skin cream lipids. Our results are consistent with previous reports that certain ingredients in cosmetics can alter the composition of the SSSM and thus affect the dermal bioaccessibility of PFAS from dust. The magnitude and nature of the these effects are compound-specific and are dependent on the composition of the personal care products (Pawar et al., 2017; Pont et al., 2004; Walters et al., 1997). Other factors that are hypothesised to affect the bioaccessibility of PFAS from indoor dust are: skin contact time, as well as lipid content and ionic strength of the tested cosmetics. Further studies are needed to investigate the bioaccessibility of PFAS from other sources e.g., from PFAS containing fabrics and cosmetics as well as their subsequent dermal uptake and the effects of different personal care products.

3.3.3. Preliminary estimates of human dermal exposure to PFAS from indoor dust

In the absence of an experimentally determined value, a conservative value of 50% is suggested for dermal absorption by the EU's Scientific Committee of Consumer Safety (SCCS) (SCCS, 2021). Thus, using 50% of the $f_{bioaccessible}$ values obtained for the most physiologically relevant sweat:sebum mixture (1:1), human dermal exposure to target PFAS via contact with indoor dust was estimated (eq. 2) (U.S. EPA, 2011) for both adults and toddlers.

$$DED = \frac{C_{dust} * BSA * DAS * F_A * IEF}{BW} \qquad (2)$$

where *DED*=daily exposure dose (ng/kg bw/day), C_{dust}=PFAS concentration in dust (ng/g), *BSA*=body surface area exposed (cm^2), *DAS*=dust adhered to skin (mg/cm^2), F_A=fraction absorbed by the skin (unitless) (here F_A = 50% of

$f_{bioaccessible}$), *IEF*=indoor exposure fraction (hours spent over a day in an indoor environment) (unitless), BW=body weight (kg).

The exposure parameters applied in eq. 2 were obtained from the USEPA exposure factors handbook (U.S. EPA, 2011) and are summarised in table 3-14. Two exposure scenarios were applied:

i) **Summer:** assuming head, forearms, hands, thighs, lower legs and feet were exposed to dust (i.e., person wearing shorts and t-shirt).

ii) **Winter:** Assuming head and hands exposed to dust (i.e. person wearing full-length trousers, long-sleeve top and socks).

The dermal exposure of two age groups (adults and toddlers) were estimated based on previously reported concentrations of PFAS in household dust by Gebbink et al., 2015. Data from this study were chosen as information on other major pathways of exposure were provided alongside PFAS concentrations in dust. Our estimates (table 3-1) highlight the potentially high dermal exposure to PFAS from contact with indoor dust, particularly in summer. When our dermal exposure values are compared to the EFSA recommended tolerable weekly intake of 4.4 ng/kg bw/week (for the sum of PFOS, PFOA, PFHxS, and PFNA), the exposure during summer can be up to 0.8 ng/kg bw/week for just two out of the four PFAS (PFOS and PFOA) via the dermal pathway alone. For toddlers, the EFSA limit is almost exceeded with PFOS and PFOA accounting for up to 3.2 ng/kg bw/week via dermal exposure to dust. The paper by Gebbink et al did not include PFHxS and PFNA in their study and thus the dermal exposures to PFHxS and PFNA were not calculated.

Table 3-1: Estimated human daily exposure dose (DED in pg/kg bw/day) to selected PFAS via the dermal pathway from household dust based on contact with 1:1 sweat:sebum mixture.

	DED (pg/kg bw/day)			
PFAS	**Adult Summer**	**Toddler Summer**	**Adult Winter**	**Toddler Winter**
PFOS	69.6	284.1	24.1	86.7
PFBA	2.0	8.4	0.7	2.5
PFHxA	6.2	25.1	2.1	7.7
PFOA	43.0	175.6	14.9	53.6
PFDA	2.0	8.1	0.7	2.5
PFDoDA	2.0	8.3	0.7	2.5

The assumption that all $f_{bioaccessible}$ will proceed to penetrate the skin barrier, can be considered a worst-case scenario, as it is highly unlikely that all the bioaccessible fraction will be absorbed, thus a more conservative value of 50% $f_{bioaccessible}$ was used (Pawar et al., 2017; SCCS, 2021). The two factors governing human dermal uptake of chemicals from house dust to the general circulation are: bioaccessibility and the percutaneous penetration rate. The outermost layer of human skin, the *stratum corneum* presents the main barrier to dermal penetration of organic chemicals. There, the major transport mechanism involved in the dermal uptake of organic chemicals is passive diffusion, which is regulated by compound-specific physicochemical properties. For compounds bound to particulate matter i.e. household dust however, the chemical's release from particles into the fluids on the skin surface can have a bigger impact on the resulting dermal uptake. A compound's physicochemical properties would, in theory, make it suitable for dermal uptake, however, if the dermal bioaccessibility is low, the resulting dermal uptake will be minimal (Luo et al., 2020; Pawar et al., 2017; Zeng et al., 2019). Part of the bioaccessible fraction of a chemical could then pass through the *stratum corneum* where it could either be metabolised *in situ* or enter the systemic circulation

($f_{bioavailable}$) through the viable epidermis and dermis layers by diffusion (Ragnarsdóttir et al., 2022). Further studies are needed to determine the subsequent percutaneous penetration rate of various PFAS. Importantly, we highlight that dust is not the only possible source of dermal exposure to PFAS. Dermal uptake from PFAS-containing fabrics and/or cosmetics (Schultes et al., 2018; Xia et al., 2022), could make a substantial additional contribution to exposure that is not accounted for in our estimates and studies of dermal exposure to PFAS arising from such materials are urgently needed.

The calculated dermal exposure of adults was compared to that arising from other pathways as reported previously (Gebbink et al., 2015) (figure 3-4). Given our assumption that 50% the dermal bioaccessible fraction will reach the bloodstream (worst-case scenario), our results were compared to the high exposure scenario reported (95th percentile of each input parameter) (Gebbink et al., 2015).

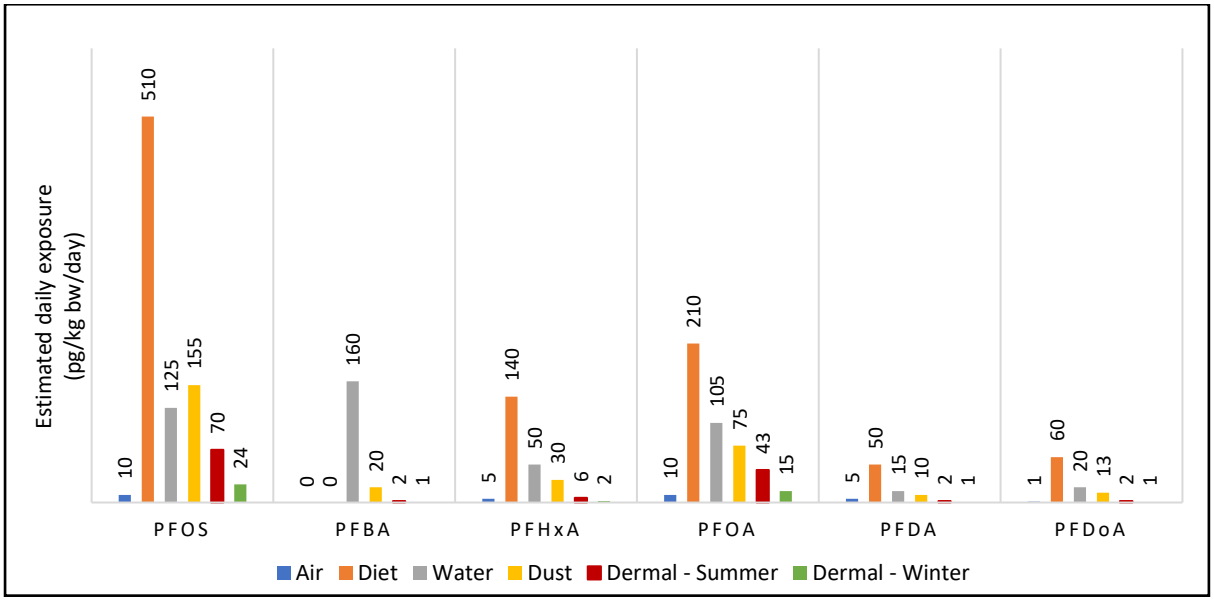


Figure 3-4: Comparison of estimated adult human dermal exposure via contact with dust and other pathways of exposure to target PFAS (high exposure scenario)(Gebbink et al., 2015).

The comparison reveals that under the specific scenarios considered here, diet is the most significant exposure pathway for most of our target PFAS. However, for PFOS and PFOA

the possible daily exposure via dermal exposure via indoor dust was significant. Furthermore, dermal exposure via indoor dust during summer exceeded that via air for all compounds except PFDA. While assuming 50% of the bioaccessible fraction will reach the bloodstream could be an overestimation, we are only accounting for one source of dermal exposure (indoor dust) when many other potential such sources are known i.e. fabrics and cosmetics (Schultes et al., 2018; Xia et al., 2022). Given recent studies have shown positive correlations between the use of personal care products and serum PFAS levels (Serrano et al., 2021; Thépaut et al., 2021); it is clear that further studies are needed to better understand the dermal uptake of PFAS and subsequently the potential contribution of dermal exposure to human body burdens of PFAS.

3.4. Study limitations

It is difficult to exactly mimic *in vivo* situations e.g., the friction on a person's skin surface when they move, so while we tried to closely mimic this *in vitro* by stirring the dust/SSSM/cosmetics test mixtures, we recognise that this does not necessarily accurately reflect real-life dermal exposure conditions and introduces uncertainties into our estimations of possible dermal uptake of PFAS.

3.5. Supporting Information

3.5.1. Synthetic sweat and sebum preparation:

Synthetic sweat and sebum mixtures (SSSM) simulating physiological fluid were prepared using over 25 chemical components according to a previously reported US patent (Stefaniak and Harvey, 2008). Table 3-2 lists the components used in the SSSM preparations. Artificial sweat and sebum mixtures were prepared separately, the sweat mixture was pH adjusted to that of normal human skin (5.3 ± 0.1). Sweat:sebum mixtures were prepared at five different, physiologically relevant ratios (100% sweat, 95:5 sweat:sebum, 1:1 sweat:sebum and 100% sebum) using drops of Tween-80 to prevent phase-separation and simulate naturally secreted SSFL.

Table 3-2: Chemical composition of synthetic human sweat/sebum mixture (SSSM) applied in this study based on a previously published patent (Stefaniak and Harvey, 2008).

Sweat Ingredients	**Measured Conc.**	**Company**
Electrolytes and Ionic Constituents	(g/L)	
Sodium Sulfate	5.83 x 10-2	Sigma Aldrich
Copper Chloride anhydrous	1.60 x 10-4	Merck
Ammonium Hydroxide	1.82 x 10-1	Fisher
Iron sulfate Heptahydrate	2.72 x 10-3	Fisher
Lead- Reference Solution 1000 ppm	2.49 x 10-5	Sigma Aldrich
Manganese- Reference Solution 1000 ppm	1.38 x 10-4	Sigma Aldrich
Nickel- Reference Solution 1000 ppm	2.46 x 10-5	Sigma Aldrich
Zinc - Reference Solution 1000 ppm	8.5 x 10-4	Sigma Aldrich
Sodium Bicarbonate	2.52 x 10-1	FSA
Potassium chloride	4.55 x 10-1	VWR
Magnesium Chloride Hexahydrate	1.67 x 10-2	Sigma Aldrich
Sodium Phosphate Anhydrous Monobasic	4.84 x 10-2	Sigma Aldrich
Calcium Chloride Dihydrate	7.65 x 10-1	Fisher
Sodium chloride	5.84 x10-2	Fisher
Organic Acids and Carbohydrates		
Acetic Acid	7.81 x 10-3	Sigma Aldrich
Butyric Acid	2.11 x 10-4	Sigma Aldrich
D(+) –Glucose	3.06 x 10-2	Sigma Aldrich
Lactic Acid	1.57 x 100	Sigma Aldrich

Essential Amino Acid Mix	2.5 mM each : 17 AA	Sigma Aldrich
Nitrogenous Substances		
Ammonium Chloride	9.92 x 10-3	Fisher
Urea	6.01 x 10-1	Sigma Aldrich
Creatinine	9.50 x 10-3	Sigma Aldrich
SEBUM		
Squalene	0.5151	Sigma Aldrich
Palmityl Palmitate (saturated)	0.9718	Sigma Aldrich
Triolein (Unsaturated)	0.5345	Sigma Aldrich
Cholesteryl Oleate	0.0972	Sigma Aldrich

3.5.2. Personal care products ingredients list

3.5.2.1. Moisturising cream

Aqua, Glycerin, Paraffinum Liquidum, Polyglyceryl-3 Methylglucose Distearate, Dimethicone, Cetyl Palmitate, Cetyl Alcohol, Panthenol, Phenoxyethanol, Caprylyl Glycol, Carbomer, Potassium Hydroxide, Tocopheryl Acetate, Bisabolol, Acrylates/C10-30 Alkyl Acrylate Crosspolymer, Disodium EDTA, Pantolactone, Borago Officinalis Seed Oil, Potassium Carbonate, Pentylene Glycol, Urea, Lactic Acid, Sodium Lactate, Serine, Sorbitol, Sodium Chloride Allatoin.

3.5.2.2. Sunscreen

Aqua, Homosalate, Butyl Methoxydibenzoylmethane, Ethylhexyl Salicylate, Butylene Glycol Dicaprylate/Dicaprate, Alcohol Denat., Bis-Ethylhexyloxyphenol Methoxyphenyl Triazine, Ethylhexyl Triazone, Isopropyl Palmitate, Phenylbenzimidazole Sulfonic Acid, Silica, Tapioca Startch, Diethylamino Hydroxybenzoyl Hexyl Benzoate, Behenyl Alcohol, Cetearyl Alcohol, Methylpropanediol, Glycerin, Glycyrrhiza Inflata Root Extract, Tocopheryl Acetate, Sodium Stearoyl Glutamate, Xanthan Gum, Carbomer, Acrylates/C10-30 Alkyl Acrylate

Crosspolymer, Dimethicone, Sodium Chloride, Sodium Hydroxide, Trisodium EDTA, Ethylhexylglycerin, Phenoxyethanol, Linalool, Limonene, Benzyl Alcohol, Alpha-Isomethyl Ionone, Geraniol, Citronellol, Coumarin, Parfum.

3.5.2.3. Deodorant stick

Cyclopentasiloxane, Aluminum Zirconium Tetrachlorohydrex GLY, Stearyl Alcohol, C12-15 Alkyl Benzoate, PPG-14 Butyl Ether, Hydrogenated Castor Oil, Dimethicone, Parfum, Polyethylene, Helianthus Annuus Seed Oil, Steareth-100, BHT, Tocopheryl Acetate, Alpha-Isomethyl Ionone, Benzyl Alcohol, Benzyl Salicylate, Cinnamyl Alcohol, Citronellol, Coumarin, Geraniol, Hexyl Cinnamal, Hydroxycitronellal, Isoeugenol, Limonene, Linalool.

3.5.2.4. Foundation

Aqua / Water, Dimethicone, Isododecane, Cyclohexasiloxane, Glycerin, Peg-10 Dimethicone, Methyl Methacrylate Crosspolymer, Butylene Glycol, Pentylene Glycol, Synthetic Fluorphlogopite, Disteardimonium Hectorite, Hydroxyethylpiperazine Ethane Sulfonic Acid, Cetyl Peg/Ppg-10/1 Dimethicone, Sodium Chloride, Polyglyceryl-4 Isostearate, Hexyl Laurate, Caprylyl Glycol, Phenoxyethanol, Disodium Stearoyl Glutamate, Tocopherol, Panthenol, Aluminum Hydroxide, Hydroxyethyl Urea, Tin Oxide, Hydrated Silica, Methicone, Pentaerythrityl Tetra-Di-T-Butyl Hydroxyhydrocinnamate [+/- May Contain: Ci 77891 / Titanium Dioxide, Ci 77491, Ci 77492, Ci 77499 / Iron Oxides, Mica, Ci 77510 / Ferric Ammonium Ferrocyanide, Ci 15985 / Yellow 6 Lake, Ci 42090 / Blue 1 Lake, Ci 45410 / Red 28 Lake, Ci 15850 / Red 7].

3.5.3. Sample Extraction and clean-up

3.5.3.1. Dust samples

Dust sample extraction and preparation was based on a previously reported method (Harrad et al., 2020). Triplicate samples (ca. 60 mg each) of unexposed SRM2585 were analysed separately in addition to the exposed dust samples. Briefly, each sample was spiked with 30 μL internal standard mixture followed by the addition of 7 mL of MeOH (0.1% NH_4OH).

Samples were then vortexed for 2 min and ultrasonicated at 20°C for 30 min. The samples were then centrifuged at 3500 RPM for 5 min and the supernatant collected into a new tube. The procedure was repeated two more times and the three fractions combined and concentrated to ~0.5 mL under a gentle stream of nitrogen at 38°C. For clean-up, samples were loaded onto a pre-conditioned (6 mL MeOH + 0.1% NH_4OH) EnviCarb™ (3 mL/250 mg, Merck) SPE cartridge. PFAS were eluted with 5 mL methanol containing 0.1% NH_4OH, the samples concentrated to near dryness before being reconstituted to 200 μL in MeOH containing $^{13}C_4$-PFOS recovery determination (or syringe) standard and transferred to autosampler vials for analysis.

3.5.3.2. SSSM samples

The extraction and preparation of SSSM supernatant samples was based on a method previously reported (Harrad et al., 2019). In short, each sample was spiked with 30 μL internal standard mixture before being loaded onto a Chromabond™ PFAS (6 mL/300mg, Chromabond) SPE cartridge. Cartridges were pre-conditioned with 12 mL MeOH (0.1% NH_4OH) followed by 12 mL MilliQ water. After sample addition, cartridges were dried under vacuum for 5 min. PFAS were eluted with 12 mL MeOH (0.1% NH_4OH) and the eluent collected and concentrated to ~0.5 mL under gentle N_2-flow at 38°C. Samples were then loaded onto a pre-conditioned (6 mL MeOH + 0.1% NH_4OH) EnviCarb™ (3 mL/250 mg, Merck) SPE cartridge. PFAS were eluted with 2 mL methanol (0.1% NH_4OH), with the eluate concentrated to incipient dryness and reconstituted to 200 μL in MeOH containing $^{13}C_4$-PFOS recovery determination standard before transfer to autosampler vials for analysis.

Table 3-3: PFAS concentrations determined in SRM2585 (Organics in indoor dust) in this study (n=6) and concentrations reported elsewhere.

PFAS	Average concentrations (ng/g)	Harrad et al., 2019 (ng/g)	Reiner et al., 2015 (ng/g)
PFBA	214.3 ± 30.3		249
PFPeA	285.8 ± 10.3		226
PFHxA	372.5 ± 80.6		279
PFHpA	372.7 ± 58.9		259
PFOA	659.1 ± 93.5	438.0	561
PFNA	95.1 ± 19.8	59.9	101
PFDA	45.5 ± 12.9		38.6
PFUdA	38.4 ± 10.4		47
PFDoA	31.8 ± 7.5		37
PFTrDA	96.0 ± 43.2		30
PFTeDA	17.7 ± 4.5		19.3
PFBS	31.4 ± 19.1	84.2	
PFHxS	1535.5 ± 212.4	1510.0	1400
PFHpS	27.7 ± 7.0		
PFOS	1860.8 ± 203.9	2500.0	2280
PFNS	13.3 ± 4.3		
PFDS	465.2 ± 52.1		

Table 3-4: Recoveries (expressed as average ± SD percent) of the isotopically labelled internal (surrogate) standards in the analysed samples.

Sample type	M2PFTeDA	M4PFHpA	M5PFPeA	M6PFDA	M7PFUdA	M8PFOA	M8PFOS
100% Sweat	58.5 ± 8.8	74.4 ± 4.5	74.8 ± 6.6	111.1 ± 3.2	71.6 ± 5.1	91.0 ± 3.4	85.2 ± 6.0
95:5 Sweat:sebum	22.0 ± 1.1	101.4 ± 10.3	10.9 ± 10.7	185.7 ± 11.9	81.0 ± 21.4	139.6 ± 13.4	107.1 ± 4.1
1:1 Sweat:Sebum	29.3 ± 10.7	118.6 ± 14.6	32.2 ± 19.5	128.1 ± 2.9	70.2 ± 2.1	152.6 ± 19.3	104.9 ± 2.4
100% Sebum[a]	8.4 ± 7.1	23.2 ± 16.0	22.8 ± 9.8	27.6 ± 8.7	16.4 ± 6.3	23.2 ± 11.9	20.8 ± 13.3
1:1 SSSM/Foundation	50.8 ± 71.1	117.7 ± 21.7	42.8 ± 83.0	151.7 ± 5.0	81.0 ± 26.9	137.6 ± 14.8	115.0 ± 7.1
1:1 SSSM/Moisturizer	31.4 ± 1.4	127.8 ± 1.2	25.5 ± 17.7	146.2 ± 5.0	72.9 ± 7.2	147.0 ± 2.5	115.8 ± 2.2
1:1 SSSM/Sunscreen	38.7 ± 3.8	156.6 ± 28.0	120.1 ± 17.0	153.2 ± 7.9	97.2 ± 57.5	190.6 ± 23.4	126.4 ± 6.6
1:1 SSSM/Deodorant	42.5 ± 7.6	161.5 ± 8.1	116.3 ± 28.5	143.7 ± 1.8	61.1 ± 6.6	197.1 ± 7.2	108.5 ± 8.9
Sample type	**MPFBA**	**MPFBS**	**MPFDoA**	**MPFHxA**	**MPFHxS**	**MPFNA**	
100% Sweat	56.8 ± 16.7	109.5 ± 7.2	50.0 ± 5.2	70.0 ± 9.1	87.0 ± 4.2	98.3 ± 3.6	
95:5 Sweat:sebum	28.2 ± 23.4	11.6 ± 23.4	58.7 ± 44.2	30.5 ± 2.0	77.4 ± 13.0	135.3 ± 5.8	
1:1 Sweat:Sebum	12.9 ± 1.4	78.6 ± 34.3	57.5 ± 13.4	69.1 ± 4.6	136.4 ± 11.6	112.9 ± 8.0	
100% Sebum[a]	16.3 ± 8.6	31.3 ± 11.8	12.6 ± 2.3	19.8 ± 17.0	25.5 ± 17.4	22.6 ± 13.3	
1:1 SSSM/Foundation	20.2 ± 48.2	78.3 ± 27.1	72.6 ± 30.5	76.4 ± 9.5	123.3 ± 22.7	135.7 ± 7.9	
1:1 SSSM/Moisturizer	12.4 ± 6.8	79.6 ± 11.7	63.0 ± 4.3	78.3 ± 8.7	130.8 ± 4.1	133.3 ± 3.3	
1:1 SSSM/Sunscreen	55.4 ± 18.6	232.9 ± 53.1	91.4 ± 46.3	168.3 ± 39.1	168.0 ± 29.7	126.5 ± 6.9	
1:1 SSSM/Deodorant	63.3 ± 19.0	173.3 ± 54.4	62.5 ± 3.0	157.1 ± 32.2	154.3 ± 15.4	108.9 ± 4.9	

[a]The low recoveries in 100% sebum samples is theorised to be due to high lipid content rendering the extraction and clean-up process more difficult.

Table 3-5: Effect of the composition of synthetic sweat and sebum mixtures on the bioaccessibilty ($f_{bioaccessible}$ (%)) of target PFAS from indoor dust.

	100% Sweat	**95:5 Sweat:Sebum**	**1:1 Sweat:Sebum**	**100 % Sebum**
PFBA	92.0 ± 7.9	95.4 ± 7.7	91.7 ± 10.8	67.4 ± 2.8
PFPeA	80.5 ± 10.4	111.6 ± 8.6	91.3 ± 7.1	76.4 ± 3.8
PFHxA	100.5 ± 4.4	71.8 ± 4.4	87.8 ± 7.5	79.4 ± 4.9
PFHpA	87.2 ± 4.8	83.2 ± 3.1	74.9 ± 2.3	82.3 ± 2.5
PFOA	74.9 ±7.9	79.2 ± 10.1	69.6 ± 5.0	82.5 ± 3.9
PFNA	50.2 ± 7.6	54.7 ± 2.3	63.4 ± 6.8	86.8 ± 2.1
PFDA	24.0 ± 1.5	19.5 ± 1.9	51.3 ± 10.1	100.9 ± 4.6
PFUdA	14.2 ± 3.4	19.0 ± 2.5	56.5 ± 8.4	93.8 ± 5.1
PFDoA	7.0 ± 4.7	11.8 ±2.9	55.7 ± 12.2	90.0 ± 2.75
PFTrDA	1.3 ± 0.7	13.4 ± 3.2	10.2 ± 6.3	23.8 ± 2.9
PFTeDA	<MDL[a]	23.0 ± 9.3	72.4 ± 21.9	103.3 ± 0.54
PFBS	68.9 ± 1.1	93.3 ± 6.8	76.6 ± 9.4	72.6 ± 8.1
PFHxS	71.0 ± 5.0	75.3 ± 7.4	74.3 ± 6.4	83.3 ± 3.9
PFHpS	48.9 ± 6.1	52.7 ± 1.7	58.8 ± 7.0	69.4 ± 4.7
PFOS	33.0 ± 5.7	28.1 ± 3.1	60.7 ± 13.7	91.2 ± 2.5
PFNS	13.4 ± 2.2	14.1 ± 1.4	61.4 ± 14.5	84.8 ± 3.7
PFDS	6.1 ± 0.7	14.5 ± 2.2	63.0 ± 9.7	90.8 ± 8.6

[a] Compound below MDL

Table 3-6: Mass balance for target PFAS after dust exposure to 100% sweat (n = 6).

	SSSM (%)	Dust (%)	Sum (%)
PFBA	92.0 ± 7.9	6.8 ± 0.6	98.8 ± 7.9
PFPeA	80.5 ± 10.4	8.1 ± 1.1	88.5 ± 10.4
PFHxA	100.5 ± 4.4	10.1 ± 1.6	110.6 ± 4.6
PFHpA	87.2 ± 4.8	12.2 ± 1.6	99.3 ± 5.1
PFOA	74.9 ±7.9	24.7 ± 3.7	99.6 ± 8.7
PFNA	50.2 ± 7.6	47.7 ± 5.2	97.9 ± 9.2
PFDA	24.0 ± 1.5	84.8 ± 5.5	108.8 ± 5.7
PFUdA	14.2 ± 3.4	91.1 ± 6.7	105.3 ± 7.6
PFDoA	7.0 ± 4.7	96.3 ± 7.2	103.3 ± 8.6
PFTrDA	1.3 ± 0.7	58.2 ± 12.2	59.5 ± 12.2
PFTeDA	<MDL[a]	99.4 ± 6.4	99.4 ± 6.4
PFBS	68.9 ± 1.1	13.2 ± 2.5	82.1 ± 2.7
PFHxS	71.0 ± 5.0	22.5 ± 3.3	93.5 ± 6.0
PFHpS	48.9 ± 6.1	38.7 ± 2.6	97.2 ± 6.7
PFOS	33.0 ± 5.7	71.0 ± 3.8	104.0 ± 6.8
PFNS	13.4 ± 2.2	85.7 ± 8.0	99.0 ± 8.2
PFDS	6.1 ± 0.7	93.6 ± 10.6	99.7 ± 10.6

[a] Compound below MDL

Table 3-7: Mass balance for target PFAS after dust exposure to 95:5 sweat:sebum (n = 6).

	SSSM (%)	Dust (%)	Sum (%)
PFBA	95.4 ± 7.7	1.5 ± 1.2	96.9 ± 7.8
PFPeA	111.6 ± 8.6	2.2 ± 1.7	113.8 ± 8.8
PFHxA	71.8 ± 4.4	4.9 ± 0.6	76.7 ± 4.4
PFHpA	83.2 ± 3.1	8.9 ± 0.8	92.2 ± 3.2
PFOA	79.2 ± 10.1	21.7 ± 3.0	100.9 ± 10.6
PFNA	54.7 ± 2.3	57.6 ± 2.7	112.2 ± 3.5
PFDA	19.5 ± 1.9	86.2 ± 4.9	105.7 ± 5.3
PFUdA	19.0 ± 2.5	84.1 ± 7.9	103.0 ± 8.2
PFDoA	11.8 ±2.9	82.8 ± 6.7	94.6 ± 7.2
PFTrDA	13.4 ± 3.2	62.0 ± 0.5	75.5 ± 3.2
PFTeDA	23.0 ± 9.3	44.5 ± 10.2	67.5 ± 13.8
PFBS	93.3 ± 6.8	4.9 ± 0.7	98.2 ± 6.9
PFHxS	75.3 ± 7.4	24.6 ± 1.7	99.8 ± 7.6
PFHpS	52.7 ± 1.7	41.3 ± 2.8	94.0 ± 3.3
PFOS	28.1 ± 3.1	77.9 ± 1.4	106.0 ± 3.4
PFNS	14.1 ± 1.4	24.4 ± 7.7	38.5 ± 7.9
PFDS	14.5 ± 2.2	77.5 ± 3.0	92.1 ± 3.7

Table 3-8: Mass balance for target PFAS after dust exposure to 1:1 sweat:sebum (n = 6).

	SSSM (%)	Dust (%)	Sum (%)
PFBA	91.7 ± 10.8	10.3 ± 1.6	102.1 ± 10.9
PFPeA	91.3 ± 7.1	10.2 ± 2.4	101.5 ± 7.5
PFHxA	87.8 ± 7.5	13.7 ± 2.0	101.5 ± 7.8
PFHpA	74.9 ± 2.3	14.4 ± 0.7	89.3 ± 2.4
PFOA	69.6 ± 5.0	18.4 ± 1.3	88.0 ± 5.1
PFNA	63.4 ± 6.8	33.7 ± 6.1	97.2 ± 9.1
PFDA	51.3 ± 10.1	37.1 ± 6.6	88.4 ± 12.1
PFUdA	56.5 ± 8.4	39.0 ± 5.5	95.5 ± 10.0
PFDoA	55.7 ± 12.2	37.4 ± 9.3	93.2 ± 15.3
PFTrDA	13.5 ± 64.0	62.9 ± 16.7	76.4 ± 17.8
PFTeDA	53.8 ± 6.1	36.2 ± 8.7	90.1 ± 9.6
PFBS	76.6 ± 9.4	8.6 ± 0.8	85.2 ± 9.4
PFHxS	74.3 ± 6.4	24.3 ± 4.2	98.6 ± 7.6
PFHpS	58.8 ± 7.0	25.5 ± 6.5	84.3 ± 9.5
PFOS	60.7 ± 13.7	33.5 ± 10.3	94.2 ± 17.1
PFNS	61.4 ± 14.5	26.6 ± 6.2	87.9 ± 15.8
PFDS	63.0 ± 9.7	24.5 ± 7.3	87.5 ± 12.1

Table 3-9: Mass balance for target PFAS after dust exposure to 100% sebum (n = 6).

	SSSM (%)	Dust (%)	Sum (%)
PFBA	67.4 ± 2.8	22.0 ± 1.0	89.4 ± 3.0
PFPeA	76.4 ± 3.8	26.2 ± 4.0	102.5 ± 5.6
PFHxA	79.4 ± 4.9	17.6 ± 2.5	97.0 ± 5.5
PFHpA	82.3 ± 2.5	15.0 ± 2.8	97.2 ± 3.7
PFOA	82.5 ± 3.9	10.7 ± 2.5	93.2 ± 4.6
PFNA	86.8 ± 2.1	10.0 ± 1.3	96.8 ± 2.5
PFDA	100.9 ± 4.6	7.2 ± 0.6	108.1 ± 4.6
PFUdA	93.8 ± 5.1	7.7 ± 0.9	101.1 ± 5.1
PFDoA	90.0 ± 2.7	8.9 ± 1.2	98.9 ± 3.0
PFTrDA	23.8 ± 2.9	17.8 ± 2.5	41.6 ± 3.8
PFTeDA	103.3 ± 0.5	9.2 ± 1.7	112.5 ± 1.7
PFBS	72.6 ± 8.1	13.8 ± 0.9	86.4 ± 8.1
PFHxS	83.3 ± 3.9	12.0 ± 2.0	95.4 ± 4.4
PFHpS	69.4 ± 4.7	9.0 ± 1.0	78.4 ± 4.8
PFOS	91.2 ± 2.5	8.8 ± 2.3	99.9 ± 3.4
PFNS	84.1 ± 3.7	6.1 ± 0.5	90.2 ± 4.4
PFDS	90.8 ± 8.6	3.9 ± 0.4	94.7 ± 8.6

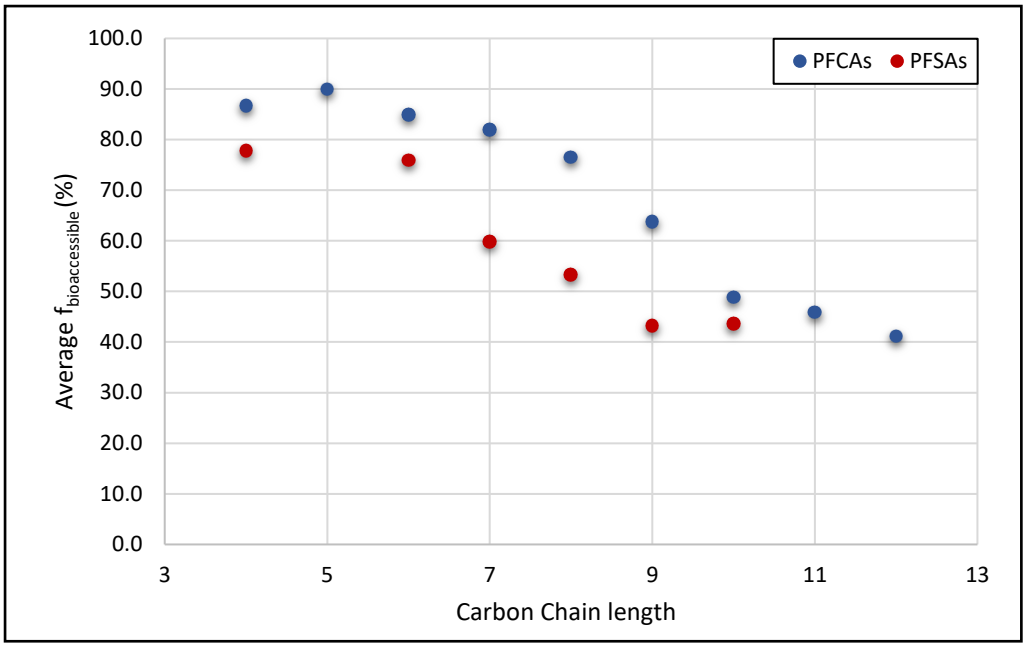


Figure 3-5: Average values of $f_{bioaccessible}$ in all SSSM mixtures against PFAS carbon chain length.

Table 3-10: Mass balance for target PFAS after dust exposure to 1:1 sweat:sebum in combination with foundation (n = 3).

	SSSM (%)	Dust (%)	Sum (%)
PFBA	85.5 ± 8.9	13.4 ± 1.4	98.9 ± 9.0
PFPeA	84.3 ± 13.7	13.2 ± 3.1	97.5 ± 14.0
PFHxA	91.5 ± 11.9	12.4 ± 1.7	103.9 ± 12.0
PFHpA	77.4 ± 12.3	14.5 ± 0.3	92.0 ± 12.4
PFOA	68.8 ± 2.4	24.3 ± 3.0	93.1 ± 3.8
PFNA	56.1 ± 9.4	30.0 ± 3.5	86.2 ± 10.0
PFDA	49.2 ± 18.4	40.5 ± 10.4	89.7 ± 21.1
PFUdA	59.9 ± 10.2	40.1 ± 16.4	100.0 ± 19.4
PFDoA	46.4 ± 13.7	66.1 ± 15.5	112.5 ± 20.7
PFTrDA	10.4 ± 8.4	69.6 ± 0.3	80.1 ± 8.4
PFTeDA	47.8 ± 14.1	54.1 ± 11.7	101.9 ± 18.3
PFBS	74.5 ± 9.4	11.2 ± 1.6	85.6 ± 14.2
PFHxS	70.5 ± 6.4	22.5 ± 5.1	93.0 ± 5.1
PFHpS	52.9 ± 7.0	20.3 ± 5.8	73.2 ± 8.03
PFOS	46.3 ± 13.7	26.4 ± 12.0	72.7 ± 15.7
PFNS	40.7 ± 14.5	21.9 ± 10.3	62.6 ± 18.2
PFDS	42.3 ± 9.6	24.1 ± 9.5	66.4 ± 13.5

Table 3-11: Mass balance for target PFAS after dust exposure to 1:1 sweat:sebum in combination with moisturiser (n = 3).

	SSSM (%)	Dust (%)	Sum (%)
PFBA	82.9 ± 5.4	27.6 ± 1.1	110.6 ± 5.5
PFPeA	71.0 ± 9.9	33.3 ± 5.5	104.3 ± 11.4
PFHxA	83.3 ± 10.3	32.6 ± 2.4	115.8 ± 10.5
PFHpA	66.7 ± 4.4	32.3 ± 2.9	99.0 ± 5.3
PFOA	63.6 ± 5.5	29.1 ± 6.0	92.7 ± 8.2
PFNA	56.2 ± 4.4	30.4 ± 0.9	86.7 ± 4.5
PFDA	55.3 ± 7.0	33.3 ± 3.4	88.6 ± 7.8
PFUdA	60.4 ± 10.2	34.9 ± 0.1	95.2 ± 10.2
PFDoA	60.2 ± 13.0	33.8 ± 4.8	93.9 ± 13.9
PFTrDA	8.9 ± 2.9	77.4 ± 8.4	86.3 ± 8.9
PFTeDA	64.5 ± 10.5	26.2 ± 0.9	90.7 ± 10.5
PFBS	64.6 ± 8.3	28.5 ± 8.9	93.2 ± 12.2
PFHxS	70.0 ± 4.1	24.2 ± 3.3	94.2 ± 5.3
PFHpS	55.9 ± 5.6	22.2 ± 1.4	78.1 ± 5.8
PFOS	60.8 ± 4.9	26.0 ± 0.7	86.8 ± 0.7
PFNS	60.1 ± 1.5	19.3 ± 0.5	79.4 ± 1.6
PFDS	57.5 ± 1.8	20.7 ± 0.2	78.2 ± 1.8

Table 3-12: Mass balance for target PFAS after dust exposure to 1:1 sweat:sebum in combination with sunscreen (n = 3).

	SSSM (%)	Dust (%)	Sum (%)
PFBA	66.7 ± 9.4	24.4 ± 3.1	91.2 ± 9.9
PFPeA	55.6 ± 3.5	14.3 ± 2.6	69.9 ± 4.4
PFHxA	92.2 ± 7.7	20.8 ± 4.8	113.0 ± 9.1
PFHpA	75.3 ± 6.8	22.1 ± 4.2	97.5 ± 8.0
PFOA	67.9 ± 3.2	22.8 ± 2.9	90.8 ± 4.3
PFNA	64.0 ± 3.3	29.0 ± 1.7	93.0 ± 3.7
PFDA	64.2 ± 4.7	35.7 ± 2.1	99.9 ± 5.1
PFUdA	67.0 ± 7.3	36.5 ± 1.4	103.6 ± 7.5
PFDoA	<MDL[a]	35.8 ± 2.9	35.8 ± 2.9
PFTrDA	<MDL[a]	28.4 ± 2.1	28.4 ± 2.1
PFTeDA	<MDL[a]	24.9 ± 2.7	24.9 ± 2.7
PFBS	65.5 ± 7.1	16.4 ± 1.8	81.9 ± 7.4
PFHxS	75.3 ± 2.7	23.3 ± 2.0	98.6 ± 3.4
PFHpS	56.7 ± 3.5	19.4 ± 0.2	76.1 ± 3.5
PFOS	73.3 ± 2.5	27.7 ± 2.0	100.9 ± 3.2
PFNS	63.7 ± 5.4	22.0 ± 4.3	85.7 ± 6.9
PFDS	49.9 ± 1.3	18.8 ± 2.2	68.7 ± 2.6

[a] Compound below MDL

Table 3-13: Mass balance for target PFAS after dust exposure to 1:1 sweat:sebum in combination with deodorant (n = 3).

	SSSM (%)	Dust (%)	Sum (%)
PFBA	86.8 ± 5.6	21.2 ± 1.7	107.9 ± 5.9
PFPeA	59.4 ± 1.3	11.5 ± 1.0	70.9 ± 1.6
PFHxA	101.1 ± 4.1	14.1 ± 1.4	115.1 ± 4.3
PFHpA	84.1 ± 1.9	15.8 ± 1.5	100.0 ± 2.4
PFOA	70.9 ± 1.7	17.6 ± 1.2	88.6 ± 2.1
PFNA	74.2 ± 2.1	24.0 ± 2.3	98.1 ± 3.1
PFDA	75.3 ± 2.3	29.7 ± 2.1	105.0 ± 3.1
PFUdA	73.9 ± 3.7	26.9 ± 3.0	100.7 ± 4.8
PFDoA	<MDL[a]	28.7 ± 0.6	28.7 ± 0.6
PFTrDA	<MDL[a]	18.8 ± 4.4	18.8 ± 4.4
PFTeDA	100.8 ± 11.0	28.9 ± 1.9	129.7 ± 11.1
PFBS	78.7 ± 1.1	11.7 ± 2.3	90.4 ± 2.5
PFHxS	83.7 ± 2.7	16.4 ± 1.8	100.13.2
PFHpS	68.5 ± 3.4	14.2 ± 1.2	82.7 ± 3.6
PFOS	85.6 ± 0.5	17.3 ± 2.1	102.8 ± 2.2
PFNS	82.1 ± 3.8	15.6 ± 1.3	97.6 ± 4.0
PFDS	57.5 ± 1.2	12.4 ± 1.3	70.0 ± 1.8

[a] Compound below MDL

Table 3-14: Parameters used in dermal exposure assessment of target PFAS:

a. Dust adhered to skin (U.S. EPA, 2011):

Dust adhered to skin (mg/cm^2)		
	Adults	**Toddler**
Head	0.024	0.054
Arms	0.038	0.048
Hands	0.160	0.170
Legs	0.019	0.051
Feet	0.140	0.200

b. Skin Surface Area (U.S. EPA, 2011), calculated based on two seasons: i) Summer: Assuming head, forearms, hands, thighs, lower legs and feet exposed to dust and ii) Winter: Assuming head and hands exposed to dust.

Surface Area (cm^2)				
	Adult		**Toddler**	
	Male	**Female**	**Male**	**Female**
Head	1360.0	1140.0	615.5	592.8
Forearms	1460.0	1090.0	425.6	418
Hands	1070.0	870.0	364.8	372.4
Thighs	4113.0	3560.0	1140	1185.6
Lower legs	2710.0	2300.0	782.8	790.4
Feet	1380.0	1210.0	494	478.8

c. PFAS concentration in dust (obtained from Gebbink et al., 2015), absorbed fraction (F_A = bioaccessible fraction), indoor exposure fraction (IEF) and body weight (BW)(U.S. EPA, 2011).

	C (ng/g)	F_A	IEF		BW (kg)	
			Adult	Toddler	Adult	Toddler
PFOS	180.0	0.61	0.17	0.25	70	15
PFBA	3.5	0.92	0.17	0.25	70	15
PFHxA	11.0	0.88	0.17	0.25	70	15
PFOA	97.0	0.70	0.17	0.25	70	15
PFDA	6.1	0.51	0.17	0.25	70	15
PFDoDA	5.7	0.56	0.17	0.25	70	15

4. DERMAL BIOAVAILABILITY OF PFAS

This chapter includes material taken verbatim from the following article:

Ragnarsdóttir, O.; Abdallah, M. A.-E.; Harrad, S. 2023. Dermal Bioavailability of Perfluoroalkyl Substances (PFAS) using *in vitro* 3D-Human Skin Equivalent Models. *Under review in Environment International, January 2024.*

O.R. conducted the experiments, interpreted the data, wrote the original draft and was the corresponding author. S.H. and M. A.-E. A. conceived and designed the experiment, assisted with the interpretation of the data, reviewed, and edited the manuscript.

4.1. Introduction

Per- and polyfluoroalkyl substances (PFAS) are a class of synthetic organic chemicals comprising thousands of compounds. Their hydrophobic and lipophobic properties along with their chemical and thermal stability has made them popular for use in a wide range of industries and consumer products (Buck et al., 2011; Glüge et al., 2020a). PFAS were first detected in human serum in 2001 (Hansen et al., 2001). Since then, significant human health effects of PFAS have been highlighted i.e., lowered immune response to vaccination (Abraham et al., 2020; Grandjean et al., 2012, 2017a), impaired liver function (Salihovic et al., 2018a) and decreased birth weight (Meng et al., 2018; Sagiv et al., 2018). Such findings led the European Food Safety Authority (EFSA), to set a recommended tolerable weekly intake of 4.4 ng/kg bw/week for the sum of four PFAS (perfluorooctanoic acid (PFOA), perfluoronoananoic acid (PFNA), perfluorohexane sulfonic acid (PFHxS), and perfluorooctane sulfonic acid (PFOS)) in 2020 (EFSA CONTAM Panel, 2020).

Diet and drinking water are considered the main pathways of human exposure to PFAS followed by indoor air and dust (Sunderland et al., 2019). More recently, PFAS have been identified in a wide range of products that come into contact with skin, i.e. cosmetics, hand sanitizers, water-repellent clothing and even school uniforms (Schultes et al., 2018; van der Veen et al., 2020; Whitehead et al., 2021; Xia et al., 2022). Furthermore, significant

correlations have been reported between the use of personal care products and PFAS concentrations in both human serum and breast milk (Colles et al., 2020; Kang et al., 2016; Serrano et al., 2021; Thépaut et al., 2021). Additional correlations have been found between serum levels and PFAS detected in hand wipe samples (Kim et al., 2019; Poothong et al., 2019).

Of the areas of the body, the forehead, scalp, and neck have the second highest rate of topical absorption (Law et al., 2020), these areas are likely to be frequently exposed via the use of personal care products, increasing the likelihood of dermal uptake of the PFAS used in these products. Several other factors can affect dermal absorption such as molecular weight, compound-specific physicochemical properties (e.g., log K_{OW}), as well as the dose, the compounds vehicle and its pH, duration of exposure, skin surface area exposed, in addition to the skin site of exposure (i.e., skin thickness and number of hair follicles) (Law et al., 2020; Lipinski et al., 2001).

Two factors play a role in the process of dermal uptake of a chemical from a source material. In the first step a chemical needs to be released from the source material, i.e., fabric or dust, for it to be available for dermal absorption. This fraction which is released into the body's fluids (in the case of skin this is a mixture of sweat and sebum) is referred to as the *bioaccessible* fraction (Ertl and Butte, 2012; Pawar et al., 2017). This can be a rate limiting step in dermal absorption and has been previously reported for PFAS by our group (Collins et al., 2015; Ragnarsdóttir et al., 2023). The second step in the process would be the transdermal permeation of the *bioaccessible* fraction through the skin and into the systemic circulation. It is not guaranteed that all the *bioaccessible* fraction will reach the systemic circulation. The fraction that does reach the systemic circulation is referred to as the *bioavailable* fraction (Ertl and Butte, 2012; Ragnarsdóttir et al., 2023).

A few studies have investigated possible dermal permeation of PFAS (Abraham and Monien, 2022; Chen et al., 2022; Kissel et al., 2023). An *in vivo* study tested the dermal permeation of 15 PFAS in male Sprague-Dawley rats and found that a fraction of both perfluoroalkyl carboxylates (PFCAs) and perfluoroalkyl sulfonates (PFSAs) were able to penetrate rat skin. The study found that perfluoroheptanoic acid (PFHpA) and perfluorobutane sulfonic acid (PFBS) showed the greatest absorption efficiency with 16% and 18% of the applied dose being absorbed respectively, 144 h after exposure. This study also found serum PFAS concentration peaked 8-72 h after dermal exposure, which is significantly later than after oral exposure (1-24 h) (Chen et al., 2022). Another study used a single human subject, exposed to $^{13}C_4$-PFOA mixed into a commercial sunscreen. A peak serum concentration (132 ng/L) was observed 22 days after application supporting the suggestion that dermal exposure can be long-lasting and indeed contribute to total body burdens of PFAS (Abraham and Monien, 2022). Additionally, a paper estimating the dermal absorption of neutral PFAS from the gas phase, identified 11 PFAS, e.g. N-Methyl- and N-Ethyl-perfluorobutyl sulfonamido ethanol (N-MeFBSE and N-EtFBSE) as well as N-Methyl- and N-Ethyl-perfluorohexyl sulfonamido ethanol (N-MeFHxSE and n-EtFHxSE) for which dermal uptake could be a significant pathway compared to inhalation (Kissel et al., 2023).

Although modelling can be a good tool to evaluate the possible dermal uptake of a huge group of chemicals such as PFAS, there are certain limitations in the absence of reliable experimental data. Models are based on physicochemical properties of the compounds, which for surfactants like PFAS can be difficult to determine (Wang et al., 2011). Additionally, when evaluating the possible dermal uptake of compounds from indoor air the hydration of the stratum corneum can fluctuate based on the skins environment which can influence the barrier function of the skin. This could affect the accuracy of the model if not accounted for in its calculations (Weschler and Nazaroff, 2014).

While *in vivo* studies have the benefit of a complete metabolic and physiological system, there are several ethical and technical limitations to such studies, especially those involving human subjects (Ragnarsdóttir et al., 2022). Furthermore, human skin barrier functions can vary based on age, race and skin hydration, making it more desirable to have more than one subject in dermal uptake studies, which in turn raises further ethical questions (Law et al., 2020). While ethical concerns also apply to the use of *in vivo* animal models they remain in use, albeit in decline. However, uncertainties with data derived from animal studies arise due to interspecies variation (e.g., number of hair follicles, intercellular subcutaneous lipids and the skin barrier function) (Abdallah et al., 2015b). One study comparing *in vitro* human and rat skin dermal permeation of 14 substances with various physicochemical properties found that human skin was less permeable for all target compounds. No constant factor of difference could be identified (Van Ravenzwaay and Leibold, 2004b). In another study which also included an *in vivo* rat model, they found that for 9 out of 12 tested chemicals, *in vitro* human skin was less permeable than the *in vivo* rat skin while the *in vitro* rat skin was more permeable than human skin for all tested compounds (Van Ravenzwaay and Leibold, 2004a). A third study found that a higher fraction of tetrabromobisphenol A Bis(2,3-dibromopropyl) ether (TBBPA-BDBPE) permeated through both *in vivo* and *ex vivo* rat skin compared to *ex vivo* human skin (Knudsen et al., 2019). Thus, basing human dermal exposure estimates only on data from rat models can lead to overestimation in risk assessment.

3D-human skin equivalent (3D-HSE) models are commercially available, multilayer dermal tissues that mimic the histological and physiological properties of normal human skin. These models make it possible to conduct dermal permeation studies without the use of human or animal subjects in line with the 3R principles (replacement, reduction and refinement) (Ragnarsdóttir et al., 2022). These models were originally developed for the pharmaceutical industry but have been used in previous permeation studies for hazardous

industrial chemicals, where they have shown similar barrier function as excised human skin (Abdallah et al., 2015b; Schäfer-Korting et al., 2008). A study from 2006 comparing the permeation of three 3D-HSE models, human excised skin and pig skin using 9 different chemicals with varying physicochemical properties found that while the permeation through the 3D-HSE models were higher than those of the ex vivo human skin, these models would still be feasible for *in* vitro dermal uptake studies (Schäfer-Korting et al., 2008). Since this study, the 3D-HSE models have been further developed to enhance their barrier function. Using such models listed under the "enhanced barrier function" category, our research group has successfully substituted human *ex vivo* skin with 3D-HSE models to investigate the dermal absorption of various brominated and chlorinated organophosphate flame retardants. While the permeability was slightly increased for the 3D HSE models compared to excised human skin for some of the tested chemicals, the difference was not significant ($p > 0.05$) (Abdallah et al., 2016, 2015b). In the present study, 3D-HSE models (also marketed as having "enhanced barrier function") were applied, for the first time, to investigate the dermal bioavailability of 17 PFAS (10 PFCAs and 7 PFSAs). We compare the dermally bioavailable fractions that permeated the skin barrier to the fraction retained within the skin tissue, and the unabsorbed fractions after 36 h exposure. Finally, the permeation coefficient (K_p), flux (J_{ss}) and lag time (t_{lag}) were determined, providing novel insights into the dermal bioavailability of the studied PFAS.

4.2. Materials and Methods

4.2.1. Materials

Experiments were conducted according to the OECD guidelines for *in vitro* dermal absorption testing (OECD, 2004a). The supplier instructions of the 3D-HSE models were also taken into consideration. The study protocol received ethical approval (ERN_19-0779) from the University of Birmingham. Dulbecco's Modified Eagle Medium (DMEM), HPLC grade methanol, ammonium hydroxide, ammonium acetate, Optima LC-MS grade methanol, and Optima LC/MS grade water were obtained from Fisher Scientific (Loughborough, UK). Native

and mass labelled PFAS standards were purchased from Wellington Laboratories Inc. (Guelph, Canada). Target compounds included C_{5-14} PFCAs and C_{4-10} PFSAs. PFAS stock solutions (10 ng/μL) were prepared in methanol.

4.2.2. Test Matrices and Permeation Assay Protocol

Episkin RHE/L/13 (1.07 cm^2) human skin equivalent kit was obtained from Episkin (Lyon, France). Upon receipt, tissues were equilibrated overnight with the supplied maintenance medium at 5% CO_2 at 37°C before the start of exposure. Figure 4-3 in the Supporting Information compares the 3D-HSE models and excised human skin. According to OECD guidelines (OECD, 2004a) 500 ng/cm^2 (100 μL) net loading of each target PFAS was applied to each skin tissue based on the exposed surface area. The Episkin tissues were mounted in Franz-type diffusion cells using special inserts constructed for this model and a DMEM-based culture medium was used as receptor fluid (RF). Figure 4-4 depicts the experimental set-up. All experiments were performed in triplicate. Following 30 minute equilibration, target PFAS were applied to the skin surface in the donor compartment. The DMEM-based receptor fluid was sampled (2 mL) at fixed time points (0.5, 1, 2, 4, 8, 10, 12, 14, 16, 19, 22, 24, 28, 32, and 36 h) and immediately replaced with fresh fluid. After 36 h the skin surface was washed thoroughly with cotton buds impregnated with methanol (MeOH, 5 times). The donor compartment was then washed (5 x 1 mL) with MeOH before the tissues were removed from the inserts and stored for analysis. Finally, the receptor compartment was washed with 5 x 1 mL aliquots of MeOH. Due to the high number of samples generated, the cost of analysis in the present study and the fact that negligible permeation was detected for C ≥ 9 PFCAs and C ≥ 8 PFSAs after 24 h, no further time-points were collected past 24 h for those compounds.

4.2.3. Sample Extraction and Chemical Analysis

Each permeation assay generated five different types of samples comprising: receptor fluid ((RF) at 15 timepoints and receptor compartment wash (which together with RF represent the

absorbed fraction); skin surface wash (cotton buds), and donor compartment wash (which combined comprise the *unabsorbed fraction*), plus skin tissue (*skin depot*). Samples were extracted based on a method previously reported (Harrad et al., 2019). In short, receptor fluid samples (n = 180) were extracted using Chromabond™ PFAS (6 mL/300 mg, Chromabond) SPE cartridges followed by clean-up using EnviCarb™ SPE cartridges. Skin samples (n = 27) were homogenized in 2 mL MeOH followed by 5 min sonication and centrifugation. The samples were concentrated to *ca* 1 mL and PFAS were extracted using the same protocol as receptor fluid samples. Cotton bud samples (n = 27) were extracted with basic MeOH by ultrasonication followed by a clean-up by passing through 0.2 μm syringe filters. Donor and receptor compartment washes (n = 54) were concentrated down using a gentle N_2 flow followed by cleanup using 0.2 μm syringe filters or EnviCarb™ SPE cartridges. A detailed description of sample extraction methods is provided as Supporting Information.

Target PFAS were analyzed on a Sciex Exion UPLC coupled to a Sciex 5600+ qTOF MS operated in negative mode based on a previously reported method (Harrad et al., 2019). Detailed instrumental parameters are provided in Supporting Information.

4.2.4. Quality Assurance and Quality Control

All experiments were performed in triplicate. In addition, a "field" blank comprising of a skin tissue exposed to solvent only but otherwise treated as a sample, was included in each sample batch (n = 3). No target compound was detected in concentrations above the limit of detection (LOD) in the blank samples so no blank correction was needed. The barrier function of the 3D-HSE models have been tested with the use of positive and negative controls. Triton-X-100 was used as a positive control and showed approximately 100% permeation, while the negative control (decabromodiphenyl ethane) showed 0% permeation 24 hours after exposure. Identification and quantification of target analytes were performed according to the relative retention times to the corresponding isotope labelled surrogate standard and the accurate mass

of each target PFAS. The robustness of the experimental approach was investigated by calculating the mass balance. Mass balance results revealed generally good recoveries overall (77-113%, of the target compounds). Further details on QA/QC measures including method accuracy, precision, and limits of quantification for each compound are provided in chapter 2. Methodology.

4.2.5. Data Analysis

Using Fick's first law of diffusion, a quantitative description of the target compound permeation through the skin barrier was obtained (equation 1) (Niedorf et al., 2008)

$$J_{ss} = \frac{\Delta m}{\Delta t * A} = \frac{D * K * \Delta C}{\Delta x} \qquad (1)$$

Where J_{ss} = steady-state flux [ng/cm^2*h]; Δm = permeated mass [ng]; Δt = time interval [h]; D = diffusion coefficient [cm^2 /h]; K = partition coefficient; A = area [cm^2]; Δc = concentration difference [ng/cm^3]; Δx = thickness of membrane [cm].

When using infinite-dose configurations, where the donor concentrations far exceed the concentrations in the receptor compartment ($C_D >> C_A$), Δc can be replaced by the known donor concentration, C_D, and the permeated mass per time assumed a constant. Thus, an independent measure of membrane resistance against permeation of the test compound, the apparent permeation coefficient (**P_{app}**) can be calculated (equation 2)

$$P_{app} = \frac{J_{ss}}{C_D} \qquad (2)$$

For each compound with a significant permeation after 36 h, cumulative permeation of the compound in the receptor fluid per unit area (ng/cm^2) were plotted against time (hours). Steady state conditions were indicated by a linear regression line ($R^2 \geq 0.9$), where the slope represents the flux (**J_{ss}**). Using a method described by Niedorf et al., 2008 the lower and upper boundary

of the linear range (i.e., steady state conditions) was determined (a summary flow chart is provided in the Supporting Information Figure 4-5).

The lag time ($\mathbf{t_{lag}}$), with non-detectable flux could then be determined. The lag time represents the time of each compound's partition into and diffusion through the skin and into the receptor fluid following the application of each test compound to the skin models. The $\mathbf{t_{lag}}$ represents the time intercept (x intercept) of the regression line over the steady-state region of the permeation curve. Thus, $\mathbf{t_{lag}}$ can be calculated (Equation 3)

$$t_{lag} = -\frac{b_0}{J_{ss}} \qquad (3)$$

where $\mathbf{b_0}$ is the y-intercept of the linear regression line.

4.3. Results and Discussion

4.3.1. Dermal Bioavailability of PFAS

Results are presented as the average of 3 replicates ± standard deviation (SD) and grouped in three major compartments: the directly absorbed dose (cumulative mass in receptor fluid samples + receptor compartment wash), the skin (mass detected in the skin tissue at the end of the exposure period) and the unabsorbed dose (mass in skin surface wash and donor compartment wash at the end of the exposure period). Mass balance was calculated by comparing the sum of recovered analyte masses in all system compartments to the dose applied to the skin at the beginning of exposure. Table 4-1 lists the dermally absorbed fractions of target PFAS as well as the PFAS distribution in other fractions in the *in vitro* model compartments at the end of the exposure period. For target PFCAs and PFSAs, the dermally absorbed fractions decreased with increasing carbon chain length.

Table 4-1: Distribution of target PFAS (expressed as % of exposure dose ± standard deviation) in different compartments of the in vitro diffusion system after 36 or 24[a] hour exposure to 500ng/cm^2.

	Absorbed fraction[b]	Skin-epidermis	Unabsorbed fraction[c]	Total recovery
PFPeA	58.9 ± 1.9	17.3 ± 3.5	16.6 ± 2.3	92.8 ± 2.6
PFHxA	36.4 ± 4.1	17.3 ± 3.4	23.5 ± 5.5	77.1 ± 4.4
PFHpA	28.8 ± 3.3	31.8 ± 6.3	32.2 ± 5.9	92.8 ± 5.3
PFOA	13.5 ± 2.8	38.3 ± 5.4	50.9 ± 5.0	102.7 ± 4.6
PFNA	0.9 ± 0.1	67.0 ± 7.3	36.9 ± 9.0	104.8 ± 6.7
PFDA[a]	0.1 ± 0.02	60.7 ± 7.9	33.9 ± 9.4	94.7 ± 7.1
PFUdA[a]	N/A[d]	66.5 ± 11.6	44.5 ± 14.6	111.0 ± 10.7
PFDoA[a]	N/A	31.3 ± 19.5	66.0 ± 18.8	97.2 ± 19.1
PFTrDA[a]	N/A	29.2 ± 1.4	84.2 ± 15.0	113.4 ± 10.7
PFTeDA[a]	N/A	9.0 ± 2.1	77.1 ± 2.4	86.0 ± 2.3
PFBS	48.7 ± 4.2	19.6 ± 4.2	15.9 ± 0.5	84.2 ± 3.4
PFPeS	43.9 ± 2.6	24.4 ± 2.9	25.0 ± 2.4	93.3 ± 2.6
PFHxS	21.9 ± 1.3	33.2 ± 1.5	41.6 ± 3.6	96.8 ± 2.4
PFHpS	6.4 ± 1.3	44.3 ± 1.5	46.5 ± 3.6	97.2 ± 2.4
PFOS[a]	1.3 ± 0.02	60.3 ± 5.0	26.0 ± 5.0	86.6 ± 4.1
PFNS[a]	N/A	68.3 ± 19.6	31.4 ± 5.3	99.7 ± 11.7

[a]PFAS with the last time-point collected at 24 h.

[b]Receptor fluid + receptor compartment wash.

[c]Skin surface wash + donor compartment wash.

[d]Concentration below LOD.

The absorbed fraction of target PFCAs was highest for PFPeA with over half (58.9%) of the applied dose being absorbed after 36 h. For PFSAs, PFBS had the highest absorbed fraction (48.7%), slightly lower compared to PFPeA, yet substantial. Absorbed fractions then decreased for both PFCAs and PFSAs with increasing carbon chain length. In general, PFCAs had higher dermally absorbed fractions after 36 h compared to PFSAs. The compounds with

highest absorbed fractions (C ≤ 7 PFCA and C ≤ 6 PFSA) fall under or very close to the Lipinski's criteria of $\log K_{OW} < 5$ and molecular weight < 500 Da (Lipinski et al., 2001). While these criteria were developed for evaluation of drug delivery, our results show good compliance via the observed decreasing dermal absorbed fraction with increasing carbon chain length and $\log K_{OW}$ of the studied PFAS (Figure 4-1) (*Chemspider*, 2023; Wang et al., 2011).

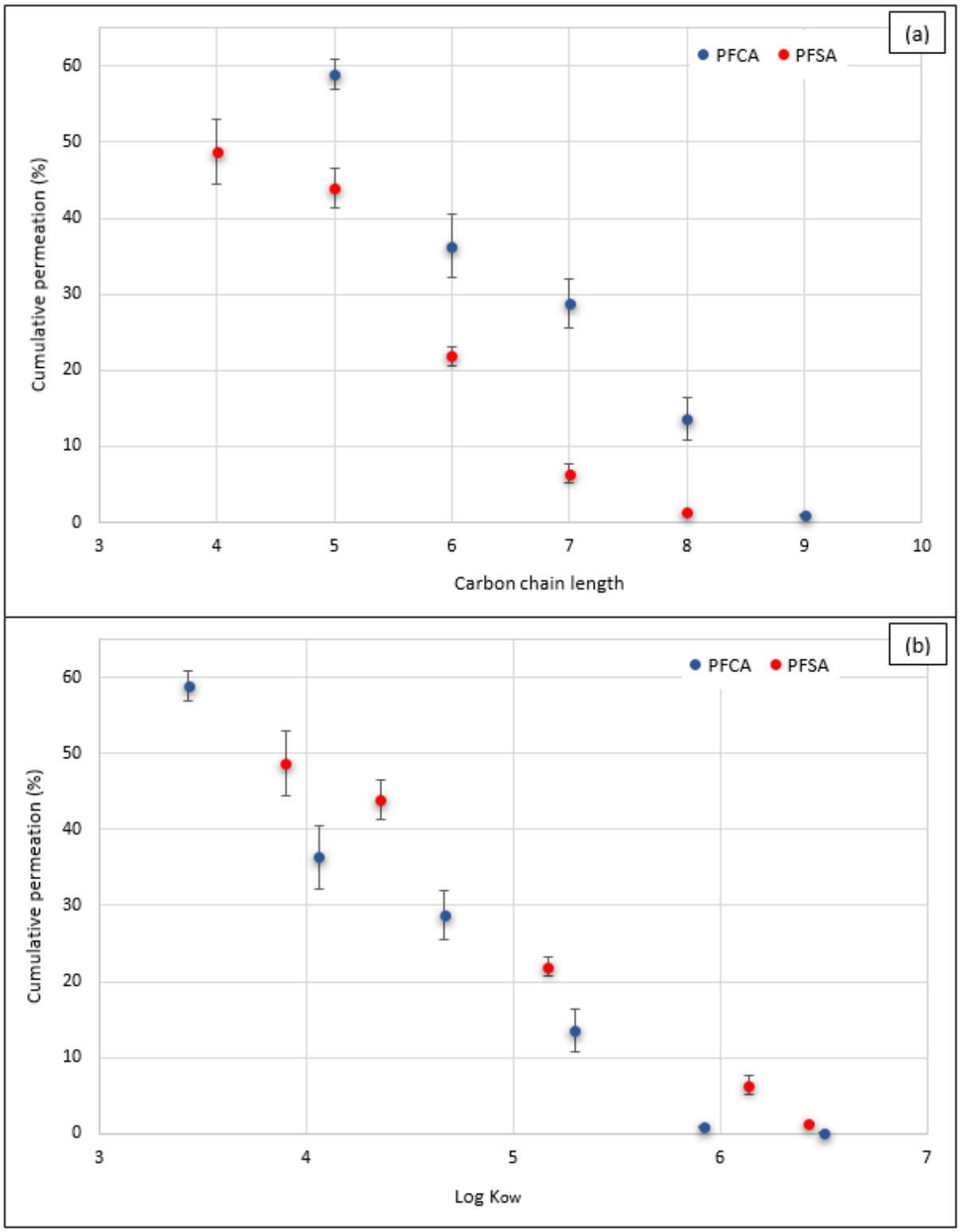


Figure 4-1: Association of cumulative permeation of PFAS after 36 hours and C chain length (a) and logKow (b) Error bars represent the cumulative standard deviation (n = 3). Included are values for compounds with C ≤ 9 and C ≤ 8 for both PFCAs and PFSAs respectively.

Previous studies have shown that the vehicle chosen for the application of chemicals onto the skin can affect the dermal uptake of those chemicals (Abrams et al., 1993; Chiang et al., 2012). Some organic solvents can delipidate the skin leading to an increased percutaneous absorption of drugs. PFAS amphiphilic properties further complicate the choice of an appropriate vehicle which would not affect the permeability of the skin in any way. A common solvent used in dermal uptake studies, acetone, has for example been shown to increase permeation of amphiphilic compounds (Chiang et al., 2012). Although alcohols could have some skin drying effects which could enhance dermal permeation, they are less occlusive than oil based vehicles which are used to enhance the permeation of lipophilic compounds (Law et al., 2020). Furthermore, PFAS themselves have been used in cosmetics to increase percutaneous permeation (Glüge et al., 2020a). Other anionic surfactants such as sodium lauryl sulfate in water also have been shown to increase dermal permeation (Okasaka et al., 2019). Thus, methanol was chosen as a vehicle for the PFAS as they are readily soluble in methanol, and given the low volume used, the solvent evaporated relatively quickly after the single application, leaving the PFAS on the skin surface. Finally, methanol should not affect the skin surface pH and thus its effect on the permeation should be minimal. It cannot however be completely excluded as a factor on the dermal uptake of PFAS which is a limitation of this study.

There is a strong negative correlation between chain length and absorbed fractions for both PFSAs ($r = -0.97$, $p = 0.004$) and PFCAs ($r = -0.97$, $p = 0.001$). Additionally, functional groups seem to play a role in dermal permeation as PFCAs generally have a higher absorbed fraction compared to the PFSA with the same carbon chain length. These trends were also reported in a recent *in vivo* rat study which included C_4-C_{14} PFCAs (excluding PFTrDA) as well as PFBS, PFHxS and PFOS (Chen et al., 2022). Furthermore, physicochemical properties, e.g., $\log K_{OW}$ seem to influence permeation as there is a clear negative correlation between

$\log K_{OW}$ and permeation for both PFCAs ($r = -0.97$; $p \leq 0.001$) and PFSAs ($r = -0.99$; $p \leq 0.001$). The PFAS mass retained within the skin increased with increasing carbon chain length, peaking for PFUnDA (C = 11) and PFNS (C = 9). The mass retained within the skin then decreased for higher carbon chain compounds. A previous study on the dermal uptake of brominated flame retardants (BFRs) from indoor dust showed similar trends with a negative correlation between the $\log K_{OW}$ ($p < 0.05$) and the permeated fraction while a positive correlation was seen for $\log K_{OW}$ and the fraction of BFRs retained within the skin ($p < 0.05$). These BFRs are examples of chemicals which do not fit Lipinski's rule of 5 but can still permeate the human skin barrier (Abdallah and Harrad, 2018). The reason for the lower skin retention of the shorter chain PFAS is likely due to their ability to permeate through the skin and enter the receptor fluid. Longer carbon chain PFAS were able to enter the skin cells, and while a steady state was not reached, it may be expected that these long carbon chain PFAS will be less likely to reach the bloodstream but rather be removed by desquamation (Ragnarsdóttir et al., 2022). However, a study on one human subject exposed topically to mass labelled $^{13}C_4$-PFOA mixed into sunscreen revealed absorption was very slow, with plasma levels reaching a maximum (132 ng/L), 22 days after application of a single 110 μg dose (Abraham and Monien, 2022). Furthermore, a study on rats found that the peak times of PFAS in the bloodstream after dermal exposure (8-72 h) were significantly longer than seen after oral exposure (1-24 h), suggesting dermal permeation of PFAS, while slower, could exert a substantial influence on the total body burden (Chen et al., 2022). Keeping this in mind, it could be possible for the fraction of the PFAS still detected in the skin tissue after 36 h to slowly cross the skin barrier and enter the blood stream. Further research is required to understand the potential slow diffusion of long chain PFAS through the human skin barrier. The 3D-HSE model is limited to 36 hours as cell viability assays performed by our group as part of the QA/QC protocol revealed > 50% cell death after 36 hours; hence our exposure experiments were limited to 36 hours.

Franko et al. investigated the dermal permeation potential of PFOA using *ex vivo* human full thickness skin and epidermis[42]. They saw similar absorbed fractions (24%) for both skin models after 24 h with an additional 45% and 23% of the applied dose found within the skin models. Our findings show a lower permeation of PFOA through the skin (13.5%) but a similar fraction detected within the 3D-HSE models (38.3%) and the full thickness skin. There are some differences between the two studies; specifically, the time of exposure 36 h in the current study vs 24 h (Franko et al.), as well as a difference in skin surface loadings (500 ng/cm^2 in our study compared to 780 x 10^3 ng/cm^2 in that of Franko et al.)), which could explain the differences in the results, especially when expressed as percent of the applied exposure dose. It is important to note that the fraction of the chemical that is permeated is dependent on the applied dose and thus using only the % values for future estimations of dermal uptake from other sources by itself could lead to over-estimations of human exposure to PFAS via dermal uptake (Kissel, 2011).

4.3.2. Dermal flux (J_{ss}) and Permeation Coefficients (P_{app})

In an infinite dose application, the permeation through the skin becomes the rate-limiting step while the concentration gradient is maximized (OECD, 2004a). A plot of the cumulative absorbed mass of each target compound (ng/cm^2) against time (h) (Figure 4-2 a and b) can then be prepared. The curves show a similar profile for PFCAs with permeation decreasing with increasing carbon chain length.

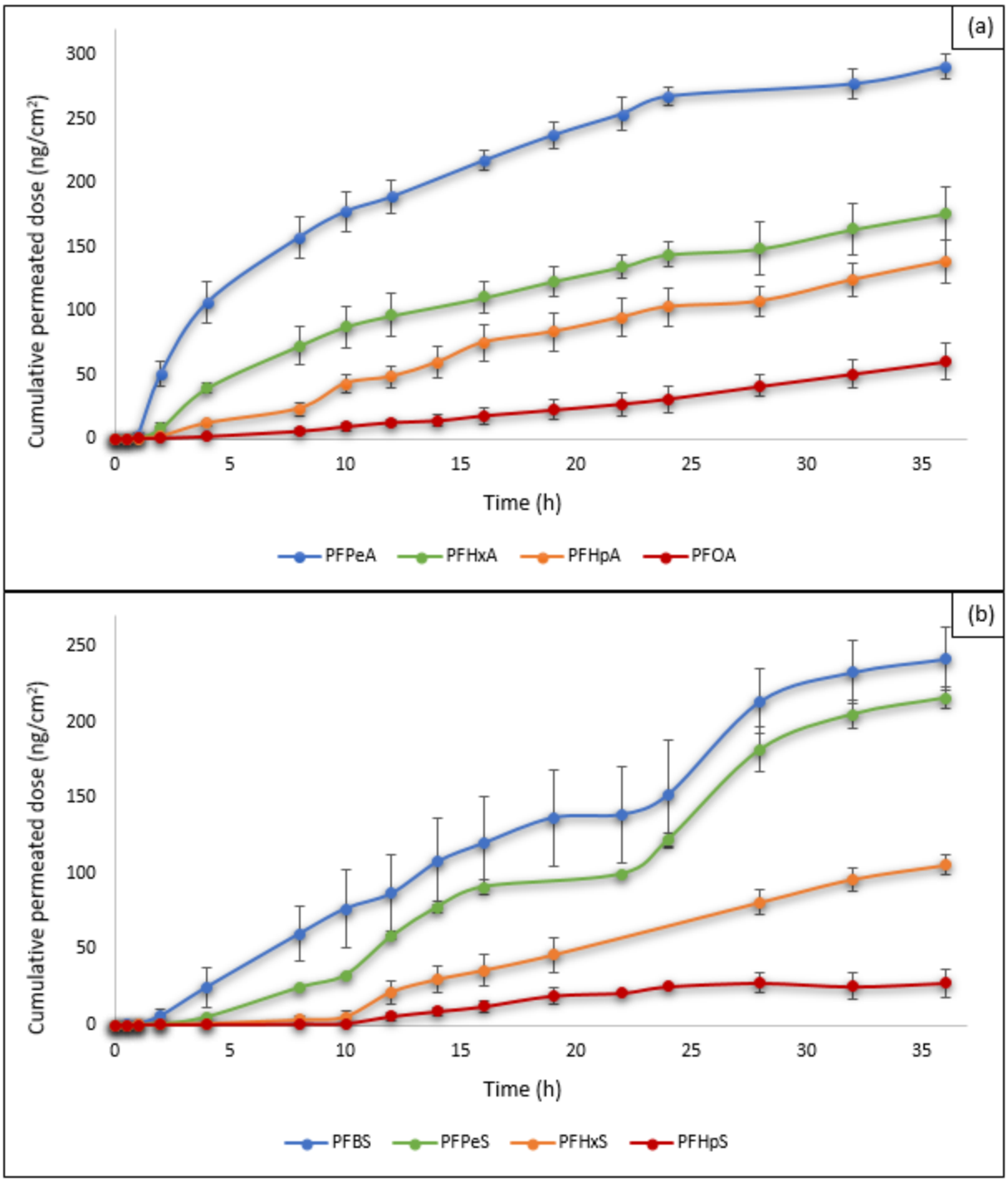


Figure 4-2: Cumulative permeation (ng/cm^2) of PFCAs (a) and PFSAs (b) into the receptor fluid following exposure of 500 ng/cm^2 of target PFAS to 3D-HSE models for 36 hours. Error bars represent the cumulative standard deviation (n = 3).

The steady state range of the curve was subsequently identified (Figure 4-6 a and b) according to the method of Niedorf et al, with a minimum of 5 data points and the linear range required to establish each curve (Figure 4-5 and table 4-3) (Niedorf et al., 2008). Thus, it was possible to estimate the permeability constant (**P_{app}**, [cm/h]), dermal flux (**J_{ss},**

[ng/cm^2·h]) and lag time (**t_{lag},** [h]) for each target compound that displayed significant permeation through the 3D-HSE models (Table 4-2). The general trend observed was a decrease in the permeation coefficient (**P_{app}**) with increasing chain length as well as a lower **P_{app}** for PFSAs compared to PFCAs of a similar carbon chain length. Furthermore, a negative correlation between the estimated **P_{app}** of each target PFAS and their logK_{ow} values ($r = -0.82$, $p = 0.01$) was observed. This trend is in agreement with previous studies of the dermal uptake of halogenated flame retardants where more lipophilic (higher log K_{ow}) compounds (α-HBCDD (**P_{app}** = $2.5 \cdot 10^{-4}$) and TBBP-A (**P_{app}** = $2.9 \cdot 10^{-3}$)) had lower **P_{app}** values compared to less lipophilic chemicals i.e. TCEP (**P_{app}** = $2.2 \cdot 10^{-2}$), TCIPP (**P_{app}** = $1.6 \cdot 10^{-2}$) and TDCIPP (**P_{app}** = $0.5 \cdot 10^{-2}$) (Abdallah et al., 2016, 2015b).

Table 4-2: Flux (J_{ss}, [ng/cm^2·h]), permeation coefficient (P_{app}, [cm/h]) and lag time (t_{lag}, [h]) values estimated from infinite exposure of 3D-HSE models to 500 ng/cm^2 of the target PFAS with significant permeation after 36 h.

	Flux (Jss) (ng/cm^2 · h)	**Permeation coefficient (P_{app}) (cm/h)**	**Lag time (h)**
PFPeA	21.65	$4.33 \cdot 10^{-2}$	0.17
PFHxA	8.99	$1.80 \cdot 10^{-2}$	0.52
PFHpA	4.05	$8.10 \cdot 10^{-3}$	0.14
PFOA	1.91	$3.82 \cdot 10^{-3}$	6.21
PFBS	7.07	$1.41 \cdot 10^{-2}$	0.17
PFPeS	7.01	$1.40 \cdot 10^{-2}$	4.40
PFHxS	3.75	$7.50 \cdot 10^{-3}$	6.85
PFHpS	0.99	$1.98 \cdot 10^{-3}$	5.78

Franko et al. previously estimated the permeation coefficient for PFOA in different ionization states and donor solution pH through *ex vivo* human epidermis[43]. They found (Franko et al., 2012) that for PFOA in the un-ionized form (3000 µg/mL in H_2O, pH = 2.5), **P_{app}** = $5.5 \cdot 10^{-2}$ while the ionized form of the compound (3000 µg/mL in a buffered

solution, pH = 5.5) had more than 1000-fold lower $\mathbf{P_{app}} = 4.4 \cdot 10^{-5}$. Our results ($\mathbf{P_{app}} = 3.82 \cdot 10^{-3}$) are 10-fold lower than those reported for the un-ionized form of PFOA by Franko et al. The difference could be associated with a combination of factors including the difference in the dosing vehicle, the skin barrier, exposure time and dosage between the two studies (Frederiksen et al., 2018). It is also worth noting that Franko et al. did not present the curves used for the estimations of $\mathbf{P_{app}}$, so it is unclear whether steady-state conditions were reached in their study.

The ability of other anionic surfactants e.g., sodium lauryl sulfate (SLS) to increase skin permeation has been well studied (Okasaka et al., 2019; Walters et al., 1993; Williams and Barry, 2012). The anionic surfactants themselves can penetrate and interact with the skin altering its barrier properties e.g., by binding to proteins in the stratum corneum. Over short exposure periods, anionic surfactants permeate poorly through the skin but at longer application times, permeation increases. While it has been shown that anionic surfactants can permeate the skin, the mechanism of permeation has been debated (Morris et al., 2019; Morris et al., 2022; Williams and Barry, 2012). As SLS is most commonly used in personal care products that are only applied on the skin for short periods of time i.e., soaps and shampoos, most studies focus on short term exposures (Morris et al., 2019; Morris et al., 2019). A longer exposure study however, found SLS in both receptor fluid and within the skin 24 h after exposure. Similarly to PFAS, a steady state was not reached 24 h after SLS exposure (Morris et al., 2019).

4.4. Conclusion

The current study provides information on the dermal bioavailability of 17 PFAS. Substantial dermal absorption (> 5% of exposure dose) was seen for C ≤ 8 PFCAs and C ≤ 7 PFSAs. The shortest carbon chain compounds examined, PFPeA (58.9 %) and PFBS (48.7%) had the highest absorbed fractions of PFCAs and PFSAs respectively, with absorbed fractions

of PFAS decreasing with increasing carbon chain length. A previous study showed pH can impact the dermal penetration potential of PFAS (Franko et al., 2012). While PFAS are more likely to be present in the ionized form on the skin surface (e.g., in personal care products), it has been shown that they are still capable of permeating the skin (Abraham and Monien, 2022). Similarly, other anionic surfactants are also able to penetrate the skin (Morris et al., 2019). Thus, the dermal route should not be dismissed as a possible route of human exposure to PFAS.

Finally, the permeation coefficients ($\mathbf{P_{app}}$) provided can be used to estimate human dermal uptake of PFAS in short term exposure scenarios. To the best of our knowledge this is the first time such coefficients are presented for seven out of the eight PFAS included in this study (PFOA excluded). These permeation coefficients should aid in future human dermal exposure estimation models. Further studies that mimic real-life exposure scenarios would further assist the current understanding of the relative contribution of the dermal exposure pathway to human body burdens of PFAS, compared to other, well-established exposure routes.

4.5. Supporting Information

4.5.1. Experimental

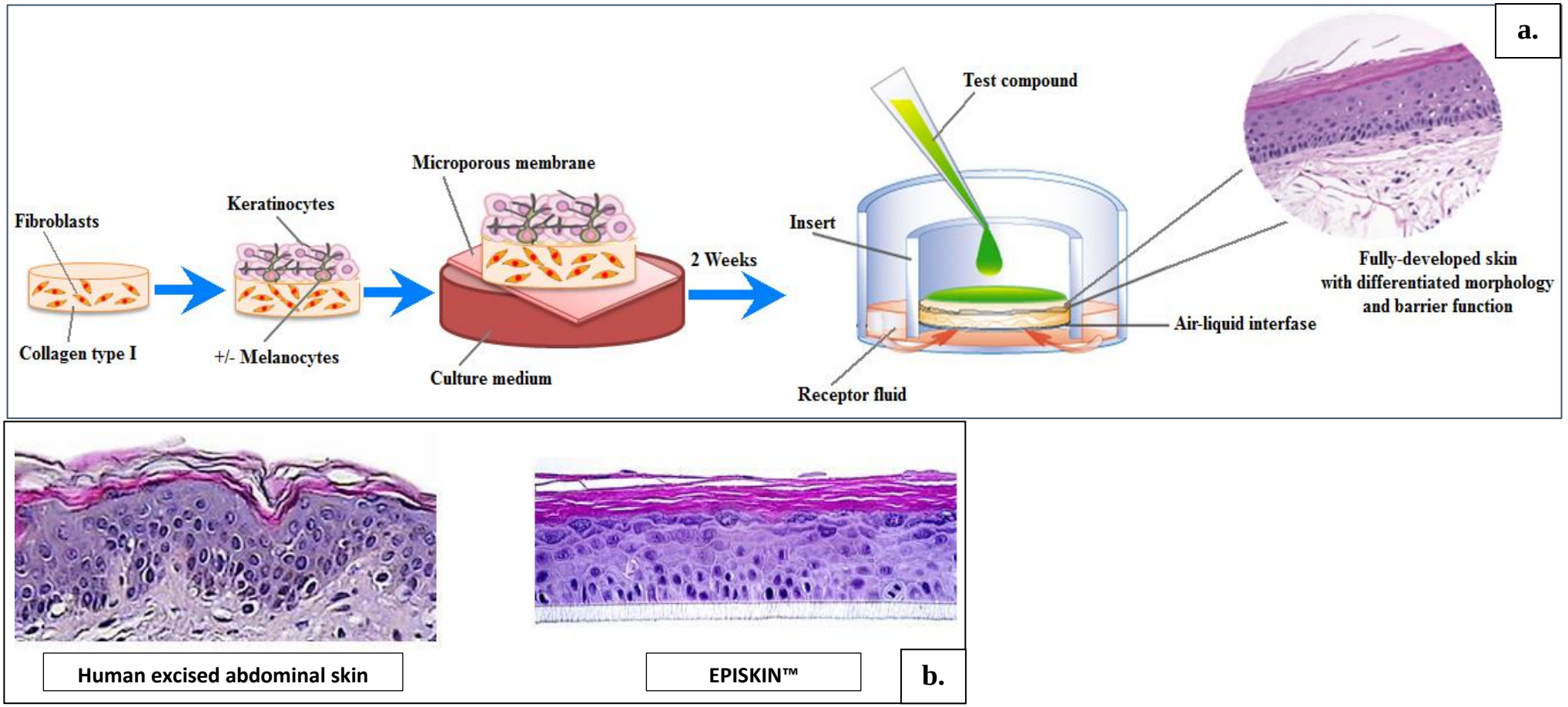


Figure 4-3: General stages of development of 3D human skin equivalent (3D-HSE) model (a). Histological comparison between excised human skin and EPISKIN™(3D-HSE model) tissue (b). Figure published previously by Abdallah et al., 2015b.

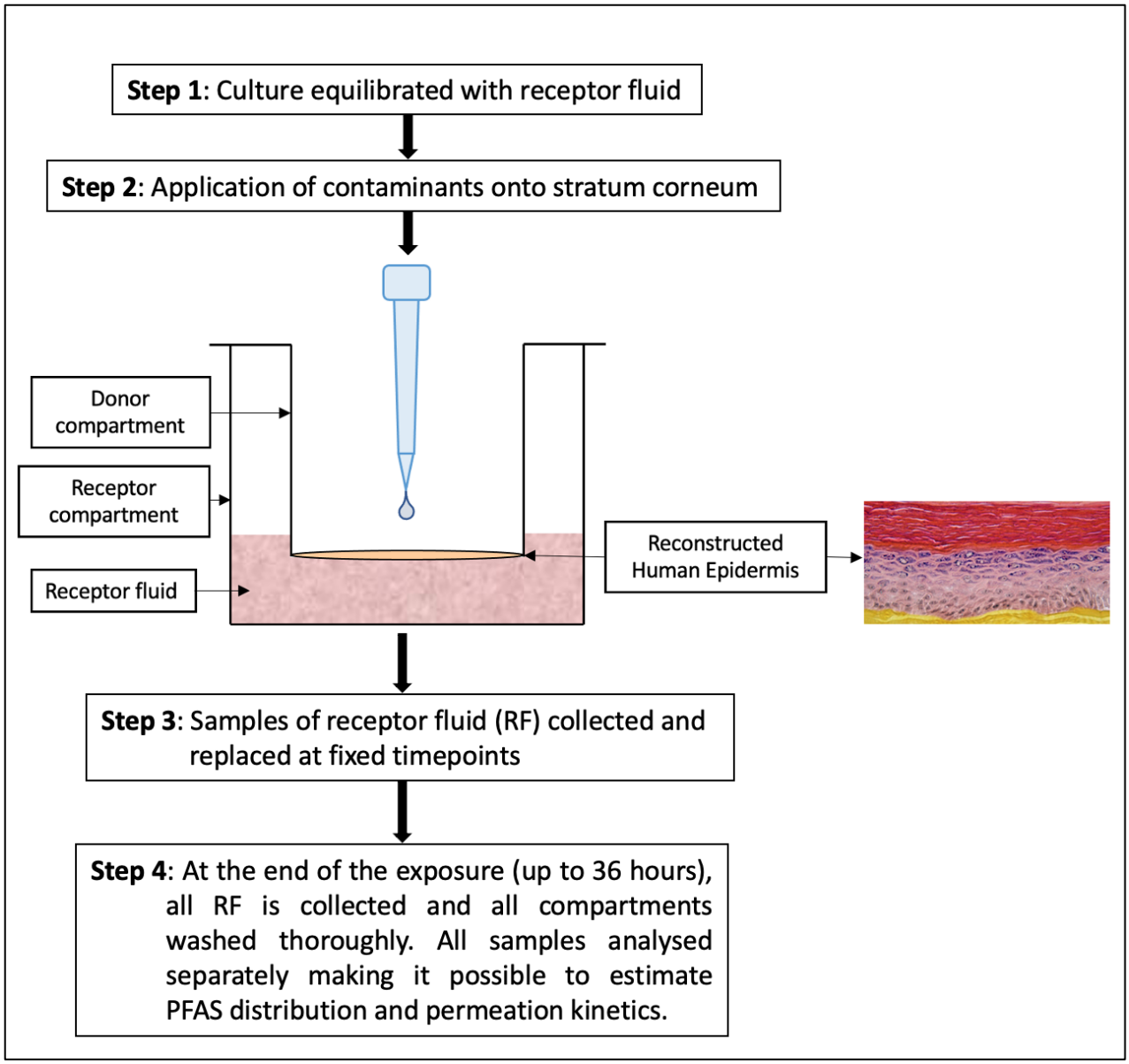


Figure 4-4: Experimental protocol applied during dermal permeation experiments.

4.5.1.1.Cell viability

The viability of the skin models were tested based on the guidelines of EPISKIN™ models. An MTT (3-(4,5-dimethylthiazol-2-yl)-2,5-diphenyltetrazolium bromide) assay was performed using a standard kit purchased from each provider. Acceptable MTT results (i.e. Formazan concentration ≥ 1.5 mg/ml) were achieved following up to 36 h of exposure.

4.5.2. Analysis of PFAS – Sample extraction and clean-up

4.5.2.1.Receptor fluid samples

Extraction and preparation of receptor fluid samples (n = 240) was based on a method previously reported (Harrad et al., 2019). In short, each sample was spiked with 30 μL internal standard mixture before being loaded onto a Chromabond™ PFAS (6 mL/300mg, Chromabond) SPE cartridge. Cartridges were pre-conditioned with 6 mL MeOH (0.1% NH_4OH) followed by 6 mL MilliQ water. After sample addition, cartridges were dried under vacuum for 5 min. PFAS were eluted with 12 mL MeOH (0.1% NH_4OH) and the eluent collected and concentrated to ~0.5 mL under gentle N_2-flow at 38°C. Samples were then loaded onto a pre-conditioned (6 mL MeOH + 0.1% NH_4OH) EnviCarb™ (3 mL/250 mg, Merck) SPE cartridge. PFAS were eluted with 5 mL methanol (0.1% NH_4OH), with the eluate concentrated to incipient dryness and reconstituted to 200 μL in MeOH before transfer to autosampler vials for analysis.

4.5.2.2.Skin samples

Skin sample (n = 30) extraction and preparation was based on a previously reported method (Harrad et al., 2020). Briefly, each sample was spiked with 30 μL internal standard mixture followed by the addition of 2 mL of MeOH (0.1% NH_4OH). Samples were then homogenised for 2 min and ultrasonicated at 20°C for 5 min. The samples were then centrifuged at 3500 RPM for 5 min and the supernatant collected into a new tube. The procedure was repeated two more times and the three fractions combined and concentrated to ~0.5 mL under a gentle stream of nitrogen at 38°C. The samples were then loaded onto Chromabond™ PFAS (6 mL/300mg, Chromabond) SPE cartridges which were pre-conditioned with 6 mL MeOH (0.1% NH_4OH) followed by 6 mL MilliQ water. After sample addition, cartridges were dried under vacuum for 5 min. PFAS were eluted with 12 mL MeOH (0.1% NH_4OH) and the eluent collected. The samples concentrated to near dryness before being reconstituted to 200 μL in MeOH and transferred to autosampler vials for analysis.

4.5.2.3.Skin surface wash samples

Skin surface wash (cotton, n = 30) sample extraction and preparation was based on a previously reported method (Harrad et al., 2020). Briefly, each sample was spiked with 30 μL internal standard mixture followed by the addition of 2 mL of MeOH (0.1% NH_4OH). Samples were then vortexed for 2 min and ultrasonicated at 20°C for 5 min. The samples were then centrifuged at 3500 RPM for 5 min and the supernatant collected into a new tube. The procedure was repeated two more times and the three fractions combined and concentrated to ~1 mL under a gentle stream of nitrogen at 38°C before being passed through a 0.22 μm syringe filter. The samples were then concentrated to incipient dryness and reconstituted to 200 μL in MeOH before transfer to autosampler vials for analysis.

4.5.2.4.Donor and receptor compartment wash samples

Donor and receptor compartment (n = 30 each) wash samples were each sample was spiked with 30 μL internal standard mixture and vortexed for 30 seconds. Donor wahs samples were then concentrated to ~1 mL under a gentle stream of nitrogen at 38°C before being passed through a 0.22 μm syringe filter. Receptor wash samples were concentrated to to ~0.5 mL under gentle N_2-flow at 38°C before being loaded onto a pre-conditioned (6 mL MeOH + 0.1% NH_4OH) EnviCarb™ (3 mL/250 mg, Merck) SPE cartridge. PFAS were eluted with 5 mL methanol (0.1% NH_4OH). All samples were then concentrated to incipient dryness and reconstituted to 200 μL in MeOH containing before transfer to autosampler vials for analysis.

4.5.3. Results and discussion – supporting information.

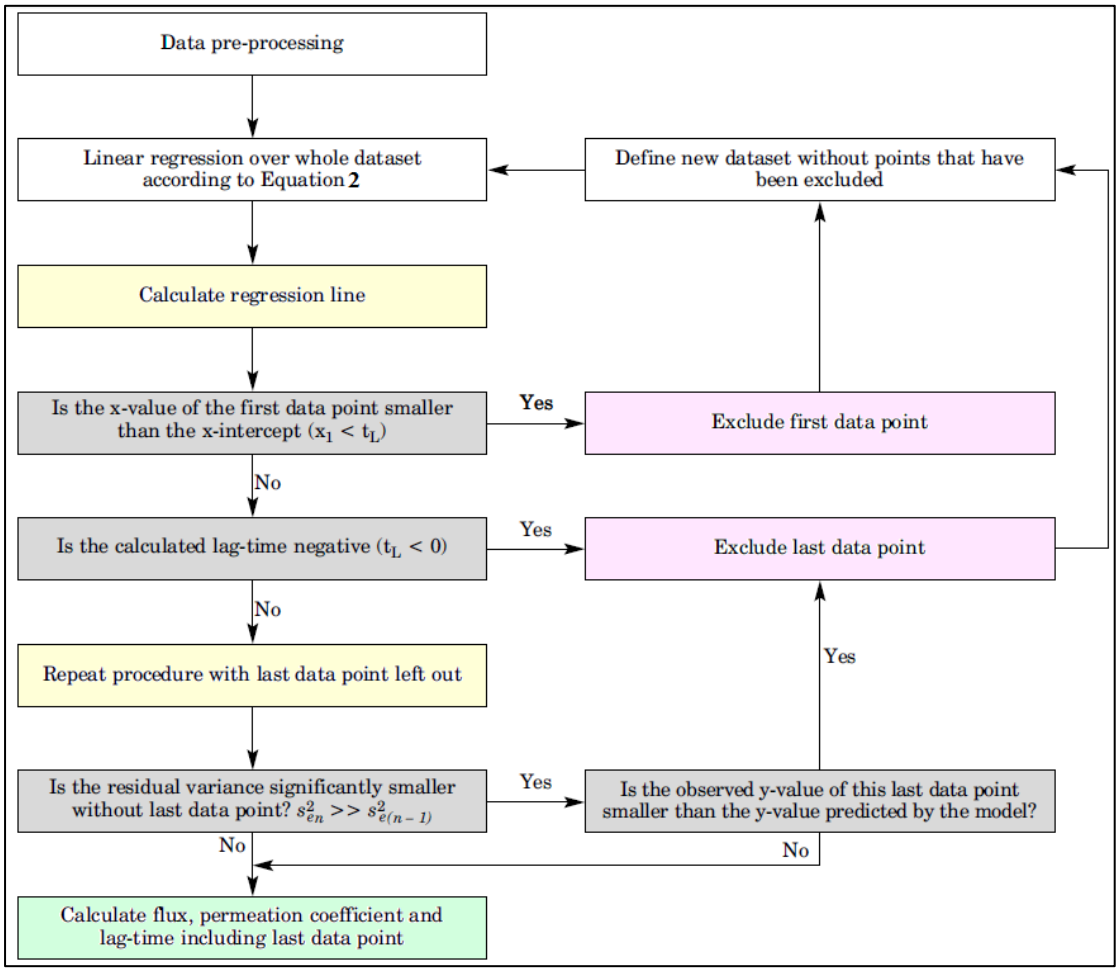


Figure 4-5: Flowchart of the applied algorithm for identification of the steady state range as described by Niedorf et al., 2008.

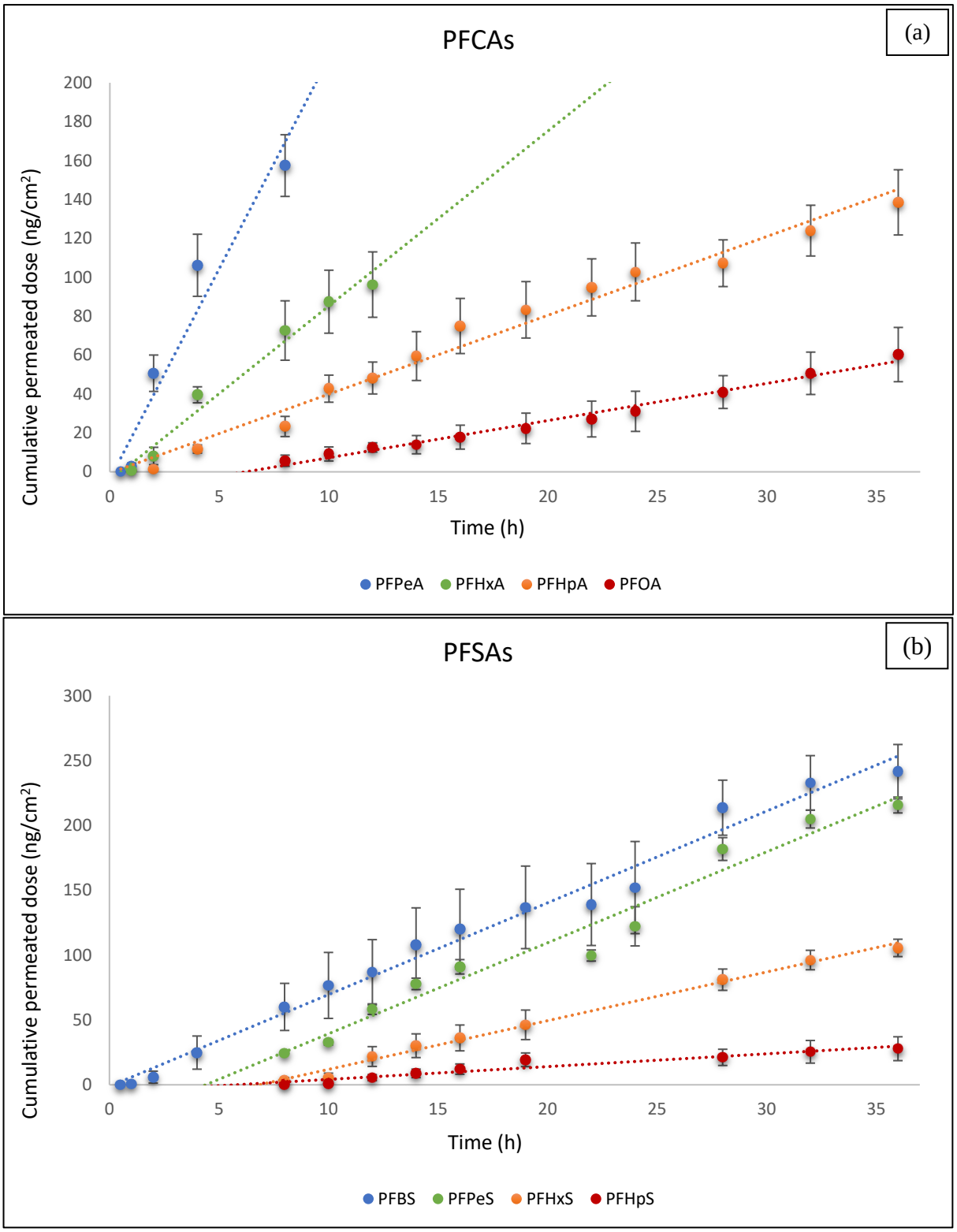


Figure 4-6: A representative curve displaying cumulative permeation (ng/cm²) of target PFCAs (a) and PFSAs (b) at the linear-range region ($R^2 \geq 0.9$), following the parameters described in Figure 4-5. Error bars represent 1 standard deviation (n = 3).

Table 4-3: Linearity coefficient (R^2) and probability statistics (p) for the linear correlations established between cumulative permeated dose (ng/cm^2) of target PFAS over time (hours) over the established steady-state period.

	R^2	P
PFPeA	0.941	0.006
PFHxA	0.977	0.0002
PFHpA	0.978	$1.66 \cdot 10^{-10}$
PFOA	0.985	$1.82 \cdot 10^{-9}$
PFBS	0.986	$2.40 \cdot 10^{-13}$
PFPeS	0.965	$4.11 \cdot 10^{-7}$
PFHxS	0.992	$8.68 \cdot 10^{-9}$
PFHpS	0.926	$3.27 \cdot 10^{-5}$

5. EVALUATION OF HUMAN EXPOSURE TO PFAS VIA DERMAL CONTACT WITH INDOOR DUST

5.1. Introduction

Per- and polyfluoroalkyl substances (PFAS) are a class of synthetic organofluorine compounds. This group comprises thousands of compounds, which are chemically and thermally stable as well as having hydrophobic and lipophobic properties. These properties have made the use of PFAS common in various industries, since the 1940s, as well as in a broad range of consumer products (Buck et al., 2011; Glüge et al., 2020a). Ever since the presence of PFAS in human sera was highlighted in 2001, their effects on human health have been a concern (EFSA CONTAM Panel, 2020; Hansen et al., 2001). Studies have linked human exposure to PFAS to significant health effects, such as lowered immune response to vaccination (DeWitt et al., 2019a; Grandjean et al., 2017a), impaired liver function (Salihovic et al., 2018a; Sen et al., 2022a), in addition to decreased birth weight and higher risk of preterm birth (Meng et al., 2018; Sagiv et al., 2018). This led the European Food Safety Authority (EFSA), in 2020, to set a recommended tolerable weekly intake of 4.4 ng/kg bw/week for the sum of four PFAS (perfluorooctanoic acid (PFOA), perfluoronoananoic acid (PFNA), perfluorohexane sulfonic acid (PFHxS), and perfluorooctane sulfonic acid (PFOS))(EFSA CONTAM Panel, 2020).

Human exposure to PFAS can happen through various pathways. Diet is widely considered the main pathway of exposure to PFAS, with seafood being a major contributor to the total dietary exposure (Gebbink et al., 2015; Sunderland et al., 2019; Trudel et al., 2008). Drinking water is also considered a major source of PFAS exposure (Sunderland et al., 2019). Due to this, regulatory limits on PFAS in drinking water have been proposed both in the US (0.004 ng/L for PFOA, 0.02 ng/L for PFOS, 10 ppt for GenX and 1000 ng/L for PFBS) (U.S. EPA, 2023) and the EU, which implemented a new drinking water directive (DWD) in 2023 setting a limit of 0.5 μg/L for the sum of total PFAS or 0.1 μg/L for a defined sum of 20 PFAS

in drinking water, a goal which member states have until 2026 to comply with (European Union, 2020). Other, less significant exposure pathways are indoor air inhalation and dust ingestion (Poothong et al., 2020; Ragnarsdóttir et al., 2022; Trudel et al., 2008).

There are two factors involved in human dermal uptake of chemicals from a source material to the general circulation. *Bioaccessibility* refers to the fraction of chemicals that are released from a matrix (e.g. dust) into the body's fluids (a mixture of sweat and sebum). Bioavailability however, is defined as the fraction of a chemical that reaches the systemic circulation (Ertl and Butte, 2012; Pawar et al., 2017; Ruby et al., 1996). A combination of data on bioaccessibility and subsequent percutaneous penetration is necessary to fully understand the extent of human dermal uptake of chemicals (*e.g.*, PFAS) (Abdallah et al., 2012; Pawar et al., 2017).

Current knowledge on the dermal pathway compared to other pathways of human exposure to PFAS is lacking (Ragnarsdóttir et al., 2022). This is due to the expectation that most PFAS will be in the ionised form at skin surface pH, leading to the assumption that dermal uptake would be less likely. However, recent *in vivo* and *in vitro* studies have shown that the transdermal permeation of PFAS is possible under normal physiological conditions (Abraham and Monien, 2022; Chen et al., 2022; Ragnarsdóttir et al., 2024). A study involving one human volunteer exposed to mass labelled PFOA fortified sunscreen found that 1.6% of the applied mass was absorbed through the skin. The permeation appeared to be slow, with the peak PFOA plasma levels being detected 22 days after exposure (Abraham and Monien, 2022). Another study using male Sprague-Dawley rats exposed to 15 PFAS, found that fractions of both perfluoroalkyl carboxylates (PFCAs) and perfluoroalkyl sulfonates (PFSAs) were able to penetrate the rat skin. Moreover, they reported a peak of PFAS in the systemic circulation at 8-72 h, which is significantly later than what has been reported after oral administration (1-24h) (Chen et al., 2022). This corroborates what was observed in the human study, i.e. that

dermal exposure can be long-lasting and contribute to total human body burdens of PFAS. Finally, an *in vitro* study exposing 3D-human skin equivalent (3D-HSE) models to 10 PFCAs (C_5-C_{14}) and 6 PFSAs (C_4-C_9) in methanol for 36 hours was conducted (chapter 4 of this thesis). The study found that lower chain compounds relatively readily permeated, with permeation decreasing with increasing chain lengths. The highest permeation was seen for PFPeA (59%) and PFBS (49%). The longer chain compounds included, ≥ C_{10} PFCAs and ≥ C_9 PFSA were not directly absorbed. They were however detected within the skin tissues themselves with C11 and C9 being detected at the highest concentrations within the skin (67% and 68% respectively), which could indicate a very slow permeation of the longer chain compounds (Ragnarsdóttir et al., 2024). It is important to note that the dose applied at the start of exposure experiments can impact the fraction that permeates through the skin (Kissel, 2011). The *in vitro* study provided permeation coefficients ($\mathbf{P_{app}}$) for eight of the studied PFAS which had the highest permeation. These coefficients are independent of the applied dose and can thus be used in estimations of human exposure via dermal contact over a range of doses under various exposure scenarios (Ragnarsdóttir et al., 2024).

Several potential sources of human dermal exposure to PFAS have been identified (Ragnarsdóttir et al., 2022). One possibly important source of exposure is personal care products. PFAS have been identified in cosmetics from all over the world, i.e., sunscreen, foundations, moisturisers, and hand sanitisers (Fujii et al., 2013; Glüge et al., 2020a; Schultes et al., 2018; Whitehead et al., 2021). These products can contain PFAS in quite high concentrations, for example, cosmetics and sunscreens from Japan were found to contain PFCAs in concentrations up to 5.9 μg/g in cosmetics and 19 μg/g respectively (Fujii et al., 2013). Another possible source of dermal exposure is fabrics treated with PFAS. Studies have identified PFAS, e.g., in durable water repellent clothing as well as children's school uniforms and car seats (van der Veen et al., 2020; Wu et al., 2021; Xia et al., 2022; Zhu and Kannan,

2020). Finally, PFAS have been identified in indoor dust from all over the world, which can be a continuous source of dermal exposure to PFAS (Eriksson and Kärrman, 2015; Harrad et al., 2019).

Against this backdrop, the aim of this chapter is to evaluate the possible impact of human dermal exposure to indoor dust on PFAS body burdens, based on the permeation coefficients ($\mathbf{P_{app}}$) and dermal bioaccessibility of PFAS previously derived and reported by our research group (Ragnarsdóttir et al., 2024, 2023). Using this data, more accurate estimations can be made on the dermal exposure of PFAS. While only one of many possible sources of dermal exposure to PFAS is considered here (i.e., dermal contact with indoor dust), the significance of the dermal pathway to human PFAS exposure and its contribution to total human body burdens is highlighted for the first time.

5.2. Materials and Methods

PFAS concentrations in dust from multiple countries have been published previously (Eriksson and Kärrman, 2015; Poothong et al., 2020). The PFAS concentrations identified in dust in two selected studies were used here to estimate human exposure to PFAS via dermal uptake from dust for five countries (table 5-1). Where median values were below LOD, half of the LOD values for each compound were used for the estimation.

Table 5-1: Median dust concentrations (ng/g) from various countries used for dermal uptake estimations. Concentrations published by Eriksson and Kärrman, 2015 and Norwegian concentrations published by Poothong et al., 2020.

	Sweden (ng/g)	Japan (ng/g)	Canada (ng/g)	Australia (ng/g)	Norway (ng/g)
PFBA	<1.97	10.3	3.54	6.77	NA
PFPeA	<0.36	4.5	1.62	0.55	NA
PFHxA	7.05	12	7.44	4.77	0.40
PFHpA	1.46	6.54	4.75	2.18	<0.1
PFOA	14.4	25.5	21	13.5	3.60
PFNA	1.96	35.8	13.5	2.97	0.80
PFBS	1.24	1.33	3.44	1.29	<0.03
PFHxS	0.15	0.76	3.75	4.32	0.06
PFOS	2.77	3.91	7.29	9.72	<0.01

5.2.1. Estimations of human dermal uptake of PFAS from dust

Individual uptakes of PFAS from dermal contact with dust were estimated based on exposure parameters obtained from the USEPA exposure factors handbook (U.S. EPA, 2011). A summary of these parameters can be found in table 5-2. This study focused on 4 (C_5-C_8) PFCAs and 4 (C_4-C_7) PFSAs for which the permeation coefficient was available.

Table 5-2: Parameters used in dermal exposure assessment of target PFAS:

a. Dust adhered to skin (U.S. EPA, 2011):

Dust adhered to skin (mg/cm^2)		
	Adults	**Toddler**
Head	0.024	0.054
Arms	0.038	0.048
Hands	0.160	0.170
Legs	0.019	0.051
Feet	0.140	0.200

b. Skin Surface Area calculated based on two seasons described above (U.S. EPA, 2011).

Surface Area (cm^2)				
	Adult		**Toddler**	
	Male	**Female**	**Male**	**Female**
Head	1360.0	1140.0	615.5	592.8
Forearms	1460.0	1090.0	425.6	418
Hands	1070.0	870.0	364.8	372.4
Thighs	4113.0	3560.0	1140	1185.6
Lower legs	2710.0	2300.0	782.8	790.4
Feet	1380.0	1210.0	494	478.8

c. Permeation coefficients (P_{app}) (chapter 4 of this thesis and Ragnarsdóttir et al., 2024), bioaccessible fraction ($F_{bioaccessible}$, chapter 3 of this thesis and Ragnarsdóttir et al., 2023), t = time spent indoors and body weight (BW)(U.S. EPA, 2011).

	P_{app} (cm/h)	$F_{bioaccessible}$ (unitless)	T (h)		BW (kg)	
			Adult	Toddler	Adult	Toddler
PFPeA	$4.33 \cdot 10^{-2}$	0.91	4	6	80	15
PFHxA	$1.80 \cdot 10^{-2}$	0.88	4	6	80	15
PFHpA	$8.10 \cdot 10^{-3}$	0.75	4	6	80	15
PFOA	$3.82 \cdot 10^{-3}$	0.70	4	6	80	15
PFBS	$1.41 \cdot 10^{-2}$	0.74	4	6	80	15
PFPeS	$1.40 \cdot 10^{-2}$	0.74	4	6	80	15
PFHxS	$7.50 \cdot 10^{-3}$	0.59	4	6	80	15
PFHpS	$1.98 \cdot 10^{-3}$	0.61	4	6	80	15

Two exposure scenarios were applied for each of the following two age groups (toddlers and adults):

i. **Summer:** assuming head, forearms, hands, thighs, lower legs, and feet were exposed to dust (i.e., person wearing shorts and t-shirt).

ii. **Winter:** Assuming head and hands exposed to dust (i.e., person wearing full-length trousers, long-sleeve top and socks).

based on the following equations. Firstly, the dose of PFAS (ng/cm^2) was determined (eq. 1)

$$Dose = C_{dust} * DAS * f_{bioaccessible} \quad (1)$$

Where C_{dust} = PFAS concentration in dust (ng/g), DAS = dust adhering to skin (g/cm^2), and $f_{bioaccessible}$ = bioaccessible fraction (fraction of PFAS available for dermal uptake (unitless)).

These values were based on values from chapter 3 of this thesis and Ragnarsdóttir et al., 2023.

From there, the flux (ng/cm^2 · h) could be determined (eq. 2)

$$Flux = P_{app} * Dose \quad (2)$$

Where P_{app} = Permeation coefficient (values from chapter 4 of this thesis and Ragnarsdóttir et al., 2024) (cm/h))

Finally, the mass permeated (ng) and the resulting body burdens (pg/kg bw/day) were estimated (eq. 3 and 4)

$$Mass\ permeated = Flux * t * BSA \quad (3)$$

$$Body\ burden = \frac{mass\ permeated}{BW} \quad (4)$$

Where t = time of exposure (h), BSA=body surface area exposed (cm^2), and BW=body weight (kg).

5.3. Results and discussion

5.3.1. Dermal uptake of PFAS from indoor dust

It is important to account for both the biaccessibility and bioavailability of a chemical when estimating dermal uptake. For compounds bound to particulate matter, their release into the skin's surface fluids (bioaccessibility) can be a limiting factor (Luo et al., 2020; Pawar et al., 2017; Zeng et al., 2019). Once bioaccessible, that fraction of a chemical can then pass through the outermost layer of the skin (the *stratum corneum)* where it could either be metabolised *in situ* or enter the systemic circulation (i.e., becomes bioavailable) through the viable epidermis and dermis layers (Ragnarsdóttir et al., 2022).

Considering both the dermal bioaccessibility and bioavailability of PFAS, human exposure to PFAS via dermal contact with dust was estimated for two age groups of residents

of four countries. Out of the four countries, PFAS concentrations in dust were highest in Japan followed by Canada which resulted in the highest dermal exposures for the residents of those countries. Our estimates (presented in table 5-3) of the weekly exposure to PFAS highlight the significance of dermal exposure as an exposure pathway, especially in summer. Total PFAS exposure via dermal uptake from dust during summer ranged from 25-767 pg/kg bw/week and 91-2761 pg/kg bw/week for adults and toddlers, respectively. In general, dermal uptake of PFAS from dust was 10 times lower in winter compared to the summertime, ranging from 2-70 pg/kg bw/week for adults and 10-300 pg/kg bw/week for toddlers. This is unsurprising as people are more covered up in the wintertime leading to a smaller skin surface area exposed. The dermal uptake from dust for the Norwegian population was significantly lower compared to the populations of other countries.

While PFOA was the compound detected at the highest concentrations in dust samples from all countries, PFHxA is the compound with the highest contribution to human body burdens of PFAS via dermal contact to dust, ranging from 10-296 pg/kg bw/week for adults and 35-1064 pg/kg bw/week for toddlers in summer for all countries except Norway. The second highest contributing compounds were PFOA (highest for Norway) and PFPeA ranging from 15-106 pg/kg bw/week and 0-277 pg/kg bw/week respectively for adults and 54-380 pg/kg bw/week and 0-998 pg/kg bw/week respectively for toddlers.

Table 5-3: Weekly human exposure to PFAS via dermal contact with dust based on age group, country, and time of year (1a. summer, 1b. winter) (pg/kg bw/week). Sum of the EFSA 4 is provided for comparison with EFSA TWI of 4400 pg/kg bw/week.

a.	**Adults**					**Toddlers**				
	Sweden	Japan	Canada	Australia	Norway	Sweden	Japan	Canada	Australia	Norway
PFPeA	11	277	100	34	0	42	998	359	122	0
PFHxA	174	296	183	117	10	625	1064	659	423	35
PFHpA	14	62	45	21	0	50	223	162	74	2
PFOA	60	106	87	56	15	215	380	313	201	54
PFNA	0	0	0	0	0.0	0	0	0	0	0
PFBS	20	22	56	21	0	73	78	201	75	1
PFPeS	0	0	0	0	0	0	0	0	0	0
PFHxS	1	5	26	30	0	4	19	93	107	1
PFHpS	0	0	0	0	0	0	0	0	0	0
PFOS	0	0	0	0	0	0	0	0	0	0
∑PFAS	**268**	**767**	**497**	**279**	**25**	**966**	**2761**	**1788**	**1003**	**91**
EFSA 4	**61**	**111**	**113**	**86**	**15**	**218**	**399**	**406**	**308**	**55**

b.	**Adults**					**Toddlers**				
	Sweden	Japan	Canada	Australia	Norway	Sweden	Japan	Canada	Australia	Norway
PFPeA	0	25	9	3	0	7	109	39	13	0
PFHxA	16	27	17	11	1	68	116	72	46	4
PFHpA	1	6	4	2	0	5	24	18	8	0
PFOA	5	10	8	5	1	23	41	34	22	6
PFNA	0	0	0	0	0	0	0	0	0	0
PFBS	2	2	5	2	0	8	8	22	8	0
PFPeS	0	0	0	0	0	0	0	0	0	0
PFHxS	0	0	2	3	0	0	2	10	12	0
PFHpS	0	0	0	0	0	0	0	0	0	0
PFOS	0	0	0	0	0	0	0	0	0	0
∑PFAS	**25**	**70**	**46**	**26**	**2**	**105**	**300**	**194**	**109**	**10**
EFSA 4	**6**	**10**	**10**	**8**	**1**	**24**	**43**	**44**	**34**	**6**

When comparing our estimated dermal exposure from dust to the EFSA recommended weekly intake of 4.4 ng/kg bw/week for the sum of four PFAS (PFOA, PFNA, PFHxS, and PFOS), the exposure to adults during summer can be up to 0.1 ng/kg bw/week (Canada and Japan) from dermal exposure to dust alone. With multiple other sources of dermal exposure to PFAS, it is likely that exposure via dermal contact with dust is a minor pathway of human dermal exposure to PFAS (Ragnarsdóttir et al., 2022). For toddlers, however dermal uptake via contact with dust is a more significant source of exposure with Canadian and Japanese toddlers being exposed to 0.4 ng/kg bw/week for the sum of PFOA and PFHxS. This difference can be explained by the fact that toddlers have more dermal contact with dust compared to adults as well as a higher ratio of skin surface area to body weight.

The previous study (chapter 4) was limited by the survival of the skin cells (36 h). This led to a limitation of this study, the lack of the permeation coefficients ($\mathbf{P_{app}}$) for PFOS and PFNA. Thus they could not be included in this study even though they were identified in dust samples from all countries (Eriksson and Kärrman, 2015). Their direct permeation was negligible after 36 h, however both compounds were identified within the skin itself at the end of exposure which could result in a slow permeation (Ragnarsdóttir et al., 2024).

5.3.2. Dermal exposure to PFAS via dermal contact with dust; comparison to other exposure pathways

The estimated adult uptake of PFAS via dermal exposure to dust was compared to other pathways reported previously for a Norwegian population (Poothong et al., 2020). It is important to stress that only dermal exposure to PFAS via contact with dust is included here. This is likely to be only one of many sources of dermal exposure to PFAS, which would lead to a higher total human exposure to PFAS via the dermal pathway (Ragnarsdóttir et al., 2022). The comparison of the different pathways is presented in figure 5-1. Median exposures were compared to our results as median dust concentrations were used for the dermal uptake estimates. Unsurprisingly, diet is the main exposure pathway for all compounds. However,

while it was a minor pathway, dermal contact to dust during summer did contribute to the total body burden of PFCAs. The dermal exposure from dust was less prominent in the winter for PFCAs. PFOA was the compound with the highest contribution to human body burdens after dermal exposure to dust in summer (2.1 pg/k bw/day), followed by PFHxA (1.4 pg/k bw/day). In general, dermal contact to dust did not contribute significantly to human exposure to PFSAs. This is both due to the lower permeation of PFSAs compared to PFCAs of the same chain length, as well as their lower concentration in the dust samples compared to PFCAs. For indoor exposure to PFCAs, it is clear that the dermal pathway is a potentially important exposure pathway, which should not be dismissed in future exposure estimations, especially considering other sources of dermal exposure to PFAS, i.e., personal care products.

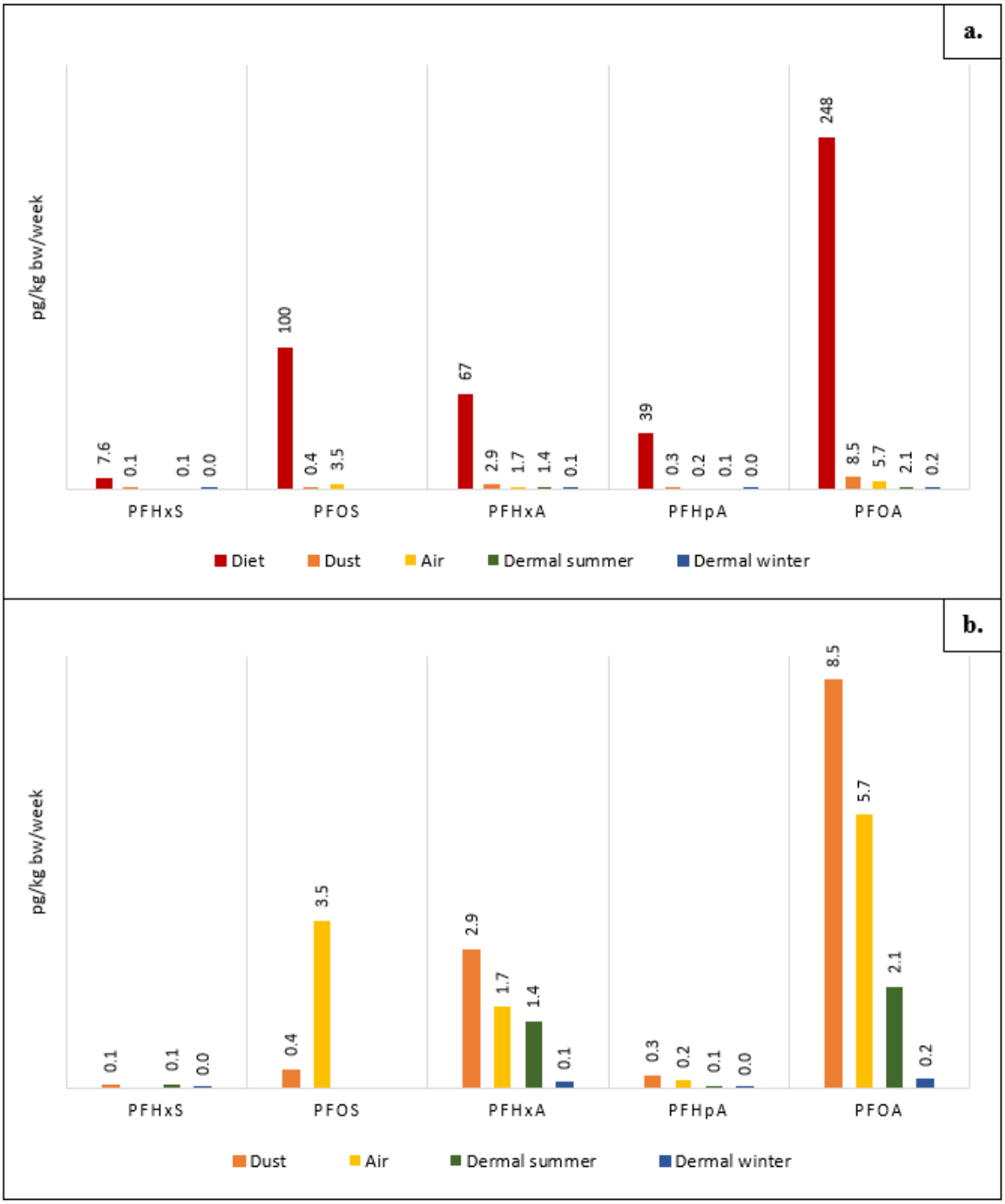


Figure 5-1: Human exposure to PFAS via dermal contact to dust compared to other known exposure pathways including (1a.) and excluding (1b.) diet.

It is important to emphasise that only one source (dust) of dermal exposure is included in the current study. This is likely to be a minor pathway compared to fabrics and/or personal care products. Recent studies have shown positive correlations between the use of personal care

products and serum PFAS levels indicating them as an important source of dermal exposure to PFAS (Serrano et al., 2021; Thépaut et al., 2021).

In general, human exposure to PFSAs were lower than to PFCAs as a result of dermal contact with indoor dust. This is not surprising considering the lower concentrations of PFSAs found in dust samples. Similar patterns are seen for other sources of dermal exposure to PFAS with fabric samples having been found to contain higher concentrations of PFCAs than PFSAs (Greenpeace, 2016; Xia et al., 2022; Zhu and Kannan, 2020). Similarly, cosmetics both from the European and North American market had higher concentrations of PFCAs than PFSAs, with no PFSAs being detected above the LOD in European cosmetic samples (Harris et al., 2022; Pütz et al., 2022; Schultes et al., 2018; Whitehead et al., 2021). Furthermore, PFCAs more readily permeate the dermal barrier compared to PFSAs of the same carbon chain length (Ragnarsdóttir et al., 2024) as was seen in the study presented in chapter 4 of this thesis. Collectively, this suggests that dermal exposure is likely greater for PFCAs compared to PFSAs.

5.4. Conclusion and future research

This study highlights the importance of human dermal uptake as an exposure pathway to PFAS. Even though only dust was considered here as a possible source of dermal exposure to PFAS, it did contribute to total huma exposure to PFAAs, albeit less than other indoor exposure pathways. Accounting for other sources of dermal exposure to PFAS (e.g., fabrics and/or cosmetics) would likely result in even higher contribution body burdens of PFAS. Thus, it is important for future exposure assessments not to dismiss this exposure pathway.

Precursor compounds to both PFCAs and PFSAs have been identified in both fabric and cosmetic samples (Harris et al., 2022; Pütz et al., 2022; Xia et al., 2022). In cosmetics, polyfluoroalkyl phosphates (PAPs) and fluorotelomer sulfonic acids (FTASs) have been detected in high concentrations while PAPs, fluorotelomer alcohols (FTOHs), and

fluorotelomer acrylates and methacrylates (FTAcs/FTMAcs) have been identified in fabric samples(Xia et al., 2022). The studies of the dermal permeation potential of precursor ions are limited. However, an *in vivo* rat study found that both 6:2 and 8:2 diPAPs were able to permeate through the skin with 7.8% and 7.2% of the applied dose having permeated respectively after 144h (Chen et al., 2022). Future studies to better understand both the direct permeation of the precursor ions as well as the possible dermal metabolism potential of those compounds, would further aid understanding of the contribution of the dermal pathway to human PFAS body burdens.

6. IN VITRO METABOLISM OF NOVEL PFAS

This chapter includes material taken verbatim from the following article:

> Licul-Kucera, V.; Ragnarsdóttir, O.; Frömel, T; van Wezel, A.P.; Knepper, T.P.; Harrad, S.; Abdallah, M. A.-E.; 2023. Interspecies comparison of metabolism of two novel prototype PFAS. *Under review in Chemosphere, October 2023.*

O.R. assisted with the development of the experimental protocol, assisted with the interpretation of the data, and writing the manuscript. V.L-K. performed the experiments, interpreted the data, and wrote the manuscript. T.F, A. v W., T. P. K., and S.H. reviewed, and edited the manuscript. M. A.-E. A. conceived and designed the experiment, assisted with the interpretation of the data, reviewed, and edited the manuscript.

6.1. Introduction

Per- and polyfluoroalkyl substances (PFAS) are a diverse group of synthetic chemicals widely used in many industrial and consumer applications as processing aids, e.g., emulsifiers, surfactant, lubricants, water-and oil repellents, inert media (Glüge et al., 2020b). PFAS have received increasing attention in the last years as studies have shown their ubiquitous distribution in the environment (Björnsdotter et al., 2021; Coggan et al., 2019; Cousins et al., 2022; González-Barreiro et al., 2006; Gremmel et al., 2017; Janousek et al., 2019). This stems from their physicochemical properties namely, high persistence (vP) and either high bioaccumulation potential (vB) or high mobility (vM). These properties both carry a level of concern for human exposure through the food chain or drinking water respectively (Hale et al., 2020). Significant health effects of PFAS have been suggested by several studies linking PFAS exposure to hepatic (Salihovic et al., 2018b; Sen et al., 2022b), renal (Stanifer et al., 2018) and thyroid dysfunction (Preston et al., 2021), preterm birth (Gardener et al., 2021) and immunotoxicity (DeWitt et al., 2019b; Grandjean et al., 2017b).

Based on the abovementioned risks, several jurisdictions have implemented restrictions on the use of certain PFAS over the past twenty years, e.g., under Stockholm Convention (United Nations Environment Programme, 2022, 2019, 2009) or REACH (Registration,

Evaluation, Authorisation and Restriction of Chemicals) (European Chemical Agency, 2022, 2020, 2019; European Commission, 2021). However, they mostly cover legacy PFAS – perfluoroalkyl carboxylic acids (PFCAs) and perfluoroalkane sulfonic acids (PFSAs) – which contain 4 to 14 carbon atoms in the chain. ECHA proposed a major legislative step towards the phase-out of all PFAS which fulfil the definition of Organisation for Economic Co-operation and Development and (OECD) for PFAS, namely "[...] that contain at least one fully fluorinated methyl (CF_3-) or methylene (-CF_2-) carbon atom (without any H/Cl/Br/I attached to it)" (Federal Institute for and Occupational Safety and Health, National Institute for Public Health and the Environment, Swedish Chemicals Agency, Norwegian Environment Agency, 2023; OECD, 2021). However, some PFAS which fulfil this definition, are excluded as they are fully degradable (Federal Institute for and Occupational Safety and Health, National Institute for Public Health and the Environment, Swedish Chemicals Agency, Norwegian Environment Agency, 2023).

According to the European Chemicals Agency (ECHA), manufacturers must demonstrate that the substance does not adversely affect the environment and human health (European Chemicals Agency, 2017). Environmental fate studies – including vPvB (high persistence (vP) and high bioaccumulation potential (vB)) assessment – are essential parts of the risk evaluation of any chemical intended to be released to the environment. These studies mostly include determination of the distribution amongst different environmental compartments and investigation of its microbial degradation and transformation pathway(s). While vPvB assessment is required, the use of ADME (absorption, distribution, metabolism, elimination) data is not mandatory (European Chemicals Agency, 2017). However, ADME profiling is intensively applied and obligatory in the pharmaceutical industry (Kola and Landis, 2004; Tsaioun et al., 2016). Drug development also proves that pharmacokinetic studies are essential in understanding the behaviour of a chemical in any organism, as they provide

additional information about a chemical that vPvB assessment cannot. Metabolic stability assays – as part of the ADME assessment – are performed to understand the susceptibility of a chemical to undergo biotransformation in the body (Van den Eede et al., 2013).

Chemicals can be eliminated by the organism unchanged, but the vast majority undergoes enzymatic functionalization and/or conjugation reactions that facilitate their elimination and protect the organism against an accumulation of lipid-soluble compounds (Osakwe, 2016). The liver plays an essential role in the metabolism, distribution, and excretion of xenobiotics (Sen et al., 2022b). Perfluoroalkyl acids (PFAAs) e.g., PFOA and PFOS are not metabolized and are poorly eliminated from the body but are reabsorbed via the enterohepatic circulation. The half-lives of PFAAs in humans can range from 1 month (PFBS) up to 8.5 years (PFOS), and increase with carbon chain length (Lau et al., 2007). PFAS precursors, e.g., fluorotelomer alcohols (FTOHs) can be metabolized, with both *in vitro* and *in vivo* studies showing the metabolism of these compounds in humans. Unfortunately, these compounds can then form the more persistent PFAAs, although they are considered minor metabolites (Fasano et al., 2006; Martin et al., 2005; Nabb et al., 2007a). Similar trends are seen with PFAS in nature. Under normal environmental conditions, PFAAs are hardly broken down and precursor compounds that are degradable in the environment will ultimately form persistent break-down products like PFAAs (Wang et al., 2017).

In a recent study, the environmental fate of two novel PFAS surfactants with a trifluoromethoxy headgroup was investigated (Licul-Kucera et al., 2023). These chemicals are covered by the OECD PFAS definition, however, they were expected, in theory, to degrade completely, i.e., mineralize in the environment. However, the study found that while only 2.5% and 1.2% of the starting surfactant was detected after 126 days, the unequivocal final mineralization of the investigated surfactants was not observed. Therefore, it is important to assess the possible fate of these chemicals in organisms of higher trophic level prior to the final

decision about their legislation. In the present study we investigate the *in vitro* phase I metabolism of these prototype PFAS surfactants in human and rat S9 subcellular fractions. We provide first insights into the *in vitro* pharmacokinetics of these novel chemicals in humans and rat and compare the differences in the rate of metabolism as well as interspecies metabolic profiles. Our aim is to understand the suitability of these novel chemicals – that are also PFAS according to both the Buck- and OECD-definition – as more environmentally-friendly alternatives to current PFAS (Buck et al., 2011; OECD, 2021; Wang et al., 2021).

6.2. Materials and Methods

6.2.1. Chemicals

6.2.1.1. Novel prototype PFAS chemicals

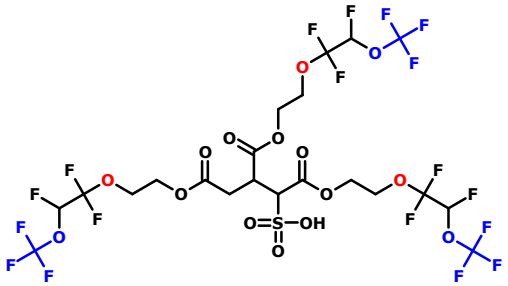
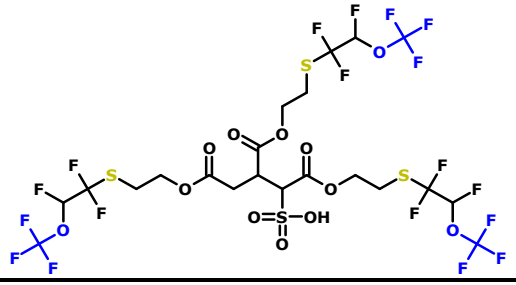
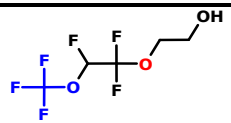
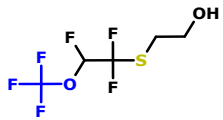
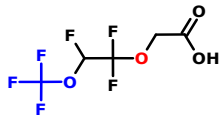
The novel prototype PFAS were designed and synthesized by Merck KGaA (Darmstadt, Germany). These chemicals are in the developmental phase and not yet available on the market. They are abbreviated as CF_3-O-SURF and CF_3-S-SURF in this study. The theoretically expected transformation products (TPs), abbreviated as CF_3-O-ALC, CF_3-S-ALC, CF_3-O-CA, CF_3-S-CA and CF_3-CA were also synthesized and measured during the study. The synthesized standards of CF_3-O-SURF and CF_3-S-SURF contained 1.3 and 3.5 w/w% impurity from CF_3-O-ALC and from CF_3-S-ALC, respectively. The structure, molecular formula and molecular weight of the prototype PFAS and their TPs are presented in Table 6-1. More details about the molecular structure of the prototype PFAS are available in section 6.3.1.

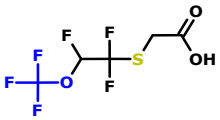
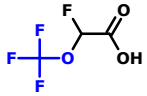
6.2.1.2. Further standards and chemicals

Perfluoropropionic acid (PFPrA), perfluoropropane sulfonic acid (PFPrS), perfluorohexanoic acid (PFHxA), perfluorononanoic acid (PFNA) and perfluorodecanoic acid (PFDA) were used as internal standards (IS). Their supplier and purity were given in Table 6-5. Water and methanol (MeOH) (both LiChrosolv®, ultrahigh-performance liquid chromatography−mass spectrometry (UHPLC−MS) grade) and dimethyl sulfoxide (DMSO) (≥99.7% purity) were obtained from Merck KGaA (Darmstadt, Germany). Ammonium acetate (>99% purity) was

bought from Fluka (Munich, Germany). Rat liver S9 fractions (pooled, from male Sprague-Dawley donors) were purchased from Merck KGaA (Darmstadt, Germany), while human hepatic S9 fractions (pooled, from three male donors) were bought from Biopredic International (Saint-Grégoire, France). Specifications of the S9 fractions are provided in section 6.5.1. The reagents of the nicotinamide adenine dinucleotide phosphate (NADPH) regenerating system, namely glucose-6-phosphate dehydrogenase (G6P-DH) from *S. cerevisiae* and glucose-6-phosphate (G6P) disodium salt hydrate (≥98% purity) were purchased from Merck KGaA, while the nicotinamide adenine dinucleotide phosphate disodium salt ($NADP^+$) (≥98% purity) was obtained from Carl Roth GmbH (Karlsruhe, Germany). Components of the incubation phosphate buffer medium, namely dipotassium phosphate (K_2HPO_4) (≥99% purity), magnesium chloride hexahydrate ($MgCl_2 \cdot 6H_2O$) (≥99.5% purity) and disodium ethylenediamine-tetraacetate dihydrate ($Na_2EDTA \cdot 2H_2O$) (≥99% purity) were purchased from Carl Roth GmbH (Karlsruhe, Germany).

Table 6-1. General information about the targeted chemicals of this study. Adapted from (Licul-Kucera et al., 2023).

Name	Abbreviation	Structure	Formula	Molecular weight ($gmol^{-1}$)
Parent substances				
1,5-dioxo-1,5-bis({2-[1,1,2-trifluoro-2-(trifluoromethoxy)ethoxy]ethoxy})-3-({2-[1,1,2-trifluoro-2-(trifluoromethoxy)ethoxy]ethoxy}carbonyl)pentane-2-sulfonic acid	CF_3-O-SURF		$C_{21}H_{20}F_{18}O_{15}S$	886.41
1,5-dioxo-1,5-bis(2-{[1,1,2-trifluoro-2-(trifluoromethoxy)ethyl]sulfanyl}ethoxy)-3-[(2-{[1,1,2-trifluoro-2-(trifluoromethoxy)ethyl]sulfanyl}ethoxy)carbonyl]pentane-2-sulfonic acid	CF_3-S-SURF		$C_{21}H_{20}F_{18}O_{12}S_4$	934.61
Possible metabolites				
2-[1,1,2-trifluoro-2-(trifluoromethoxy)ethoxy]ethan-1-ol	CF_3-O-ALC		$C_5H_6F_6O_3$	228.09
2-{[1,1,2-trifluoro-2-(trifluoromethoxy)ethyl]sulfanyl}ethan-1-ol	CF_3-S-ALC		$C_5H_6F_6O_2S$	244.16
[1,1,2-trifluoro-2-(trifluoromethoxy)ethoxy]acetic acid	CF_3-O-CA		$C_5H_4F_6O_4$	242.07

{[1,1,2-trifluoro-2-(trifluoromethoxy)ethyl]sulfanyl}acetic acid	CF_3-S-CA		$C_5H_4F_6O_3S$	258.14
Fluoro(trifluoromethoxy)acetic acid	CF_3-CA		$C_3H_2F_4O_3$	162.04

6.2.2. *In vitro* incubation

A series of test assays with different initial surfactant (CF_3-O-SURF, CF_3-S-SURF) concentrations (1, 2, 5, 10, 20, 50, 100, 200 µmol/L (µM)) were performed. Test assays were prepared by adding 1 mg/mL of RL-S9 or HL-S9 and 2.5 µL of the corresponding CF_3-O-SURF/ CF_3-S-SURF dosing solution (final concentration 1-200 mM, prepared in DMSO) to phosphate buffer (pH=7.4, 50 mM K_2HPO_4, 3 mM $MgCl_2 \cdot 6H_2O$, 1.2 mM $Na_2EDTA \cdot 2H_2O$). They were then pre-incubated for 5 min at 37 °C, with constant shaking. After that NADPH regenerating system (final concentration: 1.0 mM $NADP^+$, 5.0 mM G6P and 2 units/mL G6P-DH) was added to make a final volume of 250 µL. Samples were then incubated at 37 °C, with constant shaking, for 120 min (detailed preliminary optimization of incubation parameters in chapter 6.5.2 and figure 6-2). Finally, 250 µL of ice-cold MeOH was added to stop the reaction.

6.2.3. Sample preparation and clean-up

Following incubation, samples were vortexed for 10 s and centrifuged at 4000 rpm for 10 min. The supernatant was collected and then filtered through a 0.2 µm filter. An aliquot of the sample (depending on the initial concentration of parent substance) was then transferred to an autosampler vial and completed to 200 µL volume with 50/50 v/v% MeOH/H_2O and 10 µL of the mix of IS to have a final concentration of 7, 2.5, 1, 1 and 1 µg/L for PFPrA, PFPrS, PFHxA, PFNA or PFDA in the injected sample, respectively.

6.2.4. Quality Assurance and Quality Control

Applicability and reliability of the incubation method was tested with different control assays run in parallel to each sample batch. Activity of the liver enzymes was checked by the positive control assay, where the test compounds were replaced by metoprolol, a substance, whose metabolism is well-documented in the literature. Reagent blank assay was prepared by adding pure solvent (DMSO) instead of the dosing solution, to determine any background contamination. Heat-inactivated negative control assay was prepared identically to the test assays, but prior to the addition of NADPH regenerating system, it was incubated at 80 °C for

15 min. In this way, enzymes were heat-inactivated, and this control sample enabled the determination of any non-enzymatic transformation or loss processes (e.g., sorption). In the cofactor-free control assay the test compounds were incubated in the presence of S9 enzymes, but in the absence of the NADPH cofactor. Test assays were prepared in triplicates, while heat-inactivated negative control and cofactor-free control assays were prepared in unicates at different concentration levels. One positive control and reagent blank was prepared for each separate batch of samples.

The MS spectra of the injected positive control assays showed the characteristic peaks of metoprolol metabolites (Figure 6-3). The activity of enzymes was therefore justified. No parent compounds or metabolites were found in the reagent blank assays; therefore, no blank correction was needed.

6.2.5. Instrumental Analysis

Quantification was based on a calibration plot which included the parent compounds as well as those transformation products (TPs) for which reference standards were available. Targeted analysis was performed by liquid chromatography–tandem mass spectrometry (LC-MS/MS). For quantification, the internal standard calibration approach was used. As for the target analytes the corresponding mass-labelled chemical was not available, the non-mass labelled PFCA or PFSA which was the closest eluting to the corresponding target substance – namely PFPrA, PFPrS, PFHxA, PFNA or PFDA– was used as IS. Further details are provided in Table S1. Method performance was assessed with the calibration range, instrumental and method limit of detection (LOD) and limit of quantification (LOQ), and recovery described in section 6.5.4. Results are presented in Table 6-6.

Additional TPs for which reference standards were not available, were identified using an established non-targeted screening workflow on the high-resolution mass spectrometer

(HRMS) software. More details on non-targeted screening are provided in the SI section (Sections 6.5.5. and 6.5.6.).

6.2.6. Kinetic modelling

By using OriginPro 2018 software (version SR1-b9.5.1.195, OriginLab Corporation, Northampton, MA, USA), metabolite formation rate against the surfactant (CF_3-O-SURF, CF_3-S-SURF) concentration was plotted and different enzymatic kinetic models were fitted, namely the Michaelis-Menten equation, the Hill equation, and the substrate-inhibition equation (Lipscomb and Poet, 2008).

The model which best described all cases was the Michaelis-Menten equation (Equation 1) (Lipscomb and Poet, 2008).

$$v = \frac{Vmax \times [S]}{K_m + [S]} \quad \text{(Eq. 1)}$$

In the case of the Michaelis-Menten model, the apparent intrinsic *in vitro* clearance (CL_{int}) based on the formation of a certain metabolite can be calculated according to Equation 2 (Lipscomb and Poet, 2008).

$$CL_{int} = \frac{v}{[S]} = \frac{V_{max}}{K_m} \text{(Eq. 2)}$$

As in this study CL_{int} only expresses the metabolic capacity of 1 mg of S9 fraction in the liver, it is more informative to scale up by the protein density of the liver and express the metabolic capacity of 1 g of liver tissue (based on the corresponding subcellular fraction). This intrinsic *in vitro* hepatic clearance ($CL_{int,\ liver}$) on grams of liver basis, can be determined according to Equation 3 (Nishimuta et al., 2014).

$$CL_{int,\ liver} = CL_{int} \times p \quad \text{(Eq. 3)}$$

In the abovementioned equations *v* is the initial velocity of the reaction, V_{max} is the maximum rate of enzymatic reaction which is possible for that specific chemical-enzyme interaction, [S]

is the surfactant (CF_3-O-SURF, CF_3-S-SURF) concentration, K_m is the Michaelis-Menten constant, and p is the amount of protein per gram of the liver.

After fitting the Michaelis-Menten model, the parameters of the nonlinear function –V_{max} and K_m – were automatically calculated by the software. V_{max} is the rate of the reaction at which the enzyme shows the highest turnover, while K_m is the concentration required to achieve 50% of this maximum reaction rate. For calculation of $CL_{int,liver}$, the following parameters were applied: 121 mg protein·g liver^{-1} for HL-S9 (Nishimuta et al., 2014), and 136 mg protein·g liver^{-1} for RL-S9 (Zhou et al., 2020).

6.3. Results and Discussion

6.3.1. Metabolic pathways

Possible metabolic pathways were predicted by using fundamental knowledge of phase I enzymatic reactions (Lentz et al., 2013) and based on previous findings from microbial biotransformation of the same chemicals (Licul-Kucera et al., 2023). The prototype chemicals are trifunctional esters with aconitic acid – a naturally occurring, tricarboxylic acid – base, which is esterified by adding alcohols made of a trifluoromethoxy group linked to a fluorinated (thio)ethylene glycol derivative. On this basis, initial de-esterification of the surfactants catalyzed by esterase enzymes to release the alcohol, followed by oxidation of the free alcohol to a carboxylic acid by cytochrome P450 (CYP) enzymes via the formation of an aldehyde intermediate was hypothesized. As these carboxylic acids possess a -CHF-CF_2-O/S-CH_2- moiety in the molecule, there is a potential for the consecutive elimination of two HF molecules, initially producing CF_3-CA and then labile trifluoromethanol which further decomposes to HF and CO_2 at ambient temperature (Zachariah et al., 1995). The proposed transformation pathway is presented on Figure 6-4.

6.3.2. Metabolic profile by targeted analysis

6.3.2.1. CF_3-O-SURF

In the case of CF_3-O-SURF, no abiotic hydrolysis was observed in the heat-inactivated control nor in the cofactor-free control assays. This is in accordance with our previous finding (Licul-Kucera et al., 2023), that the abiotic hydrolysis of the surfactants was only experienced under highly basic conditions (pH=9) but not in nearly neutral medium such as the phosphate buffer (pH=7.4).

When incubating with RL-S9, as expected two metabolites, CF_3-O-ALC and CF_3-O-CA were produced. CF_3-O-ALC was detected in similar amounts in the cofactor-free control assay indicating that the biotic hydrolysis is not CYP-induced. Similar results were observed in a study where esters of p-hydroxybenzoic acid were incubated with HL-S9 without addition of NADPH regenerating system, yet esterase hydrolysis still occurred (Obringer et al., 2021). Oxidation of CF_3-O-ALC to CF_3-O-CA was most likely induced by CYP enzymes, confirmed by the observation that CF_3-O-CA was exclusively detected in test assays but not in the cofactor-free control assays. It is based on the functioning mechanism of CYP enzymes as – in contrast to esterases – they require a reducing agent (usually reduced nicotinamide adenine dinucleotide phosphate, NADPH) (Parkinson et al., 2015).

In the case of incubation with HL-S9, only one metabolite, the oxidation product CF_3-O-CA was detected. Possible explanations to this are that the CF_3-O-ALC was produced in an amount <LOD or that the oxidative transformation by CYP occurred more quickly in HL-S9 than in RL-S9. Less plausible is that the transformation of CF_3-O-SURF to CF_3-O-CA in human fractions followed a different pathway than in rat S9 and that CF_3-O-ALC is not an intermediate step in the oxidation. Roberts et al. (2012) also found some species-specific differences in the kinetics of the brominated diester bis(2-ethylhexyl) 2,3,4,5 tetrabromophthalate (TBPH). After the incubation with human liver microsomes, no loss of

TBPH or production of hydrolysis metabolite was observed. However, it was slowly metabolized in the presence of porcine hepatic carboxylesterase (Roberts et al., 2012).

6.3.2.2. CF_3-S-SURF

The metabolic profile of CF_3-S-SURF was similar to that of CF_3-O-SURF. First, no abiotic hydrolysis was observed neither in the heat-inactivated control nor in the cofactor-free control assays. During the incubation with RL-S9, both CF_3-S-ALC and CF_3-S-CA were detected. CF_3-S-ALC was also present in the cofactor-free control assays when using RL-S9. The sole detected metabolite with HL-S9 was CF_3-S-CA. This difference in the metabolic profile with the enzymes from two distinct species may be explained in similar fashion to CF_3-O-SURF.

6.3.3. Metabolic profile by non-targeted analysis

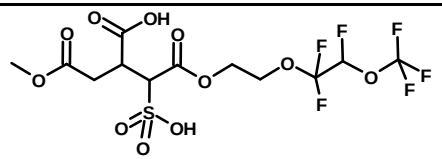
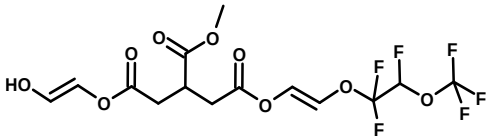
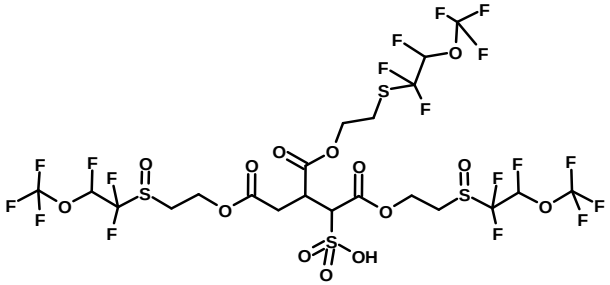
Following the post-acquisition data filtration steps (described in section 6.5.6.), two additional metabolites with unequivocal molecular formula and possible structure (at least level 3 identification confidence, according to Schymanski et al(Schymanski et al., 2014) of CF_3-O-SURF was found (Table 6-2). The structures were confirmed using the spectral information, e.g., production of acetate adducts, isotope patterns and diagnostic MS/MS fragments produced in MS/MS.

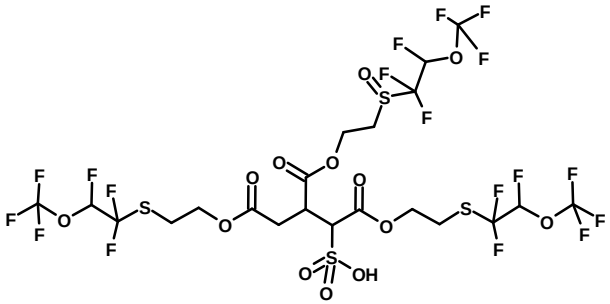
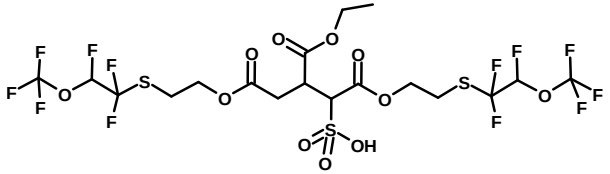
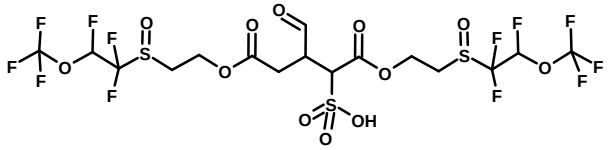
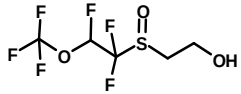
TP-NTS-O1 was an intermediate likely produced from CF_3-O-SURF by cleaving two moieties of the fluorinated wings of the molecule. TP-NTS-O2 originated from TP-NTS-O1 by cleaving the sulfonate group.

However, for CF_3-S-SURF, five additional transformation products with a minimum of level 3 identification confidence were identified (Table 6-2). TP-NTS-S1 was a di-oxidized molecule where the two oxygen atoms were either both linked to one of the thioether groups or to two different ones. The relative position of the two oxygens could not be determined in our experiments (level 3). TP-NTS-S2 was a mono-oxidized molecule where the single oxygen atom was linked to one of the equivalent thioether groups. Based on the diagnostic fragments,

the isotope pattern and the experimental context, the structure could unambiguously be assigned (level 2b). The third metabolite (TP-NTS-S3) was likely produced from the CF_3-S-SURF by cleaving a moiety of the fluorinated wing of the molecule. TP-NTS-S4 was probably formed from TP-NTS-S1 by cleaving a moiety of the fluorinated wings of the molecule. Like in TP-NTS-S1, the relative position of the two oxygens could not be unequivocally determined (level 3). The smallest metabolite (TP-NTS-S5) identified by HRMS was the oxidized CF_3-S-ALC, where the oxygen atom was linked to the thioether group. This structure was confirmed based on the presence of the MS/MS fragment $CHOS^-$ which unequivocally determined the position of the oxygen. Moreover, this molecule was also detected in the form of an acetate adduct which is a typical phenomenon reported for fluorinated alcohols (Berger et al., 2004). In RL-S9 incubations, TP-NTS-S1 was not present, while in samples incubated with HL-S9, TP-NTS-S3 was not detected. These metabolites – except TP-NTS-S2 – were detected with very low intensities. Table 6-2 summarizes the information of the findings of the non-targeted analysis.

Table 6-2: Metabolites of CF_3-O-SURF and CF_3-S-SURF identified by HRMS.

Name	Observed in samples incubated with S9 from H/R/H+R*	Formula	Proposed structure	m/z theoretical	Mass error (ppm)	Retention time (min)	Confirmation level (Schymanski et al., 2014)
CF_3-O-SURF							
TP-NTS-O1	R	$C_{12}H_{14}F_6O_{11}S$		479.0089	0.2	5.18	2b
TP-NTS-O2	R	$C_{14}H_{14}F_6O_9$		439.0469	0.2	6.96	3
CF_3-S-SURF							
TP-NTS-S1	H	$C_{21}H_{20}F_{18}O_{14}S_4$		964.9376	1.0	9.39	3

TP-NTS-S2	H+R	$C_{21}H_{20}F_{18}O_{13}S_4$		948.9427	-5.3	9.89	2b
TP-NTS-S3	R	$C_{18}H_{20}F_{12}O_{11}S_3$		734.9903	0.3	9.40	3
TP-NTS-S4	H+R	$C_{16}H_{16}F_{12}O_{12}S_3$		722.9539	1.4	7.56	3
TP-NTS-S5	H+R	$C_5H_6F_6O_3S$		258.9869	-3.9	6.22	2b

*Abbreviations:

H = human

R = rat

H+R = both human and rat

6.3.4. Metabolism kinetics

As the decrease in the concentration of the parent substances in the given test time was too small to be monitored over time, the formation of metabolites analysed be targeted analysis was monitored rather than the loss of surfactants (CF_3-O-SURF, CF_3-S-SURF). The production of metabolites was plotted against the dosing concentration of the parent compound. The estimated kinetic parameters for formation of the metabolites as well as the calculated *in vitro* hepatic clearance values are presented in Table 6-3. Comparable calculations were not performed for the metabolites analyzed be non-targeted analysis as these could not be quantified because of lack of standards.

6.3.4.1. CF_3-O-SURF

The plotted results showed formation of metabolite CF_3-O-CA was best fitted by the Michaelis-Menten model both in the HL-and RL-S9 incubation (Fig. 6-1B). However, CF_3-O-ALC – which was only present in the RL-S9 assays – did not fit any of the possible enzyme kinetic models (Fig. 6-1A). In fact, it did not reach saturation in the observed concentration range, indicating that steady state was not achieved. The lack of steady state condition for CF_3-O-ALC precluded the determination of its kinetic parameters using kinetic models.

The predicted maximum metabolic rates (V_{max}) for production of the metabolite CF_3-O-CA were 512 (±20) and 3974 (±192) fmol min^{-1} mg $protein^{-1}$ in HL-S9 and RL-S9 assays, respectively (Table 6-3). K_m values were 136 (±10) and 66 (±8) µM for HL-S9 and RL-S9, respectively (Table 6-3). The corresponding CL_{int} and $CL_{int,liver}$ values calculated according to Eq. 2 and 3 are reported in Table 6-3.

6.3.4.2. CF_3-S-SURF

For CF_3-S-SURF, formation of both CF_3-S-ALC and CF_3-S-CA metabolites was best fitted to the Michaelis-Menten model (Fig. 6-1C and 6-1D). However, as stated above, CF_3-S-ALC was only detected during reaction with RL-S9. The V_{max} value for

production of metabolite CF_3-S-ALC in RL-S9 was 562 750 (±19 633) fmol min^{-1} mg $protein^{-1}$. For CF_3-S-CA, the calculated V_{max} were 5 016 (±842) and 4 675 (±90) fmol min^{-1} mg $protein^{-1}$ in the HL-S9 and RL-S9 assays, respectively (Table 3). K_m values were 178 (±52) and 29 (±2) µM for HL-S9 and RL-S9, respectively (Table 3). The corresponding CL_{int} and $CL_{int,liver}$ values calculated based on Eq. 2 and 3 are presented in Table 6-3.

Table 6-3: Kinetic parameters derived from Michaelis-Menten model for the formation of CF_3-O-CA and CF_3-S-CA following incubation with RL- and HL-S9

Metabolite	Species	V_{max} (fmol·min^{-1}·mg^{-1})	K_m (µM)	CL_{int} (nL·min^{-1}·mg^{-1})	$CL_{int, liver}$ (µL·min^{-1}·g liver^{-1})
CF_3-O-ALC	**Human**	-	-	-	-
	Rat	-	-	-	-
CF_3-S-ALC	**Human**	-	-	-	-
	Rat	562 749 ± 19 633	126 ± 9	4459 ± 2288	606 ± 311
CF_3-O-CA	**Human**	512 ± 20	136 ± 10	4 ± 2	0.45 ± 0.24
	Rat	3 973 ± 192	66 ± 8	61 ± 25	8.23 ± 3.39
CF_3-S-CA	**Human**	5 016 ± 842	178 ± 52	28 ± 16	3.41 ± 1.96
	Rat	4 675 ± 90	29 ± 2	162 ± 52	22.0 ± 7.1

6.3.5. Inter-species metabolic comparison

The metabolic profile of CF_3-O-SURF and CF_3-S-SURF observed with the human and rat *in vitro* S9 assays only differed in terms of the presence of the corresponding alcohol CF_3-O-ALC or CF_3-S-ALC only following the RL-S9 incubation. This, however, might be linked to the deviation in the rate of the hydrolysis reaction as described under section 3.2.1 above.

Nabb et al. found no difference in the type of metabolites formed when an isotopically labelled PFAS, 8:2 fluorotelomer alcohol (8:2 FTOH) was incubated with rat, mouse, and human liver microsomes and cytosol (Nabb et al., 2007a). The

production of species-specific metabolites in one study, however, was reported for other halogenated substances. For instance, the various diastereomers of the brominated flame retardant, hexabromocyclododecane (HBCDD) produced metabolites which were exclusively detected either with rat or trout S9 fractions (Abdallah et al., 2014). A metabolic product of another flame retardant, TBPH, was exclusively formed *in vitro* by porcine enzymes, but not in human or rat subcellular fractions (Roberts et al., 2012). When incubating a short-chained chlorinated paraffin, 1, 2, 5, 5, 6, 9, 10-heptachlorodecane (HeptaCD) with chicken and human microsomes, two metabolites were detected in human liver microsomal assays, while only one metabolite was identified in chicken liver microsomal assays (Lin et al., 2022).

The conspicuous species differences in our study were revealed by comparing the metabolic rate obtained using HL-S9 with that observed when using RL-S9 enzymes. The $CL_{int,liver}$ values indicate that the metabolism of both parent substances was significantly higher in rats than in humans. Specifically, formation rates of CF_3-O-CA and CF_3-S-CA were about 18-times and 6.5-times faster in rats than in humans, respectively (Fig. 6-1). Similarly, metabolism of 8:2 FTOH was 10-times faster by rat liver microsomes (RLM) than by human liver microsomes (HLM) (Nabb et al., 2007a). Also, degradation of 2-ethylhexyl-2,3,4,5-tetrabromobenzoate (TBB) occurred significantly faster in the presence of RLM than with HLM; however, it was similar to the rate seen with porcine liver enzymes. For HBCDD diastereomers, the metabolic rate was much slower in trout than rat (Abdallah et al., 2014); while for HeptaCD it was faster for human than for chicken liver microsomes (Lin et al., 2022).

In the current study, the two studied surfactants (CF_3-O-SURF, CF_3-S-SURF) are congeners (i.e., chemical substances which are related to each other by structure). When comparing the CL_{int} values of the two congeners, CF_3-S-CA formation was 7.5

and 2.7-times higher than formation of CF_3-O-CA by HL-S9 and RL-S9, respectively (Fig. 6-1B and 6-1D). Abdallah et al. (2014) also reported different metabolic rates of three HBCDD diastereomers during phase I metabolism. Whereas β-HBCDD underwent rapid biotransformation, α-HBCDD was the most resistant to metabolic degradation in both rat and trout (Abdallah et al., 2014). In another hepatic *in vitro* metabolic study, TBB was easily metabolized even without the addition of any cofactor, while no metabolites were detected for TBPH in human or rat subcellular fractions, only by porcine carboxylesterase (Roberts et al., 2012).

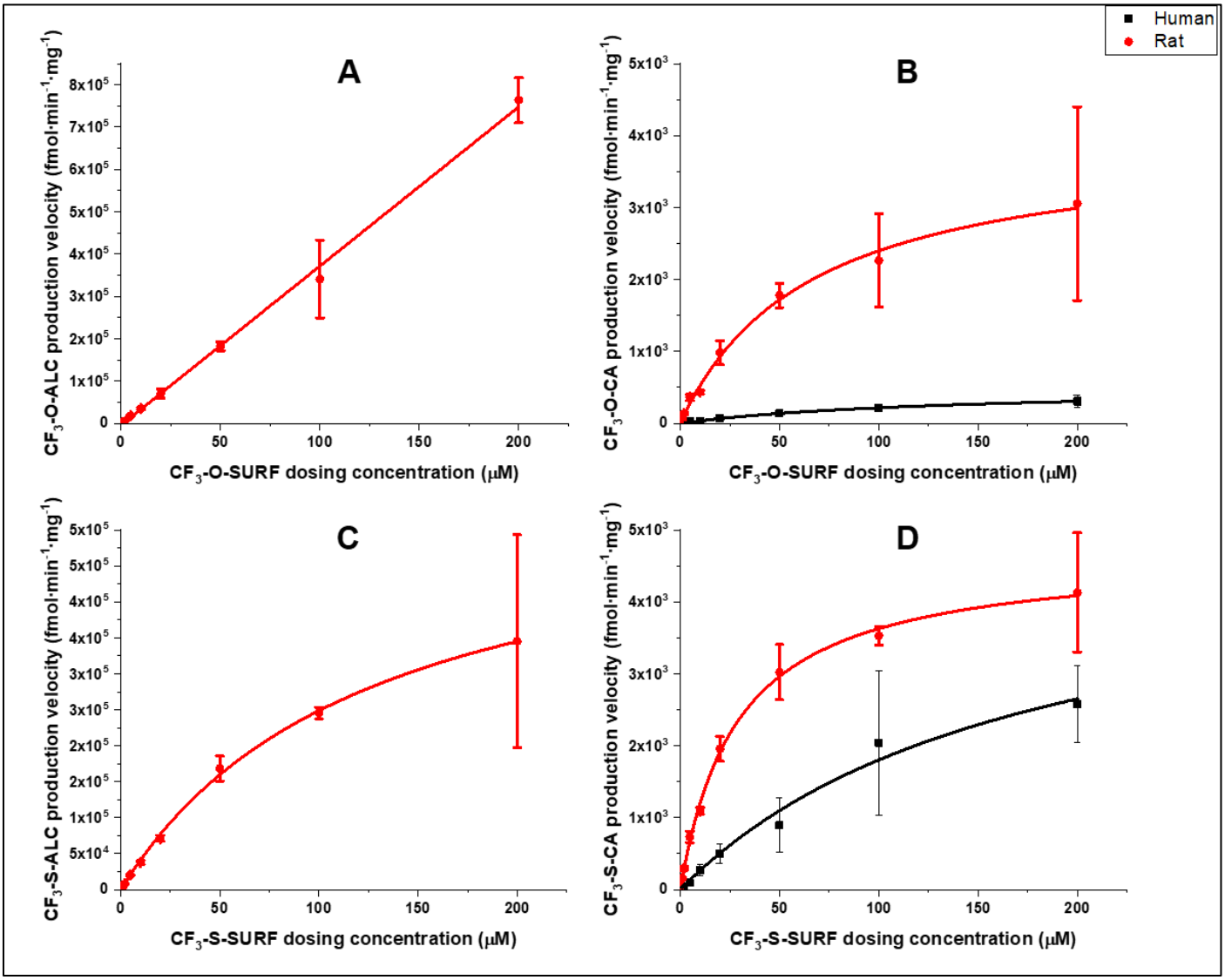


Figure 6-1: Kinetics of A) CF_3-O-ALC, B) CF_3-O-CA, C) CF_3-S-ALC and D) CF_3-S-CA production during incubation with rat and human S9 hepatic fractions, using the Michaelis-Menten model. Error bars represent standard deviations. (n=3).

6.3.5.1. The fate of the prototype PFAS chemicals in different species

The $CL_{int, liver}$ values of the novel prototype PFAS addressed in this study were found to be several orders of magnitude smaller than those for PFAS reported elsewhere (Table 6-4). The transformation rate of metabolite CF_3-O-CA by HL-S9 was about 10^5-times and 1.5×10^3-times lower than the degradation rate of 6:2 FTOH and 8:2 FTOH with HLM (Daramola and Rand, 2021; Li et al., 2009; Nabb et al., 2007b). Moreover, the transformation rate of metabolite CF_3-S-CA by HL-S9 was about 10^4-times and 2×10^2-times lower than the degradation rate of 6:2 FTOH and 8:2 FTOH when incubating with HLM, respectively (Daramola and Rand, 2021; Nabb et al., 2007a). A summary of $CL_{int, liver}$ values of the novel prototype PFAS and several other PFAS is presented in Table 6-4.

When determining the transformation rate of CF_3-S-SURF by RL-S9, the formation rate of CF_3-O-ALC and CF_3-S-ALC should be considered as they exceeded substantially those of CF_3-O-CA and CF_3-S-CA. However, as the steady state condition for CF_3-O-ALC was not achieved, the exact clearance values for this metabolite could not be calculated. Despite this, its formation rate was shown to be at least of the same order of magnitude to that of CF_3-S-ALC: Moreover, the production rate of CF_3-S-ALC by RL-S9 in this study was only about 3-times slower than degradation of 8:2 FTOH by RLM (Nabb et al., 2007a). Overall, these results suggest that metabolism of CF_3-O-SURF and CF_3-S-SURF is slow in humans, but faster in rats. Therefore, the present study highlights that extrapolation of kinetic rates between species or structurally similar substances can lead to serious over-or underestimation.

Table 6-4: Comparison of the intrinsic in vitro hepatic clearance values of PFAS

Substance	Species	Type of subcellular fraction	$CL_{int, liver}$ ($\mu L \cdot min^{-1} \cdot g\ liver^{-1}$)	Reference
CF_3-S-ALC	Rat	S9	606 ± 311	This study
CF_3-O-CA	Human	S9	0.45 ±0.24	This study
CF_3-S-CA	Human	S9	3.41 ± 1.96	This study
6:2 FTOH*	Human	microsomes	48 720	(Daramola and Rand, 2021)
8:2 FTOH*	Human	microsomes	638	(Li et al., 2016)
8:2 FTOH**	Rat	microsomes	1 832	(Nabb et al., 2007a)

*The study solely reported CL_{int} value. Hereby $CL_{int, liver}$ was calculated using Eq. 3, assessing the microsomal protein/gram of liver tissue (p) being 58 mg·g $liver^{-1}$.

** The study solely reported the $CL_{int, liver}$ value normalized to bodyweight. Hereby $CL_{int, liver}$ was calculated using the following equation, where w is the weight of liver (g) per kilogram bodyweight, being 12.5 g/0.25 kg for rat according to (Nabb et al., 2007a).

$$CL_{int,liver,bw} = \frac{CL_{int,liver,bw}}{w}$$

It has been shown in previous studies that the metabolism of the PFAS precursors FTOHs lead to the production of more toxic, e.g., fluorotelomer aldehyde, and/or highly persistent and bioaccumulative (PFAAs) metabolites (Butt et al., 2010; Li et al., 2016; Martin et al., 2005; Nabb et al., 2007a). On the contrary, these prototype chemicals metabolize to short-chained products which have a similar structure to metabolites

investigated by Folkerson et al. and have been found non-bioaccumulative (Folkerson et al., 2021). Further knowledge about the bioaccumulation, mobility and toxicity of the parent substances and their metabolites, is crucial to come to risk assessment for the tested prototype surfactants CF_3-O-SURF and CF_3-S-SURF.

6.4. Study limitations

In vitro assays are low-cost models for predicting the metabolic activity of a xenobiotic. Despite the extensive use of this methodology in the pharmaceutical industry, it has been reported that *in vivo* clearance calculated based on *in vitro* clearance values is often over-or underpredicted when compared to empirical studies (Wood et al., 2017). For example, when Folkerson et al. investigated both *in vitro* and *in vivo* metabolism of a prototype surfactant in rat, the *in vitro* experiment underestimated the metabolic rate *in vivo* (Folkerson et al., 2021). These results suggest the need for *in vivo* studies to realistically determine the half-life of xenobiotics. However, in terms of the identification of produced metabolites, the *in vitro* assay provided an adequate representation of the *in vivo* system.

Another limitation of this study is that only phase I metabolism was investigated. However, as shown in previous studies, fluorinated substances often also produce phase II conjugates in relevant amounts. In the case of FTOHs, glucuronide, sulfate, glutathione and taurine conjugates were identified during *in vitro* incubations (Li et al., 2016; Martin et al., 2005; Nabb et al., 2007a). According to Martin et al. and Li et al., phase II conjugation is the major transformation and excretion route of 8:2 FTOH (Li et al., 2016; Martin et al., 2005). In an *in vivo* experiment, rats were dosed with polyfluoroalkyl phosphate esters. After its hydrolysis to FTOH, glucuronide conjugates were observed at 2 hr and 6 hr postdosing, and sulfate conjugates were detected between 6 hr and 2 days postdosing (D'eon and Mabury, 2011). Also, even though the S9

fraction used in this study are pools from more than one individual, intra-species variations (e.g., sex, age) could not be accounted for.

Therefore, further studies investigating phase II metabolism, as well as *in vivo* experiments are required for comprehensive understanding of metabolic pathways and kinetics, and to be able to assess the health effects of these compounds. Overall, the present study enhances understanding the fate and behavior of these novel prototype fluorinated compounds in different types of organisms. Through characterization of formed metabolites and comparison of transformation rates across species, our results may serve as a basis for future risk evaluation.

6.5. Supporting Information

6.5.1. Specification of S9 fraction

CERTIFICATE OF ANALYSIS by Biopredic International

Human Hepatic S9 Fractions, Pooled

Catalog reference: S2067, Batch number: SLCM5659

NUMBER OF DONORS	**POOL OF 3 DONORS**	
ETHNICITY	Not available	
DONOR NR.	**Sex**	**Age (years old)**
DONOR 1	Male	61
DONOR 2	Male	62
DONOR 3	Male	26
CRITERIA	**Specifications**	**Results**
PROTEIN CONTENT PER VIAL (MG/VIAL)	≥ 10	12

CERTIFICATE OF ANALYSIS by Sigma-Aldrich

Rat, Hepatic S9 Fractions, Pooled

Catalog reference: FRA259, Batch number: FRA259264

NUMBER OF DONORS		**NOT AVAILABLE**
BREED		Sprague-Dawley
SEX		Male
CRITERIA	**Specifications**	**Results**
PROTEIN CONTENT PER VIAL (MG/VIAL)	≥ 20	20

6.5.2. Optimization of incubation time

The optimal incubation time was selected based on experimental evaluation where a test assay containing 5 µM of CF_3-O-SURF was incubated with RL-S9. Test assay was prepared as described in 2.2 and samples were taken after 0, 10, 30, 60, 120-, 180-, 240- and 360-min incubation. After that the samples were cleaned up according to 2.3 and the concentration of the metabolite CF_3-O-CA measured on LC-MS/MS as described in 2.5.

The incubation time was determined based on two criteria: i) it should fit into the linear range of the transformation rate – incubation time relation and ii) the concentration of the produced metabolites should be quantifiable.

Based on the results presented on Figure 6.2 the formation of the metabolite increased until 180 min incubation, however, the linearity was fulfilled only in the 0-120 min range. To maximize the metabolite formation, 120 min was selected as optimal incubation time.

6.5.3. Targeted LC-MS/MS analysis

Nexera XR HPLC system (Shimadzu Germany GmbH, Duisburg, Germany) was hyphenated to an Sciex QTrap 5500 System (AB Sciex Germany GmbH, Darmstadt,

Germany). Reversed phase (RP) LC separation was achieved using an XSelect HSS T3 column (Waters, Milford, MA, USA; dimensions: 50 x 2.1 mm, 3.5 μm) equipped with the corresponding pre-column (5 x 2.1 mm, 3.5 μm). The RPLC eluents consisted of 95% water and 5% MeOH (v/v, eluent A) and 5% water and 95% MeOH (v/v, eluent B), both with 5 mM ammonium acetate. The gradient started at 0% eluent B, increased to 100% B in 6 min, and held it for 4 min. Then eluent B decreased to 0% from 10-10.5 min and it was held for 5 min. The total run time was 15.5 min, the injection volume was 10 μL and the flow rate was 300 μL/min. The oven temperature was maintained at 23 °C.

All target compounds were measured in negative electrospray ionization mode. The optimized source temperature was 300 °C, the spray voltage was -4000 V. Nitrogen was used as curtain gas and ion source gas 1 and 2 at a flow rate of 40, 50 and 65 psi, respectively. More details about the LC-MS/MS measurement, including the multiple reaction monitoring (MRM) parameters for each analyte are presented in Table S1. Applicability and performance of the targeted LC-MS/MS method was detailed in Section 6.5.4 and table 6.6.

6.5.4. Analytical performance of the LC-MS/MS method

Calibration and quantitation of the target analytes was performed by internal standard approach, using the surrogate standards mentioned in paragraph 6.2.1.2. As no isotopically labelled standards for the target analytes were available, surrogate standards were selected based on the structural and elution similarity to the target compounds. Applicability of the surrogate compounds was individually evaluated based on the trueness validation results.

As criteria for positive identification, the approach adopted from Commission Decision 2002/657/EC was used. Firstly, retention time determined in the real sample

must equal to the one in the standards within a margin of error of 5%. Secondly, where possible, two MRM transitions – a quantifier and a qualifier – for each analyte should be monitored. Thirdly, their area ratio in the real sample must be like that determined in the standards within a 20% margin of error.

A quality control (QC) standard (20 µg/L) was regularly injected between real samples in order to monitor any shifts in retention times or changes in the sensitivity of the instruments over measuring time. Calculated concentration of target analytes in the samples was corrected according to the actual QC value.

Performance of the targeted LC-MS/MS method was assessed based on parameters such as recovery, limit of detection (LOD), and limit of quantification (LOQ). Recovery was calculated according to Eq. S1.

$$Recovery(\%) = \left[\frac{c_{spiked,sample} - c_{sample}}{c_{standard}}\right] \times 100\% \quad \text{(Eq.S1)}$$

where c_{spiked} is the measured concentration of the analyte in the sample matrix spiked with the analytes and IS (in µg/L), c_{sample} is the measured concentration of the analyte in the blank sample matrix, $c_{standard}$ is the measured concentration of the analyte (in µg/L) in the standard.

Instrumental LOQ was determined by measuring standards around the expected concentration and by choosing the one which was measurable with adequate precision and accuracy. Instrumental LOD of an analyte was determined as the LOQ/3. Method performance parameters are presented in Table 6.3.

6.5.5. Non-targeted HRMS analysis

Samples were analyzed on a UPLC Nexera X2 system (Shimadzu Germany GmbH, Duisburg, Germany) hyphenated to a Sciex X500R QTOF system (AB Sciex Germany GmbH, Darmstadt, Germany). Analytes were chromatographically separated on a

RPLC column, namely Acquity UPLC® HSS T3 (Waters, Milford, MA, USA; dimensions: 50 x 2.1 mm, 1.8 µm). As eluents, 95% water and 5% MeOH (v/v, eluent A) and 5% water and 95% MeOH (v/v, eluent B), both with 5 mM ammonium acetate, were used. The gradient started at 0% eluent B and was held for 2 minutes. Then further increased to 100% B in 12 min, and held it for 2 min. Then the initial composition to 0% B returned in 0.1 min and the column was re-equlibrated for 4 min. The total run time was 20 min, the injection volume was 10 and the flow rate was 500 µL/min. The oven temperature was held on 40 °C.

All mass spectrometric experiments were performed in negative electrospray ionization mode. The ionspray voltage was -4500 V, the temperature of the ion source was 550 °C, while the curtain and the two ion source gases were 35, 45, 45 psi, respectively. For all samples, both information dependent acquisition (IDA) and DIA (Data-Independent Acquisition) analysis was carried out. In both cases, the TOF full scan with the following settings was used: m/z range = 70-1000, declustering potential = -50 V ± 30 V, collision energy = -10 V, accumulation time = 0.2 s. During IDA analysis, five candidates were selected for MS/MS analysis (excluding candidates for 3 s after one occurrence) with an intensity threshold of 500 cps. MS/MS analysis was done with the following settings: m/z range = 50-1000, declustering potential = -50 V ± 30 V, collision energy = -50 V ± 30 V, accumulation time: 0.1 s. DIA analysis was carried out with the same MS/MS settings.

Sciex OS software (AB Sciex Germany GmbH, Darmstadt, Germany; version number: 1.6.10.40973) was used for data analysis with non-targeted and suspect screening workflows. During the peak picking process, a process blank sample was used as control sample, and the peaks of those compounds at m/z was picked which had

an area at least 10-times higher the peaks at the same m/z in the control sample. The third most exhaustive peak detection sensitivity was used.

6.5.6. Workflow for the identification of further transformation products

After the included peak picking workflow of the Sciex OS software, false hits were excluded using many filter steps. In the first step, features which area was at least 10-times higher than the area of the procedural blank, were selected and all others were filtered out. The next plausibility criterion was that the area in the test assays should be at least 10-times higher compared to the area in the corresponding negative control assay. The third requirement was that the feature should be present in both the IDA and the corresponding DIA screenings. Finally, during a manual plausibility check ion-source fragments, isotopologues, unlikely adducts, hits with sum formulas not in compliance to their isotopic pattern and further unlikely ion species were removed. Additionally, features were compared to the candidates of the suspect list. Suspect list was established by suggesting possible TPs whose production during the biotransformation is plausible.

Table 6-5:. General information about the analyzed prototype molecules and their internal standards (IS), and the liquid chromatographic-tandem mass spectrometric (LC-MS/MS) method.

	Abbreviation	Formula	Manufacturer	Purity (w/w%)	IS used	Retention time [min]	Q1 [m/z]	Q3 [m/z]	DP [V]	EP [V]	CE [eV]	CXP [V]
Target analytes	CF_3-CA	$C_3H_2F_4O_3$	Merck KGaA	no information	PFPrA	1.31	161	85	-40	-10	-16	-13
	CF_3-O-CA	$C_5H_4F_6O_4$	Merck KGaA	no information	PFPrS	3.85	241	163	-45	-10	-20	-13
							241	183	-45	-10	-12	-15
	CF_3-S-CA	$C_5H_4F_6O_3S$	Merck KGaA	no information	PFPrS	4.01	257	85	-35	-10	-16	-9
	CF_3-O-ALC	$C_5H_6F_6O_3$	Merck KGaA	no information	PFHxA	4.82	287	59	-30	-10	-22	-9
	CF_3-S-ALC	$C_5H_6F_6O_2S$	Merck KGaA	no information	PFHxA	5.08	303	59	-40	-10	-22	-9
	CF_3-O-SURF	$C_{21}H_{20}F_{18}O_{15}S$	Merck KGaA	no information	PFNA	6.07	885	81	-5	-10	-126	-13
							885	721	-5	-10	-34	-51
	CF_3-S-SURF	$C_{21}H_{20}F_{18}O_{12}S_4$	Merck KGaA	no information	PFDA	6.23	933	81	-20	-10	-118	-13
							933	85	-20	-10	-136	-9
Internal standards	PFPrA	$C_3HF_5O_2$	Merck KGaA	97%	-	1.69	163	119	-20	-10	-13	-10
							163	69	-20	-10	-50	-10
	PFPrS	$C_3HF_7O_3S$	Kanto Corporation	95%	-	3.82	249	80	-40	-10	-55	-10
							249	99	-40	-10	-30	-10
	PFHxA	$C_6HF_{11}O_2$	Neochema	97%	-	5.02	313	269	-60	-10	-13	-10
							313	119	-60	-10	-32	-10
	PFNA	$C_9HF_{17}O_2$	Neochema	97%	-	5.99	463	419	-60	-10	-18	-10
							463	169	-60	-10	-29	-10
	PFDA	$C_{10}HF_{19}O_2$	Neochema	98%	-	6.21	513	469	-40	-10	-18	-10
							513	269	-40	-10	-27	-10

Table 6-6: LC-MS/MS method performance parameters determined for the quantified targeted metabolites.

Abbreviation	Mean recovery% (n=2)	± RSD %	Instrumental LOQ [µg/L]	Instrumental LOD [µg/L]	Method LOQ [µg/L]	Method LOD [µg/L]	Lowest calibration point [µg/L] (instrumental)	Highest calibration point [µg/L] (instrumental)	Nr. of calibration points
CF_3-O-CA	104%	6%	0.10	0.03	4.0	1.3	0.10	25	7
CF_3-S-CA	112%	7%	0.10	0.03	4.0	1.3	0.10	25	8
CF_3-O-ALC	116%	5%	5.00	1.67	200.0	66.7	5.00	100	4
CF_3-S-ALC	98%	5%	1.00	0.33	40.0	13.3	1.00	100	7

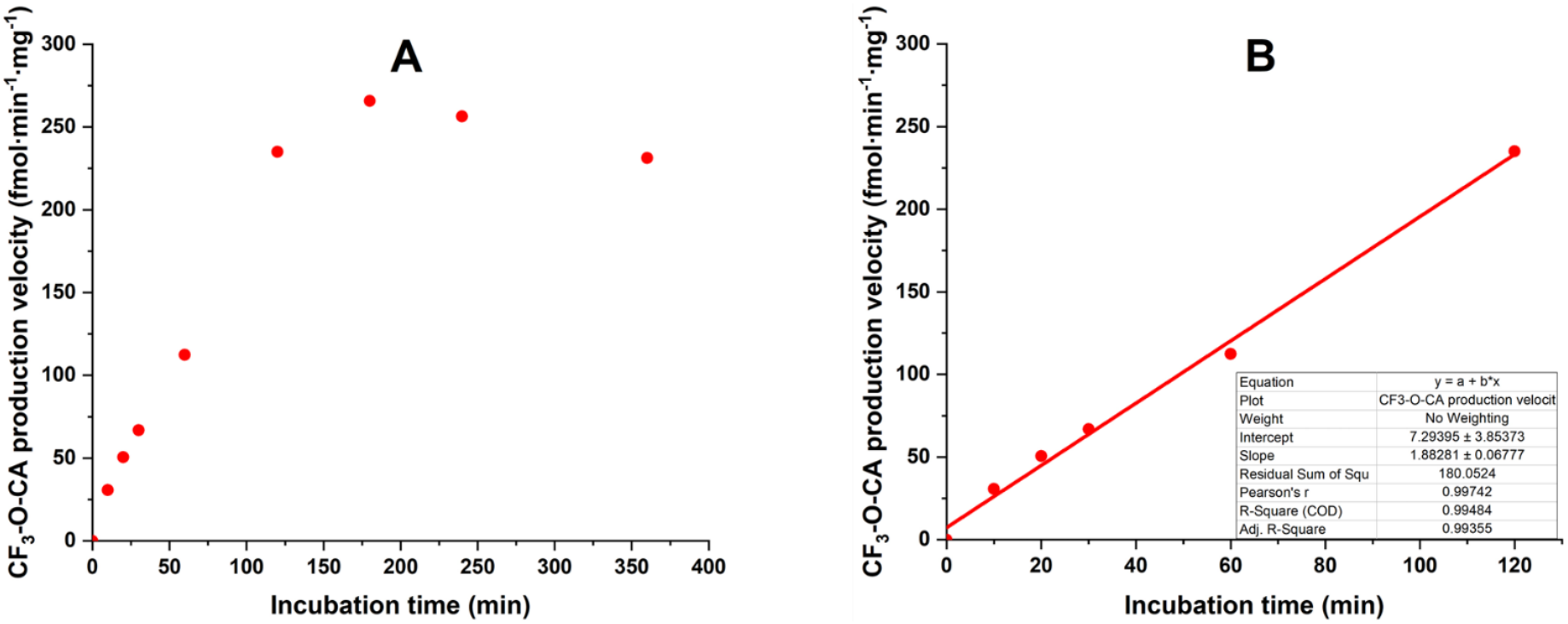


Figure 6-2: The transformation rate – incubation time relation with rat liver S9 fraction A) in the whole incubation period B) in the linear range.

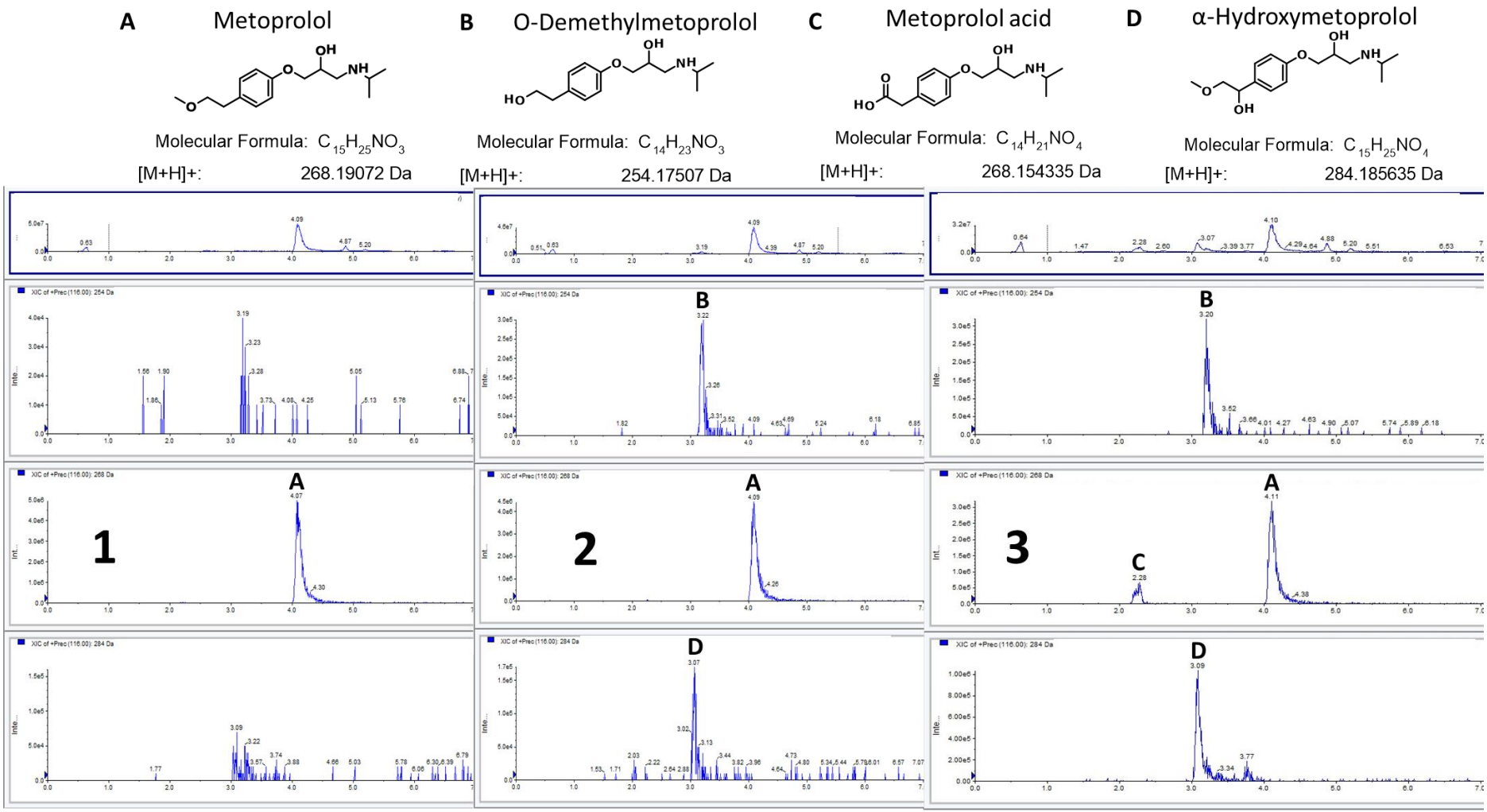


Figure 6-3: Chromatograms of positive control samples 1) before incubation 2) after 120 min incubation with human liver S9 3) after 120 min incubation with rat liver S9

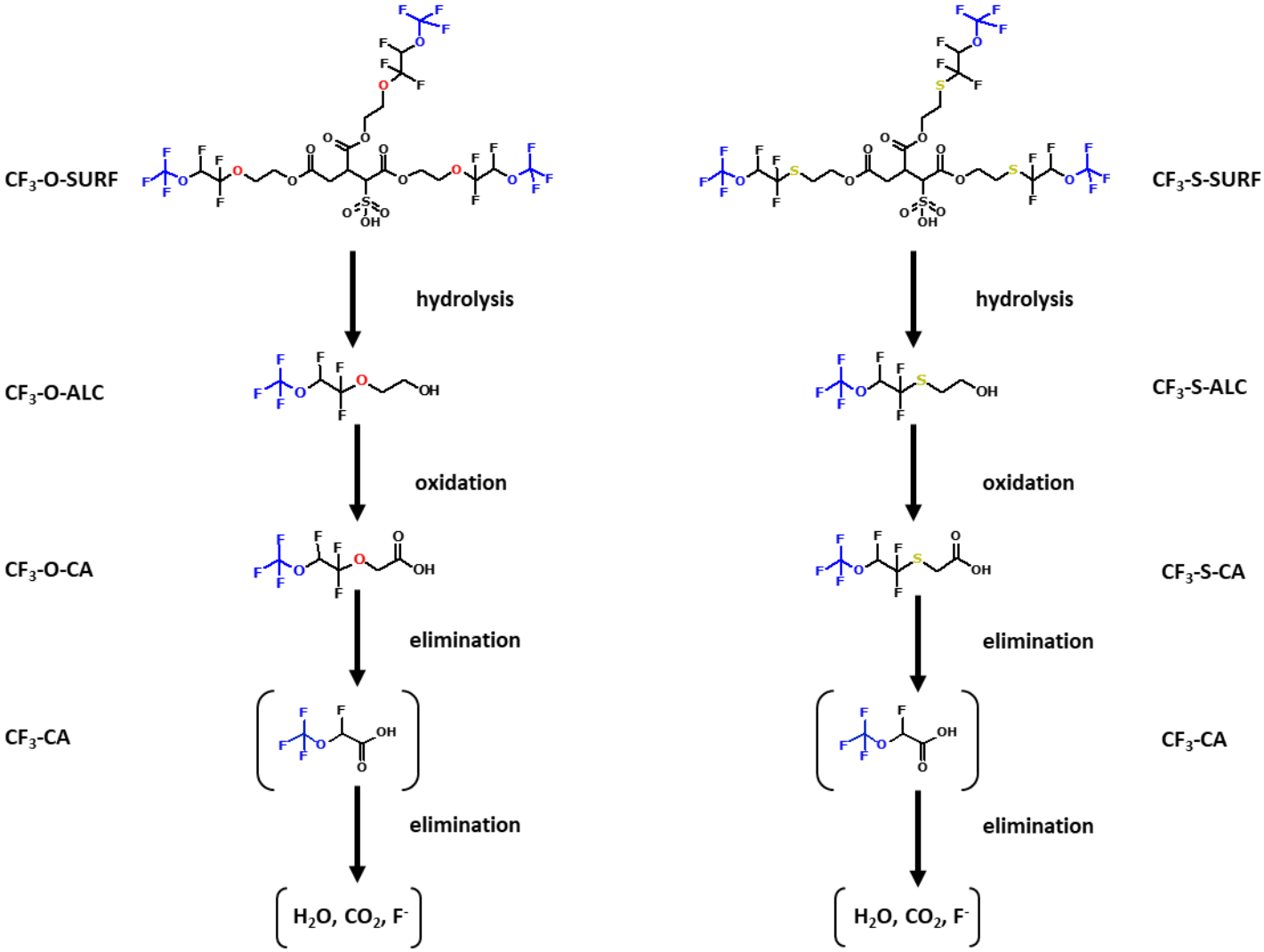


Figure 6-4: Proposed transformation pathway of the novel PFAS prototype chemicals. The metabolites in brackets were not detected in this study.

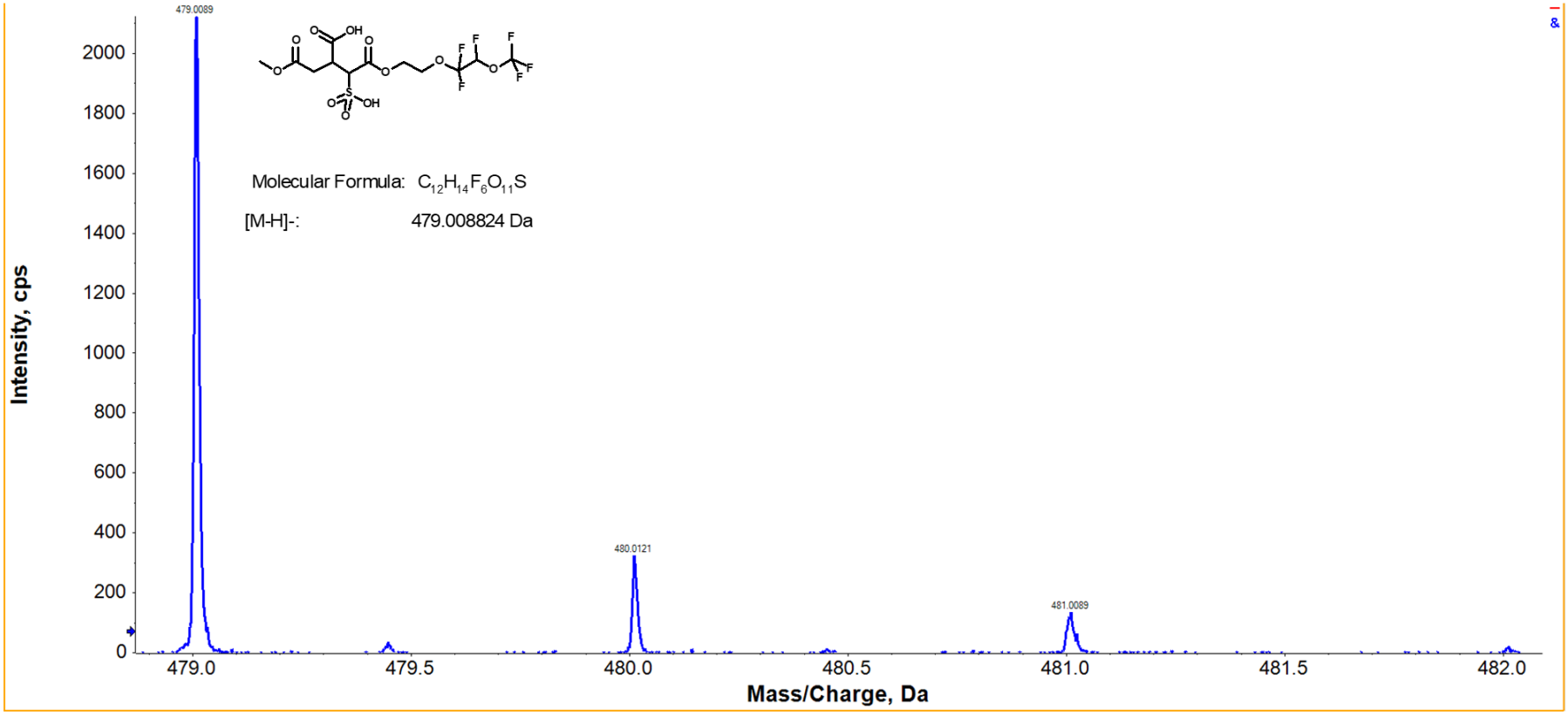


Figure 6-5: MS spectrum of TP-NTS-O1. Identified only in the RL fractions.

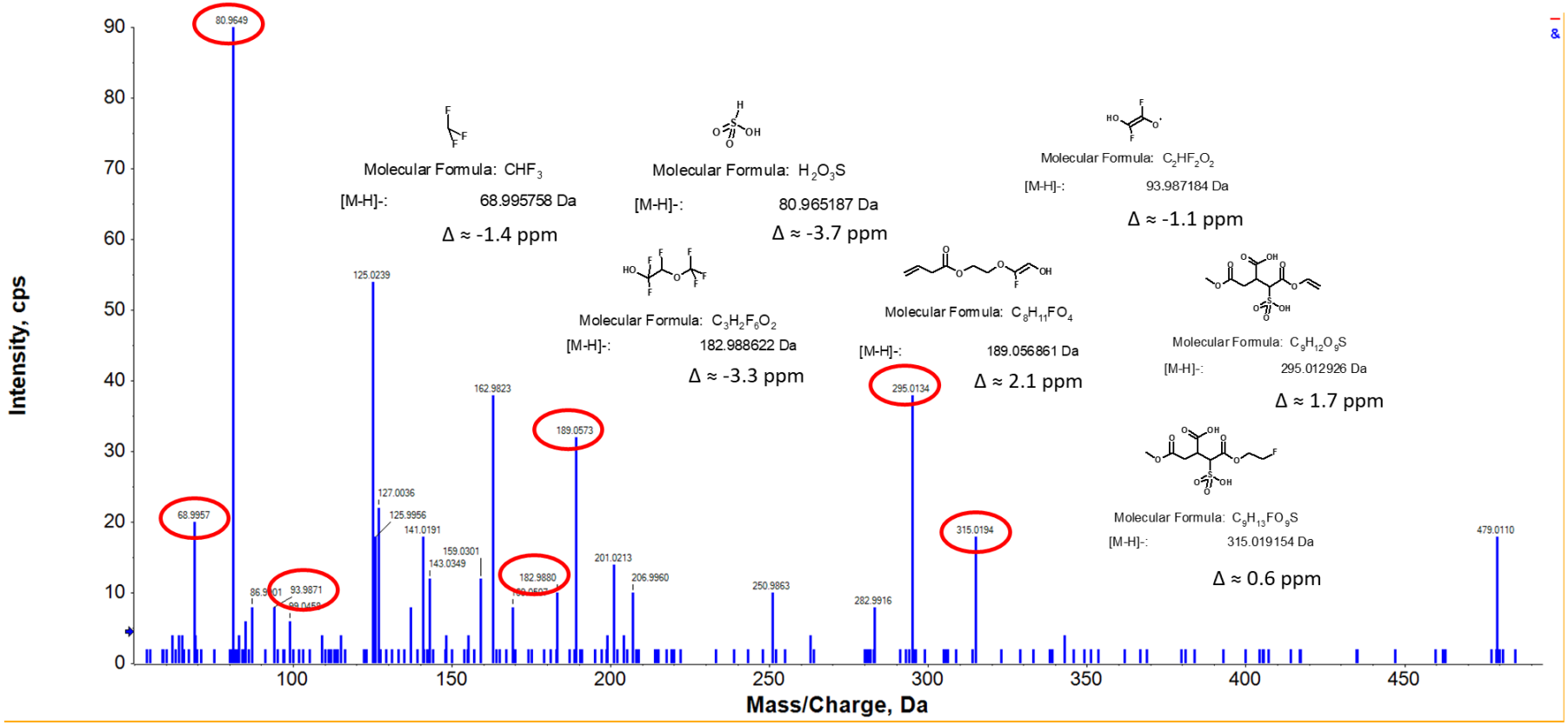


Figure 6-6: MS/MS spectrum of TP-NTS-O1.

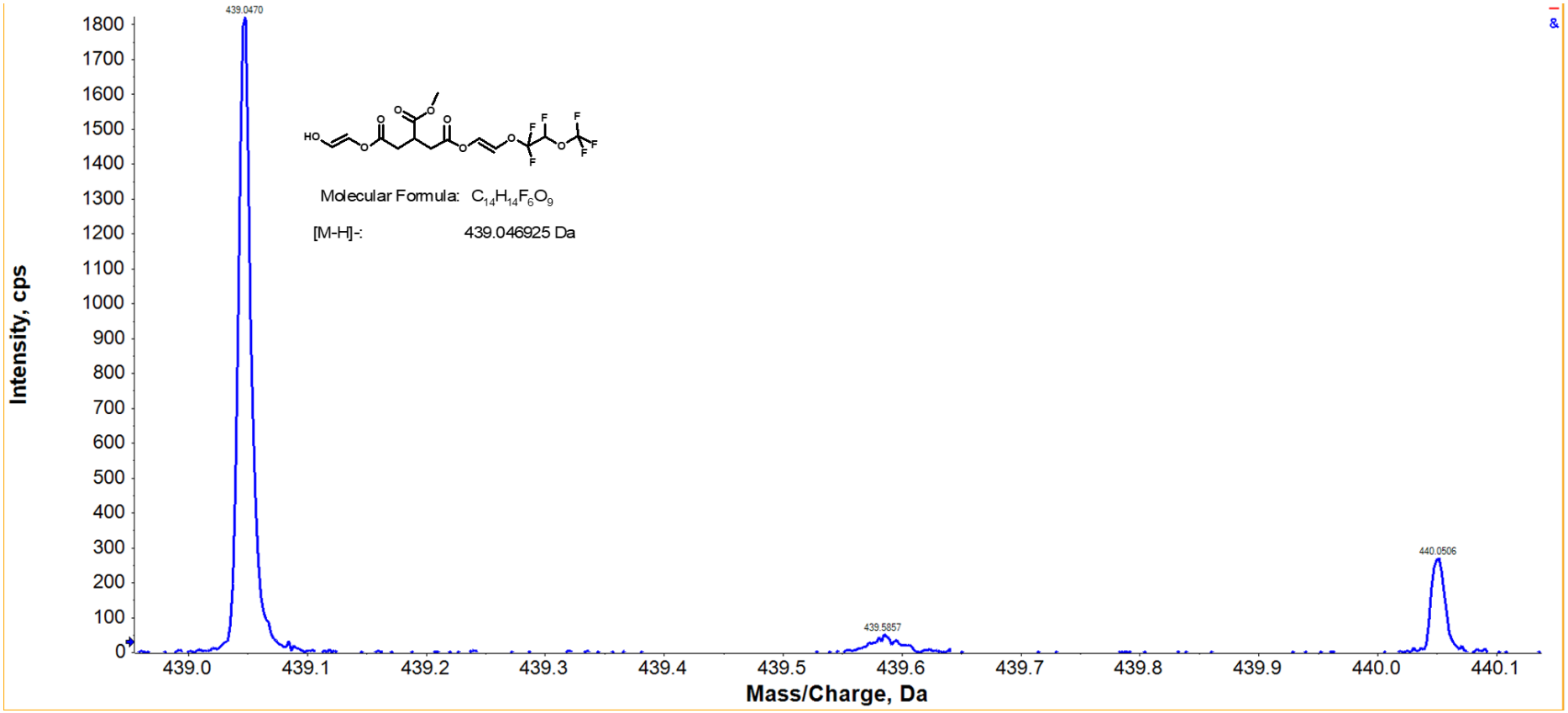


Figure 6-7: Full-scan MS spectrum of TP-NTS-O2. Identified only in the RL fractions.

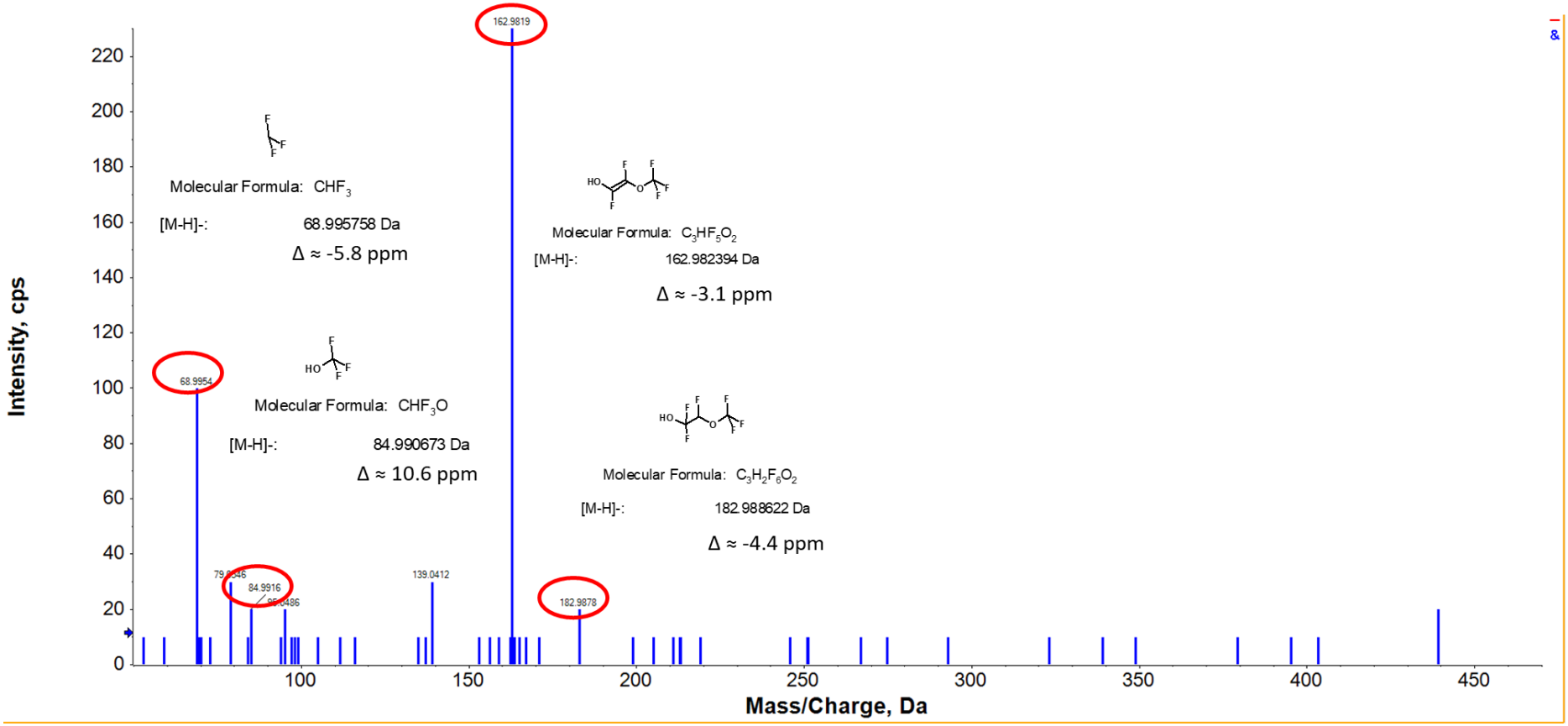


Figure 6-8: MS/MS spectrum of TP-NTS-O2.

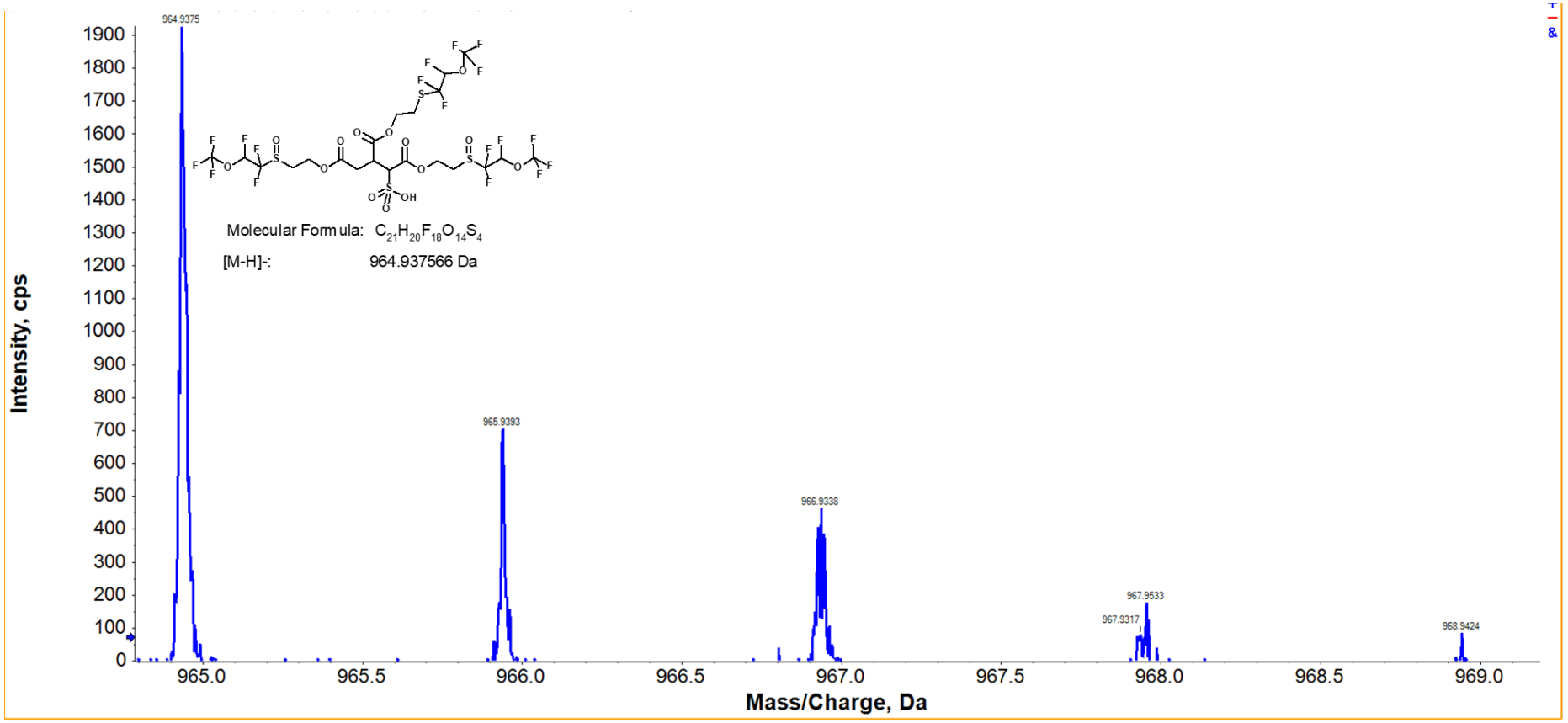


Figure 6-9: Full-scan MS spectrum of TP-NTS-S1. Identified only in the HL fractions.

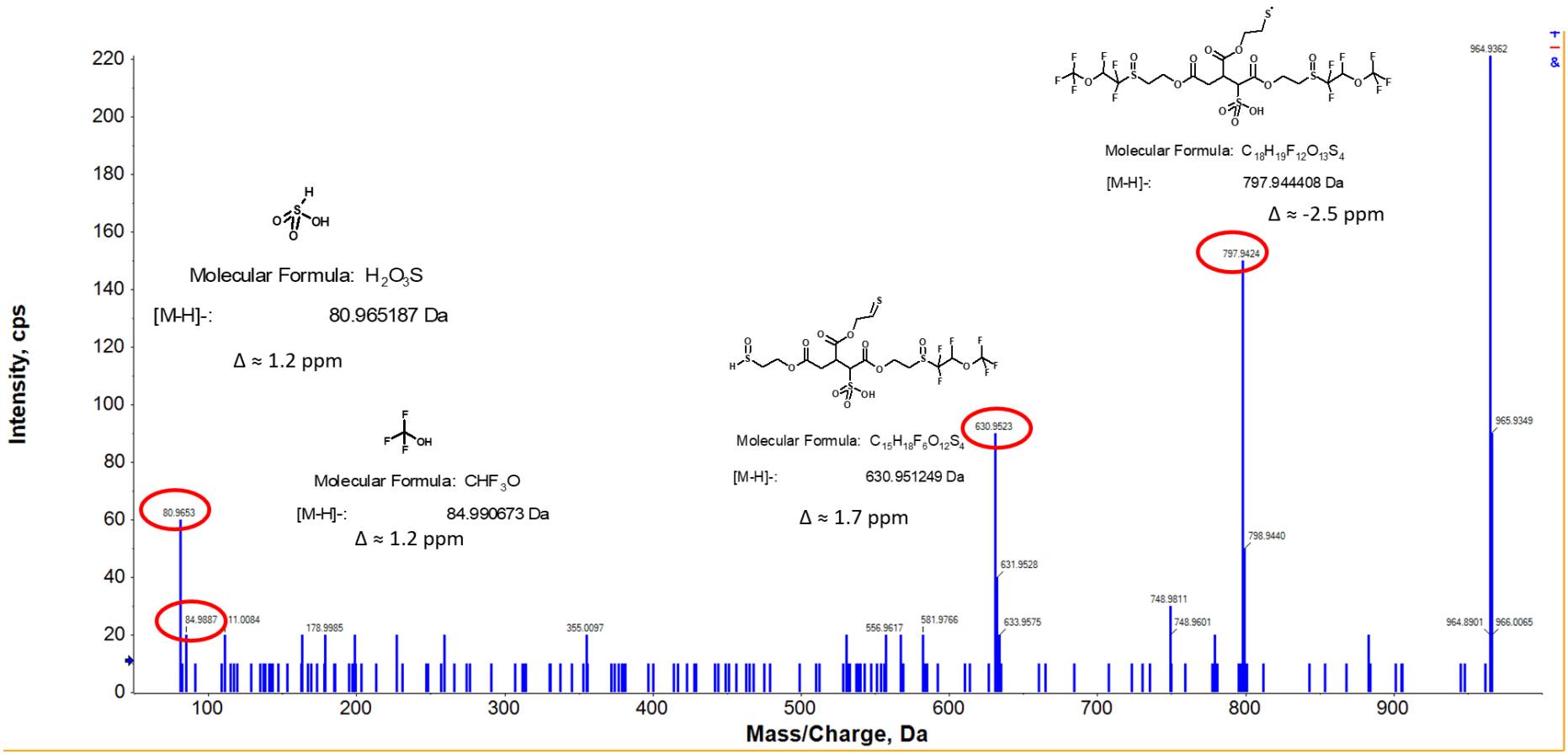


Figure 6-10: MS/MS spectrum of TP-NTS-S1.

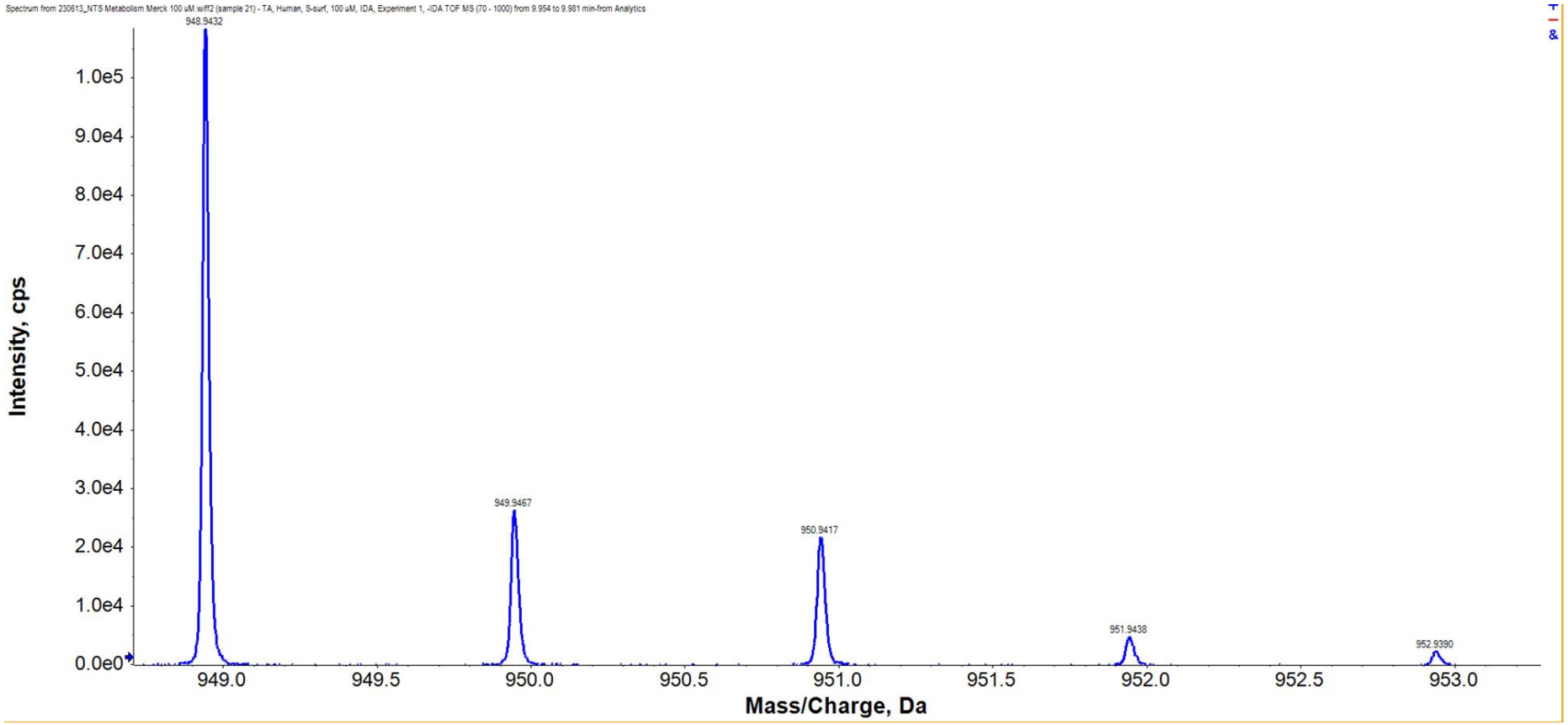


Figure 6-11: Full-scan MS spectrum of TP-NTS-S2. Identified in both the RL and HL fractions.

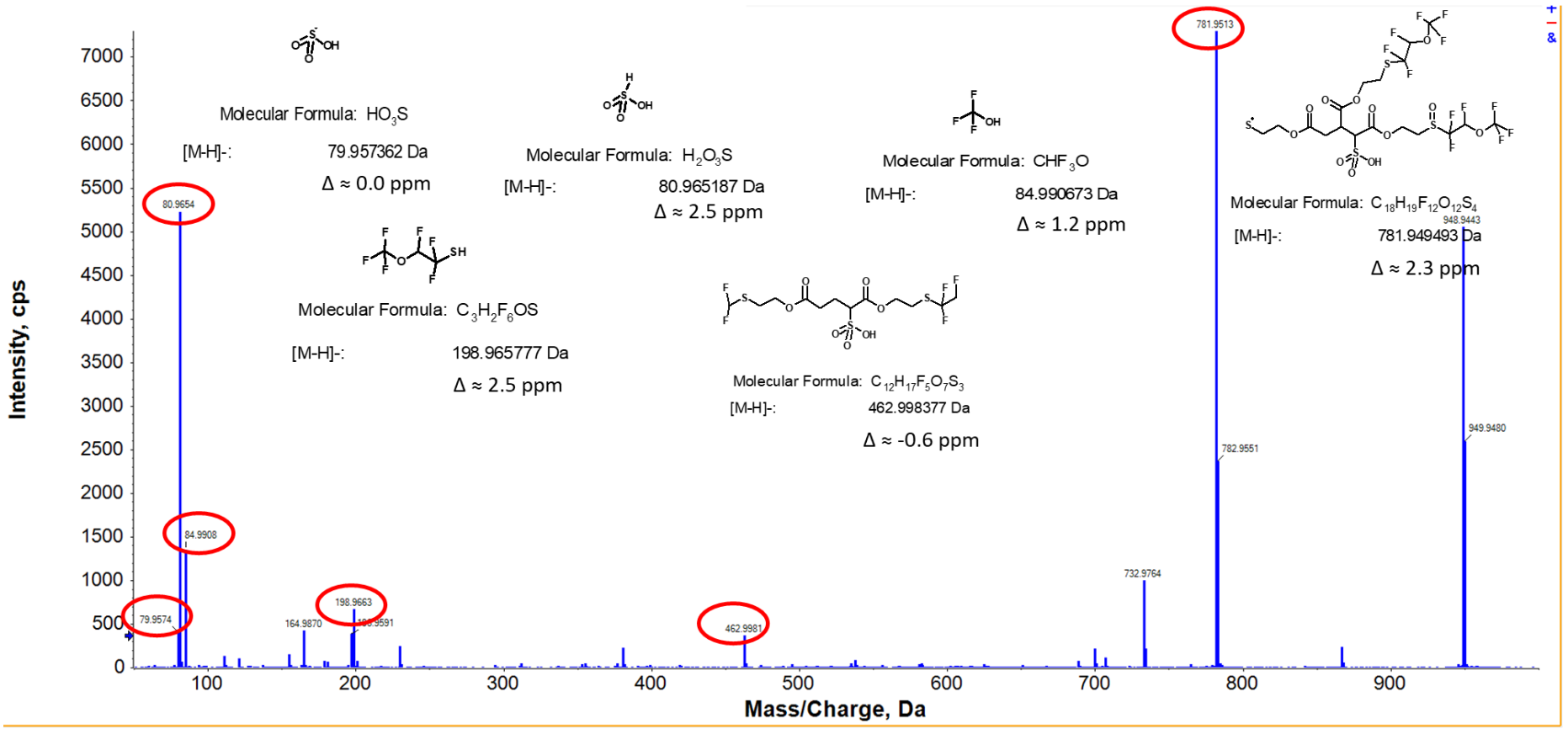


Figure 6-12: MS/MS spectrum of TP-NTS-S2.

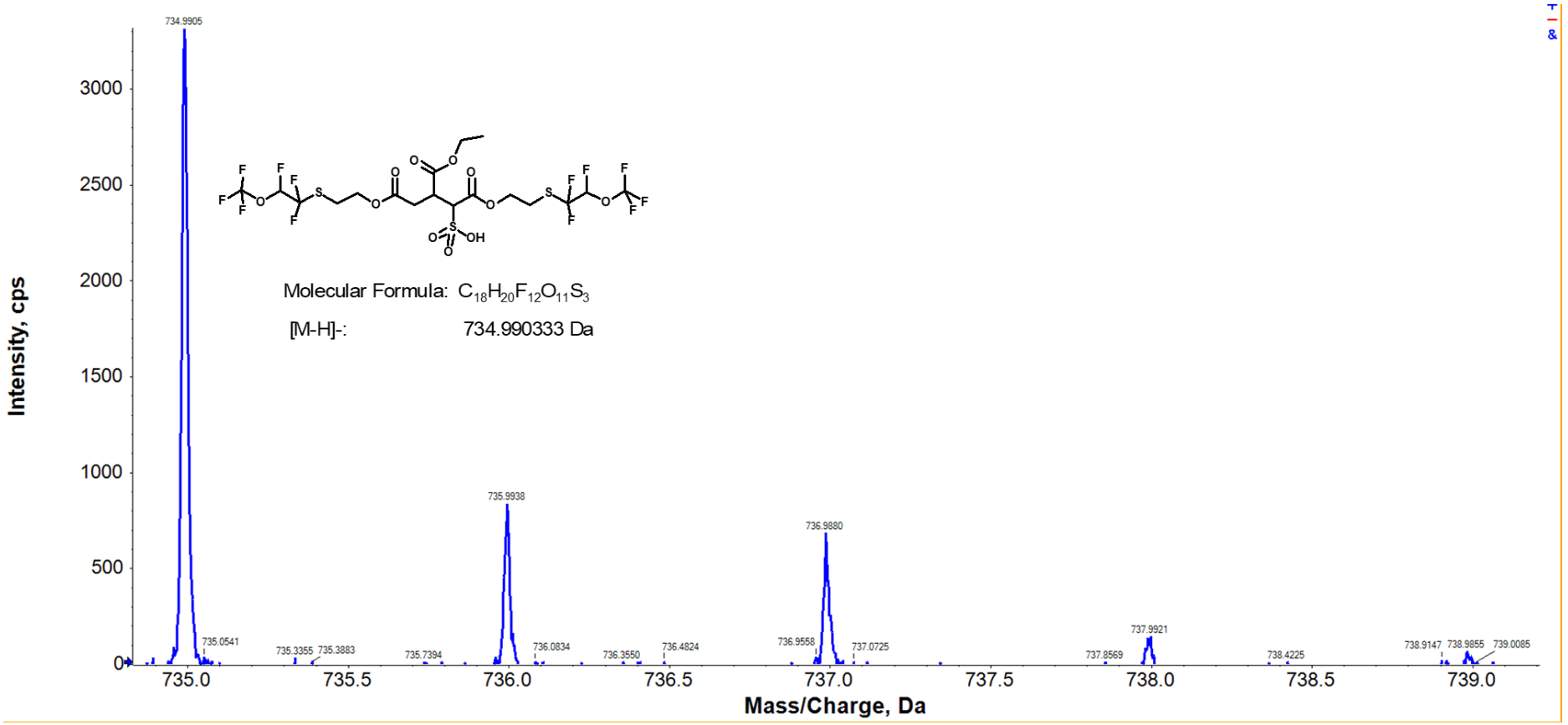


Figure 6-13: Full-scan MS spectrum of TP-NTS-S3. Identified only in the RL fractions.

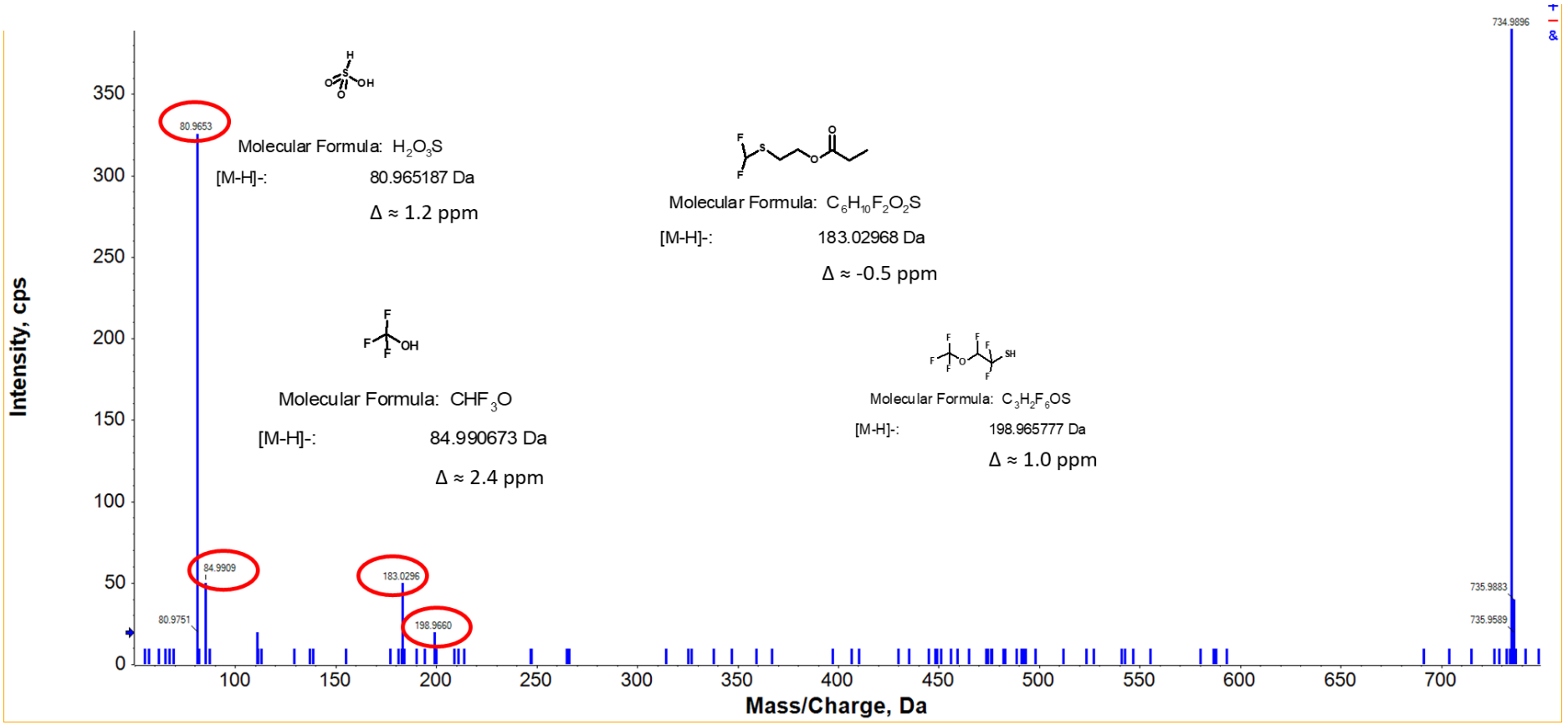


Figure 6-14: MS/MS spectrum of TP-NTS-S3.

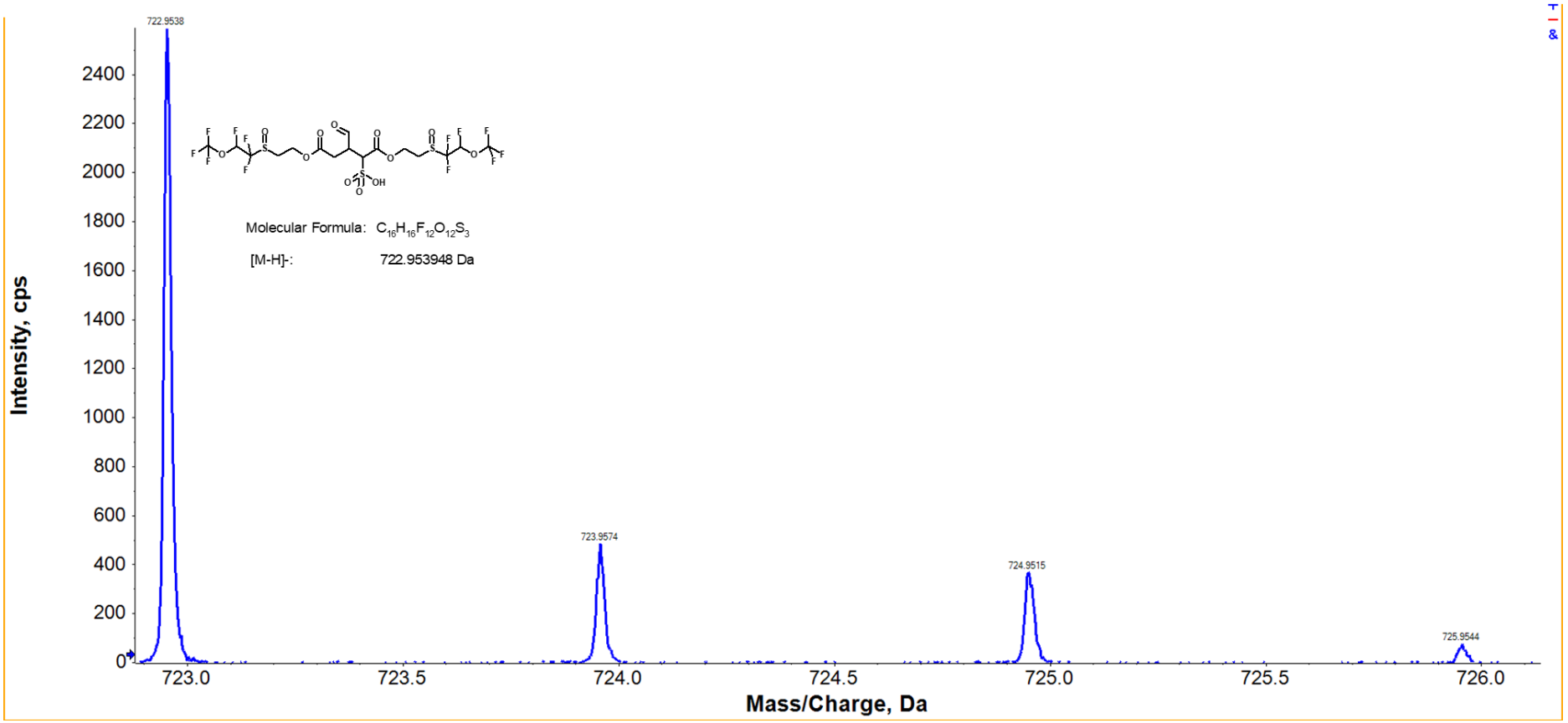


Figure 6-15: Full-scan MS spectrum of TP-NTS-S4. Identified both in the RL and HL fractions.

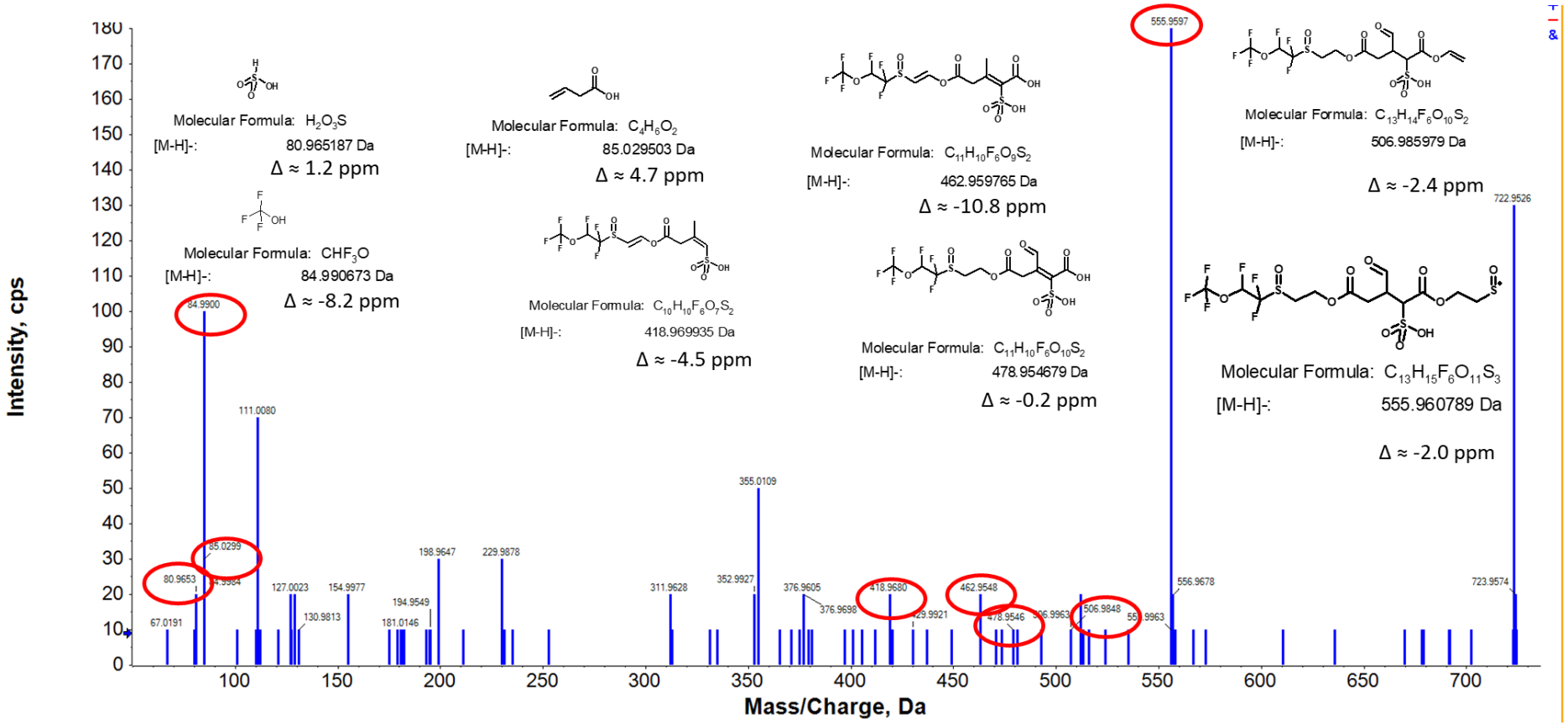


Figure 6-16: MS/MS spectrum of TP-NTS-S4.

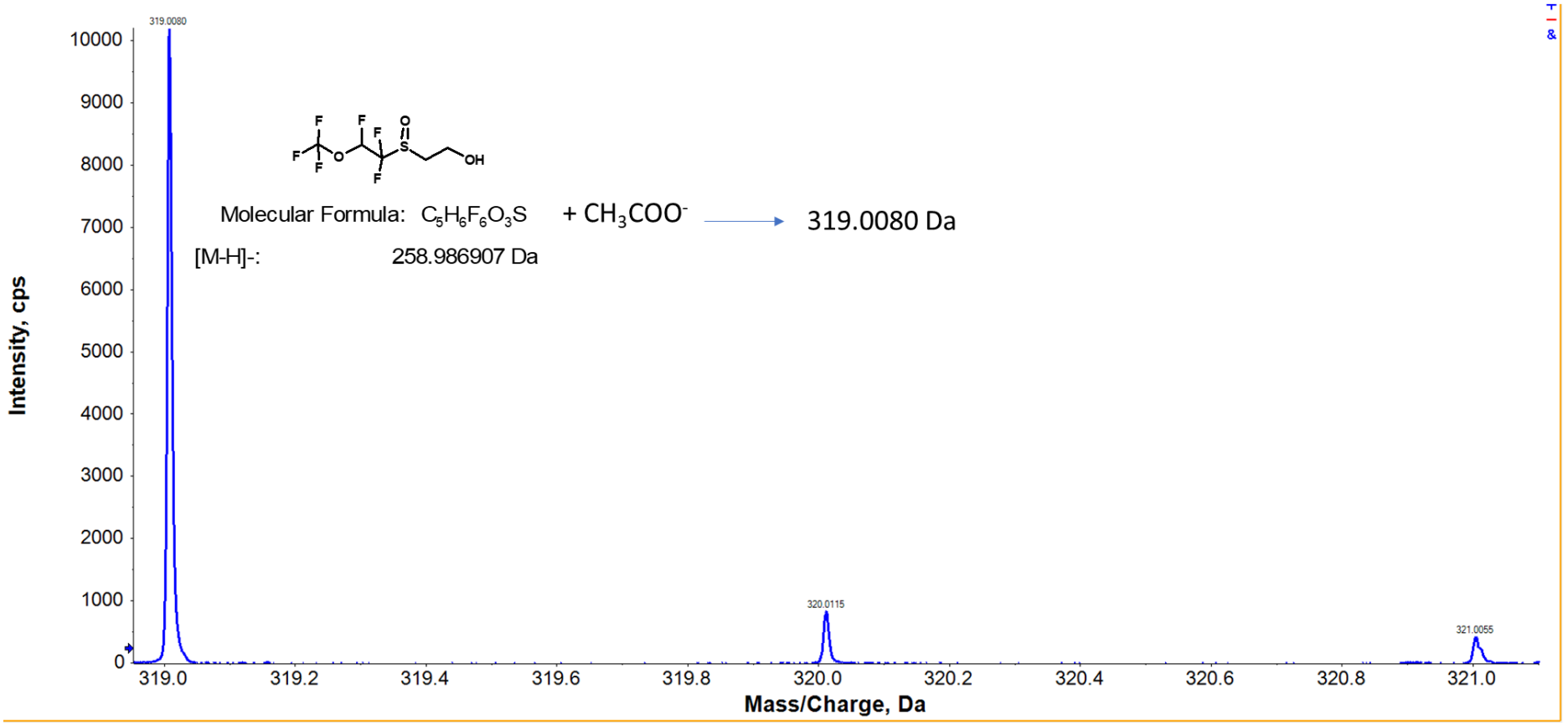


Figure 6-17: Full-scan MS spectrum of TP-NTS-S5. Identified both in the RL and HL fractions.

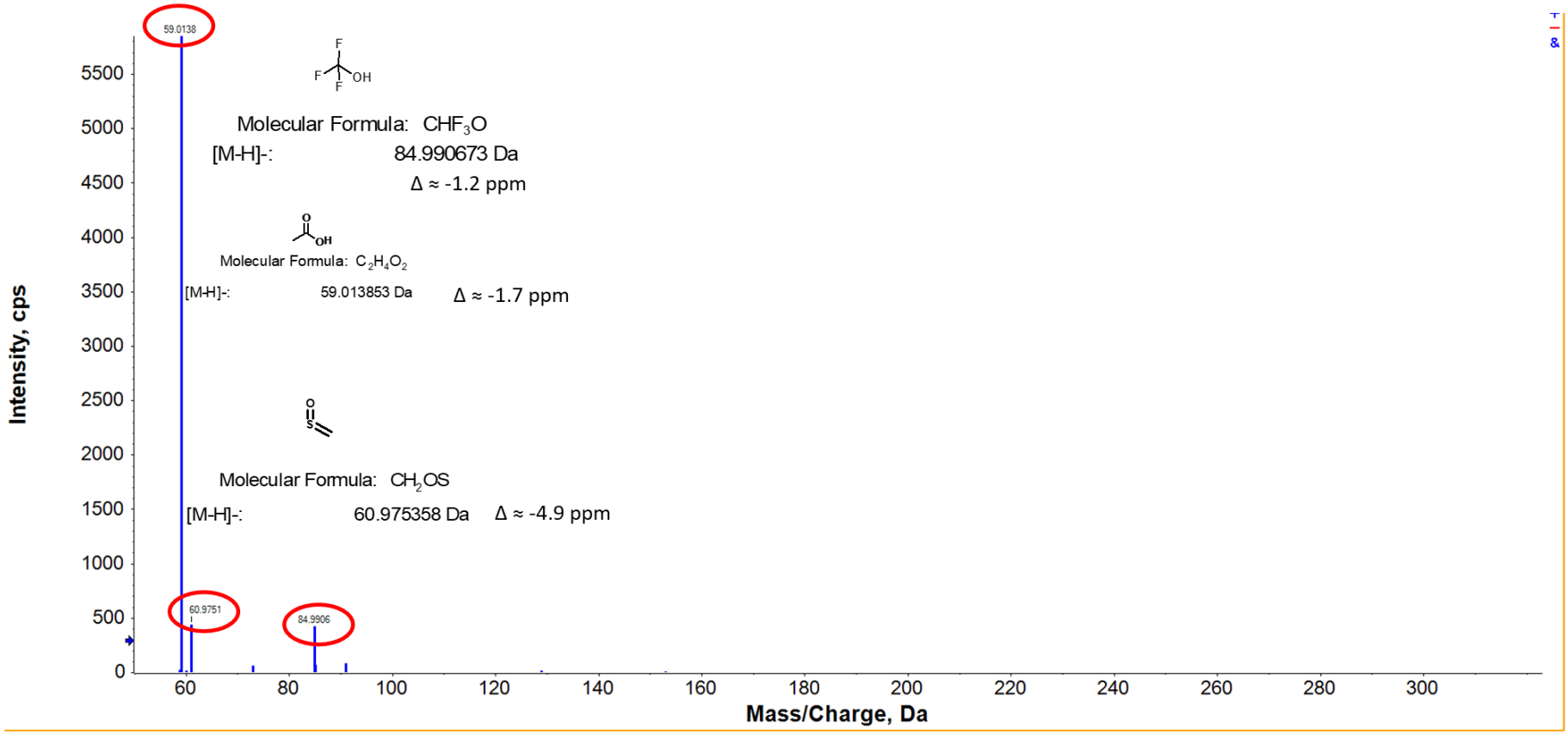


Figure 6-18: MS/MS spectrum of TP-NTS-S5.

7. SUMMARY AND CONCLUSIONS

Dermal uptake has been hitherto largely overlooked as a potentially significant pathway of human exposure to PFAS. This is both due to the fact that they are assumed to be in the ionized form at normal skin conditions and pH as well as an early study finding low permeations of APFO (Fasano et al., 2005; Trudel et al., 2008). More recently, a number of studies have identified multiple sources of dermal exposure to PFAS, such as personal care products (e.g., cosmetics, and skin care products), and fabrics (e.g., school uniforms and children's car seats) (Pütz et al., 2022; Schultes et al., 2018; Whitehead et al., 2021; Wu et al., 2021; Xia et al., 2022) Furthermore, studies on other halogenated pollutants have shown that contaminated dust contributes greatly to dermal exposure of these chemicals. The presence of PFAS in dust is well known, making dust another possible source of dermal exposure to PFAS (Eriksson and Kärrman, 2015; Harrad et al., 2019; Padilla-Sánchez and Haug, 2016). Furthermore, studies on human populations have identified correlations between PFAS serum levels and the use of personal care products indicating the dermal permeation potential of PFAS (Colles et al., 2020; Serrano et al., 2021; Thépaut et al., 2021).

These facts have led to an increased interest in the possibility of dermal permeation of PFAS. A few studies have investigated dermal uptake of PFAS using various methods, such as an *in vivo* study exposing a selection of PFAS to Sprague-Dawley rats, an *in vivo* study with a single human volunteer exposed to PFOA in sunscreen and a study modelling the dermal absorption of neutral PFAS from the gas phase (Abraham and Monien, 2022; Chen et al., 2022; Kissel et al., 2023). While these studies all contribute to the understanding of the dermal permeation potential of PFAS, they have their limitations. Several ethical and technical limitations apply to *in vivo* studies, especially those that use human subjects (Ragnarsdóttir et al., 2022). Additionally, human skin barrier functions can vary based on age, race and skin

hydration, making it more beneficial to have multiple subjects in dermal uptake studies, which then raises further ethical questions (Law et al., 2020). Animal studies have certain uncertainties due to interspecies variations of the skin (e.g., number of hair follicles, intercellular subcutaneous lipids and the skin barrier function) (Abdallah et al., 2015b). Using a modelling approach also has its limitations as they are dependent on the input data. When evaluating the possible dermal uptake of compounds from indoor air the hydration of the stratum corneum can fluctuate based on the skin's environment which can influence the barrier function of the skin. This could affect the accuracy of the model if not accounted for in its calculations (Weschler and Nazaroff, 2014). Additionally, for surfactants such as PFAS, their physicochemical properties can be difficult to determine which can affect the results of the models which are heavily based on these properties (Wang et al., 2011).

Dermal uptake of chemicals from a source material, i.e., dust or fabric is a twostep process. Firstly, compounds need to be released from the source material into the body's fluids (a mixture of sweat and sebum in the case of skin). This fraction is referred to as the *bioaccessible* fraction and this fraction is then available for dermal absorption(Ertl and Butte, 2012; Pawar et al., 2017). The second step is the transdermal permeation of this *bioaccessible* fraction through the skin and into the systemic circulation. The fraction that reaches the systemic circulation is then referred to as the *bioavailable* fraction. It is not necessary that all of the *bioaccessible* fraction will be able to permeate through the skin and become *bioavailable* (Ertl and Butte, 2012; Ragnarsdóttir et al., 2023).

Against this backdrop, this study aimed to further aid in closing the knowledge gap related to the dermal pathway as a possible exposure pathway to PFAS. To bypass the ethical and scientific complications related to extrapolation of dermal data obtained from *in vivo* studies a more ethical and sustainable *in vitro* approaches were applied to evaluate both the dermal *bioaccessibility* and the subsequent *bioavailability* of 17 PFAS.

As presented in chapter 3, the dermal bioaccessibility of 17 PFAS (C_4-C_{14} PFCAs and C_4, C_6-C_{10} PFSAs) from indoor dust to synthetic human sweat sebum mixtures (SSSM) was evaluated using physiologically based extraction tests. This study included an investigation of the effects of the composition of the SSSM and the presence of commonly applied personal care products (foundation, sunscreen, moisturiser, and deodorant) on PFAS bioaccessibility. Our results showed that the composition of the SSSM as well as the target PFAS physicochemical properties impact the bioaccessibility of all target compounds. In the most physiologically relevant SSSM (1:1 sweat:sebum) all target compounds were readily bioaccessible, with 54-92% for PFCAs and 61-77% for PFSAs becoming available for absorption. Furthermore, our study showed the impact of cosmetics on PFAS bioaccessibility, such as the presence of moisturiser which significantly decreased the total bioaccessibility of both PFCAs and PFSAs. In both cases a bigger impact was seen for longer chain compounds. This as well as the adherence of dust to skin, indicates dermal contact to dust as a possible pathway of human exposure to PFAS.

As presented in chapter 4, the dermal bioavailability of 17 PFAS (C_5-C_{14} PFCAs and C_4-C_{10} PFSAs) was assessed using *in vitro* 3D-Human Skin Equivalent models. These models have been proven to show a similar barrier function as *ex vivo* human skin while providing a more ethical way of conducting dermal uptake experiments. The models were exposed to 500 ng/cm^2 PFAS dissolved in methanol over 24-36 hours, based on an OECD protocol. The distribution of target PFAS at the end of exposure was determined based on three different fractions, absorbed, un-absorbed, and retained withing the skin tissue. The shortest chain compounds, PFPeA and PFBS had the highest absorbed fraction, 58.9% and 48.7% respectively. Carbon cain length significantly affected the permeation with absorbed fraction decreasing with increasing carbon chain length of the studied PFCAs ($r = 0.97$, $p = 0.001$) and PFSAs ($r = 0.97$, $p = 0.004$). In general, PFCAs had a higher absorbed fraction compared to

PFSAs of the same carbon chain length. Longer chain PFAS ($C_n \geq 9$) were not directly absorbed however, a large fraction of the exposed dose was detected within the skin tissue at the end of the exposure. The fraction retained was highest for PFUnDA and PFNS for which 66.5% and 68.3% was found withing the skin tissue, while neither compound was detected in the absorbed fraction. For compounds of a carbon chain length of C>11 the fraction found within the skin decreased with increasing chain length. Clear negative correlation between $\log K_{OW}$ and absorbed fraction for both PFCAs ($r = -0.97$; $p \leq 0.001$) and PFSAs ($r = -0.99$; $p \leq 0.001$), highlighting the significance of physicochemical properties on dermal penetration of PFAS. Finally, steady-state flux ($\boldsymbol{J_{SS}}$) and permeation coefficients ($\mathbf{P_{app}}$), and lag times ($\mathbf{t_{lag}}$) were determined for target compounds with significant permeation after 36 h exposure (C_5-C_8 PFCAs and C_4-C_7 PFSAs). In general, both the flux and permeation coefficient decreased with increasing chain length. The permeation coefficients can be used for future estimations of human dermal uptake of PFAS from various sources.

Chapter 5 combines the results from chapters 3 and 4 and using a PK model, evaluates human exposure to PFAS for adults and toddlers resulting from dermal exposure to dust under different exposure scenarios. Weekly human exposures via dermal contact to dust was estimated for people from four different countries of the world. The human dermal exposure to PFAS from dust varied based on time of year, country of origin and dust PFAS concentrations. Total PFAS exposure via dermal uptake from dust during summer ranged from 25-767 pg/kg bw/week and 91-2761 pg/kg bw/week for adults and toddlers, respectively. In general, dermal uptake of PFAS from dust was 10 times lower in winter compared to summertime, ranging from ranging from 2-70 pg/kg bw/week for adults and 10-300 pg/kg bw/week for toddlers. When comparing the dermal pathway to other human exposure pathways to PFAS, diet is the main pathway of exposure. Dermal contact was the smallest exposure pathway. Still, dermal contact to dust during the summer did contribute to total body burdens of PFAAs. Dermal

exposure in winter was while it was less prominent for PFAAs. This study only accounted for one source (dust) of dermal exposure. It is important to highlight that other sources such as fabrics and/or cosmetics could be a bigger source of dermal exposure to PFAS. Our results suggest that dermal contact with PFAS contaminated dust can contribute to total PFAS body burdens for both adults and toddlers.

The results presented here highlight the importance of including the dermal pathway when estimating total human exposure to PFAS. This is especially important considering the multiple sources of dermal exposure to PFAS. Further studies exposing 3D-HSE models to PFAS from various source matrices in combination to SSSM in real-life scenarios would further enhance the understanding of the dermal pathway as a source of human exposure to PFAS.

Finally, chapter 6 investigates the phase I *in vitro* metabolism of two prototype PFAS (CF_3-O-SURF and CF_3-S-SURF) in human and rat liver S9 fractions. The persistence of PFAS is a world-wide problem. However, their unique physicochemical properties make them desirable in many industries. Thus, novel PFAS which are fully degradable are being developed. Two prototype PFAS have been developed by Merck, Germany. The *in vitro* metabolism of these two PFAS was tested using human and rat liver S9 subcellular fractions as part of adsorption, distribution, metabolism, elimination assessment. The rate of metabolism as well as interspecies metabolic profiles were compared, providing the first insights into the *in vitro* pharmacokinetics of these novel compounds. The aim is to understand the suitability of these novel PFAS as more environmentally friendly alternatives to PFAS. Based on targeted analysis, rat S9 fractions produced two metabolites, while only one was detected after incubation with human S9 factions. Non-target analysis revealed additional metabolites after both human and rat metabolism, all but one in very low intensities. The metabolism of the novel prototype PFAS were found to be several orders of magnitude smaller than those reported

previously for other PFAS i.e., FTOH, suggesting a slow metabolism in humans. The metabolism was found to be faster in rats. While the metabolism appeared slow, only *in vitro* studies were performed here, which could lead to under- or overestimations in clearance values. A previous study on other PFAS replacement chemicals found that *in vitro* experiments underestimated the metabolic rate *in vivo.* Thus, to better understand the metabolic pathway and kinetics for these prototype PFAS, studies investigating phase II metabolism as well as *in vivo* experiments would be useful. However, this study enhances the understanding of the fate and behaviour of these novel prototype fluorinated compounds in two different species. Through characterization of formed metabolites and comparison of transformation rates across species, our results may serve as a basis for future risk evaluation.

The data presented in this thesis aids in closing the knowledge gap in the current understanding of human exposure to PFAS via the dermal pathway. Thus, enabling a better understanding of the overall human exposure to PFAS and the relative contribution of each exposure pathway. The presented data, both bioaccessibility and bioavailability data (i.e., $\mathbf{P_{app}}$), can be used for future exposure estimation models to determine the contribution of the dermal pathway to PFAS body burdens. To more accurately predict human exposure to PFAS from sources other than dust, e.g. cosmetics, PFAS bioaccessibilities from these sources need to be evaluated. These values can then in turn be used in addition to the $\mathbf{P_{app}}$ values presented here to model the resulting human exposure to PFAS via dermal contact to these sources. These sources of dermal exposure to PFAS (e.g. textiles, and PCPs) could potentially result in high exposures to PFAS. The cumulation of the multiple pathways of dermal exposure to PFAS also need to be considered. Doing so informs the relevant industry stakeholders as well as policymakers of the importance of considering the dermal pathway in order to reduce the risk to human health and the environment from this emerging contaminant class of high concern.

References

Abdallah, M., Gopal Pawar, Harrad, S., 2016. Human dermal absorption of chlorinated organophosphate flame retardants; implications for human exposure. Toxicology and Applied Pharmacology 291, 28–37. https://doi.org/10.1016/j.taap.2015.12.004

Abdallah, M.A.-E., Harrad, S., 2018. Dermal contact with furniture fabrics is a significant pathway of human exposure to brominated flame retardants. Environment International 118, 26–33. https://doi.org/10.1016/j.envint.2018.05.027

Abdallah, M.A.-E., Nguyen, K.-H., Moehring, T., Harrad, S., 2019. First insight into human extrahepatic metabolism of flame retardants: Biotransformation of EH-TBB and Firemaster-550 components by human skin subcellular fractions. Chemosphere 227, 1–8. https://doi.org/10.1016/j.chemosphere.2019.04.017

Abdallah, M.A.-E., Pawar, G., Harrad, S., 2015a. Evaluation of in vitro vs. in vivo methods for assessment of dermal absorption of organic flame retardants: A review. Environment International 74, 13–22. https://doi.org/10.1016/j.envint.2014.09.012

Abdallah, M.A.-E., Pawar, G., Harrad, S., 2015b. Evaluation of 3D-human skin equivalents for assessment of human dermal absorption of some brominated flame retardants. Environment International 84, 64–70. https://doi.org/10.1016/j.envint.2015.07.015

Abdallah, M.A.-E., Pawar, G., Harrad, S., 2015c. Effect of Bromine Substitution on Human Dermal Absorption of Polybrominated Diphenyl Ethers. Environ. Sci. Technol. 49, 10976–10983. https://doi.org/10.1021/acs.est.5b03904

Abdallah, M.A.-E., Tilston, E., Harrad, S., Collins, C., 2012. In vitro assessment of the bioaccessibility of brominated flame retardants in indoor dust using a colon extended model of the human gastrointestinal tract. J. Environ. Monit. 14, 3276. https://doi.org/10.1039/c2em30690e

Abdallah, M.A.E., Uchea, C., Chipman, J.K., Harrad, S., 2014. Enantioselective biotransformation of hexabromocyclododecane by in vitro rat and trout hepatic sub-cellular fractions. Environmental Science and Technology 48, 2732–2740. https://doi.org/10.1021/es404644s

Abdallah, M.A.-E., Wemken, N., Drage, D.S., Tlustos, C., Cellarius, C., Cleere, K., Morrison, J.J., Daly, S., Coggins, M.A., Harrad, S., 2020. Concentrations of perfluoroalkyl substances in human milk from Ireland: Implications for adult and nursing infant exposure. Chemosphere 246, 125724. https://doi.org/10.1016/j.chemosphere.2019.125724

Abraham, K., Mielke, H., Fromme, H., Völkel, W., Menzel, J., Peiser, M., Zepp, F., Willich, S.N., Weikert, C., 2020. Internal exposure to perfluoroalkyl substances (PFASs) and biological markers in 101 healthy 1-year-old children: associations between levels of perfluorooctanoic acid (PFOA) and vaccine response. Arch Toxicol 94, 2131–2147. https://doi.org/10.1007/s00204-020-02715-4

Abraham, K., Monien, B.H., 2022. Transdermal absorption of 13C4-perfluorooctanoic acid (13C4-PFOA) from a sunscreen in a male volunteer – What could be the contribution of cosmetics to the internal exposure of perfluoroalkyl substances (PFAS)? Environment International 169, 107549. https://doi.org/10.1016/j.envint.2022.107549

Abrams, K., Harvell, J.D., Shriner, D., Wertz, P., Maibach, H., Maibach, H.I., Rehfeld, S.J., 1993. Effect of Organic Solvents on In Vitro Human Skin Water Barrier Function. Journal of Investigative Dermatology 101, 609–613. https://doi.org/10.1111/1523-1747.ep12366068

Ackermann, K., Lombardi Borgia, S., Korting, H.C., Mewes, K.R., Schäfer-Korting, M., 2010. The Phenion® Full-Thickness Skin Model for Percutaneous Absorption Testing. Skin Pharmacol Physiol 23, 105–112. https://doi.org/10.1159/000265681

Baron, J.M., Höller, D., Schiffer, R., Frankenberg, S., Neis, M., Merk, H.F., Jugert, F.K., 2001. Expression of Multiple Cytochrome P450 Enzymes and Multidrug Resistance-Associated Transport Proteins in Human Skin Keratinocytes. Journal of Investigative Dermatology 116, 541–548. https://doi.org/10.1046/j.1523-1747.2001.01298.x

Barry, V., Winquist, A., Steenland, K., 2013. Perfluorooctanoic Acid (PFOA) Exposures and Incident Cancers among Adults Living Near a Chemical Plant. Environmental Health Perspectives 121, 1313–1318. https://doi.org/10.1289/ehp.1306615

Bartell, S.M., Calafat, A.M., Lyu, C., Kato, K., Ryan, P.B., Steenland, K., 2010. Rate of Decline in Serum PFOA Concentrations after Granular Activated Carbon Filtration at Two Public Water Systems in Ohio and West Virginia. Environmental Health Perspectives 118, 222–228. https://doi.org/10.1289/ehp.0901252

Berger, U., Langlois, I., Oehme, M., Kallenborn, R., 2004. Comparison of three types of mass spectrometer for high-performance liquid chromatography/mass spectrometry analysis of perfluoroalkylated substances and fluorotelomer alcohols. European Journal of Mass Spectrometry 10, 579–588. https://doi.org/10.1255/ejms.679

Björnsdotter, M.K., Hartz, W.F., Kallenborn, R., Ericson Jogsten, I., Humby, J.D., Kärrman, A., Yeung, L.W.Y., 2021. Levels and Seasonal Trends of C1–C4 Perfluoroalkyl Acids and the Discovery of Trifluoromethane Sulfonic Acid in Surface Snow in the Arctic. Environmental Science & Technology. https://doi.org/10.1021/acs.est.1c04776

Brede, E., Wilhelm, M., Göen, T., Müller, J., Rauchfuss, K., Kraft, M., Hölzer, J., 2010. Two-year follow-up biomonitoring pilot study of residents' and controls' PFC plasma levels after PFOA reduction in public water system in Arnsberg, Germany. International Journal of Hygiene and Environmental Health 213, 217–223. https://doi.org/10.1016/j.ijheh.2010.03.007

Buck, Robert C, Franklin, J., Berger, U., Conder, J.M., Cousins, I.T., de Voogt, P., Jensen, A.A., Kannan, K., Mabury, S.A., van Leeuwen, S.P., 2011. Perfluoroalkyl and polyfluoroalkyl substances in the environment: Terminology, classification, and origins. Integr Environ Assess Manag 7, 513–541. https://doi.org/10.1002/ieam.258

Buck, Robert C., Franklin, J., Berger, U., Conder, J.M., Cousins, I.T., Voogt, P. De, Jensen, A.A., Kannan, K., Mabury, S.A., van Leeuwen, S.P.J., 2011. Perfluoroalkyl and polyfluoroalkyl substances in the environment: Terminology, classification, and origins. Integrated Environmental Assessment and Management 7, 513–541. https://doi.org/10.1002/ieam.258

Buckley, W., R., Lewis, C.E., 1960. The "Ruster" in Industry. Journal of Occupational Medicine 2, 23–31.

Butt, C.M., Muir, D.C.G., Mabury, S.A., 2010. Biotransformation of the 8:2 fluorotelomer acrylate in rainbow trout. 2. In vitro incubations with liver and stomach S9 fractions. Environmental Toxicology and Chemistry 29, 2736–2741. https://doi.org/10.1002/etc.348

Chemspider, 2023. . Royal Society of Chemistry.

Chen, D., Zhao, Y., Xu, W., Pan, Y., Wei, Q., Xie, S., 2020. Biotransformation and tissue bioaccumulation of 8:2 fluorotelomer alcohol in broiler by oral exposure. Environmental Pollution 267, 115611. https://doi.org/10.1016/j.envpol.2020.115611

Chen, Q., Yi, S., Ye, Q., Zhu, Y., Zhong, W., Zhu, L., 2022. Insights into the Dermal Absorption, Deposition, and Elimination of Poly- and Perfluoroalkyl Substances in Rats: The Importance of Skin Exposure. Environ. Sci. Technol. 56, 16975–16984. https://doi.org/10.1021/acs.est.2c03181

Chiang, A., Tudela, E., Maibach, H.I., 2012. Percutaneous absorption in diseased skin: an overview. J of Applied Toxicology 32, 537–563. https://doi.org/10.1002/jat.1773

Coggan, T.L., Anumol, T., Pyke, J., Shimeta, J., Clarke, B.O., 2019. A single analytical method for the determination of 53 legacy and emerging per- and polyfluoroalkyl substances (PFAS) in aqueous matrices. Analytical and Bioanalytical Chemistry 411, 3507–3520. https://doi.org/10.1007/s00216-019-01829-8

Colles, A., Bruckers, L., Den Hond, E., Govarts, E., Morrens, B., Schettgen, T., Buekers, J., Coertjens, D., Nawrot, T., Loots, I., Nelen, V., De Henauw, S., Schoeters, G., Baeyens, W., van Larebeke, N., 2020. Perfluorinated substances in the Flemish population (Belgium): Levels and determinants of variability in exposure. Chemosphere 242, 125250. https://doi.org/10.1016/j.chemosphere.2019.125250

Collins, C.D., Craggs, M., Garcia-Alcega, S., Kademoglou, K., Lowe, S., 2015. 'Towards a unified approach for the determination of the bioaccessibility of organic pollutants.' Environment International 78, 24–31. https://doi.org/10.1016/j.envint.2015.02.005

Cousins, I.T., Johansson, J.H., Salter, M.E., Sha, B., Scheringer, M., 2022. Outside the Safe Operating Space of a New Planetary Boundary for Per- and Polyfluoroalkyl Substances (PFAS). Environmental Science and Technology 56, 11172–11179. https://doi.org/10.1021/acs.est.2c02765

Daramola, O., Rand, A.A., 2021. Emerging investigator series: Human CYP2A6 catalyzes the oxidation of 6:2 fluorotelomer alcohol. Environmental Science: Processes and Impacts 23, 1688–1695. https://doi.org/10.1039/d1em00307k

D'eon, J.C., Mabury, S.A., 2011. Exploring indirect sources of human exposure to perfluoroalkyl carboxylates (PFCAs): Evaluating uptake, elimination, and biotransformation of polyfluoroalkyl phosphate esters (PAPs) in the Rat. Environmental Health Perspectives 119, 344–350. https://doi.org/10.1289/ehp.1002409

DeWitt, J.C., Blossom, S.J., Schaider, L.A., 2019a. Exposure to per-fluoroalkyl and polyfluoroalkyl substances leads to immunotoxicity: epidemiological and toxicological evidence. J Expo Sci Environ Epidemiol 29, 148–156. https://doi.org/10.1038/s41370-018-0097-y

DeWitt, J.C., Blossom, S.J., Schaider, L.A., 2019b. Exposure to per-fluoroalkyl and polyfluoroalkyl substances leads to immunotoxicity: epidemiological and toxicological evidence. Journal of Exposure Science and Environmental Epidemiology 29, 148–156. https://doi.org/10.1038/s41370-018-0097-y

EFSA CONTAM Panel, (EFSA Panel on Contaminants in the Food Chain), 2020. Risk to human health related to the presence of perfluoroalkyl substances in food. EFS2 18. https://doi.org/10.2903/j.efsa.2020.6223

Eriksson, U., Kärrman, A., 2015. World-Wide Indoor Exposure to Polyfluoroalkyl Phosphate Esters (PAPs) and other PFASs in Household Dust. Environ. Sci. Technol. 49, 14503–14511. https://doi.org/10.1021/acs.est.5b00679

Ertl, H., Butte, W., 2012. Bioaccessibility of pesticides and polychlorinated biphenyls from house dust: in-vitro methods and human exposure assessment. J Expo Sci Environ Epidemiol 22, 574–583. https://doi.org/10.1038/jes.2012.50

European Chemical Agency, 2022. Inclusion of substances of very high concern in the Candidate List for eventual inclusion in Annex XIV Distribution. D(2022)9120-DC Public.

European Chemical Agency, 2020. Inclusion of Substances of Very High Concern in the Candidate List for eventual inclusion in Annex XIV. ECHA/01/2020.

European Chemical Agency, 2019. Inclusion of Substances of Very High Concern in the Candidate List for eventual inclusion in Annex XIV. ED/71/2019.

European Chemicals Agency, 2017. Guidance on Information Requirements and Chemical Safety Assessment - Chapter R.11: PBT/vPvB assessment. https://doi.org/10.2823/128621
European Commission, 2021. Commission regulation (EU) 2021/1297 of 4 August 2021 amending Annex XVII to Regulation (EC) No 1907/2006 of the European Parliament and of the Council as regards perfluorocarboxylic acids containing 9 to 14 carbon atoms in the chain (C9-C14 PFCAs), their. Official Journal of the European Union 282, 29–33.
European Union, 2020. Directive (EU) 2020/2184 of the European Parliament and of the Council of 16 December 2020 on the Quality of Water Intended for Human Consumption (No. 2020/2184).
Fang, S., Plassmann, M.M., Cousins, I.T., 2020. Levels of per- and polyfluoroalkyl substances (PFAS) in ski wax products on the market in 2019 indicate no changes in formulation. Environ. Sci.: Processes Impacts 22, 2142–2146. https://doi.org/10.1039/D0EM00357C
Fasano, W.J., Carpenter, S.C., Gannon, S.A., Snow, T.A., Stadler, J.C., Kennedy, G.L., Buck, R.C., Korzeniowski, S.H., Hinderliter, P.M., Kemper, R.A., 2006. Absorption, distribution, metabolism, and elimination of 8-2 fluorotelomer alcohol in the rat. Toxicological Sciences 91, 341–355. https://doi.org/10.1093/toxsci/kfj160
Fasano, W.J., Kennedy, G.L., Szostek, B., Farrar, D.G., Ward, R.J., Haroun, L., Hinderliter, P.M., 2005. Penetration of Ammonium Perfluorooctanoate Through Rat and Human Skin In Vitro. Drug and Chemical Toxicology 28, 79–90. https://doi.org/10.1081/DCT-39707
Fasano, W.J., Sweeney, L.M., Mawn, M.P., Nabb, D.L., Szostek, B., Buck, R.C., Gargas, M.L., 2009. Kinetics of 8-2 fluorotelomer alcohol and its metabolites, and liver glutathione status following daily oral dosing for 45 days in male and female rats. Chemico-Biological Interactions 180, 281–295. https://doi.org/10.1016/j.cbi.2009.03.015
Federal Institute for, Occupational Safety and Health, National Institute for Public Health and the Environment, Swedish Chemicals Agency, Norwegian Environment Agency, T.D.E.P.A., 2023. Annex XV Restriction Report, Proposal for Restriction, Substance Names(s): Per- and polyfluoroalkyl substances (PFASs).
Folkerson, A.P., Joudan, S., Mabury, S.A., D'eon, J.C., 2021. In Vivo Transformation of a Novel Polyfluoroether Surfactant. Environmental Toxicology and Chemistry 00, 1–9. https://doi.org/10.1002/etc.5230
Franko, J., Meade, B.J., Frasch, H.F., Barbero, A.M., Anderson, S.E., 2012. Dermal Penetration Potential of Perfluorooctanoic Acid (PFOA) in Human and Mouse Skin. Journal of Toxicology and Environmental Health, Part A 75, 50–62. https://doi.org/10.1080/15287394.2011.615108
Frederiksen, M., Stapleton, H.M., Vorkamp, K., Webster, T.F., Jensen, N.M., Sørensen, J.A., Nielsen, F., Knudsen, L.E., Sørensen, L.S., Clausen, P.A., Nielsen, J.B., 2018. Dermal uptake and percutaneous penetration of organophosphate esters in a human skin ex vivo model. Chemosphere 197, 185–192. https://doi.org/10.1016/j.chemosphere.2018.01.032
Frederiksen, M., Vorkamp, K., Jensen, N.M., Sørensen, J.A., Knudsen, L.E., Sørensen, L.S., Webster, T.F., Nielsen, J.B., 2016. Dermal uptake and percutaneous penetration of ten flame retardants in a human skin ex vivo model. Chemosphere 162, 308–314. https://doi.org/10.1016/j.chemosphere.2016.07.100
Fu, J., Gao, Y., Cui, L., Wang, T., Liang, Y., Qu, G., Yuan, B., Wang, Y., Zhang, A., Jiang, G., 2016. Occurrence, temporal trends, and half-lives of perfluoroalkyl acids (PFAAs)

in occupational workers in China. Sci Rep 6, 38039. https://doi.org/10.1038/srep38039
Fujii, Y., Harada, K.H., Koizumi, A., 2013. Occurrence of perfluorinated carboxylic acids (PFCAs) in personal care products and compounding agents. Chemosphere 93, 538–544. https://doi.org/10.1016/j.chemosphere.2013.06.049
Fujiwara, R., Takenaka, S., Hashimoto, M., Narawa, T., Itoh, T., 2015. Expression of human solute carrier family transporters in skin: possible contributor to drug-induced skin disorders. Sci Rep 4, 5251. https://doi.org/10.1038/srep05251
Gardener, H., Sun, Q., Grandjean, P., 2021. PFAS concentration during pregnancy in relation to cardiometabolic health and birth outcomes. Environmental Research 192, 110287. https://doi.org/10.1016/j.envres.2020.110287
Gebbink, W.A., Berger, U., Cousins, I.T., 2015. Estimating human exposure to PFOS isomers and PFCA homologues: The relative importance of direct and indirect (precursor) exposure. Environment International 74, 160–169. https://doi.org/10.1016/j.envint.2014.10.013
Ghassabian, A., Vandenberg, L., Kannan, K., Trasande, L., 2022. Endocrine-Disrupting Chemicals and Child Health. Annu. Rev. Pharmacol. Toxicol. 62, 573–594. https://doi.org/10.1146/annurev-pharmtox-021921-093352
Giesy, J.P., Kannan, K., 2001. Global Distribution of Perfluorooctane Sulfonate in Wildlife. Environ. Sci. Technol. 35, 1339–1342. https://doi.org/10.1021/es001834k
Glüge, J., Scheringer, M., Cousins, I.T., DeWitt, J.C., Goldenman, G., Herzke, D., Lohmann, R., Ng, C.A., Trier, X., Wang, Z., 2020a. An overview of the uses of per- and polyfluoroalkyl substances (PFAS). Environ. Sci.: Processes Impacts 10.1039.D0EM00291G. https://doi.org/10.1039/D0EM00291G
Glüge, J., Scheringer, M., Cousins, I.T., DeWitt, J.C., Goldenman, G., Herzke, D., Lohmann, R., Ng, C.A., Trier, X., Wang, Z., 2020b. An overview of the uses of per- and polyfluoroalkyl substances (PFAS). Environmental Science Processes & Impacts implications 22, 2345–2373. https://doi.org/10.1039/d0em00291g
Godin, B., Touitou, E., 2007. Transdermal skin delivery: Predictions for humans from in vivo, ex vivo and animal models☆. Advanced Drug Delivery Reviews 59, 1152–1161. https://doi.org/10.1016/j.addr.2007.07.004
González-Barreiro, C., Martínez-Carballo, E., Sitka, A., Scharf, S., Gans, O., 2006. Method optimization for determination of selected perfluorinated alkylated substances in water samples. Analytical and Bioanalytical Chemistry 386, 2123–2132. https://doi.org/10.1007/s00216-006-0902-7
Grandjean, P., Andersen, E.W., Budtz-Jørgensen, E., Nielsen, F., Mølbak, K., Weihe, P., Heilmann, C., 2012. Serum Vaccine Antibody Concentrations in Children Exposed to Perfluorinated Compounds. JAMA 307. https://doi.org/10.1001/jama.2011.2034
Grandjean, P., Heilmann, C., Weihe, P., Nielsen, F., Mogensen, U.B., Timmermann, A., Budtz-Jørgensen, E., 2017a. Estimated exposures to perfluorinated compounds in infancy predict attenuated vaccine antibody concentrations at age 5-years. Journal of Immunotoxicology 14, 188–195. https://doi.org/10.1080/1547691X.2017.1360968
Grandjean, P., Heilmann, C., Weihe, P., Nielsen, F., Mogensen, U.B., Timmermann, A., Budtz-Jørgensen, E., 2017b. Estimated exposures to perfluorinated compounds in infancy predict attenuated vaccine antibody concentrations at age 5-years. Journal of Immunotoxicology 14, 188–195. https://doi.org/10.1080/1547691X.2017.1360968
Greenpeace, 2016. Leaving Traces. The hidden hazardous chemicals in outdoor gear. Greanpeace product test 2016.
Greenpeace, 2013. Chemistry for Any Weather - Part II. Excecutive summary - Outdoor Report 2013.

Greenpeace, 2012. Chemistry for Any Weather – Greenpeace tests out- door clothes for perfluorinated toxins report. Greenpeace.
Gremmel, C., Frömel, T., Knepper, T.P., 2017. HPLC–MS/MS methods for the determination of 52 perfluoroalkyl and polyfluoroalkyl substances in aqueous samples. Analytical and Bioanalytical Chemistry 409, 1643–1655. https://doi.org/10.1007/s00216-016-0110-z
Hale, S.E., Arp, H.P.H., Schliebner, I., Neumann, M., 2020. Persistent, mobile and toxic (PMT) and very persistent and very mobile (vPvM) substances pose an equivalent level of concern to persistent, bioaccumulative and toxic (PBT) and very persistent and very bioaccumulative (vPvB) substances under REACH. Environmental Sciences Europe 32. https://doi.org/10.1186/s12302-020-00440-4
Han, J.-S., Jang, S., Son, H.-Y., Kim, Y.-B., Kim, Y., Noh, J.-H., Kim, M.-J., Lee, B.-S., 2020. Subacute dermal toxicity of perfluoroalkyl carboxylic acids: comparison with different carbon-chain lengths in human skin equivalents and systemic effects of perfluoroheptanoic acid in Sprague Dawley rats. Arch Toxicol 94, 523–539. https://doi.org/10.1007/s00204-019-02634-z
Hansen, K.J., Clemen, L.A., Ellefson, M.E., Johnson, H.O., 2001. Compound-Specific, Quantitative Characterization of Organic Fluorochemicals in Biological Matrices. Environ. Sci. Technol. 35, 766–770. https://doi.org/10.1021/es001489z
Harrad, S., Drage, D.S., Sharkey, M., Berresheim, H., 2020. Perfluoroalkyl substances and brominated flame retardants in landfill-related air, soil, and groundwater from Ireland. Science of The Total Environment 705, 135834. https://doi.org/10.1016/j.scitotenv.2019.135834
Harrad, S., Wemken, N., Drage, D.S., Abdallah, M.A.-E., Coggins, A.-M., 2019. Perfluoroalkyl Substances in Drinking Water, Indoor Air and Dust from Ireland: Implications for Human Exposure. Environ. Sci. Technol. 53, 13449–13457. https://doi.org/10.1021/acs.est.9b04604
Harris, K.J., Munoz, G., Woo, V., Sauvé, S., Rand, A.A., 2022. Targeted and Suspect Screening of Per- and Polyfluoroalkyl Substances in Cosmetics and Personal Care Products. Environ. Sci. Technol. 56, 14594–14604. https://doi.org/10.1021/acs.est.2c02660
Haug, L.S., Huber, S., Becher, G., Thomsen, C., 2011. Characterisation of human exposure pathways to perfluorinated compounds — Comparing exposure estimates with biomarkers of exposure. Environment International 37, 687–693. https://doi.org/10.1016/j.envint.2011.01.011
Hewitt, N.J., Edwards, R.J., Fritsche, E., Goebel, C., Aeby, P., Scheel, J., Reisinger, K., Ouédraogo, G., Duche, D., Eilstein, J., Latil, A., Kenny, J., Moore, C., Kuehnl, J., Barroso, J., Fautz, R., Pfuhler, S., 2013. Use of Human In Vitro Skin Models for Accurate and Ethical Risk Assessment: Metabolic Considerations. Toxicological Sciences 133, 209–217. https://doi.org/10.1093/toxsci/kft080
Jakasa, I., Kezic, S., 2008. Evaluation of in-vivo animal and in-vitro models for prediction of dermal absorption in man. Hum Exp Toxicol 27, 281–288. https://doi.org/10.1177/0960327107085826
Janousek, R.M., Lebertz, S., Knepper, T.P., 2019. Previously unidentified sources of perfluoroalkyl and polyfluoroalkyl substances from building materials and industrial fabrics. Environmental Science: Processes and Impacts 21, 1936–1945. https://doi.org/10.1039/c9em00091g
Kang, H., Choi, K., Lee, H.-S., Kim, D.-H., Park, N.-Y., Kim, S., Kho, Y., 2016. Elevated levels of short carbon-chain PFCAs in breast milk among Korean women: Current

status and potential challenges. Environmental Research 148, 351–359. https://doi.org/10.1016/j.envres.2016.04.017
Kim, D.-H., Lee, J.-H., Oh, J.-E., 2019. Assessment of individual-based perfluoroalkly substances exposure by multiple human exposure sources. Journal of Hazardous Materials 365, 26–33. https://doi.org/10.1016/j.jhazmat.2018.10.066
Kissel, J.C., 2011. The mismeasure of dermal absorption. J Expo Sci Environ Epidemiol 21, 302–309. https://doi.org/10.1038/jes.2010.22
Kissel, J.C., Titaley, I.A., Muensterman, D.J., Field, J.A., 2023. Evaluating Neutral PFAS for Potential Dermal Absorption from the Gas Phase. Environ. Sci. Technol. 57, 4951–4958. https://doi.org/10.1021/acs.est.2c08835
Knepper, T.P., Frömel, T., Gremmel, C., van Driezum, I., Weil, H., Vestergren, R., Cousins, I.T., 2014. Understanding the exposure pathways of per- and polyfluoralkyl substances (PFASs) via use of PFASs-containing products – risk estimation for man and environment (No. (UBA-FB) 001935/E). ENVIRONMENTAL RESEARCH OF THE FEDERAL MINISTRY OF THE ENVIRONMENT, NATURE CONSERVATION AND NUCLEAR SAFETY.
Knudsen, G.A., Hughes, M.F., Birnbaum, L.S., 2019. Dermal disposition of Tetrabromobisphenol A Bis(2,3-dibromopropyl) ether (TBBPA-BDBPE) using rat and human skin. Toxicology Letters 301, 108–113. https://doi.org/10.1016/j.toxlet.2018.11.011
Knudsen, G.A., Hughes, M.F., Sanders, J.M., Hall, S.M., Birnbaum, L.S., 2016. Estimation of human percutaneous bioavailability for two novel brominated flame retardants, 2-ethylhexyl 2,3,4,5-tetrabromobenzoate (EH-TBB) and bis(2-ethylhexyl) tetrabromophthalate (BEH-TEBP). Toxicology and Applied Pharmacology 311, 117–127. https://doi.org/10.1016/j.taap.2016.10.005
Kola, I., Landis, J., 2004. Can the pharmaceutical industry reduce attrition rates? Nature Reviews Drug Discovery 3, 711–715. https://doi.org/10.1038/nrd1470
Kummu, M., Sieppi, E., Koponen, J., Laatio, L., Vähäkangas, K., Kiviranta, H., Rautio, A., Myllynen, P., 2015. Organic anion transporter 4 (OAT 4) modifies placental transfer of perfluorinated alkyl acids PFOS and PFOA in human placental ex vivo perfusion system. Placenta 36, 1185–1191. https://doi.org/10.1016/j.placenta.2015.07.119
Lane, M.E., 2013. Skin penetration enhancers. International Journal of Pharmaceutics 447, 12–21. https://doi.org/10.1016/j.ijpharm.2013.02.040
Lau, C., Anitole, K., Hodes, C., Lai, D., Pfahles-Hutchens, A., Seed, J., 2007. Perfluoroalkyl acids: A review of monitoring and toxicological findings. Toxicological Sciences 99, 366–394. https://doi.org/10.1093/toxsci/kfm128
Law, R.M., Ngo, M.A., Maibach, H.I., 2020. Twenty Clinically Pertinent Factors/Observations for Percutaneous Absorption in Humans. Am J Clin Dermatol 21, 85–95. https://doi.org/10.1007/s40257-019-00480-4
Lentz, K., Raybon, J., Sinz, M.W., 2013. Drug Metabolism and Pharmacokinetics in Drug Discovery, in: Drug Discovery: Practices, Processes, and Perspectives. pp. 99–139. https://doi.org/10.1002/9781118354483.ch4
Li, B., Zhang, T., Xu, Z., Fang, H.H.P., 2009. Rapid analysis of 21 antibiotics of multiple classes in municipal wastewater using ultra performance liquid chromatography-tandem mass spectrometry. Analytica Chimica Acta 645, 64–72. https://doi.org/10.1016/j.aca.2009.04.042
Li, Y., Fletcher, T., Mucs, D., Scott, K., Lindh, C.H., Tallving, P., Jakobsson, K., 2018. Half-lives of PFOS, PFHxS and PFOA after end of exposure to contaminated drinking water. Occup Environ Med 75, 46–51. https://doi.org/10.1136/oemed-2017-104651

Li, Z.M., Guo, L.H., Ren, X.M., 2016. Biotransformation of 8:2 fluorotelomer alcohol by recombinant human cytochrome P450s, human liver microsomes and human liver cytosol. Environmental Science: Processes and Impacts 18, 538–546. https://doi.org/10.1039/c6em00071a

Licul-Kucera, V., Frömel, T., Kruså, M., van Wezel, A.P., Knepper, T.P., 2023. Finding a way out? Comprehensive biotransformation study of novel fluorinated surfactants. Chemosphere 339. https://doi.org/10.1016/j.chemosphere.2023.139563

Lin, L., Abdallah, M.A.E., Chen, L.J., Luo, X.J., Mai, B.X., Harrad, S., 2022. Comparative in vitro metabolism of short chain chlorinated paraffins (SCCPs) by human and chicken liver microsomes: First insight into heptachlorodecanes. Science of the Total Environment 851, 158261. https://doi.org/10.1016/j.scitotenv.2022.158261

Lipinski, C.A., Lombardo, F., Dominy, B.W., Feeney, P.J., 2001. Experimental and computational approaches to estimate solubility and permeability in drug discovery and development settings 1PII of original article: S0169-409X(96)00423-1. The article was originally published in Advanced Drug Delivery Reviews 23 (1997) 3–25. 1. Advanced Drug Delivery Reviews 46, 3–26. https://doi.org/10.1016/S0169-409X(00)00129-0

Lipscomb, J.C., Poet, T.S., 2008. In vitro measurements of metabolism for application in pharmacokinetic modeling. Pharmacology and Therapeutics 118, 82–103. https://doi.org/10.1016/j.pharmthera.2008.01.006

Liu, X., Yu, G., Cao, Z., Wang, B., Huang, J., Deng, S., Wang, Y., Shen, H., Peng, X., 2017. Estimation of human exposure to halogenated flame retardants through dermal adsorption by skin wipe. Chemosphere 168, 272–278. https://doi.org/10.1016/j.chemosphere.2016.10.015

Liu, Y.-Z., Pan, L.-H., Bai, Y., Yang, K., Dong, P.-P., Fang, Z.-Z., 2020. Per- and polyfluoroalkyl substances exert strong inhibition towards human carboxylesterases. Environmental Pollution 263, 114463. https://doi.org/10.1016/j.envpol.2020.114463

Lorber, M., 2008. Exposure of Americans to polybrominated diphenyl ethers. J Expo Sci Environ Epidemiol 18, 2–19. https://doi.org/10.1038/sj.jes.7500572

Lu, Y., Meng, L., Ma, D., Cao, H., Liang, Y., Liu, H., Wang, Y., Jiang, G., 2021. The occurrence of PFAS in human placenta and their binding abilities to human serum albumin and organic anion transporter 4. Environmental Pollution 273, 116460. https://doi.org/10.1016/j.envpol.2021.116460

Luo, K., Zeng, D., Kang, Y., Lin, X., Sun, N., Li, C., Zhu, M., Chen, Z., Man, Y.B., Li, H., 2020. Dermal bioaccessibility and absorption of polycyclic aromatic hydrocarbons (PAHs) in indoor dust and its implication in risk assessment. Environmental Pollution 264, 114829. https://doi.org/10.1016/j.envpol.2020.114829

Manzano-Salgado, C.B., Casas, M., Lopez-Espinosa, M.-J., Ballester, F., Iñiguez, C., Martinez, D., Costa, O., Santa-Marina, L., Pereda-Pereda, E., Schettgen, T., Sunyer, J., Vrijheid, M., 2017. Prenatal exposure to perfluoroalkyl substances and birth outcomes in a Spanish birth cohort. Environment International 108, 278–284. https://doi.org/10.1016/j.envint.2017.09.006

Martin, J.W., Mabury, S.A., O'Brien, P.J., 2005. Metabolic products and pathways of fluorotelomer alcohols in isolated rat hepatocytes. Chemico-Biological Interactions 155, 165–180. https://doi.org/10.1016/j.cbi.2005.06.007

Meng, Q., Inoue, K., Ritz, B., Olsen, J., Liew, Z., 2018. Prenatal Exposure to Perfluoroalkyl Substances and Birth Outcomes; An Updated Analysis from the Danish National Birth Cohort. IJERPH 15, 1832. https://doi.org/10.3390/ijerph15091832

Moniz, T., Costa Lima, S.A., Reis, S., 2020. Human skin models: From healthy to disease-mimetic systems; characteristics and applications. Br J Pharmacol bph.15184. https://doi.org/10.1111/bph.15184
Morris, Stephanie A.V., Ananthapadmanabhan, K.P., Kasting, G.B., 2019. Anionic Surfactant–Induced Changes in Skin Permeability. Journal of Pharmaceutical Sciences 108, 3640–3648. https://doi.org/10.1016/j.xphs.2019.06.030
Morris, S.A.V., Kasting, G.B., Ananthapadmanabhan, K.P., 2022. Surfactant equilibria and its impact on penetration into stratum corneum. Current Opinion in Colloid & Interface Science 59, 101579. https://doi.org/10.1016/j.cocis.2022.101579
Morris, Stephanie A. V., Thompson, R.T., Glenn, R.W., Ananthapadmanabhan, K.P., Kasting, G.B., 2019. Mechanisms of anionic surfactant penetration into human skin: Investigating monomer, micelle and submicellar aggregate penetration theories. Int J Cosmet Sci 41, 55–66. https://doi.org/10.1111/ics.12511
Nabb, D.L., Szostek, B., Himmelstein, M.W., Mawn, M.P., Gargas, M.I., Sweeney, L.M., Stadler, J.C., Buck, R.C., Fasano, W.J., 2007a. In vitro metabolism of 8-2 fluorotelomer alcohol: Interspecies comparisons and metabolic pathway refinement. Toxicological Sciences 100, 333–344. https://doi.org/10.1093/toxsci/kfm230
Nabb, D.L., Szostek, B., Himmelstein, M.W., Mawn, M.P., Gargas, M.I., Sweeney, L.M., Stadler, J.C., Buck, R.C., Fasano, W.J., 2007b. In vitro metabolism of 8-2 fluorotelomer alcohol: Interspecies comparisons and metabolic pathway refinement. Toxicological Sciences 100, 333–344. https://doi.org/10.1093/toxsci/kfm230
Nicolaides, N., 1974. Skin Lipids: Their Biochemical Uniqueness. Science 186, 19–26. https://doi.org/10.1126/science.186.4158.19
Niedorf, F., Schmidt, E., Kietzmann, M., 2008. The Automated, Accurate and Reproducible Determination of Steady-state Permeation Parameters from Percutaneous Permeation Data. Altern Lab Anim 36, 201–213. https://doi.org/10.1177/026119290803600209
Nilsson, H., Kärrman, A., Rotander, A., van Bavel, B., Lindström, G., Westberg, H., 2013. Biotransformation of fluorotelomer compound to perfluorocarboxylates in humans. Environment International 51, 8–12. https://doi.org/10.1016/j.envint.2012.09.001
Nishimuta, H., Houston, J.B., Galetin, A., 2014. Hepatic, intestinal, renal, and plasma hydrolysis of prodrugs in human, cynomolgus monkey, dog, and rat: Implications for in vitro-in vivo extrapolation of clearance of prodrugs. Drug Metabolism and Disposition 42, 1522–1531. https://doi.org/10.1124/dmd.114.057372
Obringer, C., Wu, S., Troutman, J., Karb, M., Lester, C., 2021. Effect of chain length and branching on the in vitro metabolism of a series of parabens in human liver S9, human skin S9, and human plasma. Regulatory Toxicology and Pharmacology 122, 104918. https://doi.org/10.1016/j.yrtph.2021.104918
OECD, 2021. Reconciling Terminology of the Universe of Per- and Polyfluoroalkyl Substances: Recommendations and Practical Guidance, Series on Risk Management No.61. https://www.oecd.org/ chemicalsafety/portal-perfluorinated-chemicals/terminology-per-andpolyfluoroalkyl- substances.pdf (accessed 2023/09/18).
OECD, 2011. GUIDANCE NOTES ON DERMAL ABSORPTION Series on Testing and Assessment No. 156.
OECD, 2004a. Test No. 428: Skin Absorption: In Vitro Method, OECD Guidelines for the Testing of Chemicals, Section 4. OECD Publishing, Paris.
OECD, 2004b. GUIDANCE DOCUMENT FOR THE CONDUCT OF SKIN ABSORPTION STUDIES OECD SERIES ON TESTING AND ASSESSMENT Number 28.

Oesch, F., Fabian, E., Guth, K., Landsiedel, R., 2014. Xenobiotic-metabolizing enzymes in the skin of rat, mouse, pig, guinea pig, man, and in human skin models. Arch Toxicol 88, 2135–2190. https://doi.org/10.1007/s00204-014-1382-8

Okasaka, M., Kubota, K., Yamasaki, E., Yang, J., Takata, S., 2019. Evaluation of anionic surfactants effects on the skin barrier function based on skin permeability. Pharmaceutical Development and Technology 24, 99–104. https://doi.org/10.1080/10837450.2018.1425885

Olsen, G.W., Burris, J.M., Ehresman, D.J., Froehlich, J.W., Seacat, A.M., Butenhoff, J.L., Zobel, L.R., 2007. Half-Life of Serum Elimination of Perfluorooctanesulfonate,Perfluorohexanesulfonate, and Perfluorooctanoate in Retired Fluorochemical Production Workers. Environmental Health Perspectives 115, 1298–1305. https://doi.org/10.1289/ehp.10009

Olsen, G.W., Chang, S.-C., Noker, P.E., Gorman, G.S., Ehresman, D.J., Lieder, P.H., Butenhoff, J.L., 2009. A comparison of the pharmacokinetics of perfluorobutanesulfonate (PFBS) in rats, monkeys, and humans. Toxicology 256, 65–74. https://doi.org/10.1016/j.tox.2008.11.008

Osakwe, O., 2016. Preclinical In Vitro Studies: Development and Applicability, in: Social Aspects of Drug Discovery, Development and Commercialization. Academic Press, pp. 129–148.

Padilla-Sánchez, J.A., Haug, L.S., 2016. A fast and sensitive method for the simultaneous analysis of a wide range of per- and polyfluoroalkyl substances in indoor dust using on-line solid phase extraction-ultrahigh performance liquid chromatography-time-of-flight-mass spectrometry. Journal of Chromatography A 1445, 36–45. https://doi.org/10.1016/j.chroma.2016.03.058

Parkinson, A., Ogilvie, B.W., Buckley, D.B., Kazmi, F., Czerwinski, M., Parkinson, O., 2015. Biotransformation of Xenobiotics, in: Klaassen, C.D., Watkins III, J.B. (Eds.), Casarett & Doull's Essentials of Toxicology, 3e. McGraw-Hill Education, New York, NY.

Pawar, G., Abdallah, M.A.-E., de Sáa, E.V., Harrad, S., 2017. Dermal bioaccessibility of flame retardants from indoor dust and the influence of topically applied cosmetics. J Expo Sci Environ Epidemiol 27, 100–105. https://doi.org/10.1038/jes.2015.84

Pont, A.R., Charron, A.R., Brand, R.M., 2004. Active ingredients in sunscreens act as topical penetration enhancers for the herbicide 2,4-dichlorophenoxyacetic acid. Toxicology and Applied Pharmacology 195, 348–354. https://doi.org/10.1016/j.taap.2003.09.021

Poothong, S., Padilla-Sánchez, J.A., Papadopoulou, E., Giovanoulis, G., Thomsen, C., Haug, L.S., 2019. Hand Wipes: A Useful Tool for Assessing Human Exposure to Poly- and Perfluoroalkyl Substances (PFASs) through Hand-to-Mouth and Dermal Contacts. Environ. Sci. Technol. 53, 1985–1993. https://doi.org/10.1021/acs.est.8b05303

Poothong, S., Papadopoulou, E., Padilla-Sánchez, J.A., Thomsen, C., Haug, L.S., 2020. Multiple pathways of human exposure to poly- and perfluoroalkyl substances (PFASs): From external exposure to human blood. Environment International 134, 105244. https://doi.org/10.1016/j.envint.2019.105244

Preston, E. V, Webster, T.F., Henn, B.C., Mcclean, M.D., Oken, E., Rifas-shiman, S.L., Pearce, E.N., Antonia, M., Fleisch, A.F., Sagiv, S.K., 2021. Prenatal Exposure to Per- and Polyfluoroalkyl Substances and Maternal and Neonatal Thyroid Function in the Project Viva Cohort: a mixtures approach. Environ Int. 139, 1–26. https://doi.org/10.1016/j.envint.2020.105728.Prenatal

Pütz, K.W., Namazkar, S., Plassmann, M., Benskin, J.P., 2022. Are cosmetics a significant source of PFAS in Europe? product inventories, chemical characterization and

emission estimates. Environ. Sci.: Processes Impacts 24, 1697–1707. https://doi.org/10.1039/D2EM00123C
Ragnarsdóttir, O., Abdallah, M.A.-E., Harrad, S., 2023. Dermal bioaccessibility of perfluoroalkyl substances from household dust; influence of topically applied cosmetics. Environmental Research 238, 117093. https://doi.org/10.1016/j.envres.2023.117093
Ragnarsdóttir, O., Abdallah, M.A.-E., Harrad, S., 2022. Dermal uptake: An important pathway of human exposure to perfluoroalkyl substances? Environmental Pollution 307, 119478. https://doi.org/10.1016/j.envpol.2022.119478
Ragnarsdóttir, O., Mohamed Abou-Elwafa Abdallah, Stuart Harrad, 2024. Dermal Bioavailability of Perfluoroalkyl Substances using in vitro 3D Human Skin Equivalent Models. *Under review in Environment International*, 2024.
Reiner, J.L., Blaine, A.C., Higgins, C.P., Huset, C., Jenkins, T.M., Kwadijk, C.J.A.F., Lange, C.C., Muir, D.C.G., Reagen, W.K., Rich, C., Small, J.M., Strynar, M.J., Washington, J.W., Yoo, H., Keller, J.M., 2015. Polyfluorinated substances in abiotic standard reference materials. Anal Bioanal Chem 407, 2975–2983. https://doi.org/10.1007/s00216-013-7330-2
Reisinger, K., Blatz, V., Brinkmann, J., Downs, T.R., Fischer, A., Henkler, F., Hoffmann, S., Krul, C., Liebsch, M., Luch, A., Pirow, R., Reus, A.A., Schulz, M., Pfuhler, S., 2018. Validation of the 3D Skin Comet assay using full thickness skin models: Transferability and reproducibility. Mutation Research/Genetic Toxicology and Environmental Mutagenesis 827, 27–41. https://doi.org/10.1016/j.mrgentox.2018.01.003
Roberts, S.C., Macaulay, L.J., Stapleton, H.M., 2012. In Vitro Metabolism of the Brominated Flame Retardants 2- Ethylhexyl-2,3,4,5-Tetrabromobenzoate (TBB) and Bis(2-Ethylhexyl) 2,3,4,5-Tetrabromophthalate (TBPH) in Human and Rat Tissues. Chem Res Toxicol. 25, 1435–1441. https://doi.org/10.1021/tx300086x.In
Ruby, M.V., Davis, A., Schoof, R., Eberle, S., Sellstone, C.M., 1996. Estimation of Lead and Arsenic Bioavailability Using a Physiologically Based Extraction Test. Environ. Sci. Technol. 30, 422–430. https://doi.org/10.1021/es950057z
Sagiv, S.K., Rifas-Shiman, S.L., Fleisch, A.F., Webster, T.F., Calafat, A.M., Ye, X., Gillman, M.W., Oken, E., 2018. Early-Pregnancy Plasma Concentrations of Perfluoroalkyl Substances and Birth Outcomes in Project Viva: Confounded by Pregnancy Hemodynamics? American Journal of Epidemiology 187, 793–802. https://doi.org/10.1093/aje/kwx332
Salihovic, S., Stubleski, J., Kärrman, A., Larsson, A., Fall, T., Lind, L., Lind, P.M., 2018a. Changes in markers of liver function in relation to changes in perfluoroalkyl substances - A longitudinal study. Environment International 117, 196–203. https://doi.org/10.1016/j.envint.2018.04.052
Salihovic, S., Stubleski, J., Kärrman, A., Larsson, A., Fall, T., Lind, L., Lind, P.M., 2018b. Changes in markers of liver function in relation to changes in perfluoroalkyl substances - A longitudinal study. Environment International 117, 196–203. https://doi.org/10.1016/j.envint.2018.04.052
Sartorelli, P., Andersen, H.R., Angerer, J., Corish, J., Drexler, H., Göen, T., Griffin, P., Hotchkiss, S.A.M., Larese, F., Montomoli, L., Perkins, J., Schmelz, M., van de Sandt, J., Williams, F., 2000. Percutaneous penetration studies for risk assessment. Environmental Toxicology and Pharmacology 8, 133–152. https://doi.org/10.1016/S1382-6689(00)00035-1
SCCS, 2021. The SSCS Notes of Guidance for the Testing of Cosmetic Ingredients and Their Safety Evaluation 11th Revision. European Commission.

Schäfer-Korting, M., Bock, U., Diembeck, W., Düsing, H.-J., Gamer, A., Haltner-Ukomadu, E., Hoffmann, C., Kaca, M., Kamp, H., Kersen, S., Kietzmann, M., Korting, H.C., Krächter, H.-U., Lehr, C.-M., Liebsch, M., Mehling, A., Müller-Goymann, C., Netzlaff, F., Niedorf, F., Rübbelke, M.K., Schäfer, U., Schmidt, E., Schreiber, S., Spielmann, H., Vuia, A., Weimer, M., 2008. The Use of Reconstructed Human Epidermis for Skin Absorption Testing: Results of the Validation Study. Alternatives to Laboratory Animals 36, 161–187. https://doi.org/10.1177/026119290803600207

Schiffer, R., Neis, M., Höller, D., Rodríguez, F., Geier, A., Gartung, C., Lammert, F., Dreuw, A., Zwadlo-Klarwasser, G., Merk, H., Jugert, F., Baron, J.M., 2003. Active Influx Transport is Mediated by Members of the Organic Anion Transporting Polypeptide Family in Human Epidermal Keratinocytes. Journal of Investigative Dermatology 120, 285–291. https://doi.org/10.1046/j.1523-1747.2003.12031.x

Schultes, L., Vestergren, R., Volkova, K., Westberg, E., Jacobson, T., Benskin, J.P., 2018. Per- and polyfluoroalkyl substances and fluorine mass balance in cosmetic products from the Swedish market: implications for environmental emissions and human exposure. Environ. Sci.: Processes Impacts 20, 1680–1690. https://doi.org/10.1039/C8EM00368H

Schymanski, E.L., Jeon, J., Gulde, R., Fenner, K., Ruff, M., Singer, H.P., Hollender, J., 2014. Identifying small molecules via high resolution mass spectrometry: Communicating confidence. Environmental Science and Technology 48, 2097–2098. https://doi.org/10.1021/es5002105

Sen, P., Qadri, S., Luukkonen, P.K., Ragnarsdottir, O., McGlinchey, A., Jäntti, S., Juuti, A., Arola, J., Schlezinger, J.J., Webster, T.F., Orešič, M., Yki-Järvinen, H., Hyötyläinen, T., 2022a. Exposure to environmental contaminants is associated with altered hepatic lipid metabolism in non-alcoholic fatty liver disease. Journal of Hepatology 76, 283–293. https://doi.org/10.1016/j.jhep.2021.09.039

Sen, P., Qadri, S., Luukkonen, P.K., Ragnarsdottir, O., McGlinchey, A., Jäntti, S., Juuti, A., Arola, J., Schlezinger, J.J., Webster, T.F., Orešič, M., Yki-Järvinen, H., Hyötyläinen, T., 2022b. Exposure to environmental contaminants is associated with altered hepatic lipid metabolism in non-alcoholic fatty liver disease. Journal of Hepatology 76, 283–293. https://doi.org/10.1016/j.jhep.2021.09.039

Serrano, L., Iribarne-Durán, L.M., Suárez, B., Artacho-Cordón, F., Vela-Soria, F., Peña-Caballero, M., Hurtado, J.A., Olea, N., Fernández, M.F., Freire, C., 2021. Concentrations of perfluoroalkyl substances in donor breast milk in Southern Spain and their potential determinants. International Journal of Hygiene and Environmental Health 236, 113796. https://doi.org/10.1016/j.ijheh.2021.113796

Shane, H.L., Baur, R., Lukomska, E., Weatherly, L., Anderson, S.E., 2020. Immunotoxicity and allergenic potential induced by topical application of perfluorooctanoic acid (PFOA) in a murine model. Food and Chemical Toxicology 136, 111114. https://doi.org/10.1016/j.fct.2020.111114

Stanifer, J.W., Stapleton, H.M., Souma, T., Wittmer, A., Zhao, X., Boulware, L.E., 2018. Perfluorinated chemicals as emerging environmental threats to kidney health: A scoping review. Clinical Journal of the American Society of Nephrology 13, 1479–1492. https://doi.org/10.2215/CJN.04670418

Stefaniak, A.B., Duling, M.G., Geer, L., Virji, M.A., 2014. Dissolution of the metal sensitizers Ni, Be, Cr in artificial sweat to improve estimates of dermal bioaccessibility. Environ. Sci.: Processes Impacts 16, 341. https://doi.org/10.1039/c3em00570d

Stefaniak, A.B., Harvey, C.J., 2008. Artificial skin surface film liquids. US20080311613A1.

Stefaniak, A.B., Harvey, C.J., 2006. Dissolution of materials in artificial skin surface film liquids. Toxicology in Vitro 20, 1265–1283. https://doi.org/10.1016/j.tiv.2006.05.011
Stockholm Convention, 2022a. Initial indicative list of perfluorohexane sulfonic acid (PFHxS), its salts and PFHxS-related compounds. Decision SC-10/13.
Stockholm Convention, 2022b. POPRC-17/6: Long-chain perfluorocarboxylic acids, their salts and related compounds.
Stockholm Convention, 2019. Ninth Meeting of the Conference of the Parties to the Stockholm Convention.
Sunderland, E.M., Hu, X.C., Dassuncao, C., Tokranov, A.K., Wagner, C.C., Allen, J.G., 2019. A review of the pathways of human exposure to poly- and perfluoroalkyl substances (PFASs) and present understanding of health effects. J Expo Sci Environ Epidemiol 29, 131–147. https://doi.org/10.1038/s41370-018-0094-1
Thépaut, E., Dirven, H.A.A.M., Haug, L.S., Lindeman, B., Poothong, S., Andreassen, M., Hjertholm, H., Husøy, T., 2021. Per- and polyfluoroalkyl substances in serum and associations with food consumption and use of personal care products in the Norwegian biomonitoring study from the EU project EuroMix. Environmental Research 195, 110795. https://doi.org/10.1016/j.envres.2021.110795
Trudel, D., Horowitz, L., Wormuth, M., Scheringer, M., Cousins, I.T., Hungerbühler, K., 2008. Estimating Consumer Exposure to PFOS and PFOA. Risk Analysis 28, 251–269. https://doi.org/10.1111/j.1539-6924.2008.01017.x
Trudel, D., Scheringer, M., von Goetz, N., Hungerbühler, K., 2011. Total Consumer Exposure to Polybrominated Diphenyl Ethers in North America and Europe. Environ. Sci. Technol. 45, 2391–2397. https://doi.org/10.1021/es1035046
Tsaioun, K., Blaauboer, B.J., Hartung, T., 2016. Evidence-based absorption, distribution, metabolism, excretion (ADME) and its interplay with alternative toxicity methods. Altex 33, 343–358. https://doi.org/10.14573/altex.1610101
United Nations Environment Programme, 2022. Decision SC-10/13. Listing of Perfluorohexane Sulfonic Acid (PFHxS), its salts and PFHxS-related compounds.
United Nations Environment Programme, 2019. Decision: SC-9/12. Listing of Perfluorooctanoic Acid (PFOA), its Salts and PFOA-Related Compounds.
United Nations Environment Programme, 2009. Decision SC-4/17. Listing of Perfluorooctane Sulfonic Acid, its Salts and Perfluorooctane Sulfonyl Fluoride.
U.S. EPA, 2023. Proposed PFAS National Primary Drinking Water Regulation (NPDWR).
U.S. EPA, 2022. US EPA Health Advisory Levels for Four PFAS.
U.S. EPA, 2021. EPA Advances Science to Protect the Public from PFOA and PFOS in Drinking Water.
U.S. EPA, 2011. Exposure Factors Handbook.
U.S. EPA, 2004. In vitro dermal absorption rate testing of certain chemicals of interest to the oc- cupational safety and health administration; final rule. Fed Regist 2004;69:22402–41.
van de Sandt, J.J.M., van Burgsteden, J.A., Cage, S., Carmichael, P.L., Dick, I., Kenyon, S., Korinth, G., Larese, F., Limasset, J.C., Maas, W.J.M., Montomoli, L., Nielsen, J.B., Payan, J.-P., Robinson, E., Sartorelli, P., Schaller, K.H., Wilkinson, S.C., Williams, F.M., 2004. In vitro predictions of skin absorption of caffeine, testosterone, and benzoic acid: a multi-centre comparison study. Regulatory Toxicology and Pharmacology 39, 271–281. https://doi.org/10.1016/j.yrtph.2004.02.004
Van den Eede, N., Maho, W., Erratico, C., Neels, H., Covaci, A., 2013. First insights in the metabolism of phosphate flame retardants and plasticizers using human liver fractions. Toxicology Letters 223, 9–15. https://doi.org/10.1016/j.toxlet.2013.08.012

van der Veen, I., Hanning, A.-C., Stare, A., Leonards, P.E.G., de Boer, J., Weiss, J.M., 2020. The effect of weathering on per- and polyfluoroalkyl substances (PFASs) from durable water repellent (DWR) clothing. Chemosphere 249, 126100. https://doi.org/10.1016/j.chemosphere.2020.126100

van Eijl, S., Zhu, Z., Cupitt, J., Gierula, M., Götz, C., Fritsche, E., Edwards, R.J., 2012. Elucidation of Xenobiotic Metabolism Pathways in Human Skin and Human Skin Models by Proteomic Profiling. PLoS ONE 7, e41721. https://doi.org/10.1371/journal.pone.0041721

Van Gele, M., Geusens, B., Brochez, L., Speeckaert, R., Lambert, J., 2011. Three-dimensional skin models as tools for transdermal drug delivery: challenges and limitations. Expert Opinion on Drug Delivery 8, 705–720. https://doi.org/10.1517/17425247.2011.568937

Van Ravenzwaay, B., Leibold, E., 2004a. A comparison between in vitro rat and human and in vivo rat skin absorption studies. Hum Exp Toxicol 23, 421–430. https://doi.org/10.1191/0960327104ht471oa

Van Ravenzwaay, B., Leibold, E., 2004b. The significance of in vitro rat skin absorption studies to human risk assessment. Toxicology in Vitro 18, 219–225. https://doi.org/10.1016/j.tiv.2003.08.002

Vestergren, R., Cousins, I.T., Trudel, D., Wormuth, M., Scheringer, M., 2008a. Estimating the contribution of precursor compounds in consumer exposure to PFOS and PFOA. Chemosphere 73, 1617–1624. https://doi.org/10.1016/j.chemosphere.2008.08.011

Vestergren, R., Cousins, I.T., Trudel, D., Wormuth, M., Scheringer, M., 2008b. Estimating the contribution of precursor compounds in consumer exposure to PFOS and PFOA. Chemosphere 73, 1617–1624. https://doi.org/10.1016/j.chemosphere.2008.08.011

Walters, K.A., Bialik, W., Brain, K.R., 1993. The effects of surfactants on penetration across the skin. Int J Cosmet Sci 15, 260–271. https://doi.org/10.1111/j.1467-2494.1993.tb00572.x

Walters, K.A., Brain, K.R., Howes, D., James, V.J., Kraus, A.L., Teetsel, N.M., Toulon, M., Watkinson, A.C., Gettings, S.D., 1997. Percutaneous penetration of octyl salicylate from representative sunscreen formulations through human skin in vitro. Food and Chemical Toxicology 35, 1219–1225. https://doi.org/10.1016/S0278-6915(97)85471-3

Wang, Z., Buser, A.M., Cousins, I.T., Demattio, S., Drost, W., Johansson, O., Ohno, K., Patlewicz, G., Richard, A.M., Walker, G.W., White, G.S., Leinala, E., 2021. A New OECD Definition for Per- And Polyfluoroalkyl Substances. Environmental Science and Technology 55, 15575–15578. https://doi.org/10.1021/acs.est.1c06896

Wang, Z., Dewitt, J.C., Higgins, C.P., Cousins, I.T., 2017. A Never-Ending Story of Per- and Polyfluoroalkyl Substances (PFASs)? Environmental Science and Technology 51, 2508–2518. https://doi.org/10.1021/acs.est.6b04806

Wang, Z., MacLeod, M., Cousins, I.T., Scheringer, M., Hungerbühler, K., 2011. Using COSMOtherm to predict physicochemical properties of poly- and perfluorinated alkyl substances (PFASs). Environ. Chem. 8, 389. https://doi.org/10.1071/EN10143

Watkins, D.J., McClean, M.D., Fraser, A.J., Weinberg, J., Stapleton, H.M., Sjödin, A., Webster, T.F., 2011. Exposure to PBDEs in the Office Environment: Evaluating the Relationships Between Dust, Handwipes, and Serum. Environmental Health Perspectives 119, 1247–1252. https://doi.org/10.1289/ehp.1003271

Weatherly, L.M., Shane, H.L., Lukomska, E., Baur, R., Anderson, S.E., 2021. Systemic toxicity induced by topical application of heptafluorobutyric acid (PFBA) in a murine model. Food and Chemical Toxicology 156, 112528. https://doi.org/10.1016/j.fct.2021.112528

Weschler, C.J., Nazaroff, W.W., 2014. Dermal Uptake of Organic Vapors Commonly Found in Indoor Air. Environmental Science & Technology 48, 1230–1237. https://doi.org/10.1021/es405490a
Wester, R.C., Bucks, D.A.W., Maibach, H.I., Anderson, J., 1983. Polychlorinated biphenyls (PCBs): Dermal absorption, systemic elimination, and dermal wash efficiency. Journal of Toxicology and Environmental Health 12, 511–519. https://doi.org/10.1080/15287398309530445
Wester, R.C., Maibach, H.I., Bucks, D.A.W., McMaster, J., Mobayen, M., Sarason, R., Moore, A., 1990. Percutaneous absorption and skin decontamination of PCBS: In vitro studies with human skin and in vivo studies in the rhesus monkey. Journal of Toxicology and Environmental Health 31, 235–246. https://doi.org/10.1080/15287399009531453
Wester, R.C., Maibach, H.I., Sedik, L., Melendres, J., Wade, M., 1993. Percutaneous absorption of PCBs from soil: In vivo rhesus monkey, in vitro human skin, and binding to powdered human stratum corneum. Journal of Toxicology and Environmental Health 39, 375–382. https://doi.org/10.1080/15287399309531758
Whitehead, H.D., Venier, M., Wu, Y., Eastman, E., Urbanik, S., Diamond, M.L., Shalin, A., Schwartz-Narbonne, H., Bruton, T.A., Blum, A., Wang, Z., Green, M., Tighe, M., Wilkinson, J.T., McGuinness, S., Peaslee, G.F., 2021. Fluorinated Compounds in North American Cosmetics. Environ. Sci. Technol. Lett. acs.estlett.1c00240. https://doi.org/10.1021/acs.estlett.1c00240
WHO, 2006. Dermal absorption. Environmental Health crieteria, 235.
Wiegand, C., Hewitt, N.J., Merk, H.F., Reisinger, K., 2014. Dermal Xenobiotic Metabolism: A Comparison between Native Human Skin, Four in vitro Skin Test Systems and a Liver System. Skin Pharmacol Physiol 27, 263–275. https://doi.org/10.1159/000358272
Wilkinson, S.C., Maas, W.J.M., Nielsen, J.B., Greaves, L.C., van de Sandt, J.J.M., Williams, F.M., 2006. Interactions of skin thickness and physicochemical properties of test compounds in percutaneous penetration studies. Int Arch Occup Environ Health 79, 405–413. https://doi.org/10.1007/s00420-005-0056-5
Williams, A.C., Barry, B.W., 2012. Penetration enhancers. Advanced Drug Delivery Reviews 64, 128–137. https://doi.org/10.1016/j.addr.2012.09.032
Winquist, A., Steenland, K., 2014. Perfluorooctanoic Acid Exposure and Thyroid Disease in Community and Worker Cohorts: Epidemiology 25, 255–264. https://doi.org/10.1097/EDE.0000000000000040
Wong, F., MacLeod, M., Mueller, J.F., Cousins, I.T., 2014. Enhanced Elimination of Perfluorooctane Sulfonic Acid by Menstruating Women: Evidence from Population-Based Pharmacokinetic Modeling. Environ. Sci. Technol. 48, 8807–8814. https://doi.org/10.1021/es500796y
Wood, F.L., Houston, J.B., Hallifax, D., 2017. Clearance prediction methodology needs fundamental improvement: Trends common to rat and human hepatocytes/microsomes and implications for experimental methodology. Drug Metabolism and Disposition 45, 1178–1188. https://doi.org/10.1124/dmd.117.077040
Wu, Q., Kannan, K., 2019. Perfluoroalkyl Substances (PFASs) in Foodstuffs and Human Dietary Exposure, in: Gómara, B., Marina, M.L. (Eds.), Current and Future Developments in Food Science. BENTHAM SCIENCE PUBLISHERS, pp. 259–313. https://doi.org/10.2174/9789811421587119010010
Wu, Y., Miller, G.Z., Gearhart, J., Peaslee, G., Venier, M., 2021. Side-chain fluorotelomer-based polymers in children car seats. Environmental Pollution 268, 115477. https://doi.org/10.1016/j.envpol.2020.115477

Xia, C., Diamond, M.L., Peaslee, G.F., Peng, H., Blum, A., Wang, Z., Shalin, A., Whitehead, H.D., Green, M., Schwartz-Narbonne, H., Yang, D., Venier, M., 2022. Per- and Polyfluoroalkyl Substances in North American School Uniforms. Environ. Sci. Technol. 56, 13845–13857. https://doi.org/10.1021/acs.est.2c02111

Xie, S., Cui, Y., Yang, Y., Meng, K., Pan, Y., Liu, Z., Chen, D., 2020. Tissue distribution and bioaccumulation of 8:2 fluorotelomer alcohol and its metabolites in pigs after oral exposure. Chemosphere 249, 126016. https://doi.org/10.1016/j.chemosphere.2020.126016

Yeung, L.W.Y., Robinson, S.J., Koschorreck, J., Mabury, S.A., 2013a. Part I. A Temporal Study of PFCAs and Their Precursors in Human Plasma from Two German Cities 1982–2009. Environ. Sci. Technol. 47, 3865–3874. https://doi.org/10.1021/es303716k

Yeung, L.W.Y., Robinson, S.J., Koschorreck, J., Mabury, S.A., 2013b. Part II. A Temporal Study of PFOS and Its Precursors in Human Plasma from Two German Cities in 1982–2009. Environ. Sci. Technol. 47, 3875–3882. https://doi.org/10.1021/es4004153

Zeng, D., Kang, Y., Chen, J., Li, A., Chen, W., Li, Z., He, L., Zhang, Q., Luo, J., Zeng, L., 2019. Dermal bioaccessibility of plasticizers in indoor dust and clothing. Science of The Total Environment 672, 798–805. https://doi.org/10.1016/j.scitotenv.2019.04.028

Zhang, Y., Beesoon, S., Zhu, L., Martin, J.W., 2013. Biomonitoring of Perfluoroalkyl Acids in Human Urine and Estimates of Biological Half-Life. Environ. Sci. Technol. 47, 10619–10627. https://doi.org/10.1021/es401905e

Zhao, W., Zitzow, J.D., Weaver, Y., Ehresman, D.J., Chang, S.-C., Butenhoff, J.L., Hagenbuch, B., 2016. Organic Anion Transporting Polypeptides Contribute to the Disposition of Perfluoroalkyl Acids in Humans and Rats. Toxicol. Sci. kfw236. https://doi.org/10.1093/toxsci/kfw236

Zhou, Y., Oh, M.H., Kim, Y.J., Kim, E., Kang, J., Chung, S., Ju, C., Kim, W.-K., Lee, K., 2020. Metabolism and Pharmacokinetics of SP-8356, a Novel (1S)-(−)-Verbenone Derivative, in Rats and Dogs and Its Implications in Humans. Molecules 25, 1–14.

Zhu, H., Kannan, K., 2020. Total oxidizable precursor assay in the determination of perfluoroalkyl acids in textiles collected from the United States. Environmental Pollution 265, 114940. https://doi.org/10.1016/j.envpol.2020.114940